SUSTAINED DRUG DELIVERY TO REDUCE THE EXTENT OF BURN PROGRESSION

MOOGAAMBIKAI D/O THANGAVELOO

LEE KONG CHIAN SCHOOL OF MEDICINE

2024

SUSTAINED DRUG DELIVERY TO REDUCE THE EXTENT OF BURN PROGRESSION

MOOGAAMBIKAI D/O THANGAVELOO

Lee Kong Chian School of Medicine

A thesis submitted to the Nanyang Technological University
in partial fulfilment of the requirement for the degree of
Doctor of Philosophy

2024

Statement of Originality

I hereby certify that the work embodied in this thesis is the result of original research, is free of plagiarised materials, and has not been submitted for a higher degree to any other University or Institution.

17/02/2024

. . . . . .

Date

. . . . . .

Moogaambikai D/O Thangaveloo

Supervisor Declaration Statement

I have reviewed the content and presentation style of this thesis and declare it is free of plagiarism and of sufficient grammatical clarity to be examined. To the best of my knowledge, the research and writing are those of the candidate except as acknowledged in the Author Attribution Statement. I confirm that the investigations were conducted in accord with the ethics policies and integrity standards of Nanyang Technological University and that the research data are presented honestly and without prejudice.

17/04/2024

. . . . . .

Date

. . . . . .

Prof. David L. Becker

Authorship Attribution Statement

This thesis **does not** contain any materials from papers published in peer-reviewed journals or from papers accepted at conferences in which I am listed as an author.

17/02/2024

. . . . . .

Date

. . . . . .

Moogaambikai D/O Thangaveloo

Acknowledgements

I would like to thank the Ministry of Education for the funding of the Nanyang Technological University Scholarship. I would like to extend my gratitude to the Lee Kong Chian School of Medicine for conferring this scholarship award on me so that I could pursue my research interests.

I want to convey my sincere gratitude and thanks to my supervisor, Prof. David Becker, for allowing me to work in his lab and for having faith in my ability to take on various projects and collaborate with diverse people from other labs.

I would like to thank my co-supervisors Prof. David Leavesley and Asst Prof. Franklin Zhong for their unwavering support during this process. A special thank you to my mentor, Prof. Anthony Phillips, for all of his insightful advice and helpful criticism during the course of my candidature.

A huge thank you to Assoc Prof. Andrew Tan and Asst Prof. Navin Verma from the thesis advisory committee for their continuous support and guidance throughout my thesis. I would like to thank my "pre-doc" supervisor from Singapore General Hospital, Dr. Feng Jiajun, for his invaluable support and the Singapore General Hospital, Burns Unit for letting me shadow them as part of my clinical attachment to observe burn victims.

The Becker Lab graduates, Dr. Milton Kwek, Dr. Chua Jia Wang, Dr. Erica Teo, and Dr. Ong Zi Xin, deserve special recognition for inspiring me and cheering me on at every juncture of my candidature. I am especially grateful for the support and friendship of my past and present colleagues from Becker Lab: Dr. Sophia Lim, Ms. Amelia Aw, Ms. Debbie Lim, Ms. Bavani Kannan, and Mr. Toby Chin, who helped me through the difficult PhD journey and brought light into the darkness for me. I am grateful to have collaborated with Dr. Zheng Xinting and Mr. Zijie on the biosensor patch project.

A special mention goes to the 4th LKC Graduate Students Club Committee: Dr. Soon Keong, Mr. Mark Chan, Mr. Vikneshwaran, and Ms. Joleen Goh for serving the school alongside while working on our respective theses. Thanks to all my LKC and SRIS friends and peers who supported me. Special thanks to Mr. Andrew Amaladass for his encouragement and exuberant spirit, which were greatly appreciated during dark times.

I would like to thank the staff of the LKC Graduate Office and Research Administration and Support Services, with special thanks to Dr. Radek Machan and Dr. Hwee Foo Yong from the NTU Optical Bio-Imaging Centre (NOBIC), for supporting me throughout these years.

I would like to thank members of Asst Prof. Franklin Zhong, Asst Prof. Navin Verma, Prof. Maurice van Steensel, Prof. Tom Dawson, and the Asian Skin Bank from SRIS for being such a great support during the final months of my PhD. I would like to thank Prof. Phil Ingham and Asst Prof. Wilson Goh for their kind words and encouragement.

Last but not least, I want to express my sincere gratitude to my parents for their unending love and support throughout my PhD journey, as well as to my mother-in-law, brothers, sister-in-law, nephews, and nieces. Huge thanks to my cousins and dearest friends for their unwavering support. A special shoutout to my husband, Thinesh Kurunathan, for being so understanding, being a pillar of strength, and believing me in every step of the way.

Above God, Appa, this is for you.

Table of Contents

Summary

Burns are highly dynamic injuries characterized by an initial zone of necrosis that progresses to compromise surrounding tissue. Acute inflammation and cell death are the two main factors contributing to burn progression. These processes are modulated by Connexin43 (Cx43) hemichannels and gap junctions in traumatic injuries such as burns and chronic wounds. Particularly, Cx43 hemichannel mediated ATP release interacts with P2X7 to activate the NLRP3 inflammasome pathway. This study used a rat burn model to evaluate the effect of a gap junction modulator, Cx43 antisense oligodeoxynucleotides, or Cx43 hemichannel blocker, Tonabersat, for the inhibition of inflammasome activation and use as a potential treatment for burn injury. In Chapter 3, I described our rat burn model, which was created with a hand-held soldering iron, and wounds were subjected to a scoring matrix that best mimicked features of human burn wounds. In the following chapter, burn wounds were treated with topical Cx43 antisense oligodeoxynucleotide or Tonabersat using the characterized rat burn model. I evaluated the immunofluorescence expression levels of Cx43, hemichannels, inflammasome markers (NLRP3, Cas-1, and IL-1β), inflammatory markers MPO and CD68, and skin fibrosis markers αSMA and HSP47 at various timepoints. To evaluate the overall effects on burn wound healing, quantitative analysis with H&E and Masson's trichrome was performed. Our data showed that sustained release of Cx43 antisense oligodeoxynucleotide reduced protein expression of Cx43 hemichannels and gap junctions, and Tonabersat at high concentrations reduced Cx43 gap junctions protein expression. This concomitantly reduced inflammation and NLRP3 inflammasome complex assembly in rat burn injuries, leading to improved wound healing and reduced scarring. In the final two chapters, a preliminary study was conducted on a porcine scald burn model. Tonabersat and Cx43 antisense oligodeoxynucleotide were applied

topically or in a form of scaffold dressing to treat porcine scald burn wounds. I evaluated the immunofluorescence expression levels of Cx43, hemichannels, inflammasome markers NLRP3 and Cas-1, inflammatory markers MPO and CD68, and skin fibrosis makers αSMA and HSP47 at various timepoints. Finding from this study shows that Cx43 hemichannels and gap junctions play a central role in the amplification and perpetuation of inflammation in burn injury. The Cx43-targeted therapeutics mitigating burn progression might reduce the healthcare cost of burn care and allow for better functional recovery in burn patients.

List of Abbreviations

µm	Microns
µM	Micromolar
AF	Alexa Fluor
ANOVA	Analysis of variance
AS-30	Cx43 Antisense oligodeoxynucleotides (Cx43asODN) 30µM
AS-300	Cx43 Antisense oligodeoxynucleotides (Cx43asODN) 300µM
ASC	Adaptor apoptosis-associated spec-like protein
asODN or AS	Antisense oligodeoxynucleotides
AS-S	Cx43asODN scaffold
ATP	Adenosine triphosphate
Au NP	Gold nanoparticles
BJ-5ta	Immortalized human fibroblast cell line
BSA	Bovine serum albumin
Ca^{2+}	Calcium ions
Cas-1	Cleaved Caspase-1
Cx	Connexin
CXCL	C-X-C motif chemokine ligand
DAMPs	Damage-associated molecular patterns
DAPI	4′,6-diamidino-2-phenylindole
DeCtrl	Debrided control
DMEM	Dulbecco’s Modified Eagle’s medium
DMSO	Dimethyl sulfoxide
DNA	Deoxyribonucleic acid
E1	Extracellular loop 1
E2	Extracelular loop 2
ECM	Extracellular matrix
EDTA	Ethylenediamineetetraacetic acid
EGF	Recombinant human epidermal growth factor (EGF)

F-127	Pluronic F-127 gel
FBS	Fetal bovine serum
GJ	Gap junction
GSDMD	Gasdermin D
H&E	Hematoxylin and eosin
HaCaT	Immortalized human keratinocyte cell line
HC	Hemichannel
HIER	Heat induced antigen retrieval
HMGB1	High mobility group box 1
HSC	Hepatic stellate cells
HSP47	Heat shock protein 47kDa
IACUC	Institutional Animal Care and Use Committee
ICC	Immunocytochemistry
IF	Immunofluorescence
IL	Interleukin
iPSC	Induced pluripotent stem cells
IQR	Interquartile range
IκB	Inhibitory-κB Kinase
K^+	Potassium ions
kDA	Kilo Dalton
LPS	Lipopolysaccharide
MMP	Matrix metallopeptidase
MPO	Myeloperoxidase
mRNA	Messenger ribonucleic acid
MSC	Mesenchymal stem cells
MT	Masson's Trichrome
MTT	3-[4,5-dimethylthiazol-2-yl]-2,5-diphenyltetrazolium bromide
Na^+	Sodium ions
NF-κB	Nuclear factor-κB
NLRP3	NOD-like reception pyrin domain-containing protein 3
NS	Normal skin
P2X	ATP-gated P2X receptors

P2Y	Purinergic G protein coupled P2Y receptors
PAF	Platelet-activating factor
PAI-1	Plasminogen activator inhibitor 1
PAMPs	Pathogen-associated molecular patterns
PBD	Post burn day
PBS	Phosphate-buffered saline
PBS-T	Phosphate-buffered saline + Tween®20
PCL	Polycaprolactone
PDLLA	poly-D, L-lactic acid
PEG	Polyethylene glycol
PFA	Paraformaldehyde
PI	Propidium Iodide
P-S	Plain PCL/PEG scaffold
qPCR	Quantitative polymerase chain reaction
RNA	Ribonucleic acid
ROI	Region of interest
ROS	Reactive oxygen species
SD	Sprague Dawley
STZ	Streptozotocin
TAT	Transactivator of transcription
TBSA	Total burn surface area
TGFβ1	Transforming growth factor beta 1
TNF-α	Tumour necrosis factor alpha
Tona	Tonabersat
Tona-100	Tonabersat 100μM
Tona-30	Tonabersat 30μM
Tona-S	Tonabersat scaffold
TUNEL	Transferase-mediated dUTP nick-end labelling
UN	Untreated wound
VEGF	Vascular endothelial growth factor
Veh	Vehicle Control
ZO-1	Zonula occuldens-1
αSMA	Alpha smooth muscle actin

List of Figures

List of Tables

Chapter 1: Literature Review

1.1 Burn Injury

The World Health Organization (WHO) has defined a burn injury as an injury to the skin or other tissues largely caused by heat, radiation, electricity, or chemicals (WHO, 2018). Burns are a global health problem. Annually, 11 million people worldwide are estimated to be burned severely enough to require medical attention. These burns result in 180,000 deaths (WHO, 2018). Almost half occur in the Southeast Asia region. In Singapore alone, there are around 4,000 reported burn injuries and about 220 admissions to hospitals every year requiring surgical intervention (Hwee et al., 2016; Ngim & Ghulam, 1994). A cost analysis of burn treatment by an Australian burns centre estimated USD73,532 per admitted burns patient. The length of stay, operative cost, dressing, and staffing are the most significant components (Ahn & Maitz, 2012).

1.2 Burn Pathophysiology

Before focusing on the pathophysiology of burns, it is important to understand the structural anatomy of the skin (Figure 1.1). The epidermis is the outermost protective layer of the skin that mainly comprises epithelial cells and keratin (Hossler, 2014). Beneath the epidermis lies the dermis, which contains interwoven collagen bundles and elastin fibres (Wong et al., 2016). Additionally, it contains skin appendages such as hair follicles and sebaceous glands, sweat glands, nerves, stromal cells such as fibroblasts, and a vascular network to provide nutrients and oxygen to the skin (Lindberg & Lamps, 2018). The dermis is further divided into two distinct layers: the papillary dermis and the reticular dermis. The upper papillary dermis contains thin collagen fibres (average 38μm) with numerous small capillary vessels at the superficial plexus (papillary/reticular dermis interface) (Wong et al., 2016). The reticular

dermis lies beneath this and is composed primarily of thick, dense collagen fibres (average length of 80 µm) with relatively larger blood vessels, multiple adnexal structures, and nerves (Lindberg & Lamps, 2018; Wong et al., 2016). Under the dermis is the subcutaneous tissue, which is made of fat and loose connective tissue that insulates and protects the skin (Wong et al., 2016).

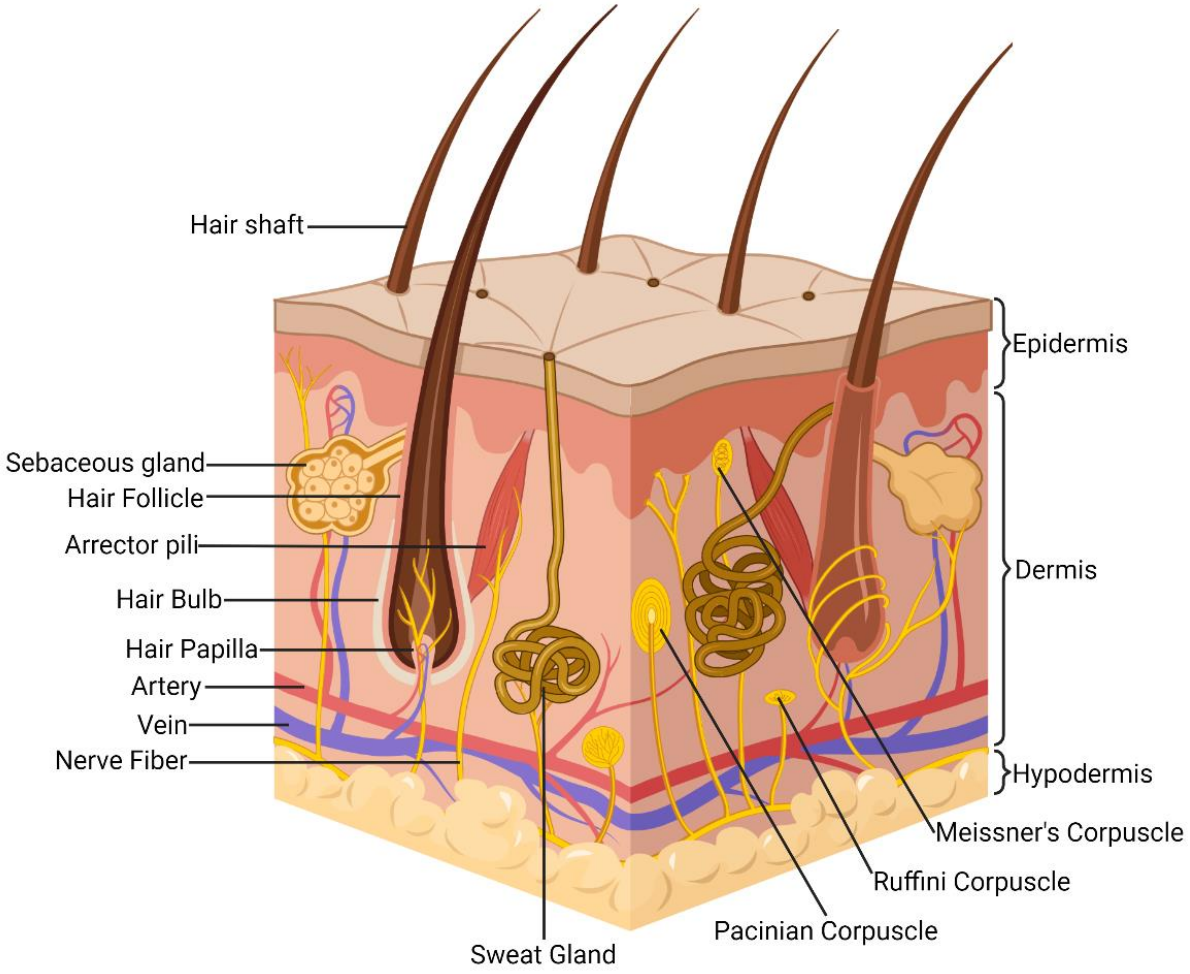

Figure 1.1 Anatomy of Skin.
A three-dimensional illustration of the skin. Created using Biorender.com.

It is important to note that the presence of skin appendages such as hair follicles, sebaceous glands, and sweat glands acts as a great source of regenerative stem cells to maintain homeostasis (Morgun & Vorotelyak, 2020). In the concept of burn injury and wound healing, if the skin appendages are undamaged, there is considered to be an ample supply of epithelial cells to repopulate the injured site and influence the rate and quality of healing (Shakespeare, 2001). On the other hand, if the injury causes the skin appendages to be destroyed, it requires debris clearance and replacement, and wound closure is likely to occur from the wound edges. This typically requires a longer time for the wound to heal and may require surgical intervention to remove necrotic tissue and preserve healthy dermis for wound recovery (Shakespeare, 2001).

Understanding the pathophysiology of burn injuries is important for effective medical treatment and management (Hettiaratchy & Dziewulski, 2004). Depending on the extent of damage caused to one or more layers of skin, it can cause a significant physiological imbalance and even death (Church et al., 2006). Typically, burns are classified according to depth of injury, including first degree burn: superficial, second degree burn: superficial-partial thickness and deep-partial thickness, third degree burn: full-thickness, and subdermal burns involving deeper structures such as fascia, muscles, and bone (Table 1.1) (Vaughn & Beckel, 2012; Warby & Maani, 2020).

Table 1.1 Classification by burn depth.

Classification	Description
Superficial Thickness	Damage to epidermal layer. Heals over few days without scarring.
Superficial-Partial Thickness	Forms blister between epidermis and dermis. Initially damage appears to be only epidermal in depth but may be determined to be partial thickness 12 to 24 hours later.
Deep-Partial Thickness	Damage to deeper dermis, hair follicles and glandular structures. Could potentially turn into full thickness burn if intervention is not introduced. Invariably causes hypertrophic scarring.
Full Thickness	Damage extends through all layers of the dermis and often injures the underlying subcutaneous tissue.
Subdermal	Damage to all layers of skin and potentially life-threatening injuries that extend into underlying soft tissue, muscle and/or bone structures.

Adapted from (Vaughn & Beckel, 2012; Warby & Maani, 2020).

The Jackson's burn wound model was designed to understand the pathophysiology of a burn wound. It describes the three concentric zones of a burn, namely; the zone of coagulation, stasis, and hyperemia (Jackson, 1953) (Figure 1.2). The central zone of coagulation sustains the greatest amount of thermal trauma, resulting in irreversible tissue damage and denaturing of proteins. This is surrounded by the zone of stasis; whereby cellular damage is less severe with viable tissues. Here, inflammatory mediators cause systemic capillary leak and intravascular fluid loss leading to decreased tissue perfusion or oedema. As such, burn resuscitation that refers to maintaining adqueate fluids and tissue oxygenation is key to combat hypovolemia and hypoperfusion (Schaefer & Nunez Lopez, 2023). The ischaemic zone of stasis may convert into full necrotic zone of coagulation if burn resuscitation and wound care are suboptimal, leading to burn wound conversion (Figure 1.3). The zone of hyperaemia surrounds the zone of stasis and is characterised by minimal cell damage and increased tissue perfusion, resulting in natural recovery (Jackson, 1953).

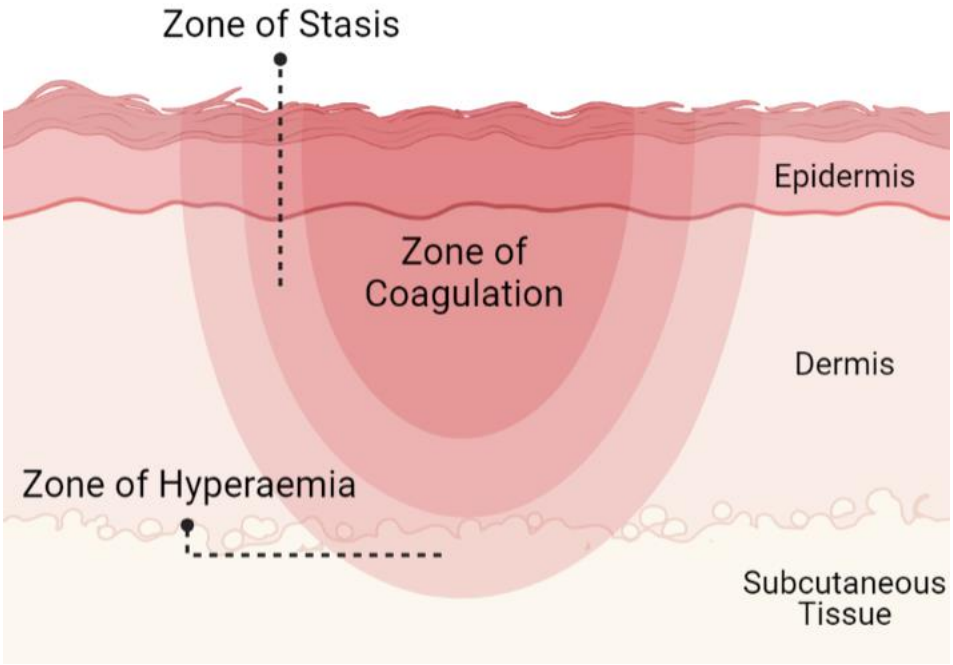

Figure 1.2 Schematic representation of Jackson's Burn Model.
Image modified from (Jackson, 1953) and created using Biorender.com.

Figure 1.3 Burn wound conversion in bilateral feet burn.
(a) initial superficial burn converted into (b) deep dermal burn. (c) Burn progressed into full thickness burn and eventually involved (d) subcutaneous tissue and fascia.

1.3 Inflammation and cell death in burn wounds

The acute inflammatory response in burn wounds is dominated by neutrophils, leading to persistently increased levels of pro-inflammatory cytokines such as TNF-α and IFN-β (Lateef et al., 2019). The acute inflammation is perpetuated by high levels of extracellular adenosine triphosphate (ATP), secreted by activated neutrophils and thus recruiting more circulating neutrophils (Eltzschig et al., 2006). This response causes collagen degradation, keratinocyte cell death, microvascular compromise, disruption of plasma membranes, DNA cross-links and strand breaks, and peptide fragmentation (Pober & Sessa, 2014; Rijken & Bruijnzeel, 2009; Shupp et al., 2010). Aside from acute inflammation, cell death is frequently observed during burn progression. In partial thickness burns, almost half of the dermal cells surrounding the zone of coagulation undergo cell death in the first week and 20% more in the third week (Gravante et al., 2008). A similar process is observed in other injuries, including brain trauma, radiation injury, and cardiac ischaemia injury, where healthy cells undergo cell death after receiving death signals from their dying neighbours (Garcia-Dorado et al., 2004; Mancuso et al., 2011; Spray et al., 2013). Pyroptosis ("pyro" for fire and "ptosis" for falling in Greek) is

an inflammatory mode of programmed cell death (McKenzie et al., 2020). The orchestration of pyroptosis is mediated by pro-inflammatory caspases, including caspase-1 (humans and rodents), caspase 4/5 (humans), and caspase 11 (rodents) (Basile et al., 2012; Liu et al., 2021; McKenzie et al., 2020; J. Ye et al., 2021). The activation of caspase-1 facilitates the maturation and release of interleukin-1β (IL-1β) and interleukin-18 (IL-18) (Pelegrin, 2021). Additionally, Gasdermin D (GSDMD), a newly identified pyroptosis executioner, is activated and releases the N-terminal fragment (GSDMD-NT) (Bae et al., 2017). The GSDMD-NT oligomerizes and forms a pore in the cell membrane, which leads to cell swelling, loss of cell membrane integrity, and the release of pro-inflammatory cytokines IL-1β and IL-18 and other intracellular components (Bae et al., 2017).

1.4 Current treatment strategies for burns

1.4.1 Debridement and Skin Graft

Typically, superficial burn wounds are dressed and left to heal on their own. Partial thickness burns, which may seem to heal naturally, could convert into a deeper burn because of the burn wound conversion phenomena. Hence, providing a definitive treatment for burn injury remains a great challenge. Early burn wound debridement (also known as escharotomy) and skin grafts remain as key standard of care for deep partial thickness and full thickness burn wounds. Local inflammatory factors and tissue ischaemia can cause further necrosis and, eventually, organ failure. In a timely manner, escharotomy must be performed to restore perfusion to prevent further loss of tissue viability (Butts et al., 2020). However, it is inevitable that debridement could involve removal of some surrounding healthy tissue and cause damage. In addition, such procedures could cause haemorrhagic shock resulting in suboptimal hemostasis after extensive debridement. Therefore, precise techniques such as enzymatic debridement and hydrosurgical

debridement system (e.g., Versajet) could counter this problem (Kakagia & Karadimas, 2018; Ziegler et al., 2020). Enzymatic debridement with collagenase clostridiopeptidase or Bromelain-based (Debrase) are shown to be less painful and improve collagen formation and vasculature in burn wounds (Legemate et al., 2018; Ozcan et al., 2002; Singer et al., 2011). Hydrosurgery uses a powerful water jet that flushes a narrow stream of water through a nozzle that causes a localised vacuum to cut accurately, irrigate, and suction tissue simultaneously without damaging viable tissues (Legemate et al., 2022). Skin grafting after hydrosurgery is shown to preserve viable dermis and improve scar quality in patients compared to conventional debridement (Legemate et al., 2018; Ziegler et al., 2020). Skin grafting is a commonly used wound closure technique in burn patients. Skin graft application aids in promoting faster wound healing and better aesthetic outcomes. In addition, it reduces complications and provides a shorter hospital stay for patients. Using a dermatome, a thin layer of skin, including epidermal and dermal layers is harvested to replace and cover affected burn areas. If the surface area to be covered is large, additional tiny slits are made in the grafted skin using a meshing technique to allow it to be stretched and applied over a larger surface area. This procedure is typical of split-thickness skin grafting (Braza & Fahrenkopf, 2022; Browning & Cindass, 2022). Full-thickness skin grafts are highly effective in achieving closure of skin defects where primary closure or healing is not possible (Prohaska & Cook, 2022). A well prepared, vascularized wound bed without infection is vital for full-thickness skin graft application and survival. Since full thickness skin grafts are obtained from another healthy part of the body, the amount of skin graft that could be obtained is limited. Hence, it is useful to cover small, affected areas (Ramsey et al., 2022) such as the nose as well as the eyelids and the ears (Trufant et al., 2016). However, the rate of failure for full thickness skin grafts remains high as the dermal component fails to absorb oxygen and nutrients from the prepared wound bed (Braza & Fahrenkopf, 2022).

1.4.2 Tissue engineering

1.4.2.1 Stem Cell Therapy

When conventional burn care strategies fail, tissue engineering helps with the repair and replacement of damaged tissue and organs. With the development of stem cell therapy, several types of stem cells have prevented burn progression and salvaged the zone of stasis. Singer and colleagues have reported that the delivery of mesenchymal stem cells (MSCs) intravenously in a rat brass comb model reduced the area of necrosis by approximately 20%, thus preventing burn progression (Singer et al., 2013). Another group has found that subcutaneous injection of MSCs into the zone of stasis reduced apoptotic cell death counts, increased tissue perfusion and tissue viability in the zone of stasis (Oksuz et al., 2013). Abbas and colleagues reported similar findings, along with reduced neutrophil infiltration, downregulated proinflammatory cytokine production, and upregulation of anti-inflammatory cytokines after MSC subcutaneous delivery. Furthermore, they reported that MSCs reduced oxidative stress and enhanced tissue perfusion through the production of proangiogenic factors and CD31 positive blood vessels, suggesting the involvement of these underlying mechanisms in the MSC treated zone of stasis (Abbas et al., 2018). Transplantation of keratinocyte derived, induced pluripotent stem cells (iPSCs) in murine models of cutaneous burn injury led to enhanced re-epithelialisation, scarless wound healing, and reduced skin fibrosis markers (Choudhury et al., 2021; Wu et al., 2019; Yan et al., 2019). An alternative to stem cell therapy in burn wounds would be the use of exosomes secreted by cultured cells. Studies have shown that human iPSC exosomes or iPSC derived MSC secreted exosomes accelerated fibroblast migration and proliferation, collagen synthesis, and angiogenesis in diabetic and non-diabetic excisional wound models (Choudhury et al., 2021; Kobayashi et al., 2018; Zhang et al., 2015).

1.4.2.2 Topical dressings

Topical dressings are widely used in burn care management. Biobrane™ is a biosynthetic dressing made of porcine dermal collagen-bonded nylon membrane on a silicon scaffold, that was first suggested for superficial partial thickness burn treatment (Farroha et al., 2013). Biobrane™ prevents moisture loss, and its transparency allows for wound inspection. One of the advantages of Biobrane™ is its stretchable properties which allow it to be used in areas with complex body contours (Feng et al., 2018; Kiong et al., 2015). As a result, pain and discomfort associated with daily dressing changes are reduced (Feng et al., 2018). Biobrane™ facilitates wound reepithelization to complete within a couple of weeks. However, Biobrane™ is not suitable for use on deep or full thickness burns (Zeng et al., 2011) and does not have anti-microbial properties to reduce infection (Sharma et al., 2019). Nanosilver dressing on burn wounds in patients has been shown to reduce pro-inflammatory cytokines TNFα and IL-1β, reduce bacteria colonisation rate, and improve healing compared to wounds treated with Sulfadiazine Silver Cream, which is an antimicrobial agent for burn wound treatment (Wu et al., 2021). Although, sulfadiazine silver cream has good antimicrobial effects, severe irritation is a big limitation that could lead to scar formation (Saeidinia et al., 2017).

As the burn wound healing process is rather complex, the properties of a dressing or an application should factor in the dynamic changes that happen as a wound heals. It is widely accepted that a warm and moist environment is essential for optimal wound healing to take place (Ousey et al., 2016). Current strategies revolve around the “wet wound” environment to facilitate the growth of granulation tissue, reduce the inflammatory response, promote cell migration and angiogenesis, and accelerate wound healing (Junker et al., 2013). Besides eliminating excess exudates, an ideal dressing must retain moisture at the wound site. In addition, it must also be comfortable and made of non-toxic and non-allergenic materials.

Moreover, it should allow oxygenation, protect against infection, and yet be cost-efficient enough to serve as a promising wound dressing (Stoica et al., 2020).

Hydrogels can be used as dermal substitutes that allow cell migration and proliferation. They also retain sufficient moisture in the environment, which is crucial for burn wound healing. Moreover, they can encapsulate stem cells or bioactive compounds to deliver to the wound bed to enhance wound healing (Choe et al., 2018). Various groups have experimented with different natural polymers, such as chitosan (Alven & Aderibigbe, 2020; T. Wang et al., 2012), dextran (Sun et al., 2011), hyaluronan (Li et al., 2018), alginate (Xu et al., 2019), collagen, and gelatin (T. Wang et al., 2012) for the production of hydrogels. Others have used synthetic materials such as polyglycolide, polylactide, and polylactide coglycolide (Metcalfe & Ferguson, 2007). These studies have shown that wide application of such hydrogels has a close resemblance to the extracellular matrix (ECM), which allows cell migration and proliferation, reduces inflammation, promotes angiogenesis, enhances granulation tissue formation, and accelerates wound healing (Stoica et al., 2020). However, the main disadvantage of such hydrogels is their poor mechanical properties, which make them non-adherent and can dislodge from their initial placement on the wound. In addition, when hydrogels swell rapidly, they could have a burst release, which may not be ideal for applications that require controlled drug release (Ghasemiyeh & Mohammadi-Samani, 2019). Some of these available products come from animal sources that carry the inherent risk of causing immune rejection (Zeng et al., 2011). To date, no products are available that completely mimic the healthy skin.

The transfer of nutrients, metabolites, and regulatory molecules from cells to the extracellular environment, as well as the reverse, can be controlled by the structure of biomaterials or scaffolds. As a result, new technology such as electrospinning is being developed to turn

biomaterials into porous intricate structures. This method processes polymeric solutions made with various solvents and polymers using the electrostatic principle. The resulting fibers have a diameter that varies from a few micrometres to nanometres (Steffens et al., 2014). MSCs were seeded onto electrospun nanofiberous scaffolds of poly-D,L-lactic acid (PDLLA) coupled with Spirulina biomass (PDLLA/Sp), which were implanted in a murine model of third degree burns. It was reported that no difference in ulceration, inflammation, and fibrosis was observed across all treatments seven days following the creation of lesions. However, the macroscopic study of the scaffold-using groups revealed improved wound contraction in contrast to the control group (Steffens et al., 2014).

Polyethylene glycol (PEG), a key excipient in numerous types therapeutic treatments that are already in clinical use and FDA approved is one of the most widely used biocompatible polymeric substances in recent times (Dethe et al., 2022; Hoang Thi et al., 2020). PEG is known for its safety and tolerance when administered to the body through multiple routes (Hoang Thi et al., 2020). When compared to nonfunctionalized nanoparticles, PEGylated nanoparticles have two key advantages: a significantly longer circulation period and significantly better hydrophilicity (Dethe et al., 2022). Some examples of FDA approved products are Genexol®-PM and OncoGel™ for anti-cancer therapy (Wang et al., 2023), COSEAL for urologic procedures and DuraSeal® for cranial procedures to facilitate natural wound healing (Wheat & Wolf, 2009). Polycaprolactone (PCL), on the other hand, has good mechanical strength with steady and slow biodegradability, and biological compatibility, making it a good wound healing material. When PCL matrix is combined with bioactive materials, very good drug and protein delivery properties result, which is an additional promising property for applications to wound healing and infection control (Al Samad et al., 2016). Gold nanoparticles (Au NP) have been shown to decrease inflammatory markers, enhance pro-angiogenic factors, and promote

wound healing in cutaneous studies (Kim et al., 2015; Leu et al., 2012). To increase the activity in the application to rat burn wound healing, the biosynthesized Au NPs were further modified and electrospun into Au-PEG/PCL scaffold. Because polymers and nanoparticles interact so strongly, mixing bioactive nanoparticles with these polymeric materials has been shown to increase nanoparticle activity. The results show that the Au-PEG/PCL scaffold was effective in promoting keratinocyte proliferation while also preventing the formation of scars. Notably, the polymeric Au-PEG/PCL scaffold demonstrated a decrease in inflammation of the injured area, supporting its use as a secure and highly effective biological wound healing agent (Wang et al., 2018). Another study showed that electrospun ibuprofen-loaded polyethylene (PEG) or nanofibrous scaffolds had no negative effects on fibroblasts viability and increased proliferation *in vitro* (Kheilnezhad & Hadjizadeh, 2022). These findings suggest that it could act as a suitable barrier to prevent abdominal adhesions, while the release of ibuprofen from a scaffold could reduce inflammation and prevent post-operative peritoneal adhesions (Kheilnezhad & Hadjizadeh, 2022).

In a rat model of full thickness burn wounds, delivery of the non-ionic surfactant Pluronic F-127 (F-127) intravenously showed a striking improvement in the rate of wound closure and decreased vascular necrosis, inflammation, and thrombosis (Paustian et al., 1993). Topical application of F-127 Pluronic gel has been shown to enable the progressive release of therapeutics that lead to improved wound healing outcomes in animal models of cutaneous, burn, spinal cord injury, and peritoneal adhesion. (Chua et al., 2022; Coutinho et al., 2005; Cronin et al., 2006; Paustian et al., 1993; Y. Zhou et al., 2022). As reviewed by Palackic and colleagues, in recent times, research has been focused on novel treatment approaches targeting detrimental inflammatory mediators and signalling pathways (Palackic et al., 2022). To

understand this further, it is important to understand how these effects could take place and the available treatments to tackle this.

1.5 Gap Junctions and Connexins (Cx)

Cellular communication is critical for the continual maintenance of tissue homeostasis (Vinken et al., 2006). Gap junctions are formed by proteins known as connexins. There are 21 connexin family members in the human genome. Each connexin is a four-pass transmembrane protein containing two-extracellular loops, one cytoplasmic loop, and N and C-terminal cytoplasmic tails (Figure 1.4 a) (Laird, 2006). Six connexin subunits oligomerize to form a connexon or hemichannel, that docks to another in an adjacent cell to form a gap junction channel (Figure 1.4 b) (Laird, 2006; Nielsen et al., 2012). These channels facilitate intercellular communication between cells for the direct cytoplasmic exchange of calcium (Ca^{2+}), sodium (Na^{+}), potassium (K^{+}) ions, and small molecules (<1 kDa), and allow electrical and biochemical coupling between cells (Goodenough et al., 1996; Valiunas et al., 2005). This function is crucial in maintaining skin homeostasis by regulating the transport of ions and other small molecules between cells (Martin & van Steensel, 2015). Gap junctional channels can also contribute to the collapse of the cell membrane by allowing entry of ions and potentially toxic molecules from neighbouring cells as a result of the bystander effect (Contreras et al., 2004; Spray et al., 2013) (Figure 1.4 b). In addition to intercellular communication, undocked connexin hemichannels can open to allow the passage of molecules (such as ATP and Ca^{2+}) from the cytoplasm to the extracellular space (Contreras et al., 2004). While the opening of these channels is tightly controlled under resting state (Contreras et al., 2003), hemichannels are triggered to open in response to proinflammatory cytokines (Retamal et al., 2007), metabolic inhibition (Contreras et al., 2002), or increase in cytoplasmic Ca^{2+} or decrease in extracellular

Ca^{2+} concentration (Lagos-Cabre et al., 2018; Lopez et al., 2016). Although, gap junctional coupling is important for cell survival, excessive opening of the hemichannel can trigger the release of inflammatory cytokines (Contreras et al., 2004).

In skin, gap junctions are widely expressed. Connexins found in the mammalian skin include Cx26, Cx30, Cx30.3, Cx31, Cx32, Cx37, Cx40, Cx43 and Cx45 (Di et al., 2001; Fitzgerald et al., 1994; Goliger & Paul, 1994; Richard, 2000; Risek et al., 1992; Wiszniewski et al., 2000; Zhang & Cui, 2017). These connexins are differentially expressed in various cell types in the layers of the epidermis and dermis (Scott & Kelsell, 2011; Scott et al., 2012). Cx43 is ubiquitously expressed in all skin cell types such as keratinocytes, fibroblasts, skin appendages, endothelial cells, melanocytes, dermal papilla cells and adipocytes (Becker et al., 2012; Burke et al., 2014; Zhang & Cui, 2017). Findings from several studies have reported increased Cx43 expression in cutaneous injuries such as chronic wounds (Becker et al., 2012; Sutcliffe et al., 2015), pressure ulcers (Kwek et al., 2021), and *ex vivo* diabetic skin (Pollok et al., 2011). Moreover, these studies suggest that Cx43 is essential for cell proliferation, cell migration, and regulating the production of extracellular matrix (ECM) during wound healing (Becker et al., 2012; Mori et al., 2006; Qiu et al., 2003). These studies indicate that Cx43 is important for the maintenance of skin homeostasis, skin barrier function and responses to environmental stimuli. In our lab, we have identified that Cx43 is upregulated in burn injury and that it plays a role in the passage of cell death signals and inflammation following burn injury (Coutinho et al., 2005; Feng et al., 2020). However, this limited knowledge in relation to Cx43 and the possible pathway that may be involved in burn injury is yet to be further explored.

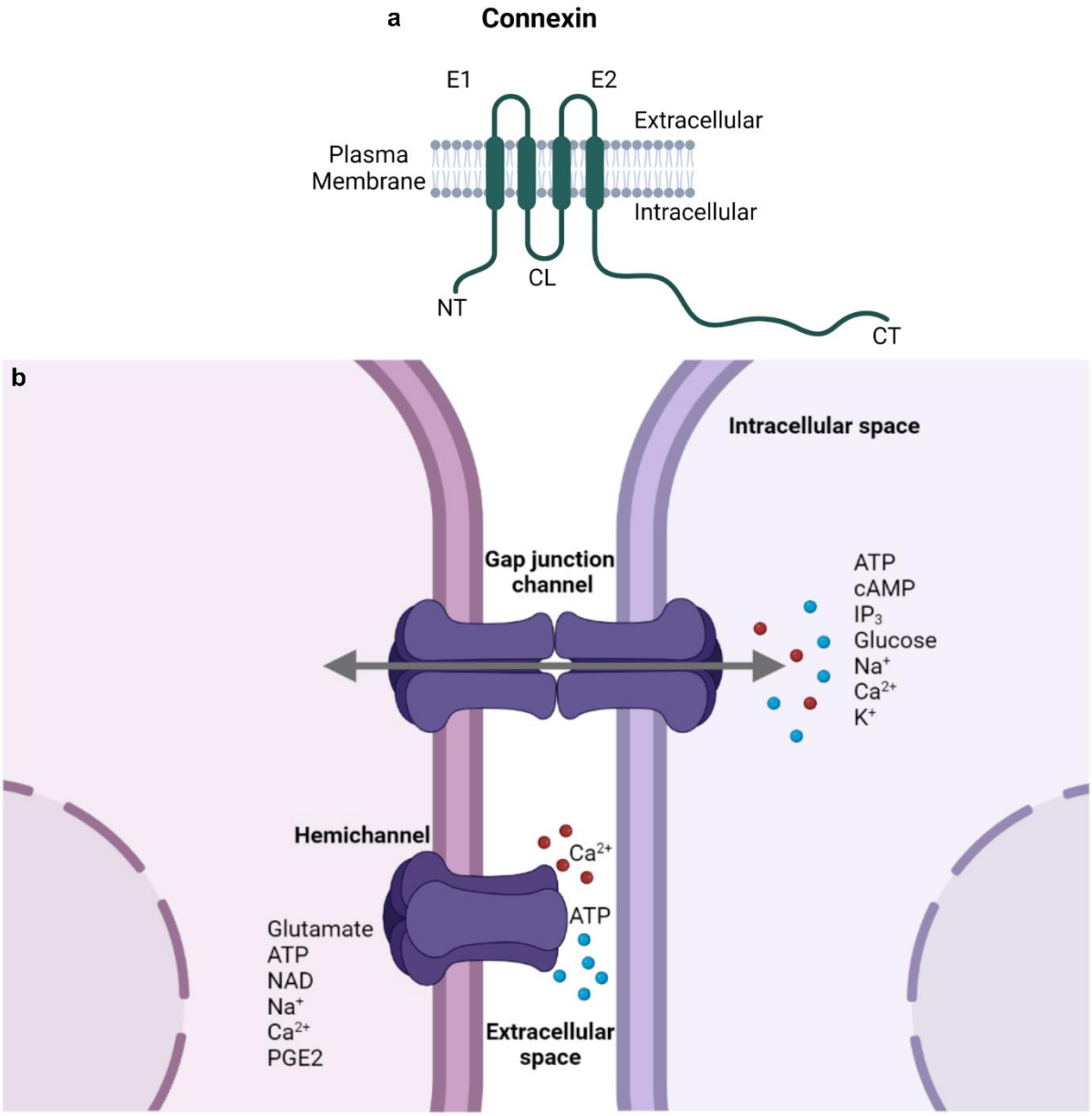

Figure 1.4. Structure and function of Connexin based channels.
(a) Structure of connexin containing four transmembrane domains with intracellular N-terminus: NT and C-terminus: CT connected by two extracellular loops: E1 and E2 and one cytoplasmic loop: CL. (b) schematic diagram representation gap junction channel allowing ion and small molecules exchange between two cells and hemichannel convey ion and small molecules between cytosol and extracellular space. ATP: Adenosine triphosphate. cAMP: Cyclic adenosine monophosphate. IP_3: Inositol 1,4,5-triphosphate. Na^+: Sodium. Ca^{2+}: Calcium. K^+: Potassium. NAD: nicotinamide dinucleotide. PGE2: Prostaglandin E2. Modified from (Vinken, 2015) and created using BioRender.com.

1.6 Hemichannel associated inflammasome activation

Lipopolysaccharide (LPS) priming in the first signal required for the activation of NLRP3 inflammasome. LPS binding to Toll-like receptor 4 (TLR4) triggers the release of pro-inflammatory cytokines like tumor necrosis factor-alpha (TNF-α) and interleukin-6 (IL-6) by immune cells (Gombault et al., 2012). This priming step is necessary to sensitize the cell to the secondary stimulus for NLRP3 activation. The second signal required for NLRP3 inflammasome activation is often provided by extracellular ATP, which is released from damaged cells during infection or injury. ATP serves as a damage-associated molecular pattern (DAMP) and activates the NLRP3 inflammasome (Gombault et al., 2012). The persistent pathologic opening of Cx43 hemichannels mediates the release of ATP into the extracellular environment (W. Chen et al., 2019). The released ATP then binds to its receptors and facilitates autocrine activation of P2X purinergic receptors such as P2X4, P2X7 and P2Y 12 receptors, as a physiological cellular communication resulting in a flux of Na^+, Ca^{2+} and K^+ ions across the pore (Acosta et al., 2021; Lohman & Isakson, 2014; Mugisho, Rupenthal, et al., 2019). The activated P2 purinergic receptors trigger a signalling molecule, the NOD-like reception pyrin domain-containing protein 3 (NLRP3) inflammasome, which recruits the adaptor apoptosis-associated spec-like protein (ASC) and pro-caspase-1 to form the inflammasome complex. Assembly of the inflammasome complex results in activation of caspase-1, and cleaves pro-inflammatory cytokines to their active forms and releases IL-1β and IL-18 (Pelegrin, 2021; Wang et al., 2020) (Figure 1.5). Cleavage of Caspase 1 also promotes Gasdermin D (GSDMD) pore formation that translocates and binds to the plasma membrane and initiates pore formation, resulting in the loss of membrane integrity and the release of cellular contents, leading to cell death by pyroptosis (Bae et al., 2017). Exposure to oxidative stress in mouse peritoneal macrophages via LPS and ATP exposure increased Cx43 expression and activated

the NLRP3 inflammasome which was abolished upon Cx43 inhibition (Huang et al., 2019). This finding was consistent in a heterozygous $Cx43^{+/-}$ mouse model compared with the Cx43 wild type (WT) mouse (Huang et al., 2019). Moreover, acute renal injury induced by LPS in the $Cx43^{+/-}$ mouse model showed significantly lower blood IL-1β, renal NLRP3 and NOX4 expression, resulting in improved renal pathological changes (Huang et al., 2019). Activation of NLRP3 is a key mediator of neuroinflammation in peripheral nerve injury. Elevated Cx43 expression was observed in models of spinal cord injury (Cronin et al., 2008; Tonkin et al., 2018). Spinal delivery of Peptide 5, an E2 Cx43 mimetic peptide, reduced Cx43 expression, improved mechanical pain hypersensitivity, and reduced spinal glial activation, suggesting that Cx43 hemichannel blockade has protective action against neuropathic pain in a mouse model of spinal cord injury (Tonkin et al., 2018).

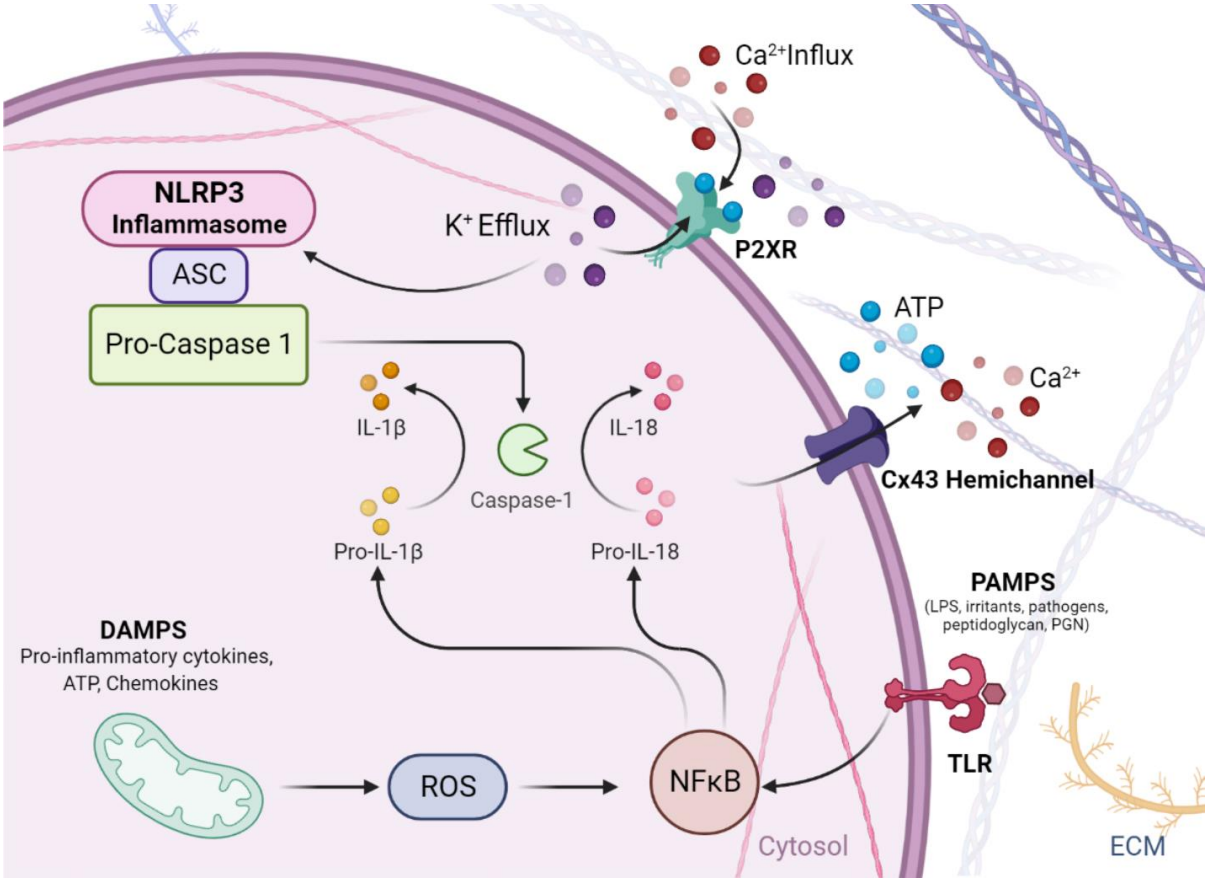

Figure 1.5. Schematic diagram of Cx43 hemichannel roles in the inflammasome pathway. ATP is released via hemichannels into the extracellular environment during pathophysiological situations such as from injury and cellular death. Extracellular ATP activates cell surface P2 purinergic receptors (E.g., ligand gated cationic P2X7 receptors). ATP binding to the P2XR receptor trigger a flux of Na^+, Ca^{2+} ions influx and K^+ ions efflux ions across the pore. Activation of P2X7 receptor triggers NLRP3 inflammasome complex formation by recruiting apoptosis-associated ASC and pro-caspase 1. Activated caspase-1 cleaves pro-IL-1β and pro-IL-18 to their active forms, IL-1β and IL-18. In addition to the purinergic receptor mediated pathway, pathogen-associated molecular patterns (PAMPs – such as irritants, peptidoglycans, or bacterial LPS) and cell-derived damage-associated molecular patterns (DAMPs – such as inflammatory cytokines or chemokines) bind to specific receptors such as the Toll-like receptors (TLRs). Activation of these receptors initiates the pro-inflammatory nuclear factor (NF-κβ) pathway to initiate cytokine release. Mitochondria are also at the centre of the cell death pathway that can be triggered by stimuli such as DAMPs, leading to elevation of reactive oxygen species (ROS) and the activation of the NF-κβ pathway. Inflammation alters gene expression, including upregulation of Cx43 mRNA, resulting in greater numbers of hemichannels at the cell surface where increased hemichannel opening leads to further ATP release and regulates the release of inflammatory cytokines. These cytokines may not pass through hemichannels directly, but hemichannel block significantly reduces their levels

relative to untreated tissues. Image modified from (Acosta et al., 2021; Y. Kim et al., 2016) and created using BioRender.com.

1.7 Therapeutic potential of Cx43 targeted therapeutics

Inhibiting Cx43 hemichannels is a potential therapeutic strategy to reduce the progression of injuries and diseases (Laird & Lampe, 2018). However, some connexin hemichannel blockers such as glycyrrhetinic acid and carbenoxolone can benon-specific and can also block gap junctions and pannexins (Buckley et al., 2021; Sahu et al., 2014). At least three distinct strategies can be employed to downregulate Cx43 hemichannels: 1) antisense oligodeoxynucleotides – prolonged use of this approach will ultimately reduce the amount of Cx43 protein available for gap junction couplings, 2) small molecule hemichannel inhibitors such as Tonabersat (Kim, Griffin, Nor, et al., 2017; Mat Nor et al., 2020) and 3) mimetic peptides such as Gap19, Gap26, Gap27, Peptide 5 and ACT1 (Coutinho et al., 2020; Ghatnekar et al., 2009; O'Quinn et al., 2011; Qing et al., 2021).

1.7.1 Cx43 antisense oligodeoxynucleotide (Cx43asODN)

Cx43 can be targeted using a very specific antisense oligodeoxynucleotide (asODN) approach. Antisense molecules are designed to reduce specific protein expression and rely on the ability of short segments of complementary DNA or modified DNA, to target specific sequences of endogenous mRNA (Rinaldi & Wood, 2018). The resulting RNA-DNA heteroduplex is then the target of endogenous RNase H endonuclease activity that cleaves the duplex and ultimately results in a significant reduction of the target protein (Di Fusco et al., 2019). The asODNs are usually synthesized in lengths of thirteen to thirty-five nucleotides. The asODN in the body are complementary to the relevant mRNA strand, and a minimum ODN size of 12 to 15 bases is

required to recognise a specific gene (Mahato et al., 2005). Our Cx43asODN is a 30 base long unmodified asODN sequence that has been tested in humans in various cutaneous wounds such as venous leg ulcers and diabetic foot ulcers, as well as persistent corneal epithelial defects (Becker et al., 2012; Gilmartin et al., 2016; Grupcheva et al., 2012; Laird & Lampe, 2018). Downregulation of Cx43 or blocking these channels has been shown to reduce the propagation of the death signals and prevent cellular apoptosis of the healthy neighbouring cells in brain trauma, radiation injury, and cardiac ischaemia (Du et al., 2017; Frantseva et al., 2002; Lin et al., 1998; Mancuso et al., 2011). However, as an unmodified oligonucleotide, efficient and often sustained delivery is critical as Cx43asODNs are rapidly broken down in the systemic circulation (Agrawal et al., 1995; McDouall et al., 2022; Myers & Dean, 2000). Hence, most research groups employ topical application of Cx43asODN incorporated into a thermo-reversible gel, Pluronic F-127, to sites of injury and this remains in practice to date (Cronin et al., 2006; Kwek et al., 2021; Law et al., 2006). In recent times, Cx43asODN was delivered in combination with cell-penetrating peptide such as Xentry-KALA (XK) or Xentry-Protamine (XP), which aided stability and bioavailability (Coutinho et al., 2018). It was found that this coupling method decreased Cx43 expression in ARPE-19 cells when introduced to hypoxic and physiologic conditions (Coutinho et al., 2018). However, further validation in animal models is required to determine if this stability and bioavailability stands true for systemic delivery.

1.7.2 Tonabersat

Tonabersat, a benzopyran compound (cis-6-acetyl-4S-(3-chloro-4-fluoro-benzoylamino)-3,4-dihydro-2,2-dimethyl-2H-benzo [b]pyrane-3 S-ol (SB-220453), was first developed as an antimigraine agent (Chan et al., 1999a; Dahlof et al., 2009; Sarrouilhe et al., 2014; Silberstein, 2009). Tonabersat has potent anticonvulsant activity with good therapeutic potential in several

rat and cat seizure models of focal and generalised epileptic seizures (Chan et al., 1999b; Herdon et al., 1997; Parsons et al., 2001; Upton et al., 1997). The pharmacological profile from numerous studies encouraged the use of Tonabersat as a potential treatment for migraine headache. A preclinical study has shown that Tonabersat can prevent increased gap junctional activity in cortical spreading depression and reduce neurogenic inflammation associated with migraines (Damodaram et al., 2009). While the clinical trials have demonstrated good safety profiles, they have failed to progress beyond Phase II for the treatment of migraine (Goadsby et al., 2009). Recent studies that explored gap junctional activity in retinal disease have found that Tonabersat acts as a Cx43 hemichannel blocker with the potential to reduce inflammation, restore and improve overall functionality (Kim, Griffin, Nor, et al., 2017; Louie et al., 2021; Mat Nor et al., 2020; Mugisho, Rupenthal, et al., 2019). *In vitro* hyperglycaemia stimulation with inflammatory cytokines IL-1β and TNFα in human retinal pigment epithelial cells (ARPE-19) to mimic diabetic retinopathy, induced NLRP3 and cleaved-caspase 1 inflammasome complex formation. Treatment with 100 µM Tonabersat prevented NLRP3 complex formation, reduced cleavage of caspase-1 into its active form and prevented the release of cytokines (Lyon et al., 2020). A light damaged retina animal model of age-related macular degeneration and a spontaneous diabetic retinopathy rat model exhibited increased Cx43 protein expression, inflammation, and clinical features of retinal damage. Oral delivery of Tonabersat closed connexin hemichannels, suppressed macrophage-mediated inflammation and inhibited inflammasome assembly leading to better retinal function, vasculature, and anatomical integrity (Mat Nor et al., 2020). Human retinal *ex vivo* model of diabetic retinopathy exposed to high glucose and pro-inflammatory cytokines IL-1β and TNFα expressed increased inflammation and activation of the NLRP3 inflammasome pathway, but this was abolished with the treatment of Tonabersat suggesting that the use of Cx43 hemichannel blockers may be beneficial in disease models (Louie et al., 2021). Since Cx43 is found to be upregulated in

burn wounds in human tissues and mouse burn model (Coutinho et al., 2005; Feng et al., 2020), Tonabersat could potentially be a novel therapeutic for treatment of burn injury.

1.7.3 Mimetic peptides

1.7.3.1 Gap19

There are several mimetic peptides that act as hemichannel blockers. One of them is Gap19, which is derived from the cytoplasmic loop of Cx43, which does not interfere with gap junction function. Gap19 (Sequence: KQIEIKKFK) peptide is known to specifically block Cx43 hemichannels without affecting gap junctions By blocking Cx43 hemichannels, Gap19 can prevent the flow of ions and molecules between the extracellular environment and the cytoplasm of a cell without significantly interfering the ability of hemichannels to dock and form gap junctions (Acosta et al., 2021; King et al., 2021) (Figure 1.6). However, the precise mechanism of Gap19 on Cx43 hemichannel is being explored by researchers to gain deeper understanding of its effects and potenital therapeutic applications. Oxygen glucose deprivation to in vitro astrocytes, increased dye uptake of Ethidium bromide via Cx43 hemichannels and reduced cell viability. Treatment with the Gap19 peptide inhibited Cx43 hemichannel activity and protected against astrocytic cell death via the JAK2/STAT3 signalling pathway (B. Chen et al., 2019). In addition, in a mouse model of brain ischaemia/reperfusion injury, Gap19 decreased cleaved caspase-3 and Bax protein levels and prevented cellular damage and protected against neurological deficits post ischaemia (B. Chen et al., 2019). Gap19 is commonly linked to HIV-derived transactivator of transcription (TAT) internalisation sequence that promotes membrane permeability and reduces the concentration that is required for half-maximal Cx43 hemichannel inhibition (Ramadan et al., 2020). Ionizing radiation is commonly used for diagnostic and therapeutic purposes in cancer treatment. However, it also causes some radiation toxicity to healthy tissues during treatment and can lead to the

breakdown of endothelial cells (Hoorelbeke et al., 2020; Ramadan et al., 2020). In addition, irradiation induced Cx43 hemichannel opening and thus increased extracellular ATP release, ROS production, and cellular uptake of propidium iodide in irradiated brain endothelial cells (Hoorelbeke et al., 2020). Treatment with TAT-Gap19, abolished ATP release via Cx43 hemichannel blocking and prevented DNA damage in brain endothelial cells (Hoorelbeke et al., 2020). In addition, Ramadan and colleagues have reported that application of TAT-Gap19 blocked heart endothelial Cx43 hemichannels and reduced oxidative stress, cell death, inflammatory responses, and senescence and thus preventing ionizing radiation induced endothelial cell damage (Ramadan et al., 2020). Furthermore, blocking Cx43 hemichannel function with TAT-Gap19 reduced pro-fibrotic genes including extracellular matrix proteins, cell contractility related molecules and promoted scarless gingival wound healing (Tarzemany et al., 2017). In vascular eye conditions, hypoxic injury can stimulate the opening of the Cx43 hemichannel and result in increased proinflammatory cytokines. Gap19 conjugated to cell penetrating peptide, Xentry (XG19) was shown to reduce Cx43 hemichannel mediated ATP release in retinal epithelial cells exposed to hypoxic conditions (Coutinho et al., 2020). Moreover, Cx43 hemichannel blocking with XG19 improved cell survival during hypoxic conditions, suggesting it to be a potential treatment for hypoxic disease conditions (Coutinho et al., 2020). Gap19 has been shown to have protective effects against cardiac ischaemic/reperfusion injury, cardiomyocyte cell death, and neuroinflammation (Abudara et al., 2014; N. Wang et al., 2013; Yin et al., 2018).

1.7.3.2 Gap26

Gap26 (Sequence: VCYDKSFPISHVR) is a hemichannel blocker that targets the extracellular loop 1 (E1) of Cx43. Gap26 peptide is not connexin specific and has equal effects in Cx43, Cx40 and Cx26 (King et al., 2021) (Figure 1.6). This non-selective connexin peptide was

shown to inhibit hemichannel docking that is essential for gap junction formation. In human keratinocytes and dermal fibroblasts, Gap26 successfully inhibited gap junction intercellular communication. However, this effect was more prominent in migrating keratinocytes as they express a variety of connexins, and due to the non-selective target, Gap26 may be more effective in preventing function in these migrating cells (Wright et al., 2009). Hyperoxia exposed Type II alveolar epithelial cells of rats and neonatal rats, expressed increased ROS production and Cx43 expression and communication. Upon treatment with Gap26, oxidative stress, via the ASK1-JNK/p38 pathway, was abolished, and Cx43 gap junction mediated cell death was prevented in *in vitro* and *in vivo* neonatal rats, resulting in improved alveolar development (Qing et al., 2021). Cx43 involvement in ischaemic stroke is widely reported (Nakase et al., 2003; Orellana et al., 2014; Schulz et al., 2015). Cx43 expression in neonatal rats subjected to hypoxia/ischaemia brain injury increased in a time dependent manner and peaked at day 7. Administration of Gap26 after ischaemia injury promoted internalization and accelerated degradation of Cx43 in the cytoplasm via the ubiquitin proteasome pathway and decreased extracellular glutamate and cleaved caspase-3 expression. This suggests that Cx43 hemichannels play an important role in protecting against neuronal cell death, resulting in improved brain functional activities and motor coordination (Li et al., 2015).

1.7.3.3 Gap27

Gap27 (Sequence: SRPTEKTIFII) derived from the E2 of Cx43 hemichannel functions (amino acids 204-214) (Evans & Boitano, 2001) (Figure 1.6). In human fibroblasts and keratinocytes, Gap27 increased cell migration and proliferation, without altering Cx43 protein levels (Evans & Boitano, 2001). Treatment with Gap27 has been reported to accelerate wound healing and enhance cell proliferation in *in vitro* skin models (Faniku et al., 2018), *ex vivo* skin models (Pollok et al., 2011), and human dermal fibroblasts *in vitro* hyperglycaemic/hyperinsulinemia

conditions (Wright et al., 2012). Gap27 treatment of oral mucosal *in vitro* promoted cell migration and reduced matrix metallopeptidase (MMP) and transforming growth factor beta 1 (TGFβ1) expression involved in ECM turnover and downregulated pro-fibrotic ECM molecules such as collagen type I (Tarzemany et al., 2015). Cx43 is also involved in corneal wound healing (Elbadawy et al., 2016; Grupcheva et al., 2012). Treatment with Gap27 enhanced *in vitro* wound closure of human corneal epithelial cells from 6 hours to 24 hours post injury and accelerated wound closure after 3 days. It also improved epithelium stratification by day 5 post treatment in human corneas *ex vivo* (Elbadawy et al., 2016). A single bolus application of Gap27 injection into the jugular vein reduced infarct size up by 61% in a rat model of myocardial infarction relative to control rats. However, co-administration of Gap26/27 did not confer additional protective action to ischaemic hearts suggesting that a saturating level of Gap26/27 protection was reached (Hawat et al., 2012). Continuous administration of Gap27 for 4 weeks via osmotic minipumps in a rat model of a high-output heart failure resulted in significantly improved cardiac mechanical functions, reduced cardiac hypertrophy and decreased arrhythmogenesis (Lucero et al., 2020).

*1.7.3.4 **Peptide 5***

Peptide 5 is a synthetic peptide corresponds to the extracellular loop 2 (EL2), Sequence: VDCFLSRPTEKT of Cx43 and overlaps with Gap27 by seven amino acids (O'Carroll et al., 2008). This peptide was created by evaluating the ability of different Cx43 EL domain sequences for their best ability to prevent neuronal death in an in vitro model of spinal cord injury (O'Carroll et al., 2008). It can selectively target either gap junction or hemichannel. In an early study using rodent ex vivo spinal cord injury treated with Peptide 5 showed reduced swelling in a dose depenedent manner. Low concentration of 5μM Peptide 5 selectively inhibited hemichannels while high concentration 500μM inhibited both hemichannel opening

and gap junctional communication (O'Carroll et al., 2008). Kim and colleagues have demonstrated that for blocking of hemichannels, the precise sequence specificity of Peptide 5 is crucial but less so for the uncoupling of gap junction channels in human cerebral microvascular endothelial cells and human retinal pigment epithelial cells under ischaemia-reperfusion conditions. Although, the seven overlapping Gap27 amino acids, SRPTEKT motif is essential to Peptide 5 function, it is insufficient to prevent hemichannel inhibition. However, Peptide 5 and SRPTEKT motif both reduced gap junction communication (Kim, Griffin, Harris, et al., 2017). In addition, it can selectively target pathological opening of hemichannels without affecting normal functions of gap junctions. Administration of Peptide 5 to lumbar spinal injury abatement model lowered NLRP3 protein expression and thus led to reduction in neuroinflammation (Tonkin et al., 2018). In addition, Peptide 5 treatment to IL-1β and TNF-α intravitreally injected mouse model to induce diabetic retinopathy reduced Cx43 protein expression and prevented upregulation of inflammasome complex markers, NLRP3 and ASC. Concomitantly, the treatment lowered the vascular beading and dilation, signs observed in an advanced condition of diabetic retinopathy (Mugisho, Green, et al., 2019). Even though Peptide 5 has been reported to targets inflammatory condtion of retinal and spinal diseases, there are no studies that reported on skin diseases and burn injury.

1.7.3.5 ACT1

Alpha-connexin carboxyl-terminal (ACT1) peptide (Sequence: RPRPDDLEI) corresponds to a short sequence located in the Cx43 C-Terminus. When linked to an antennapedia internalization sequence (Figure 1.6), treatment with ACT1 in cutaneous injury reduced neutrophil accumulation at the wound bed, improved epidermal structural integrity and reduced granulation tissue formation with minimal scarring in mouse and pig models at 10 days and 30 days, respectively post treatment (Ghatnekar et al., 2009). Myocardial infarction and

dysfunctional cardiac pumping can result in heart failure. Cx43 gap junction reorganization during myocardial infarction was shown to promote deadly cardiac arrhythmias (Kieken et al., 2009). ACT1 application to cryoinjured myocardial infarcted hearts in mice enhanced Cx43-pS368 and was associated with stabilization of Cx43 and reduced arrhythmias and left ventricular dilation (O'Quinn et al., 2011; Ongstad et al., 2013). This was also reported in ischaemia-reperfusion injury (Jiang et al., 2019). In corneal wounds in a diabetic rat model, ACT1 delivered in F-127 Pluronic gel or using polymeric alginate-poly-l-ornithine (A-PLO) microcapsules for sustained delivery promoted wound closure compared to control groups, and reduced interferon inducible T-cell alpha chemoattractant (ITAC) and TNFα and reduced EMT markers such as TGFβ2, Keratin 8 and Glut4 (Moore et al., 2014). Grek and colleagues evaluated the efficacy and safety of ACT1 in a multi-center, within patient-controlled trial. Patients with two bilateral incisional wounds were randomised to early application of ACTl delivered in F-127 Pluronic gel after wound creation and 24 hours later. They found that ACT 1 treatment of human laparoscopic incisional wounds significantly improved scar pigmentation, thickness, and surface roughness at 9 months post treatment (Grek et al., 2017). Subsequently, the group went on to test ACT1 incorporating the zonula occludens-1 (ZO-1) binding domain of Cx43 (Granexin Gel) in phase III clinical trials in chronic wounds (National Library of Medicine, 2016, January 28 - 2020, May 27).

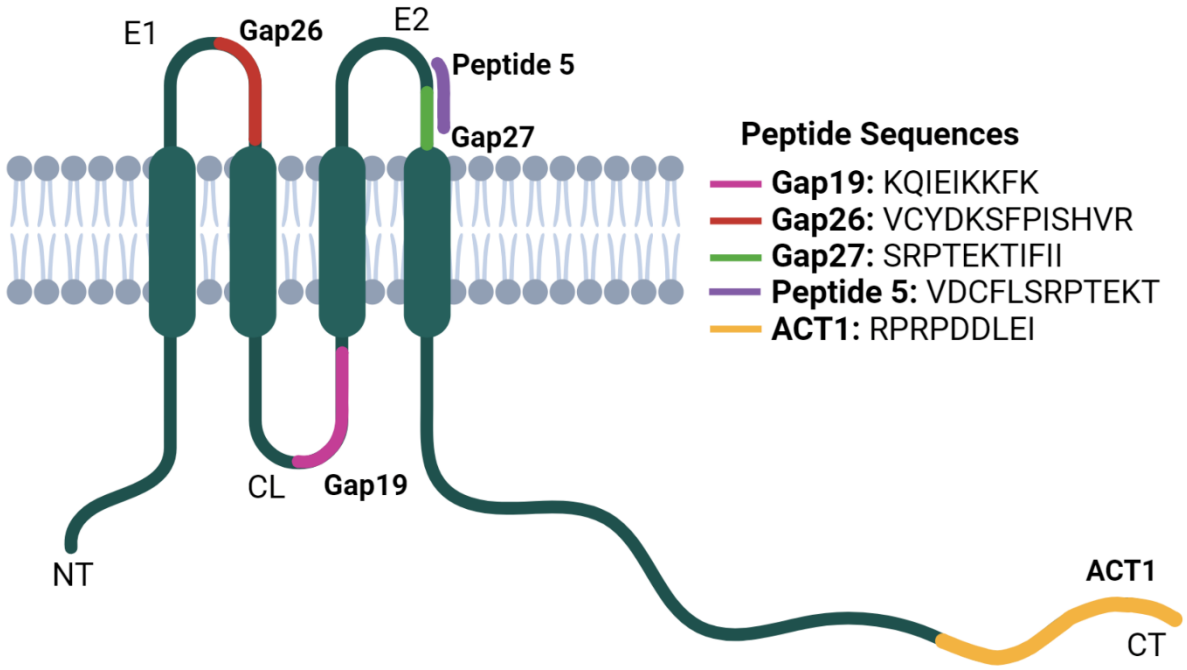

Figure 1.6 Schematic diagram of Cx43 and Cx43 mimetic peptides deriving from E1, E2, CL & CT regions.
Image adapted from (Abudara et al., 2014) and Created using BioRender.com.

Early downregulation of Cx43 function or expression may be beneficial for wound healing. Hence, I aim to deliver Cx43 targeted therapeutics as a topical application and incorporate them into a scaffold dressing to cover the wound and provide a physical barrier.

1.8 Hypothesis

That Cx43 plays an important role in the response to a burn injury that promotes inflammation and that treatment with Cx43asODN or Tonabersat will either transiently reduce Cx43 gap junction protein or directly block Cx43 hemichannel activity, respectively, to mitigate burn progression and improve wound healing.

1.9 Aims

1. To characterise deep partial thickness rat burn model.
2. To characterise the effect of Cx43 therapeutics on burn wound progression and healing outcomes in a rat burn model.
3. To characterise the effect of Cx43 therapeutics on the burn wound inflammatory response and inflammasome activation in a rat burn model.
4. Investigate the role of Cx43 and its therapeutic downregulation to reduce the inflammatory response, and NLRP3 inflammasome activation in a pig burn model.
5. In addition, to explore the use of Cx43 therapeutics incorporated scaffold dressing in pig burn model.

1.10 Thesis structure

In this thesis, reviewing existing literature in **Chapter 1** paved the pathway to first identify the research gaps in relation to Cx43, burn injury and existing treatment strategies for burn wounds. **Chapter 2** contains a detailed description of the materials and methodologies used to achieve the goals. The purpose of **Chapter 3** is to characterise the rat burn model using a scoring matrix that closely resembles the description of the depth of burn described in humans, as well as to evaluate the Cx43 protein expression pattern following burn injury. Using the characterised model, the role of Cx43 in relation to inflammasome activation in rat burn injury is investigated in **Chapter 4**. It also details the changes that occur during the early phase of burn wound healing such as the inflammatory response and inflammasome activation upon rat burn injury. Furthermore, to determine the significant contribution of Cx43 in rat burn injury, evaluation of protein levels of Cx43 and inflammasome markers upon treatment with topical application Cx43asODN or Tonabersat are described in detail. Similarly, the role of Cx43 in a porcine burn model was addressed in **Chapter 5** whereby, Cx43asODN or Tonabersat were delivered to burn wounds and protein levels of Cx43, inflammatory response and inflammasome activation were evaluated. In **Chapter 6**, the scaffold delivery method was used in an effort to sustainably improve the delivery of Tonabersat and Cx43asODN to porcine burn wounds. The effects of the scaffold therapeutic release were evaluated in a similar manner as in the previous chapter.

Chapter 2: Materials and Methods

2.1 Rat Burn Model

2.1.1 Rat

The animal study was conducted in accordance with National Advisory Committee for Laboratory Animal Research (NACLAR) guidelines. All animal protocols were approved by Institutional Animal Care and Use Committee (IACUC) of the Animal Research Facility (ARF) of Nanyang Technological University, protocol number: A19039.

Sprague Dawley (SD) rats weighing 200-250g were purchased from InVivos Pte Ltd (Singapore) and allowed to become acclimatized for 7 days before conducting burn experiments. G*Power analysis was performed to determine the number of animals required per group to achieve signifance. Sample size of four animals per group is required to achieve significance and additional one to two animals were added to each group to account for unforesseable circumstances. For the rat burn model characterisation, five animals were used to characterise superficial and deep partial thickness rat burns. Six animals per group were used for the study of topical application of Cx43 therapuetics. However, due to the quality of harvested tissues that is compromised by burn creation and tissue processing, tissues from four to six animals were quanitifed during analysis. All animals were individually housed after burn creation.

2.1.2 General anaesthetia and monitoring

Prior to burn induction, rats were anaesthetized with isoflurane at 1.5 to 2.5% with oxygen flow rate at 1-2 L/min via an induction chamber. Rats were attached to an anaesthesia nose cone and placed on a heat pad throughout the procedure. Subcutaneous injection of Buprenorphine at

0.01-0.05 mg/kg and Meloxicam at 1.0-2.0 mg/kg was given to all animals for pain management. Postoperatively, all animals received a Buprenorphine subcutaneous injection at 0.01-0.05 mg/kg for pain management for 3 to 4 days or more if animals appeared in pain. Animals were monitored daily. The animals were euthanized via CO_2 inhalation on respective harvest time points as indicated in Figure 2.4.

2.1.3 Rat burn creation

To characterise the rat burn model, five rats were used, and eight contact burns were created using a hand-held soldering iron with a round tip 8mm diameter probe as shown in (Figure 2.1) on each rat. First the hair was shaved off the back and hair removal cream Nair (Church & Dwight Co., Inc, US) was applied for 4 min. Nair was then wiped away with a wet gauze. Then eight wounds with a range of burn temperatures were tested out on the back of each rat, with applications for 10 s at the following temperatures: 50, 55, 60, 65, 70, 75, 80 and 85°C. For burn creation, the soldering iron was rested on the back of rat without any physical pressure being applied. The animals were euthanised at post burn day (PBD) 4 and burnt skin tissues were harvested to study the extent of burn depth into the skin layers.

Figure 2.1 Representative image of burn creation on rat model.

2.1.4 Scoring Matrix

Hematoxylin & Eosin (H&E) stained burn sections were subjected to a simple scoring matrix adapted and modified from Medina et al., 2018 based on a visual assessment of the tissue sections (Medina et al., 2018) (Figure 2.2) . These histological assessments have been paired with accurate burn classification (Vaughn & Beckel, 2012). The scoring parameters are as described in Table 2.1.

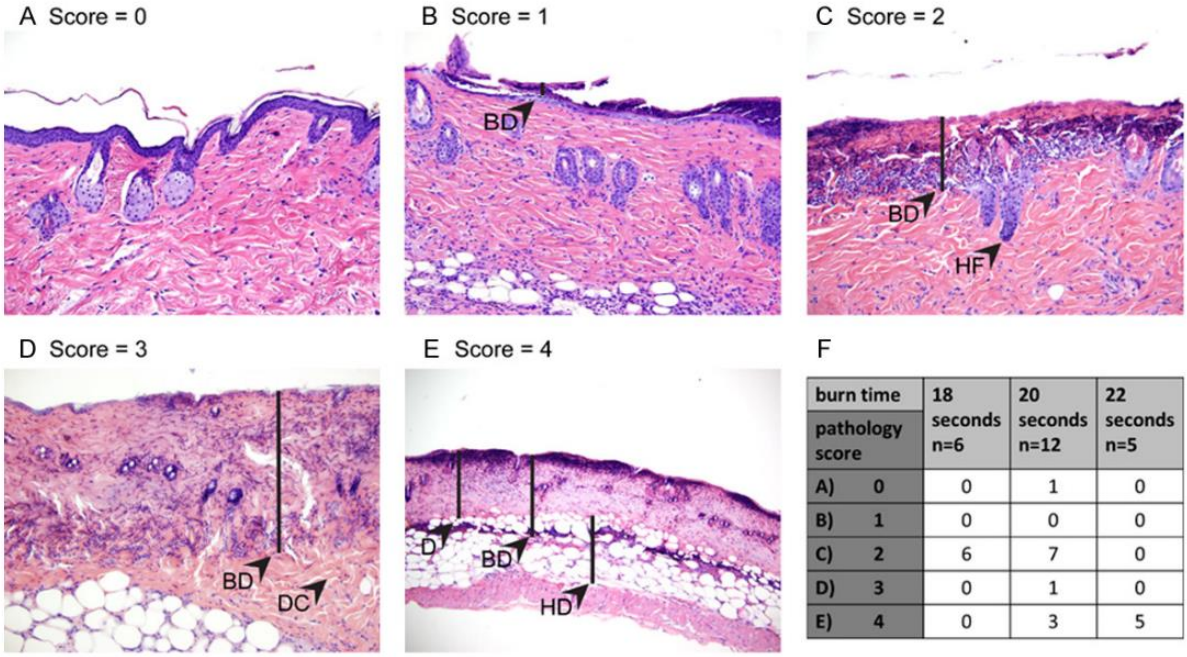

burn time / pathology score		18 seconds n=6	20 seconds n=12	22 seconds n=5
A)	0	0	1	0
B)	1	0	0	0
C)	2	6	7	0
D)	3	0	1	0
E)	4	0	3	5

Figure 2.2 Histological images taken from Medina et al., 2018 to show burn depth scores. (A) Normal Skin; Score-0. (B) Score-1; note the burn depth (BD) does not extend past the epidermis. (C) Score-2; the burn depth extends through the epidermis and into the dermis but does not extend past the base of the hair follicle (HF). (D) Score-3; the burn depth extends beneath the hair bulbs, but not completely through the dermis. Some dermal collagen (DC) remains. (E) Score-4 the burn depth extends through the dermis (D) and into the hypodermis (HD). (F) a table listing the number of animals used in experiment and how they were scored (Medina et al., 2018).

Table 2.1 Scoring matrix for assessing burn depth (adapted and modified from Medina et al., 2018 and Vaughn & Beckel, 2012).

Score	Histological Features	Burn Classification
0	Normal Skin	Normal skin
1	Cellular damage to epithelial cells within epidermis Basement membrane remains intact	Superficial thickness burn
2	Cellular damage extends beyond basement membrane into the dermis Hair bulbs remain intact Some collagen denaturation Some infiltration of leukocytes	Superficial partial thickness burn
3	Complete cellular damage to hair follicle Collagen denaturation does not extend past the deeper dermis Cellular damage to fibroblasts and endothelial cells Some migration of adipocytes into mid-dermis, large and rounded adipocytes	Deep partial thickness burn
4	Complete damage to epidermis and dermis Severe collagen denaturation, extend beyond deeper dermis into panniculus carnosus Cellular damage to fibroblast and endothelial cells Extended migration of adipocytes into dermis, large and rounded adipocytes	Full thickness burn

2.1.5 Inflammatory Score

An in-house scoring criteria was determined based on the histology obtained from the various burn temperature testing conducted on rat burn wounds. The region was defined within the burn area identifying for leukocytes with multi-lobed, bi-lobed or large spherical nucleus with deep hematoxylin staining (purple). **Score 0**: Little/no recruitment of leukocytes. **Score 1**: Some recruitment of leukocytes to burn area. **Score 2**: Moderate recruitment of leukocytes to dermis within burn area. **Score 3**: Large recruitment of leukocytes (focal accumulation around hair follicles and adipocyte). **Score 4**: Extensive recruitment of leukocytes from deep dermis to upper dermis.

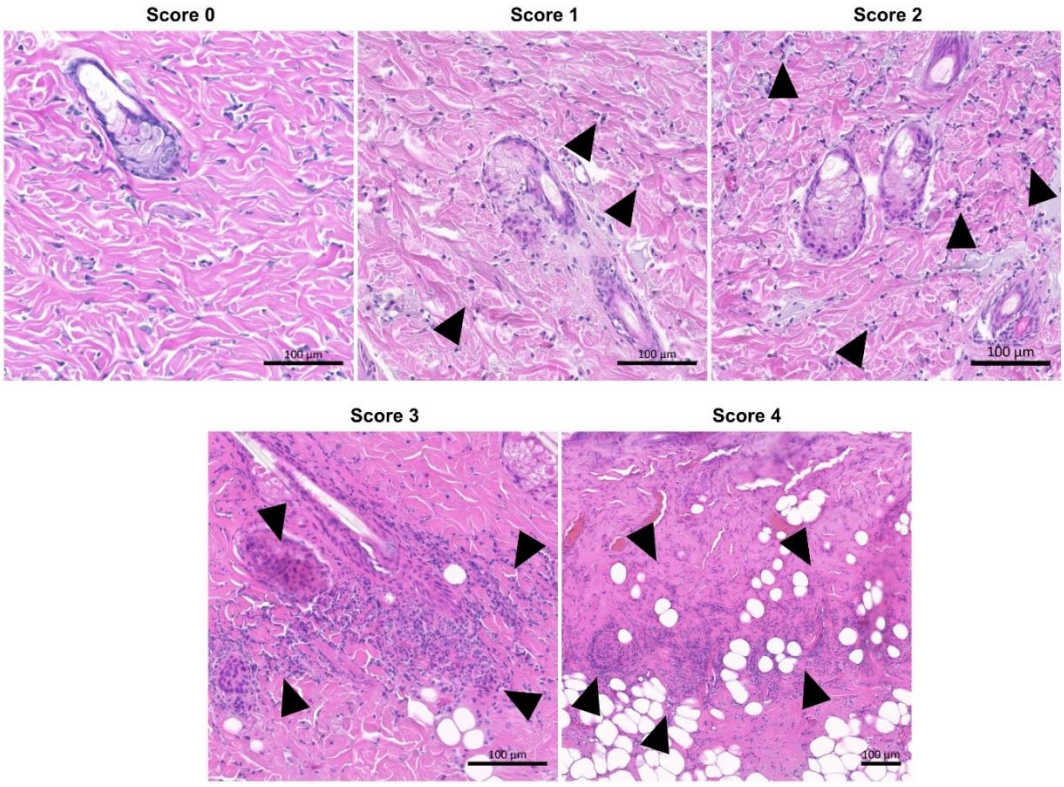

Figure 2.3 Scoring matrix for leukocyte recruitment in burn dermis.
Scoring matrix reference images graded for inflammatory response in rat burn dermis scored on PBD 1, 4 & 7. **Score 0**: Little/no recruitment of leukocytes. **Score 1**: Some recruitment of leukocytes to burn area. **Score 2**: Moderate recruitment of leukocytes. **Score 3**: Large recruitment of leukocytes (focal accumulation around hair follicles and adipocyte). **Score 4**:

Extensive recruitment from deep dermis to upper dermis. Black arrows: leukocyte recruitment in dermis, hair follicles and adipocytes.

2.1.6 Evaluation of Cx43 targeted therapeutics in rat burn model

Using the characterised rat burn model, 55°C 10 s burn wounds were created as decribed in 2.1.3. after burn creation, wounds were debrided with a gauze for penetration of therapeutics into wound. Subsequently, topical application was delivered for four consecutive days as shown in Figure 2.4. For treatment, topical application of 50µl of Cx43asODN (300 µM, AS-300, Rat sequence: 5' – GTA ATT GCG GCA CGA GGA ATT GTT TCT GTC – 3', Sigma, USA)) or Tonabersat (100 µM, Tona-100, MedChemExpres, USA) was delivered in 30% Pluronic F-127® in MilliQ H_2O. 50µl of 30% Pluronic F-127® was used a vehicle control. A debrided burn was the untreated (UN) control. All wounds were dressed with Tegaderm™ (3M) transparent film dressing and OPSITE transparent waterproof film. Tissues were harvested at PBD 1, 4, 7, 14 and 21 and processed for downstream analysis (Figure 2.4). Animals recovered and were returned to individual cages after treatment application and were monitored daily.

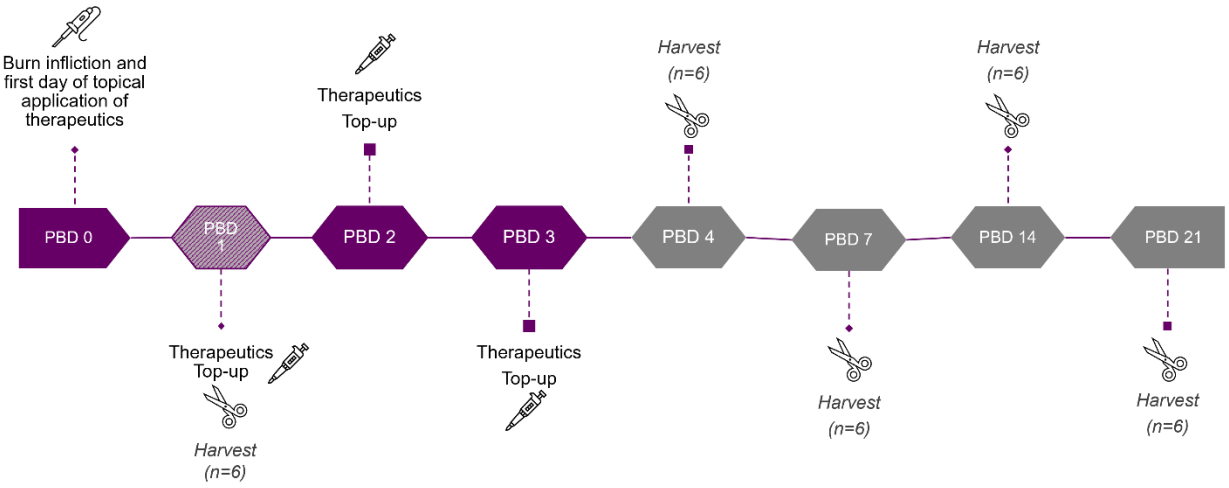

Figure 2.4 Experimental design of Topical application of Cx43asODN or Tonabersat in a rat burn model.

2.2 Porcine Burn model

2.2.1 Pig

The animal study was conducted in accordance with National Advisory Committee for Laboratory Animal Research (NACLAR) guidelines. All animal protocols were approved by Institutional Animal Care and Use Committee (IACUC) of Innoheart Pte Ltd, Singapore, protocol number INH2019/014. Three mixed breed female pigs weighing 50 to 60 kg ±5 kg were transported from Culindo Livestock (1994) Pte Ltd (Singapore) and allowed to become acclimatized for 14 days before conducting burn experiments. All procedures were performed under a general anaesthetic and all efforts were made to minimise suffering. All animals were housed individually after burn creation.

2.2.2 General anaesthetic and monitoring

Animals were anaesthetized with an intramuscular injection of Atropine (50µg/kg) and a cocktail containing Tiletamine (250mg), Zolazepam (250mg), Ketamine (2.5ml of 100mg/ml), Xylazine (2.5ml of 100mg/mg) at a final concentration of 0.05ml/kg. For maintenance, isoflurane was maintained at 1-2.5% in oxygen (1-3 L/min flow). Intramuscular injection of Tramadol (2-4mg/kg) was given to all animals for postoperative pain management. Blood pressure, heart rate, and body temperature were monitored during anaesthesia. An IV cannula was placed in the lateral auricular vein and intravenous fluids (0.9% NaCl) were administered at a rate of 5ml/kg/h throughout the procedure. Animals underwent the same general anaesthetic regime at each biopsy collection time point. On PBD 21, the animals were euthanised under anaesthesia, with Pentobarbital sodium, 100mg/kg intravenously administered.

2.2.3 Burn creation

The burn creation set up was adapted from Prof Cuttle's 2016 publication (Andrews et al., 2016) (Figure 2.5 & Figure 2.6) that consisted of a water source from a heated water bath (Grant Instruments, Cambridge, UK), a submersible water pump (EBANG, China) a stainless-steel pipe (scald burn device), weighted lead rings and portable medical suction pump (Shanghai SMAF, China).

The device is well insulated with a thick rubber hose and the bottom edge was sealed with a rubber ring to ensure that there is no direct contact between the stainless-steel pipe and the skin surface. The aperture of the bottom edge of the device for direct contact between the water and skin surface was approximately 45mm. Weighted lead rings sat on top of the device to provide uniform downward pressure. The water from the heated water bath was pumped into the device at a rate of ~2 L/min, using a submersible pump, and aspirated out at an equivalent rate with a portable medical suction pump. A hand-held digital type-K thermocouple probe thermometer (Fluke Australia Pty Ltd., Australia) was used to measure the temperature of the water bath and water within the scald burn device. Every second of burn creation was logged once heated water was applied to create the scald burn. Eight burn wounds, each 45mm diameter, were created on the flank of the pig. Water temperature set at 60°C was applied for 1 min to each of the burn wounds. 30 min after of burn creation, wounds were debrided, and topical applications of treatments or scaffold delivery were applied to wounds as described in section 2.2.4 & 2.2.5.

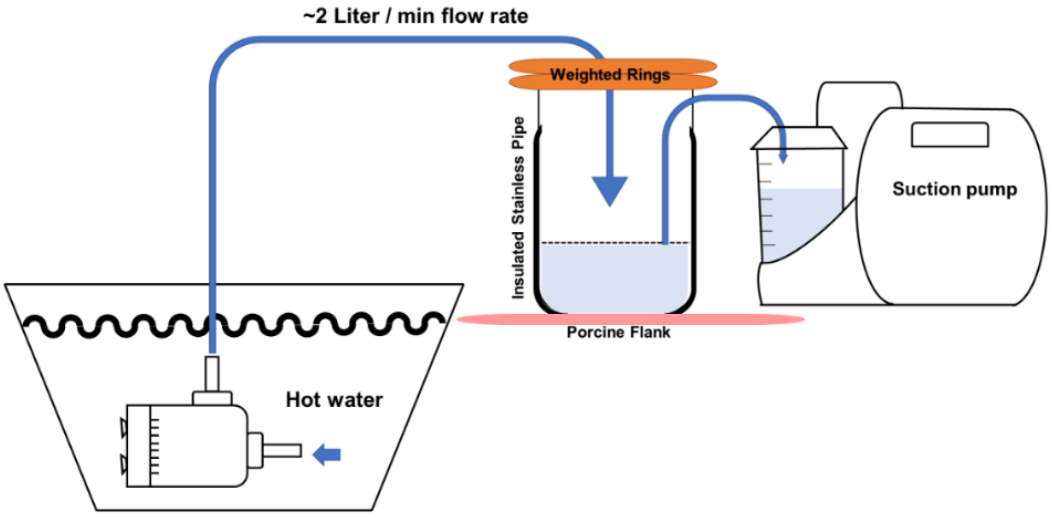

Figure 2.5 Schematic representation of scald burn device step up.

Figure 2.6 Porcine burn creation.
(a) Scald burn creation workflow. Water from heated water bath flows into the burn device and suctioned out into a water collection bottled attached to a suction pump. (b) debridement of burn wound. (c) Electrospun scaffold removal from aluminum foil sheet. (d) application of scaffold onto debrided wound. (e) Wet scaffold upon contact with burn wound exudates. (f) Topical gel application onto debrided wound dressed with Tegaderm™.

2.2.4 Topical application of Cx43asODN or Tonabersat to a porcine scald burn model

Based on the *in vitro* cell assays and previously established treatment conditions, three pigs were subjected to Cx43asODN (Pig Sequence: 5' – GTA ATT GCG GCA GGA AGA ATT GTT TCT GTC – 3', Sigma, USA) and Tonabersat (MedChemExpress, USA) treatment either in the form of topical gel application or scaffold dressing as described in Table 2.2. Cx43asODN (Sigma-Aldrich, USA) was dissolved in MilliQ H_2O at a stock concentration of 3mM. Tonabersat (Medchem Express, USA) was dissolved in dimethyl sulfoxide (DMSO, Sigma) at a stock concentration of 100mM. 500µl of Topical application of low and high concentrations of Cx43asODN (30µM and 300 µM) and Tonabersat (30µM and 100 µM) was delivered in 30% Pluronic F-127® in MilliQ H_2O to cover the surface area of burn wounds. 500µl of 30% Pluronic F-127® was used a vehicle control. Topical treatments were applied directly to debrided wound (DeCtrl). DeCtrl was also included as a control (Table 2.2). The high concentrations of Cx43asODN were used based on our previous work where we have shown that 300µM improved wound healing outcomes (Chua et al., 2022). The high concentration of Tonabersat was chosen based on Kim and colleagues publication where they have shown that low concentration of Tonabersat was able to block hemichannels and higher concentration of Tonabersat uncoupled gap junctions (Kim, Griffin, Nor, et al., 2017). All wounds were then dressed with Tegaderm™ transparent film dressing and OPSITE transparent waterproof film.

2.2.5 Scaffold delivery of Cx43asODN or Tonabersat to a porcine scald burn model

The scaffold dressings were fabricated using an electrospinning technique. Electrospinning allows polymers to possess great mechanical strength, flexibility and stiffness (Liu et al., 2019). In this study, I used a cocktail of polycaprolactone (PCL, Sigma, USA,) and polyethylene glycol (PEG, Sigma, USA) at 8:2 ratio, loaded with 6mM and 10mM of Cx43asODN or Tonabersat, respectively. The polymer solution was loaded into a 1ml Luer lock syringe and connected to the infusion pump (KD Scientific, USA). The polymer was then charged with high voltages +8 and 4kV that was applied to the needle tip and rotating drum collection as shown in Figure 2.7.

The polymer solution was electrospun onto an aluminium foil sheet (Diamond, Reynolds Consumer Products, USA) attached to a rotating drum collector rotating at 500rpm (X-Tech Engineering, Singapore). A total of 2.5ml of polymer solution produced 2 pieces of 6 x 6 cm scaffold dressing with an average of 0.1mm thickness. The scaffold dressings were freeze-dried using a freeze dryer (Labcono Corporation, USA) and UV sterilised in a biosafety cabinet prior to experimental use. After scald burn wound creation, the scaffold dressing was removed from the foil sheet and applied to the debrided wound (Table 2.2).

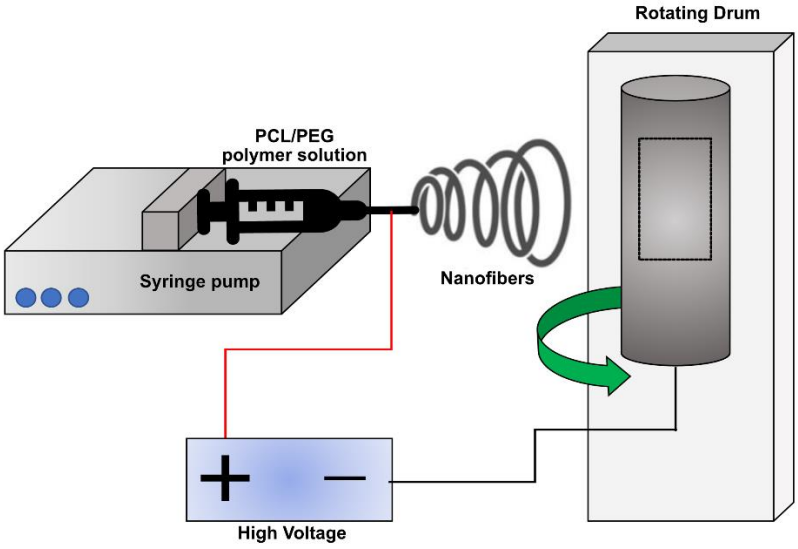

Figure 2.7 Schematic diagram of basic set up of electrospinning.
Set up consists of syringe filled with PCL/PEG polymer solution connected to an infusion pump. The base of the needle nozzle end contains the charged surface of the solution. High voltage is utilised to draw the polymer jet that stretch and split to form nanofibers in a controlled manner and collected onto an aluminium foil attached around the rotating drum.

2.2.6 Scanning Electron Microscopy

The structure of P-S, AS-S and Tona-S (Table 2.2) scaffold were evaluated by Variable Pressure-Scanning Electron Microscopy (VP-SEM) (FlexSEM 1000 II, Hitachi, Japan), at pressure 30Pa and accelerating voltage of 10kV, using a backscattered electrons (BSE) detector. SEM imaging was assisted and performed by a member of staff at Nanyang Technological Univeristy, Optical Bio-Imaging Centre (NOBIC). To quantify scaffold fiber diameter, I meaured 50 fibers from each SEM image on Image J (National Institutes of Health, USA). Six fields of view of each scaffold were measured for fiber diameter.

2.2.7 Scaffold Release Profile

Scaffold release profile was performed to determine daily concentration of Cx43asODN and Tonabersat eluted from the scaffold dressing. Briefly, three 6mm circular scaffold dressings were incubated in 50µl of 1X phosphate buffered saline (PBS) in a microcentrifuge tube for 7 days at 37°C. Daily, the 1X PBS was removed from microcentrifuge tube containing the scaffold and replenished with fresh 1X PBS. At specific intervals, 1µl of liquid from the collected samples was assayed in a NanoDrop UV spectrophotometer. Data were collected to produce daily elution graphs.

Table 2.2 List of control and treatment used on porcine burn wounds.

<table>
<tr><th colspan="2">Topical Application</th><th colspan="2">Scaffold dressing</th></tr>
<tr><td rowspan="4">Treatment</td><td>AS-30 (Cx43asODN 30µM), n=3</td><td rowspan="4">Treatment</td><td>AS-S (Cx43asODN scaffold), n=3</td></tr>
<tr><td>AS-300 (Cx43asODN 300µM), n=3</td><td rowspan="3">Tona-S (Tonabersat Scaffold), n=2</td></tr>
<tr><td>Tona-30 (Tonabersat 30µM) n=2</td></tr>
<tr><td>Tona-100 (Tonabersat 100µM), n=3</td></tr>
<tr><td>Control</td><td>Veh (30% Pluronic), n=2</td><td>Control</td><td>Plain Scaffold, n=1</td></tr>
<tr><td colspan="4">Control: DeCtrl (Debrided Control), n=3</td></tr>
</table>

2.3 Histology

2.3.1 Tissue processing and microtome sectioning

Harvested tissue samples were bisected and stored in 4% (w/v) paraformaldehyde at 4°C overnight for paraffin wax processing. Skin tissues were transferred into 70% (v/v) ethanol and processed overnight using the HistorCore PEARL (Leica, Germany) tissue processor. Subsequently, the processed tissues were embedded into paraffin blocks using the HistoCore Arcadia C embedder (Leica, Germany). Paraffin blocks were sectioned at 5µm thickness using a Leica RM2245 microtome (Leica, Germany) and mounted onto Poly-Lysine coated slides.

2.3.2 Hematoxylin & Eosin Staining

Tissue sections were stained for histological examination of Hematoxylin & Eosin (H&E) using the pre-set programme on Leica Autostainer XL (Leica, Germany). Briefly, slides were deparaffinized as shown in steps 1 to 7 and stained with Hematoxylin and Eosin (steps 8 to 14, Leica, Germany) and dehydrated with increasing percentages of alcohol and into Clearene™ (Lecia, Germany). Slides were mounted with Organo/Limonene™ mounting medium (Sigma, USA) (Table 2.3).

Table 2.3 Set programme for H&E staining on Leica Autostainer.

Step	Station	Time	Reagent	Step	Station	Time	Reagent
1	1	5 min	Clearene™	**12**	Wash 3	2 min	Deionised H_2O
2	2	5 min	Clearene™	**13**	10	5 s	Scott's Water
3	3	2 min	100% Ethanol	**14**	Wash 4	2 min	Deionised H_2O
4	4	2 min	100% Ethanol	**15**	11	2 min	70% Ethanol
5	5	2 min	95% Ethanol	**16**	12	30 s	Eosin
6	6	2 min	95% Ethanol	**17**	13	2 min	70% Ethanol
7	7	2 min	70% Ethanol	**18**	14	2 min	95% Ethanol
8	Wash 1	2 min	Deionised H_2O	**19**	15	2 min	95% Ethanol
9	8	1 min	Hematoxylin	**20**	16	2 min	100% Ethanol
10	Wash 2	3 min	Deionised H_2O	**21**	17	2 min	100% Ethanol
11	9	3 s	Acid Alcohol	**22**	18	2 min	Clearene™

2.3.3 Masson's Trichrome Staining

Tissue sections were stained for Masson's Trichrome for the examination of collagen bundles. The composition of the respective Masson's Trichrome reagents is described in Table 2.4. Briefly, the paraffin slides were deparaffinized (steps 1 to 7 as stated in Table 2.3) and submerged in Bouin's solution overnight. The next day, the slides were rinsed in running tap water for 12 min until the yellow colour on samples disappeared. To differentiate the nuclei, slides were immersed into modified Weigert's Hematoxylin working solution for 5 min, followed by 3 min of running tap water and transferred to Biebrich Scarlet working solution for 2.5 min. Subsequently, the slides were rinsed in four changes of 1% glacial acetic acid until the solution is clear and then differentiated in 5% Phosphomolybdic-tungstic acid working solution for 30 min. Excess solution was drained off the slide and it was immediately submerged into 2% light green for 20 min and rinsed with deionised water. The stained slides were dried at room temperature for 45 min and mounted with Organo/Limonene™ mounting medium (Sigma, USA).

Table 2.4 List of reagents and preparation to working solution of Masson's Trichrome staining.

Reagent	Company/Catalog	Reagent preparation to working solution
Bouin's solution	Sigma, HT10132	Used directly, reusable within the day
Weigert's Iron Hematoxylin kit working solution	Merck Millipore, 1.15973.0002	Used according to manufacturer's protocol. Mixed one part of solution A to one part of solution B
Biebrich scarlet working solution	Sigma, B6008	1% Ponceau BS
	Sigma, F8129	1% Fuchsin Acid
	Merck Millipore, 1.00062	1% Glacial Acetic acid
5% Phosphomolybdic-tungstic acid working solution	Sigma, P4006	10% Phosphotungstic acid solution in DI water
	Sigma, 79560	10% Phosphomolybdic acid solution in DI water
1% Glacial Acetic Acid solution	Merck Millipore, 1.00062	Glacial Acetic Acid
		Deionised water
2% Light Green solution	Sigma, L5382	Light Green SF Yellowish
	Merck Millipore,	2.5% Acetic acid

2.3.4 Picrosirius red staining

Briefly, the paraffin slides were deparaffinized and washed in deionised water (steps 1 to 7 as stated in Table 2.3). Slides were then immersed in Picrosirius red (Abcam, UK) for 1 h. Slides were then transferred into two changes of 0.5% acetic acid (Abcam, UK) for 5 s each followed by two changes of 100% (v/v) ethanol (Sigma, USA) for 2 min each. Slides were cleared again with two changes of Clearene (Leica, Germany) for 2 min each. Finally, slides were mounted using Organo/Limonene™ mounting medium (Sigma, USA).

2.3.5 Immunofluorescence

For immunofluorescence staining, paraffin section slides were deparaffinized in Clearene™ (Leica, Germany) and rehydrated with decreasing concentrations of ethanol in water (steps 1 to 7 as stated in Table 2.3). Antigen retrieval was performed with heated sodium citrate buffer (pH 6.0) at 99°C for 20 min in a water bath, followed by 20 min of cooling at room temperature. Slides were then permeabilized in 0.2% (v/v) Triton-X 100 in PBS for 20 min and blocked in 1% bovine serum albumin (BSA) – 0.02% Sodium Azide blocking buffer for 1 h. Primary antibodies were reconstituted in blocking buffer and incubated overnight at room temperature as indicated in Table 2.5 for rat burn model and Table 2.6 for porcine burn model. Controls without primary antibody were incubated with blocking buffer. Following removal of primary antibody solution, two washes of 1xPBS-T (0.1% Tween® 20) for 5 min followed by 1xPBS wash for 5 min were performed before 1 h of secondary antibody incubation in blocking buffer at room temperature as stated in Table 2.7. After incubation, slides were washed three times in 1xPBS for 5 min before counterstaining with DAPI (1:10,000, Cat: D1306, Life Technologies, USA). Finally, slides were washed with two washes of 1XPBS-T (0.1% Tween® 20) for 5 min followed by 1xPBS wash for 5 min prior to mounting with Citifluor AF1 (Electron Microscopy Sciences, USA) anti-fade mounting medium. Slides were imaged using TCS SP8 confocal microscope (Leica, Germany).

Table 2.5 List of antibodies uses for rat burn model.

Name	Catalogue no / Brand	Antigen Retrieval	Dilution
Rabbit anti-Connexin-43	C6219 (Sigma, USA)	Histozyme (Sigma, USA), PIER	1:1000
Rabbit anti-α smooth muscle actin (αSMA)	ab5694 (Abcam, UK)	EDTA buffer, pH8.5, HIER	1:500
Rabbit anti-Cleaved-Caspase 1 (Cas-1)	PA5-105049 (ThermoFisher Scientific, USA)	EDTA buffer, pH8.5, HIER	1:500
Rabbit anti-Hemichannel – Cx43*	Purified custom made antibody, AB3000, against a highly conserved portion of the E1 domain of Cx43 amino acid between 42 and 61, Sequence: ESAWGDEQSAFRCNTQQPGC (ThermoFisher Scientific, USA) (Glass, 2014)	EDTA buffer, pH8.5, HIER	1:2000
Rabbit anti-IL-1β	P420B (ThermoFisher Scientific, USA)	EDTA buffer, pH8.5, HIER	1:200
Rabbit anti-MMP-9	ab76003 (Abcam, UK)	EDTA buffer, pH8.5, HIER	1:200
Rabbit anti-Myeloperoxidase (MPO)	PA5-16672 (ThermoFisher Scientific, USA)	EDTA buffer, pH8.5, HIER	1:200
Rabbit anti-NLRP3	NBP2-12446 (Novus Biologicals, USA)	EDTA buffer, pH8.5, HIER	1:500
Rabbit anti-P2X7	PA5-77665 (ThermoFisher Scientific, USA)	EDTA buffer, pH8.5, HIER	1:400
Mouse anti-rat CD68, clone ED1	MCA341R (Bio-Rad Laboratories, USA)	EDTA buffer, pH8.5, HIER	1:400
Mouse anti-HSP47, E-1	sc-13150 (Santa Cruz, USA)	Histozyme (Sigma, USA), 5 min	1:500

** Rabbit anti-Hemichannel – Cx43 is a purified custom made antibody. This antibody will only bind to E1 and prevent gap junctions and therefore only stain for non-docked hemichannels.*

Table 2.6 List of antibodies used for porcine burn model.

Name	Catalogue no / Brand	Antigen Retrieval	Dilution
Rabbit anti-Connexin-43	C6219 (Sigma, USA)	Histozyme (Sigma, USA), PIER	1:1000
Rabbit anti-α smooth muscle actin (αSMA)	ab5694 (Abcam, UK)	EDTA buffer, pH8.5, HIER	1:500
Rabbit anti-Cleaved-Caspase 1 (Cas-1)	PA5-105049 (ThermoFisher Scientific, USA)	EDTA buffer, pH8.5, HIER	1:500
Rabbit anti-Hemichannel	Purified custom made antibody, AB3000, against a highly conserved portion of the E1 domain of Cx43 amino acid between 42 and 61, Sequence: ESAWGDEQSAFRCNTQQPGC (ThermoFisher Scientific, USA) (Glass, 2014)	EDTA buffer, pH8.5, HIER	1:2000
Rabbit anti-Myeloperoxidase (MPO)	PA5-16672 (ThermoFisher Scientific, USA)	EDTA buffer, pH8.5, HIER	1:200
Rabbit anti-NLRP3	NBP2-12446 (Novus Biologicals, USA)	EDTA buffer, pH8.5, HIER	1:500
Rabbit anti-P2X7	PA5-77665 (ThermoFisher Scientific, USA)	EDTA buffer, pH8.5, HIER	1:400
Mouse anti-rat CD68, clone ED1	MCA341R (Bio-Rad Laboratories, USA)	EDTA buffer, pH8.5, HIER	1:400

Mouse anti-HSP47, E-1	sc-13150 (Santa Cruz, USA)	Histozyme (Sigma, USA), 5 min	1:500

** Rabbit anti-Hemichannel – Cx43 is a purified custom made antibody. This antibody will only bind to E1 and prevent gap junctions and therefore only stain for non-docked hemichannels.*

Table 2.7 List of secondary antibodies used in this study.

Name	Catalogue no / Brand	Dilution	Reactivity
Goat anti-mouse Alexa Fluor™ 488	A-11001 (ThermoFisher Scientific, USA)	1:500	Mouse
Goat anti-rabbit Alexa Fluor™ 555	A-21428 (ThermoFisher Scientific, USA)	1:500	Rabbit

2.4 Microscopic Assessment

2.4.1 Brightfield Microscopy

H&E and Masson's Trichrome stained tissue slides were scanned using an automated high-speed digitization AxioScan.Z1 slide scanner (Zeiss, Germany) imaged with 20× NA 0.8 objective. Digitally scanned images were visualised and extracted using the Zen 3.3 software (Zeiss, Germany).

2.4.1.1 Quantification of percentage of collagen content from Masson's Trichrome stained tissues

PBD 21 Masson's trichrome stained sections were used for collagen content measurements in both rat and porcine burn models (Chapter 4, 5 & 6). H&E digitally scanned images were visualised using the Zen 3.5 software (Carl Zeiss, Germany) and three 3000µm x 3000µm regions of interest from the centre of the rat burn injury were cropped and exported. Three 3000µm x 3000µm regions of interest from each of the upper dermis, mid dermis and deep dermis of porcine burn injury were exported. These exported images were quantified for collagen content using ImageJ software (version 1.53t, National Institutes of Health, USA). First, the image was loaded onto the software and scale bar and area measurement settings were selected. Then, the image was processed for colour deconvolution with vectors for Masson's Trichrome. Colour 3 (green) was selected, and threshold "Li" was utilized. %Area of collagen content was measured using "Analyze Particles" function.

2.4.1.2 Nascent Epidermal Thickness measurements

PBD 14 and 21 H&E tissue sections were used for nascent epidermal thickness measurements for both rat and porcine burn models (Chapter 4, 5 & 6). H&E digitally scanned images were

visualised using the Zen 3.5 software (Carl Zeiss, Germany). To measure nascent epidermal thickness, the line tool was used from Zen 3.5 software to draw full thickness of epidermis excluding stratum corneum and rete like ridges. Six-line region of interest (ROI) were measured 150µm apart from one another (Ippagunta et al., 2016). These measurements were averaged to determine the thickness of nascent epidermis for each sample (Figure 2.8).

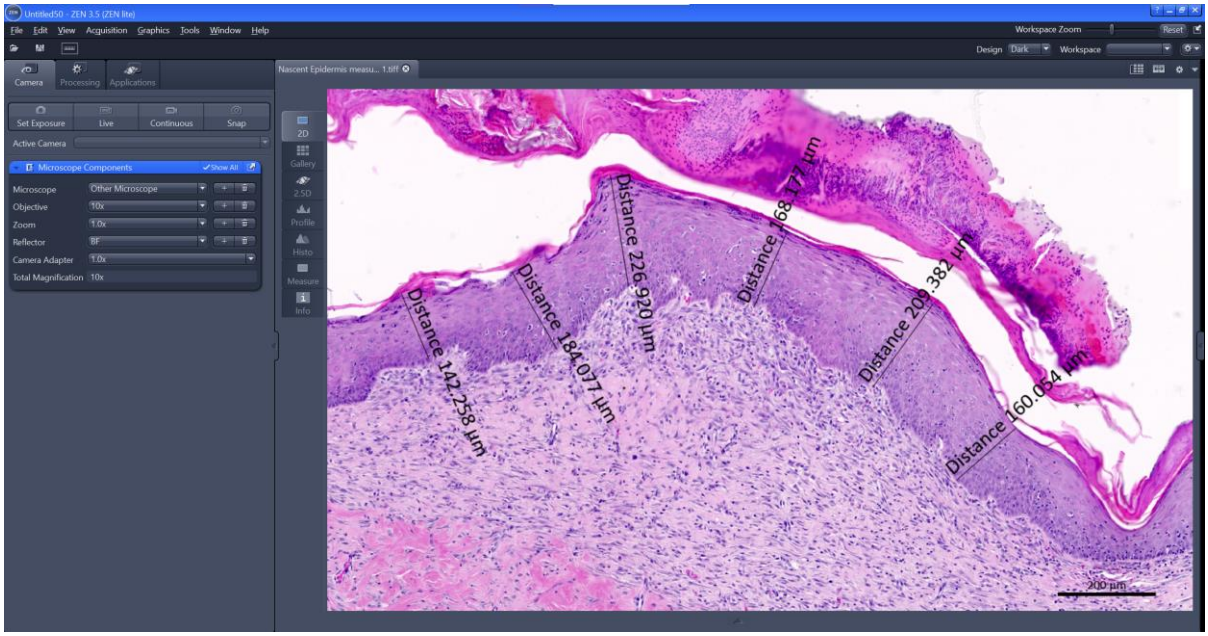

Figure 2.8 Example of Nascent epidermal thickness measurement performed on Zen 3.5 software (Carl Zeiss, Germany) using the "Line" function.

2.4.1.3 Rate of Re-epithelialisation measurement

To determine the rate of re-epithelialisation, the area of site of burn injury was first determined using H&E digitally scanned images on Zen 3.5 software (Carl Zeiss, Germany). Using the curve line tool, the total length of the burn injury site without hair follicles was mesaured. Next, using the curve tool, the gap between the nascent epidermis outgrowth from burn wound edges was measured. Then, the rate of re-epithelialisation was calculated using for the following

formula: total length of burn injury – gap between nascent epidermis outgrowth / total length of burn injury x 100%.

2.4.2 Confocal Microscopy

Immunostained slides were visualised using an upright confocal microscope TCS SP8 (Leica, Germany) with 40X 1.2 NA Plan-Apochromat or 63X 1.4 NA Plan-Apochromat. Five optical sections of 3 µm Z-Stacks were captured with a depth of 0.7µm of each Z was maintained for all images. Lasers were used sequentially to excite at 405, 488 and 555nm wavelengths. All images were acquired in 8-bit greyscale at 1024 x 1024 pixels with a frame average of 2 or 3. A minimum of 3 to 4 fields of view per tissue was obtained. All images were taken with identical parameters to allow for direct comparison of staining intensity. All images were subjected to max projection on the LasX Software (Leica, Germany) and exported for image analysis.

2.4.3 Image analysis

2.4.3.1 Region of interest (ROI) for early and late phase of burn wound healing

Early Phase

Post burn day (PBD) 1, 4, & 7 are considered as early stages of burn wound healing. As described in chapter 1, the zone of stasis is the most vulnerable area of burn injury that could convert into a zone of coagulation. To locate the zone of stasis, the zone of coagulation was identified first from H&E-stained slides that depict areas with necrosis. The area closest to zone of coagulation with surviving cells was identified as zone of stasis (Figure 2.9). Four field of view were acquired from each sample from zone of stasis for protein level quantification.

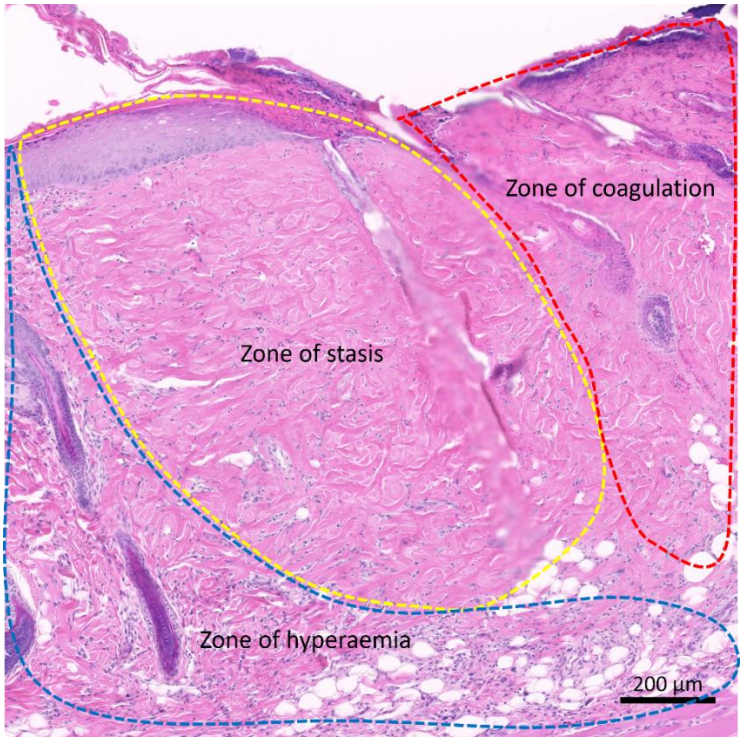

Figure 2.9 Example of chosen area of zone of stasis.

The area closest to zone of coagulation and furthest area with inflammatory zone and increased perfusion is identified as zone of stasis. All readouts for immunofluorescence were taken from this region and kept consistent for confocal imaging and analysis.

Late Phase

PBD 14 and 21 are late phases of burn wound healing. As the wound heals, the three zones of the Jackson model become indistinguishable. The centre of the wound tissue that was most damaged and recovered was identified for image analysis. Three fields of view were acquired from each sample for protein level quantification and percentage of collagen content (Figure 2.10).

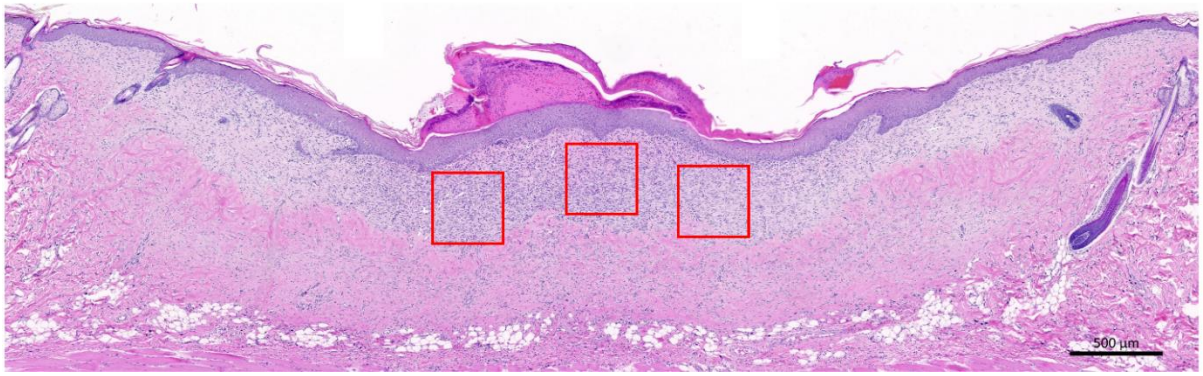

Figure 2.10 Examples of chosen area of for late phases.
Region of interests indicated in red boxes chosen at centre of burn wound on PBD 21.

*2.4.3.2 **Protein level quantifications***

Quantification of protein levels were determined by using in-house quantification algorithms using ImageJ software (version 1.53t, National Institutes of Health, USA). As mentioned above, four fields of view were chosen to study protein levels in zone of stasis at PBD 1, 4 & 7, and three fields of view were acquired for image analysis at PBD 14 & 21. An image is uploaded onto ImageJ software (Figure 2.11 a). The respective channel, red (Alex Fluor 555) or green (Alexa Fluor 488), of that image is selected after splitting (Figure 2.11 b). A specific threshold was set to include positive signals as described in Table 2.8 & Table 2.9. After thresholding, the image was converted into a binary image and protein levels were determined by analysing all particles (Figure 2.11 c). The threshold for settings were kept constant throughout image analysis. Table 2.8 and Table 2.9 shows the threshold used for each antibody for the rat burn model and porcine burn model respectively.

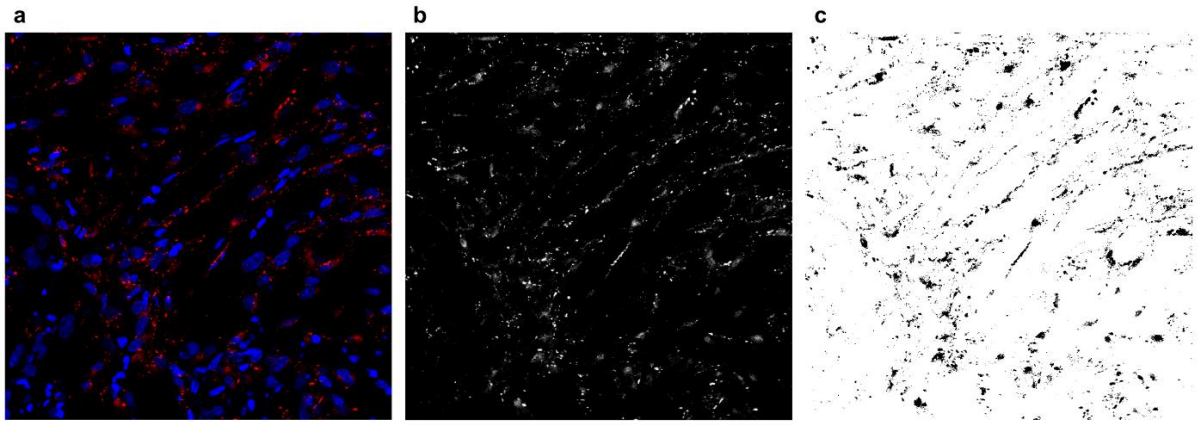

Figure 2.11 Example of image analysis workflow for Immunostained images on ImageJ software). (a) Example of original Immunofluorescence-stained image loaded. (b) Example of red channel of original image after channel splitting on ImageJ software. (c) Example of binary image of original image after threshold setting (40-255) is applied.

Table 2.8 List of threshold settings applied to each of interest of protein in rat burn model.

Early Phase		Late phase	
Protein of interest	**Threshold settings**	**Protein of interest**	**Threshold settings**
Cx43	40-255	**αSMA**	50-255
Cas-1	40-255	**HSP47**	40-255
Hemichannel	30-255	**MMP-9**	40-255
IL-1β	30-255		
NLRP3	10-255		
P2X7	10-255		

Table 2.9 List of threshold settings applied to each of interest of protein in porcine burn model.

Early Phase		Late phase	
Protein of interest	**Threshold settings**	**Protein of interest**	**Threshold settings**
Cx43	20-255	**αSMA**	40-255
Cas-1	30-255	**HSP47**	20-255
Hemichannel	30-255		
MPO	30-255		
NLRP3	40-255		
P2X7	10-255		

2.5 Molecular and biochemistry techniques

2.5.1 RNA extraction

To extract RNA from the experimental samples, harvested tissues that were previously stored in RNA*Later*™ (Invitrogen, USA) at -80°C, were thawed and transferred into recommended amounts of TRIzol™ (Invitrogen, USA). Tissues were homogenised using the Qiagen TissueLyser II (Germany) with an autoclaved metal ball added into the tube to ensure complete homogenization. The homogenization step was kept at 30 Hz for 5 min. Subsequently, chloroform was mixed with the homogenate and was rested at room temperature (RT) for 10 min followed by a spin at 12,000 x g for 15 min at RT. For RNA extraction the upper aqueous phase was collected and transferred into a fresh tube. 3M sodium acetate pH 5.2 and isopropanol was added to the aqueous phase and was allowed to precipitate at -20°C for 30 min. After precipitation, the samples were spun at 12,000 x g for 15 min at 4°C. The supernatant was carefully aspirated, and the pellet was gently washed with cold 70% molecular grade ethanol. After a flash spin for 2 min, the previous step was repeated. The pellet was air dried and 20 to 50µl of RNase-free water was added and mixed well.

2.5.2 Determination of RNA quantification

The RNA contents from tissue homogenates were determined using Nanodrop™ 2000/2000c Spectrophotometer (Thermo Fisher scientific, Massachusetts, USA). Briefly, 1µl elution buffer was loaded on the pedestal and blank reading for RNA quantification programme was executed as auto zero. Subsequently, 1µl of purified RNA was loaded for automatic concentration measurement.

2.5.3 cDNA synthesis

To generate cDNA from purified RNA contents, each sample was reverse-transcribed by using the ReverTra Ace™ cDNA synthesis kit with gDNA remover (FSQ-301, TOYOBO). Following the manufacturer's protocol, the master mix reagent contains random and oligo dT primers, optimized for efficient reverse transcription, was added and cDNA was synthesized.

2.5.4 Quantitative reverse transcription polymerase chain reaction (qRT-PCR)

cDNAs were then subjected to real-time PCR analysis using Luna® Universal qPCR Master Mix (New England BioLabs, USA) according to the manufacturer's instructions. Briefly, 10µl of Luna Universal qPCR Master Mix, 0.5µl of 10µM of forward and reverse primers, 1µl of cDNA template were mixed, and nuclease free water was used to top up to a final reaction volume of 20µl. Using the specific PCR primers (Table 2.10) and glyceraldehyde-3-phosphate dehydrogenase (GAPDH) as a housekeeping gene were purchased from IDT (Integrated DNA Technologies, USA) (Kim et al., 2020; Peinnequin et al., 2004). Two technical replicates were prepared for all samples and loaded into the Applied Biosystems QuantStudio 6 thermocycler. Thermal cycling conditions were applied as: 95°C for 10 min; followed by 40 cycles of 95°C for 15 s, and 60°C for 1 min following the manufacturer's protocol. After hybridization of specific primers, the technical values were averaged, and relative fold change of gene expression was calculated by using 2-ΔΔCt values. First, the gene of interest Ct (cycle threshold) was normalised to the housekeeping gene Ct value and subsequently, the difference between an experimental sample and an experimental control calculated. From which, the expression fold change was determined and plotted on a graph for statistical analysis.

Table 2.10 List of primer sequences used for collagen I, collagen III & housekeeping genes.

Gene	Primer Sequences
Col Iα1	F: 5'-GCT CCT CTT AGG GGC CAC T-3'
	R: 5'-CCA CGT CTC ACC ATT GGG G-3'
Col III	F: 5'-GTT CTA GAG GAT GGC TGT ACT AAA CAC A-3'
	R: 5'-TTG CCT TGC GTG TTT GAT ATT C-3'
GAPDH	F: 5'-GTA TTG GGC GCC TGG TCA CC-3'
	R: 5'-CGC TCC TGG AAG ATG GTG ATG G-3'

2.6 Statistical Analyses

2.6.1 Rat burn

All statistical analysis was performed on GraphPad Prism® 8.4 software (GraphPad Software Inc., USA). In general, all statistical comparison were made between normal skin (NS) vs untreated (UN) to establish if there was any difference between normal and injury. Subsequently, statistical comparison was made between controls and treatment as follows: UN vs Cx43asODN 300µM (AS-300), UN vs Tonabersat 100µM (Tona-100), Vehicle control (Veh) vs AS-300 & Veh vs Tona-100. Hence, data sets were subjected to One-way analysis of variance followed by Sidak's multiple comparisons test. All data are presented as means ±

S.E.M. and *n* represents the number of animals used for each time point indicated below each graph. A p-value of 0.05 was considered statistically significant.

2.6.2 Porcine burn

All statistical analysis was performed on GraphPad Prism® 8.4 software (GraphPad Software Inc., USA). In general, all statistical comparison were made between normal skin (NS) vs Debrided control (DeCtrl) to establish if there is any difference between normal and injury. Subsequently, for data sets under topical application, statistical comparison was made between controls and treatment as follows: DeCtrl vs Cx43asODN 30µM (AS-30), DeCtrl vs Cx43asODN 300µM (AS-300), DeCtrl vs Tonabersat 30µM (Tona-30), DeCtrl vs Tonabersat 100µM (Tona-100), Vehicle control (Veh) vs AS-30, Veh vs AS-300, Veh vs Tona-30 & Veh vs Tona-100. For scaffold treatment analysis, statistical comparison was made between DeCtrl vs Cx43asODN Scaffold (AS-S), DeCtrl vs Tonabresat Scaffold (Tona-S), Plain Scaffold (P-S) vs AS-S & P-S vs Tona-S. non-parametric test Kruskal-Wallis was used for sample size three and below. All data are presented as median and interquartile range (IQR). and *n* represents the number of animals used for each time point indicated below each graph. A p-value of 0.05 was considered statistically significant.

Chapter 3: Characterisation of the rat burn model

3.1 Introduction

Burn injuries are complex and underappreciated injuries that are associated with substantial mortality and morbidity (Jeschke et al., 2020). Burn injury involves multifactorial and pathophysiological events that cause structural and functional deficits to organs post injury. For instance, large surface area burns are followed by systemic problems such as hypermetabolism (Jeschke, 2016; Knuth et al., 2021; Williams et al., 2009) and sepsis (Zhang et al., 2021).

Due to the complex nature of burn injury and the involvement of various organs, *in vitro* models are limited in their ability to recapitulate the diverse pathophysiology and wound healing mechanisms. Although *in vitro* models provide insights on how a certain type of cell responds to stimulus or crosstalk in coculture studies, investigations addressing wound healing are constrained by the lack of inflammatory and vascular components in *in vitro* models (Lebeaux et al., 2013). The construction of animal models helps in understanding the cause and progression of human diseases and injuries and have proven to be of great use in discovering therapeutic agents. A plethora of animals have been employed to study burn injury, including mice, rats, dogs, rabbits, sheep, and pigs (Aijaz et al., 2022). All organisms share the underlying ability of their skin to act as a barrier against the environment. However, the structure and anatomy of the skin vary greatly between species (Table 3.1). Despite these differences, animal models have significantly enhanced our knowledge of the origins and development of many human diseases and have been shown to be a valuable tool for the development of therapeutic agents. In this chapter, I primarily focus on rodent burn models.

Table 3.1 Characteristics of skin structure of human, pig, rat, and mouse.

Trait	Human	Pig	Rat	Mouse
Hair Coat	Sparse	Sparse	Dense	Dense
Epidermis	**50–120 µm**	**–0 - 140 µm**	**35-75µm**	**<25 µm**
Dermis	Thick	Thick	Thin	Thin
Panniculus Carnosus	None	None	Present	Present
Skin architecture	Firmly attached	Firmly attached	Loose	Loose
Wound healing mechanism	Re-epithelialisation	Re-epithelialisation	Contraction	Contraction

Adapted from (Abdullahi et al., 2014).

3.1.1 Rodent models used for skin healing studies

Understanding histological differences in skin architecture is crucial if researchers want to create a model that closely resembles the human skin. Mouse and rat skin contains the major layers (epidermis and dermis) of human skin. However, the mouse skin is distinctly thinner than human skin. Unlike the mouse skin, which has a flat interphase between the epidermis and dermis, the human interphase is extremely undulated (Wong et al., 2011). When it comes to cutaneous healing studies, rats are consistently preferred for experimentation over mice. However, it is important to note that the rat skin morphology is different from human skin (Table 3.1). Rat skin is elastic and loose, unlike human skin, which is firmly attached to the underlying structures. It is because of this difference, rat wound contraction can significantly contribute to the healing of skin wounds as opposed to humans, who heal via re-epithelialisation and granulation tissue formation (Cross et al., 1995). As a result, wound contraction in rats, which is often faster than re-epithelialization shortens the total amount of time taken for wound healing. In addition, rats possess a subcutaneous panniculus carnosus

muscular layer, which is absent in human skin (Wong et al., 2011). This muscle contributes to wound healing by contracting and producing collagen. Although there are some key differences between humans and rats, finding a suitable animal model to recapitulate all features of a burn injury remains challenging. Moreover, the selection of species also depends on other factors such as the purpose of the study and restrictions on costs. Rats have been used in numerous wound healing models due to their widespread availability, small size, and tractable nature. Rats are large enough to provide an appropriate area of skin for wound studies, and smaller research animals require lesser maintenance expenses. Another reason to consider using rats for skin wound healing models is the extensive body of knowledge on rat wound healing that has been accumulated over many years of prior study (Dorsett-Martin, 2004).

To gain a comprehensive understanding of burn wound healing, there is a need for an animal model that adequately mimics these pathological states. Hence, it is ideal to use clinically relevant methods for burn wound creation in animal models. Currently, there are several methods to create burn injuries in rodent models, including scalding, contact burns, and electrical burns. Most reported skin burns are contact and scald burns; depending on the extent of the damage, the injuries are categorized as superficial, partial-thickness, full-thickness, or subdermal (Monstrey et al., 2008).

3.1.2 Scald burn

The scald burn model in rodents was first described by Walker and Mason for large area burn infliction (Walker & Mason, 1968). This method can be used to create burns with or without bacterial infection. Some studies have reported immersing the dorsal skin rat model in boiling water to create full thickness burns (Fagan et al., 1999). Although this method seemed to provide relatively reproducible burns, immersing animals in hot water remains an ethical

concern. In addition, a review by Menegat et al, reported that there were some discrepancies in burn creation that were reported in scald burn models (Menegat et al., 2019). Furthermore, creating multiple wounds on an animal with this methodology is challenging. Although rats may withstand burn wounds with more than 60% total burn surface area (TBSA), doing so leads to decreased survival and is not practical for experimentation (Kulp et al., 2012).

3.1.3 Contact Burn

The type of treatment is dependent on the degree of the burn, thus knowing this information is crucial. Skin grafts and early excision are required for full-thickness burns. With the use of wound dressings, superficial and partial-thickness burns can be treated conservatively (Cai et al., 2014). Creating contact burns with a simple set up can produce uniform and reproducible burn wounds. However, this requires proper characterisation of the burn wounds with histological evidence and testing of various temperatures with time durations to ensure the burn creation protocol is standardized prior to testing of interventions. Numerous studies have reported contact burn strategies, and I performed a database search.

The PubMed-NCBI database was searched between 1968 to 2019 to collect information on contact burns created on rat models that best recapitulate the features of different levels of burn. This was done using the following key words: “rat contact burn”, yielding a total of 98 entries, of which only full-text English and MEDLINE articles were identified. Each abstract from this search was reviewed, and only experimental studies containing rat contact burns were considered. Full inclusion and exclusion criteria are listed in Table 3.2. Other review articles, articles of burn injury created on other species, and articles that poorly described the methodology of burn creation were excluded. This narrowed the field to 33 articles that best presented the information on rat contact burns (Table 3.3).

Table 3.2 Inclusion and exclusion criteria for eligible studies.

Inclusion Criteria	Exclusion Criteria
Rat only	
In vivo	*Ex vivo*
Skin contact burn	Paw contact burn or systemic burn model
Method of contact burn eg., brass rod or comb	
Histological evaluation of depth of burn injury for at least 1 time point (within 7 days) post-burn	
Contact burns expressed as temperature	Chemical burns, laser burns, radiation burns, cold burns
Novel method or material for burn infliction and/or if method is based on previous model (quoted) but material is significantly altered or modified	Studies quoting use of previously described burn infliction method
English	Full text unavailable in English

Most of the articles used either a brass or aluminium metal plate that was preheated in boiling water without any temperature control system (Table 3.3). Studies have shown that such methodologies have resulted in variation in the burn creation and no one temperature or duration was chosen for either partial thickness or full thickness burns. The anatomical region of the burn is typically the back of the rats. Some have used a combination of locations that included the back, scapular, temporal extremities, lumbar and abdomen. Some studies did not mention the location of the wound (Mitsunaga Junior et al., 2012). None of these studies reported the use of a scoring matrix to describe full thickness or partial thickness burn. Some studies also lacked the use of histological evidence to support their results. Any researcher who conducts an experiment on a burn injury animal model, should understand their experimental set up and characterise the conditions to select those that best achieve the required depth of the burn.

Table 3.3. Summary list of publications between 1968 to 2019 reporting use of contact burns to create a skin injury.

Year	Title (reference)	Burn Mechanism (Brass or different contact method)	Size of material	Rat Strain	Rat Weight (gm)	Location on the rat	Temperature	Duration (Seconds)	Definition of burn (deep or partial)	Histology present?
1982	Genetics of natural resistance to thermal injury (Rapaport et al., 1982)	Heated metal plate	4mm	ACI, Buffalo (BUF), Fisher(F344), Lewis(L), Brown-Norwegian (BN), Osborne-Mendel(OM) Wistar Furth(WF) Sprague Dawley(SD) Wistar(W)rats	250 to 300	Back & Abdominal skin	250	2 sec for the back 1 sec for abdominal skin	Full thickness burn	Yes, but no figures published
1996	Effects of recombinant bactericidal/permeability-increasing protein (rBPI23) on neutrophil activity in burned rats (J. Hansbrough et al., 1996)	Stainless steel template	8 cm X 5.8 cm X 0.4 cm	Wistar(W)rats	200 to 300	Dorsal	250	7	Full thickness burn	No
1996	Neutrophil activation and tissue neutrophil sequestration in a rat model of thermal injury (J. F. Hansbrough et al., 1996)	Stainless steel template preheated using a thermistor	8 cm X 5.8 cm X 0.4 cm	Wistar(W)rats	200-300	Dorsal	250	7	Full thickness burn	No

1997	Hypernatremia deepens the demarcating borderline of leukocytic infiltration in the burn wound (Kuroda et al., 1997)	Round aluminium templates preheated in water bath	2 cm	Wistar(W)rats	280 to 300	Dorsal	70	5	Partial thickness 2nd deg burn	Yes
1999	Effects of topical nitroglycerin and flurbiprofen in the rat comb burn model (Gorman et al., 1999)	Brass rat - comb	55 x 19mm	Sprague Dawley(SD)	450	Dorsal			Full thickness burn	No
2000	Role of nitric oxide in the control of burn perfusion (Lindblom et al., 2000)	electrically heated aluminium rod	1 cm2	Sprague Dawley(SD)	250 to 300	Dorsal	55	Duration taken for temperature reached 55°C the probe was put in contact with the abdominal skin until the temperature reached 45°C, at which time the probe was removed	Full thickness burn	No

2001	Microvascular assessment of burn depth conversion during varying resuscitation conditions (Kim et al., 2001)	Milled aluminium plates	2x2cm	Sprague Dawley(SD)	460	Dorsal	100	various	partial to full thickness	Yes
2004	Determination of burn depth by polarization-sensitive optical coherence tomography (Srinivas et al., 2004)	cylindrical brass rod preheated in water bath	1 cm	Sprague Dawley(SD)	250 to 300		75	various	Full thickness burn	No
2005	Topical treatment of standardised burns with herbal remedies in model rats (Becic et al., 2005)	Round metal seal heated in water bath	2.5cm	Wistar(W)rats	232	Dorsal	80	14	Partial to full thickness	Yes
2008	Apoptosis and necrosis in the ischaemic zone adjacent to third degree burns (Singer et al., 2008)	brass comb with four prongs preheated in boiling water	brass comb were 20 x20 x55 mm with four 10x25-mm rectangular prongs, separated by three 5-mm-wide grooves	Sprague Dawley(SD)	300-325	Dorsal	100	30	Full thickness burn	Yes
2009	Morphological parameters for assessment of burn severity in an acute burn injury rat model (Meyerholz, Piester, Sokolich, et al., 2009)	Aluminium branding irons preheated in boiling water	2x2cm	Sprague Dawley(SD)	460	Dorsal	100	various	Partial thickness	No

2009	Pharmacologic modification to resuscitation fluid after thermal injury--is drotrecogin alfa the answer to arrest burn depth progression? (Meyerholz, Piester, McNamara, et al., 2009)	Aluminium branding irons preheated in boiling water	2x2cm	Sprague Dawley(SD)	460	Dorsal	100	various	Partial thickness burn	Yes
2010	Apoptosis is differentially regulated by burn severity and dermal location (McNamara et al., 2010)	Aluminium branding irons preheated in boiling water	2x2cm	Sprague Dawley(SD)	460	Dorsal	100	various	Partial thickness burn	Yes
2010	Effect of photodynamic therapy on the healing of cutaneous third-degree-burn: histological study in rats (Garcia et al., 2010)	"Punch" heated with blue flame of a Bunsen burner	NA	Wistar(W)rats	180-220	Dorsal	80	30	Full thickness burn	Yes
2011	Propolis and amnion reepithelialise second-degree burns in rats (Pessolato et al., 2011)	heated brass Plate	5cm2	NA	264	Dorsal	130	5	2nd degree burn	Yes
2012	*In vivo* terahertz imaging of rat skin burns (Tewari et al., 2012)	Rectangular brass bar preheated in boiling water	5mm	Sprague Dawley(SD)	200-300	Dorsal	100	20	Deep partial thickness burn	Yes
2013	Phases of the cutaneous angiogenesis process in experimental third-degree skin burns:	cone shaped stainless steel	1cm	Wistar(W)rats	280-310	Dorsal	100	5	Full thickness burn（3rd	Yes

	histological and immunohistochemical study - rat burn (Busuioc et al., 2013)								degree burn)	
2014	Digital photogrammetry and histomorphometric assessment of the effect of non-coherent light (light-emitting diode) therapy (λ640 ± 20 nm) on the repair of third-degree burns in rats (Neves et al., 2014)	test-tube containing boiling water	2.44cm	Wistar(W)rats	250-275	Dorsal	100	20	Full thickness burn (3rd degree burn)	Yes
2014	Effect of local application of epidermal growth factor on innate immunity and cell composition of destruction focus in experimental thermal injury (Osikov et al., 2014)	flat-bottom vial made of chemical glass containing boiling water	4cm	Albino Rats	200-220	Dorsal	100	30	Full thickness burn (3rd degree burn)	no
2015	Beneficial effects of hydrogen-rich saline on early burn-wound progression in rats (Guo et al., 2015)	Brass comb heading in boiling water	20mmx10mm	Sprague Dawley(SD)	250-300	Dorsal	100	20	Full thickness burn	yes
2016	Preparation of Partial-Thickness Burn Wounds in Rodents Using a New Experimental Burning	Electronically -controlled heating stamp	1cm or 2cm	Fischer 344 (F344)	200	Dorsal	80	variable	Partial and full thickness burn	yes

	Device (Sakamoto et al., 2016)									
2016	Preventing Scars after Injury with Partial Irreversible Electroporation (Golberg et al., 2016)	Preheated brass block	1cm2	Sprague Dawley(SD)	250		>95	10	Full thickness burn	yes
2016	Anti-inflammatory and burn injury wound healing properties of the shell of Haliotis diversicolor (Chen et al., 2016)	Copper block preheated in dry bath	2x2cm	Wistar(W)rats	400-450	dorsal	165	10	Full thickness burn	yes
2016	Active Dynamic Thermography is a Sensitive Method for Distinguishing Burn Wound Conversion (Prindeze et al., 2016)	Preheated brass comb	20x25mm	Sprague Dawley(SD)	NA	dorsal	100	30	Full thickness burn	yes
2016	Interaction between Macrophages and Fibroblasts during Wound Healing of Burn Injuries in Rats (Oka et al., 2016)	Aluminium cylindrical block heated in boiling water	2cm	Wistar(W)rats	310-360	dorsal	100	20s	Full thickness burn (3rd degree burn)	yes
2017	A new apparatus for standardization of experimental burn models (Arda et al., 2017)	Electronically powered copper cylinder bar	10mm	Sprague Dawley(SD)	275-300	Dorsal	60/80	10s	Partial to full thickness	yes

2017	Terahertz Imaging of Cutaneous Edema: Correlation With Magnetic Resonance Imaging in Burn Wounds (Bajwa et al., 2017)	Rectangular brass bran preheated on a hot plate	2mmx19mm	Sprague Dawley(SD)	180-200	Dorsal	200/130	10s	Partial to full thickness	yes
2017	Protease loaded permeation enhancer liposomes for treatment of skin fibrosis arisen from second degree burn (Sahu et al., 2017)	Solid aluminium bar preheated boiling water	10mm	Sprague Dawley(SD)	NA	Dorsal	95-100	13s	Partial thickness	yes
2018	Early intervention by Captopril does not improve wound healing of partial thickness burn wounds in a rat model (Akershoek et al., 2018)	Brass stamp preheated	2x2cm	Wistar(W)rats	280-291	Dorsal	100	10	Partial thickness	yes
2018	Beneficial effects of Salvia miltiorrhiza in the healing of burn wounds: an experimental study in rats (Irmak et al., 2018)	Brass bar preheated in boiling water	3x2cm	Sprague Dawley(SD)	258-379	Dorsal	100	20	Full thickness	yes
2018	Effects of carbomer 940 hydrogel on burn wounds: an *in vitro* and *in vivo* study (Hayati et al., 2018)	Brass comb preheated in boiling water	10x20mm	Wistar(W)rats	300-350	Dorsal	100	20	Full thickness	yes
2019	Developing a Simple Burn Model in Rats of Different Ages (Zheng et al., 2019)	metal column preheated in boiling water	1cm	Sprague Dawley(SD)	100-795	Dorsal	100	various	Partial to full thickness	yes

2019	Delivery of silver sulfadiazine and adipose derived stem cells using fibrin hydrogel improves infected burn wound regeneration (Banerjee et al., 2019)	Brass soldering device with thermocouple probe and thermometer	17mm	NA	NS	Dorsal	87	10	Partial thickness	yes

3.1.4 Scoring matrix for burn wound assessment

Several studies have reported the use of histological scoring matrices in relation to burn wound healing that feature the rate of re-epithelialisation, granulation tissue formation, inflammatory cells, and the presence of angiogenesis (Hazrati et al., 2010). Typically, these scoring matrices are used to describe histological changes that occur on PBD 14 and 21 when wounds undergo remodelling. To succinctly understand the histological changes that occur after a burn and the depth of burn progression, Medina and colleagues, with the help of a board of certified pathologists, described a scoring matrix as shown in Table 3.4 (Medina et al., 2018). These histological features closely reflect the human burn depth classification as reported by Vaughn and colleagues (Vaughn & Beckel, 2012). The classification of human burns was based on clinical indicators as well as their corresponding histology diagnosis and prognosis (Latarjet, 1995). In this study, I have adapted the incorporated scoring matrix to score the depth of burn wound to identify the classification of rat burns.

Table 3.4 Scoring matrix for assessing burn depth (adapted and modified from Medina et al., 2018 and Vaughn & Beckel, 2012).

Score	Histological Features (Medina et al., 2018)	Burn Classification (Vaughn & Beckel, 2012)
0	Normal Skin	Normal skin
1	Cellular damage to epithelial cells within epidermis Basement membrane remains intact	Superficial thickness burn
2	Cellular damage extends beyond basement membrane into the dermis Hair bulbs remain intact Some collagen denaturation Some infiltration of leukocytes	Superficial partial thickness burn
3	Complete cellular damage to hair follicle Collagen denaturation does not extend past the deeper dermis Cellular damage to fibroblasts and endothelial cells Some migration of adipocytes into mid-dermis, large and rounded adipocytes	Deep partial thickness burn
4	Complete damage to epidermis and dermis Severe collagen denaturation, extend beyond deeper dermis into panniculus carnosus Cellular damage to fibroblast and endothelial cells Extended migration of adipocytes into dermis, large and rounded adipocytes	Full thickness burn

3.1.5 Aims

The main aim of this chapter is to identify the ideal conditions to study deep partial thickness burns that best recapitulates the zone of stasis. Using a soldering iron as a burn creation setup, it is important to characterise the depth of burn with histological evidence to ensure a consistent burn is created. In addition, combining the Medina et al scoring system with well-established histological features of depth of burn (Table 3.4) I will evaluate the burn wounds. This assessment comprises of key features of thermal injury to different layers of the skin comprising, epidermis, dermis, hair follicles, sebaceous glands, and subcutaneous fat. In addition to that, an inflammatory scoring system is also applied that details the presence of neutrophils around the damaged area. To study the role of Cx43 expression, immunostaining analysis will be performed. The optimal conditions were then used to investigate the progression of burn injuries in rats. Collectively, these assessments facilitate the identification of the ideal model to study the role of Cx43 in rat burn injury.

3.2 Results

3.2.1 Histological changes with various temperatures tested

The histological appearance of wounds was consistent between replicates of the same burn condition (Figure 3.1). A gradient of tissue injury into the deeper layers of rat skin was observed with increasing temperature (Figure 3.1). By PBD 4, conditions of 50, 55, 60 and 65°C for 10 s show evidence of complete cellular damage to the epidermis, papillary dermis, and upper layers of the reticular dermis but did not completely damage all hair follicles (Figure 3.1). Wave like infiltration of inflammatory cells distinguished the areas of burn damage from normal tissue. For higher temperature conditions 70, 75, 80 and 85°C for 10 s showed deeper tissue injury extending into the subcutaneous tissue layer (Figure 3.1 & Figure 3.2). Since, the histological features of 50, 55, 60 and 65°C 10 s burn were found to be similar, 55°C 10 s burn was chosen as the lower temperature for in-depth descriptive analysis. Likewise, the histological features of 70, 75, 80 and 85°C 10 s burn were very similar, hence 85°C 10 s burn is described in detail as a high temperature burn. High magnification images were taken of normal skin, the burn area and burn edge of lowest and highest temperature tested for 10 s. Epidermal keratinocytes in the burn area were severely damaged by PBD 4. Wound edge epidermis was significantly hyper-thickened compared to normal skin (Figure 3.2). The dermis in the burn area was coagulated with minimal collagen interspaces in the 55°C and 85°C 10 s burns. Leukocytes were seen in a wave like zone to differentiate between the more damaged and less damaged burn areas (Figure 3.1 & Figure 3.2). Interestingly, in the 85°C burn, pockets of adipocytes can be observed in the dermis. Compared to normal skin, more inflammatory

cells are present along with fibroblasts in the burn edge region (Figure 3.2). Blood vessels appeared to be congested and nuclei of endothelial cells were condensed in the burn area of 55°C and 85°C conditions. Whereas in the burn edge of both 55°C and 85°C 10 s injuries blood vessels were packed with red blood cells and leukocytes, and endothelial cells appear normal (Figure 3.2). Minimal red blood cells can be observed in the blood vessels of normal skin (Figure 3.2). The size of hair follicles and sebaceous glands in burn edges area appeared normal except for some condensation of nuclei in the centre of hair follicles, indicative of cell death. In contrast, a complete loss of hair follicles and sebaceous glands was seen in the burn area of the 85°C burn for 10 s condition. In the 55°C burn, almost all sebaceous glands were damaged with partial loss of hair follicles (Figure 3.2). Interestingly, big round adipocytes were seen in the burn area of 55°C and 85°C on PBD 4. With increasing temperature, more and larger adipocytes were seen in the centre of dermal layer of the burn area. When compared to the normal skin, where the adipocytes were smaller and loosely organised residing in the subcutaneous layers. In the burn edge, several adipocytes were close to normal skin and also had some rounded adipocytes in the dermis (Figure 3.2).

The scoring matrix adapted from Medina and colleagues, was used to score the rat burn wounds (Table 3.4) (Medina et al., 2018). It revealed that 55°C burn is optimal to create a deep partial thickness burn, which has the 3 zones of burn injury (zone of coagulation, zone of stasis and zone of hyperemia) as described in the Jackson's burn model as shown in Table 3.5 (Jackson, 1953). Although many rat burn models have been reported (Campelo et al., 2011; Guo et al., 2017), here I was able to create consistent burns with a range of temperatures tested, and report with a histological scoring matrix and accurate burn classification. Based on this, I selected to

use 55°C and 85°C to study burn progression with histological changes that occurs on PBD 1, 4, 7 & 14.

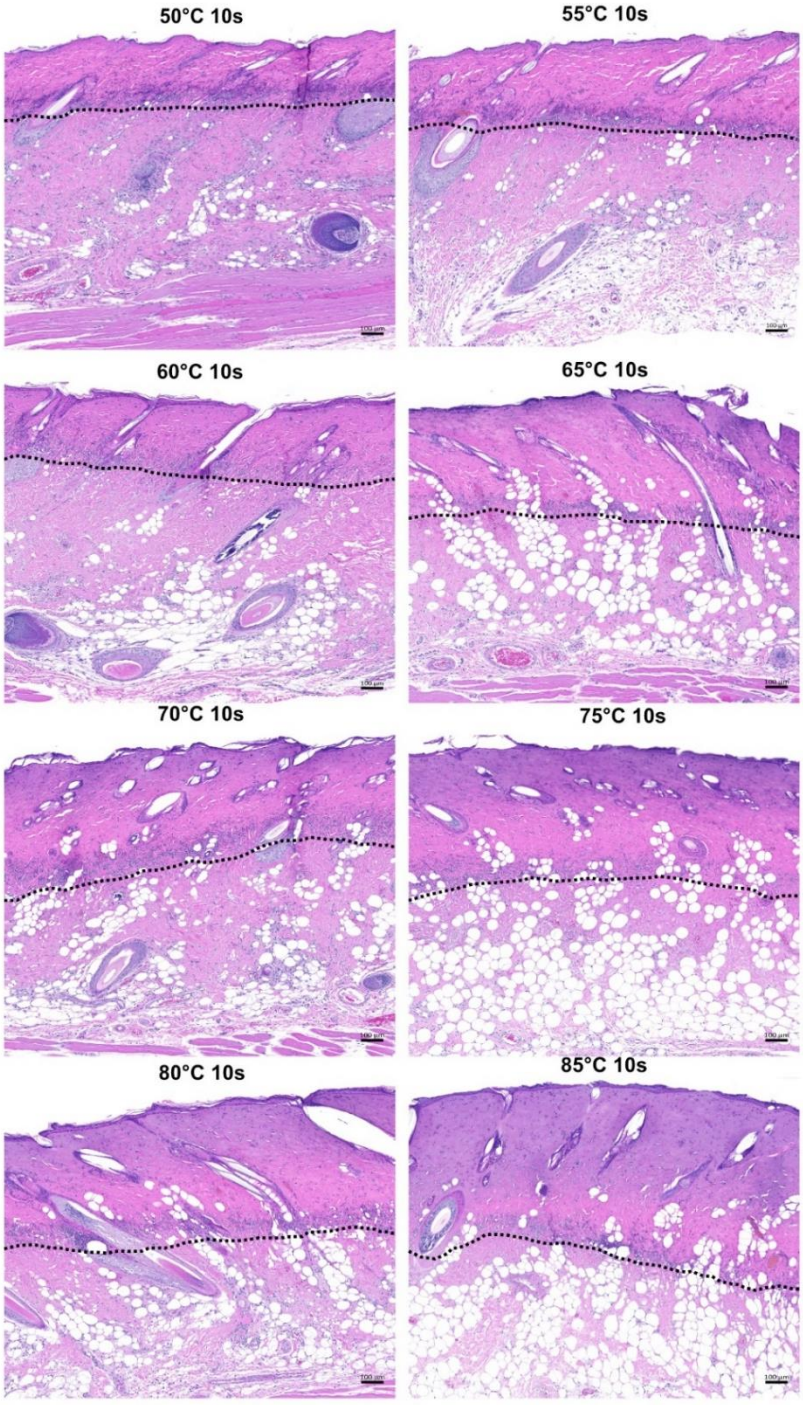

Figure 3.1 Burn depth using various temperatures for 10 s on PBD 4.
Black dotted lines represent the extent of dermal injury to deeper layers of burn tissue. Scale bar: 100µm.

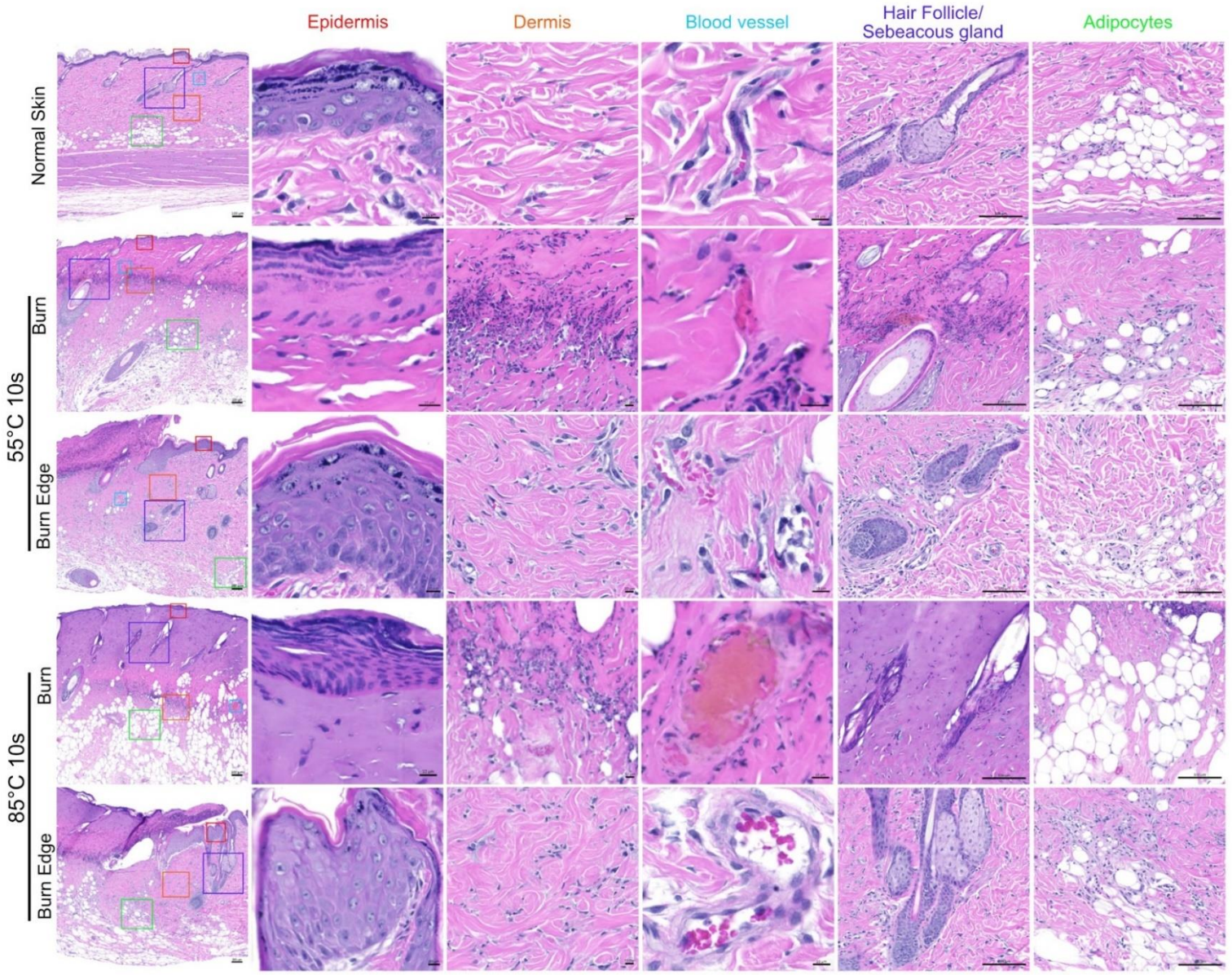
Epidermis
Dermis
Blood vessel
Hair Follicle/
Sebeacous gland
Adipocytes
Normal Skin
55°C 10s
Burn
Burn Edge
85°C 10s
Burn
Burn Edge

Figure 3.2 Histological H&E observations of rat normal skin and burn skin (burn and burn edge) at 55°C and 85°C for 10 s.
Coloured squares indicate representative histological images taken for epidermis (red square, scale bar: 10µm), dermis (orange square, scale bar: 100µm), blood vessel (blue square, scale bar: 100µm), hair follicle and sebaceous gland (purple square, scale bar: 100µm), and adipocytes (green square, scale bar: 100µm) in subcutaneous layer. First row: normal skin. Overview images scale bar: 100µm. Second row: 55°C for 10 s, burn area. Third row: 55°C for 10 s, burn edge area. Fourth row: 85°C for 10 s, burn area. Fifth row: 85°C for 10 s, burn edge area.

Table 3.5 Score table of 10 s burn creation using different temperatures (adapted and modified from (Medina et al., 2018).

Pathology Score	50°C	55°C	60°C	65°C	70°C	75°C	80°C	85°C
0	0	0	0	0	0	0	0	0
1	0	0	0	0	0	0	0	0
2	3	0	1	2	0	0	0	0
3	1	4	3	2	2	2	2	1
4	1	1	1	1	3	3	3	4

Scoring was performed on n=5 burn wounds of each temperature conditions tested. Red box indicates 55°C condition is ideal for partial thickness burn creation.

3.2.2 Burn Progression in rat burn injury

To confirm that the methodology used in this study is capable to producing progressive burn depth with increasing temperatures I harvested burn wounds of 55°C and 85°C (10s duration) and examined the histological changes and depth of burn on PBD 1, 4, 7 & 14 (Figure 3.3, Figure 3.4, Figure 3.5 & Figure 3.6). Here I show the histological differences and burn depth progression into the deeper layers. On PBD 1, histological appearances reveal immediate necrosis of the epidermis and dermis of 55°C and 85°C burn wounds (Figure 3.3 a & d). There are some immune cell infiltrates into the dermis (Figure 3.3 b, c e & f). Vascular occlusion was also present (Figure 3.3 b & f). Furthermore, cellular condensation was observed in hair follicles and sebaceous glands of 55°C and 85°C wounds and blood vessels deep in the dermis (Figure 3.3 b & e). In addition, leaky blood vessels were also observed with extravasated red blood cells in the dermis (Figure 3.3 c & g). However, there were no obvious differences observed in the two temperature conditions.

On PBD 4, I observed a clear difference in depth of burn and structure in the two conditions (Figure 3.4 a & d). As described in section 1.2.1, the dermis of 55°C and 85°C was coagulated in the upper dermis. Some surviving hair follicles and some infiltration of leukocytes in the deep dermis of 55°C burn wounds was observed. Whereas 85°C burn wounds had complete damage to hair follicles and increased number of leukocytes were visible in dermis (Figure 3.4 b & e). The presence of large and rounded adipocytes with some small adipocytes were prominent in 55°C burn wound but 85°C burn had mostly large and rounded adipocytes indicating adipocyte hypertrophy (Figure 3.4 c & f). Furthermore, the depth of burn had progressed into the deeper layers of dermis in 85°C burn wounds, much more than 55°C (Figure 3.4 a & d).

On PBD 7, the burn depth extended further into the dermis in the 55°C and 85°C wounds caused by burn progression (Figure 3.5 a). In addition, I observed increased leukocyte infiltration and cell death in the dermis as shown by nuclear condensation. A similar pattern was observed in 85°C burn wounds (Figure 3.5) with coagulated dermis in the deeper dermis. Blood vessel occlusion was also observed in both conditions (Figure 3.5).

On PBD 14, no re-epithelisation was observed in the centre of 55°C and 85°C burn wound conditions (Figure 3.6 b & e). Large blood vessels were observed in 55°C whereas 85°C had some small blood vessels (Figure 3.6 b & e). Some remodelling in the deep dermis and fibroblast migration was observed in both conditions (Figure 3.6 c & f). Increased leukocyte infiltration was seen in 85°C as compared to 55°C burn wounds (Figure 3.6 c & f).

In summary, I have shown burn progression based on histological differences at two temperatures. These observations indicate that our method of burn creation is able to create wounds in a temperature dependent and consistent manner.

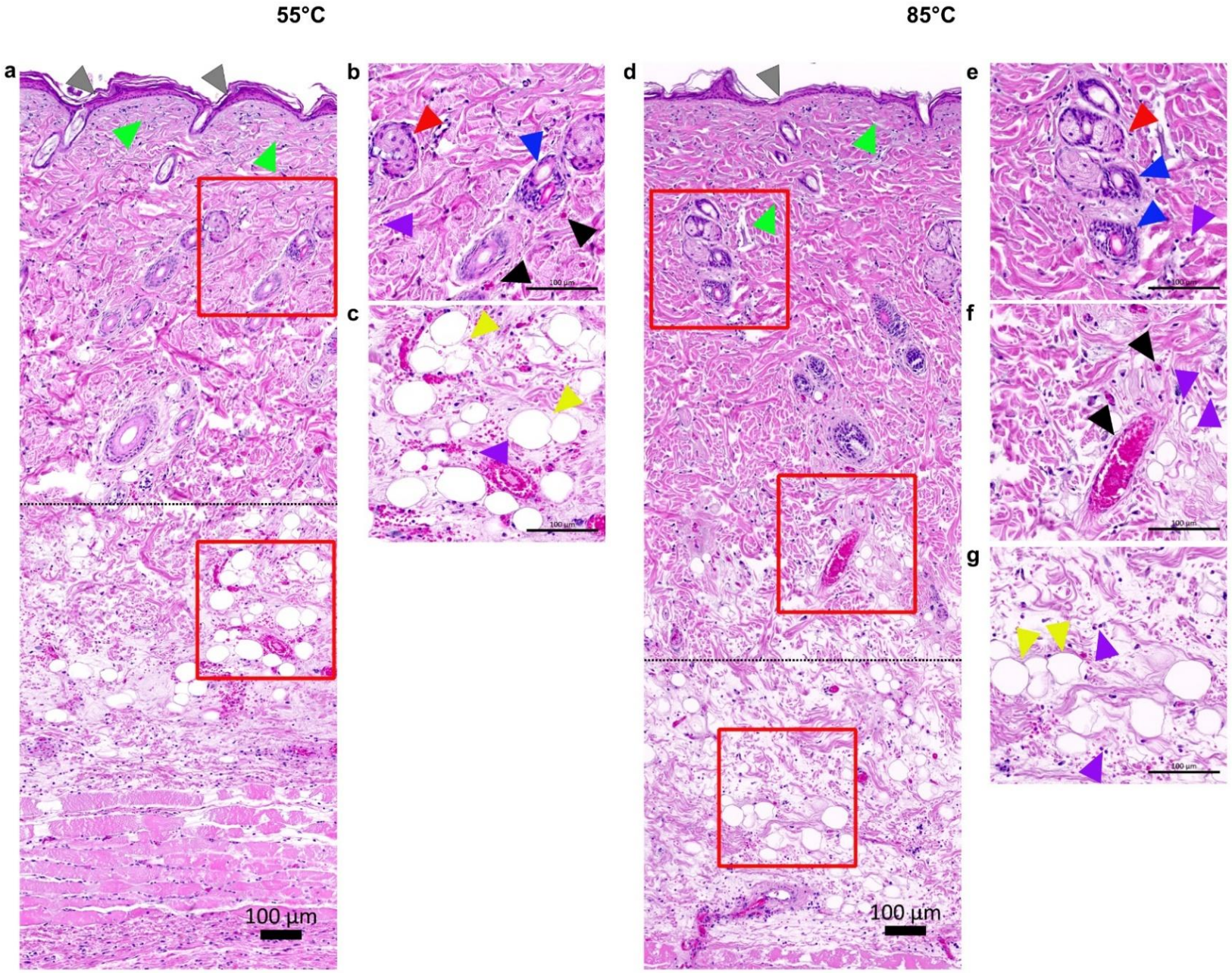
55°C
85°C
a
b
c
d
e
f
g
100 µm
100 µm

Figure 3.3 55°C and 85°C burn progression in rat burn injury on PBD 1.
(a) Representative H&E image of overview of 55°C burn wound taken from centre of wound. PBD 1 burn depth as indicated by black dotted lines. Gray arrow: damage to epidermis. Green arrow: collagen denaturation. Red boxes indicate zoomed region of interests of (b) & (c). (b) Zoomed image of 55°C burn wound. Blue arrow: damage to hair follicle. Red arrow: damage to sebaceous gland. Black arrow: blood vessel occlusion. (c) Zoomed image 55°C burn wound at deeper layers. Yellow arrow: large and rounded adipocytes. Purple arrow: leukocyte infiltration. (d) Representative H&E image of overview of 85°C burn wound taken from the centre of the wound. PBD 1 burn depth as indicated by black dotted lines. Gray arrow: damage to epidermis. Green arrow: collagen denaturation. Red boxes indicate zoomed region of interests (e), (f) &(g). (e) Zoomed image of 85°C burn wound. Blue arrow: damage to hair follicle. Red arrow: damage to sebaceous gland. Purple arrow: leukocyte infiltration. (f) Zoomed image of 85°C burn wound showing blood vessels (black arrow) and leukocyte infiltration (purple arrow). (g) Zoomed image 85°C burn wound at deeper layers. Yellow arrow: large and rounded adipocytes. Purple arrow: leukocyte infiltration. Scale bar 100μm.

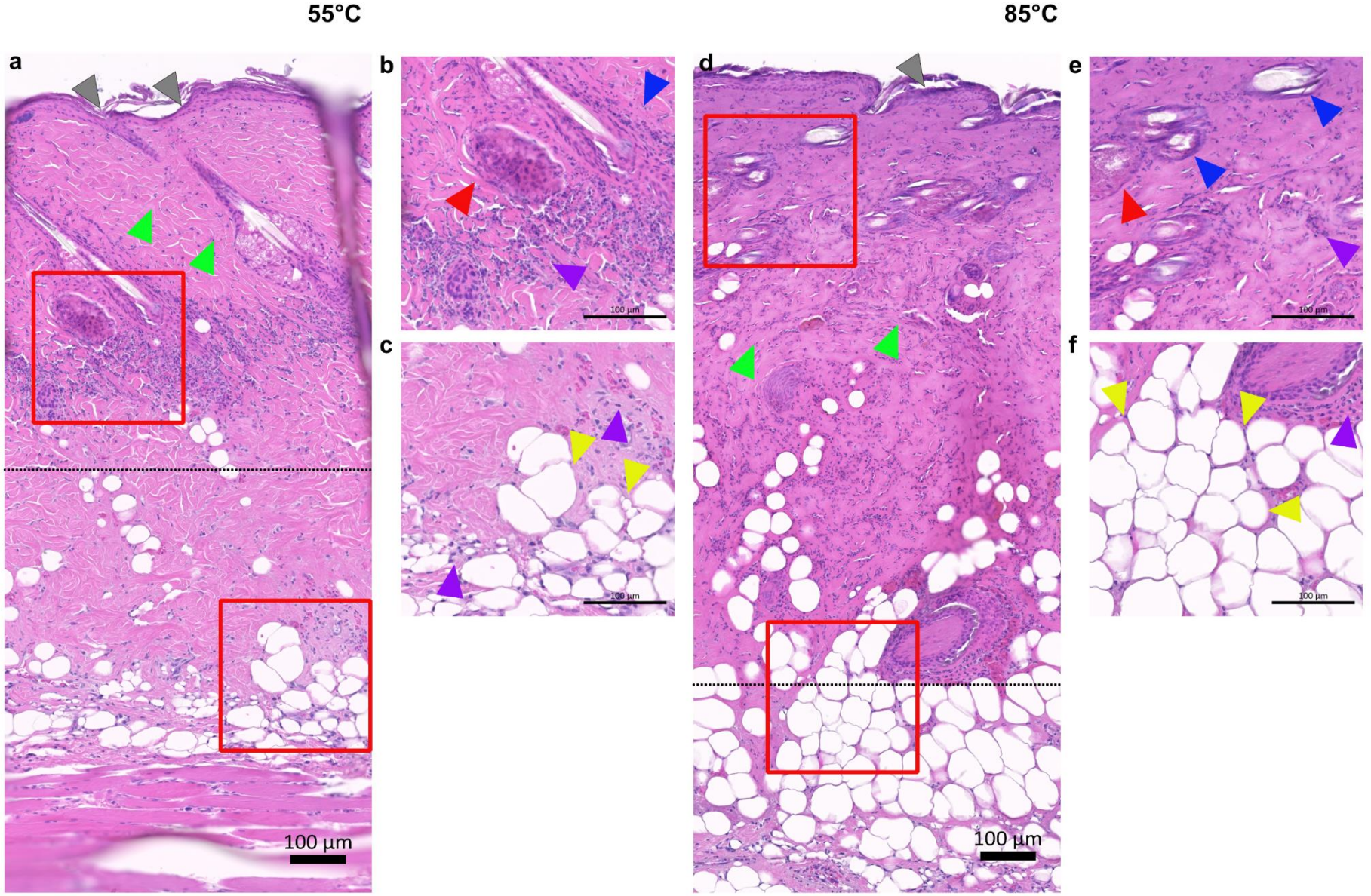
55°C
85°C
a
b
c
d
e
f
100 µm
100 µm
100 µm
100 µm
100 µm
100 µm

Figure 3.4 55°C and 85°C burn progression in rat burn injury on PBD 4.
(a) Representative H&E image of overview of 55°C burn wound taken from centre of wound. PBD 4 burn depth as indicated by black dotted lines. Gray arrow: damage to epidermis. Green arrow: collagen denaturation. Red boxes indicate zoomed region of interests of (b) & (c). (b) Zoomed image of 55°C burn wound. Blue arrow: damage to hair follicle. Red arrow: damage to sebaceous gland. Purple arrow: Leukocyte infiltration. (c) Zoomed image 55°C burn wound at deeper layers. Yellow arrow: large and rounded adipocytes. Purple arrow: leukocyte infiltration. (d) Representative H&E image of overview of 85°C burn wound taken from centre of wound. PBD 4 burn depth as indicated by black dotted lines. Gray arrow: damage to epidermis. Green arrow: collagen denaturation. Red boxes indicate zoomed region of interests (e) & (f). (e) Zoomed image of 85°C burn wound. Blue arrow: damage to hair follicle. Red arrow: damage to sebaceous gland. Purple arrow: leukocyte infiltration. (f) Zoomed image 85°C burn wound at deeper layers. Yellow arrow: large and rounded adipocytes. Purple arrow: leukocyte infiltration. Scale bar 100μm.

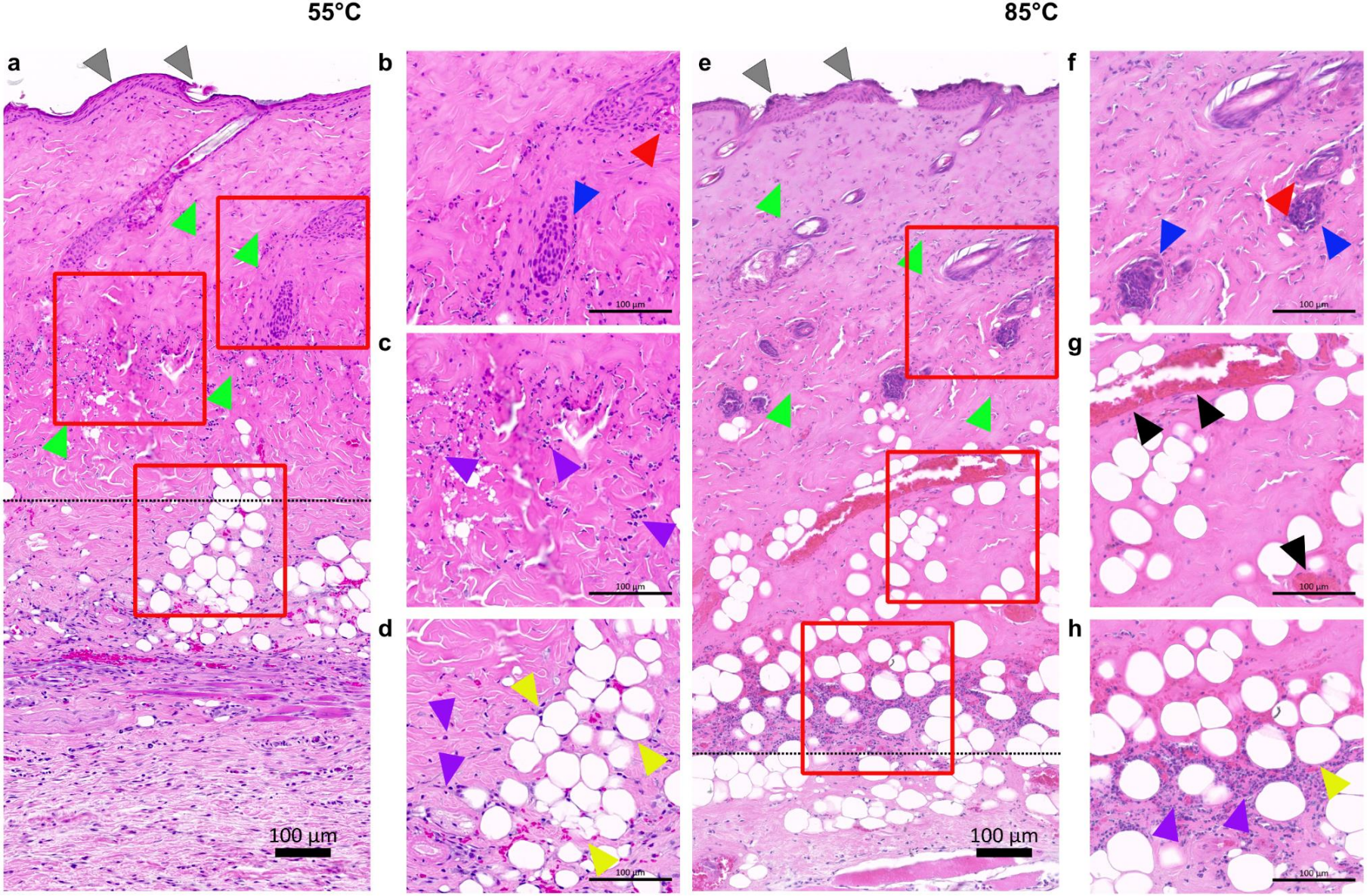
55°C
85°C
a
b
c
d
e
f
g
h
100 µm

Figure 3.5 55°C and 85°C burn progression in rat burn injury on PBD 7.
(a) Representative H&E image of overview of 55°C burn wound taken from centre of wound. PBD 7 burn depth as indicated by black dotted lines. Gray arrow: damage to epidermis. Green arrow: collagen denaturation. Red boxes indicate zoomed region of interests of (b), (c) & (d). (b) Zoomed image of 55°C burn wound. Blue arrow: damage to hair follicle. Red arrow: damage to sebaceous gland. (c) Zoomed image 55°C burn wound at centre showing coagulated dermis with leukocyte infiltration (purple arrows). (d) Zoomed image 55°C burn wound at deeper layers. Yellow arrow: large and rounded adipocytes. Purple arrow: leukocyte infiltration. (e) Representative H&E image of overview of 85°C burn wound taken from centre of wound. PBD 7 burn depth as indicated by black dotted lines. Gray arrow: damage to epidermis. Green arrow: collagen denaturation. Red boxes indicate zoomed region of interests of (f), (g) & (h) (f) Zoomed image of 85°C burn wound. Blue arrow: damage to hair follicle. Red arrow: damage to sebaceous gland. (g) Zoomed image of 85°C burn wound showing coagulated dermis with blood vessel occlusion (black arrows). (h) Zoomed image 85°C burn wound at deeper dermis. Yellow arrow: large and rounded adipocytes. Purple arrow: leukocyte infiltration. Scale bar 100μm.

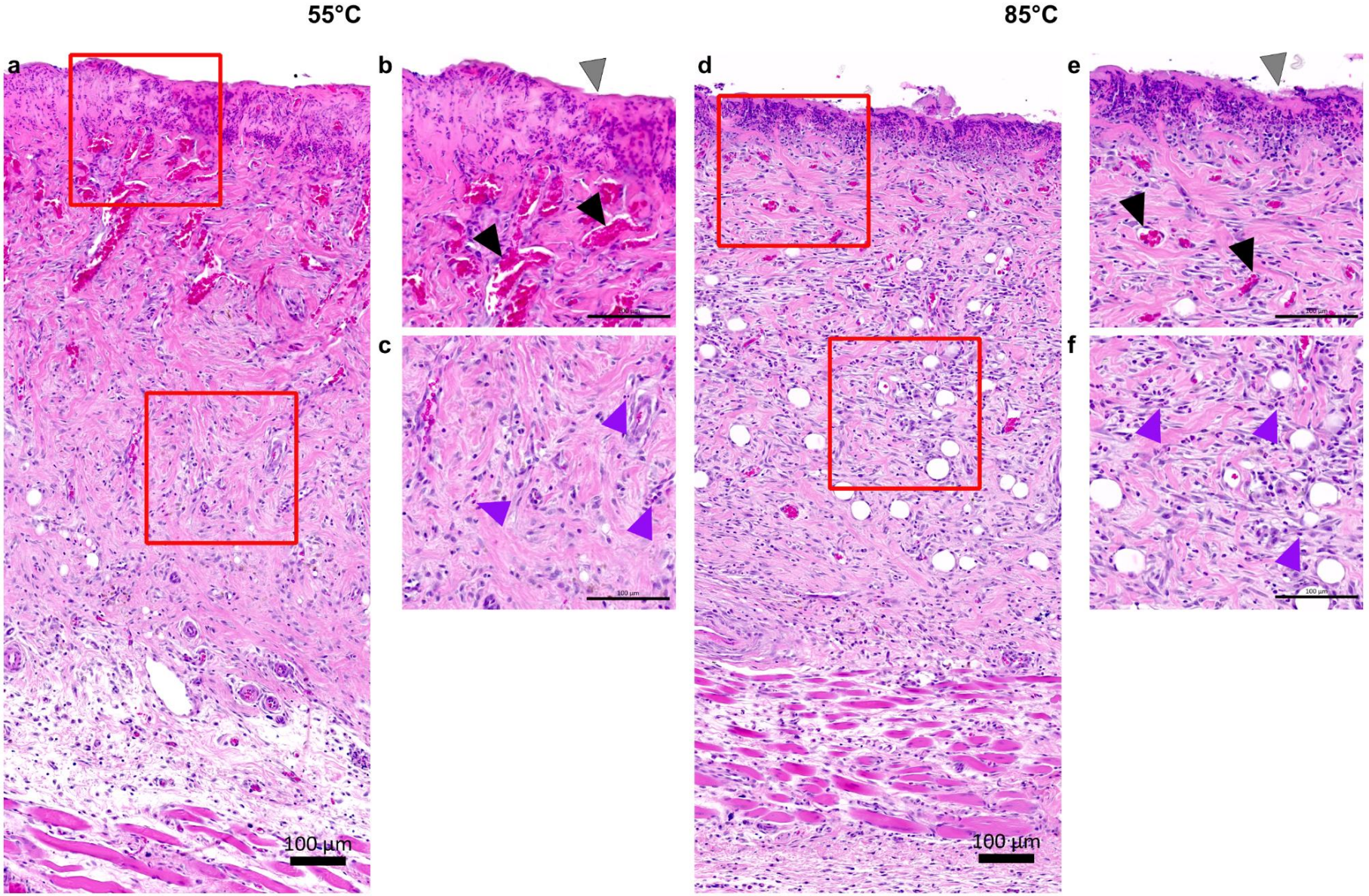
55°C
85°C
a
b
c
d
e
f
100 µm
100 µm

Figure 3.6 55°C and 85°C burn progression in rat burn injury on PBD 14.
(a) Representative H&E image of overview of 55°C burn wound taken from centre of wound. (b) Zoomed image of 55°C wound at superficial layer of dermis. Gray arrow: no re-epithelisation. Black arrow: blood vessels. Red boxes indicate zoomed region of interests of (b) & (c). (c) Zoomed image of 55°C burn wound taken from centre of dermis. Purple arrow: Presence of leukocytes. (d) Representative H&E image of overview of 85°C burn wound taken from centre of wound. (e) Zoomed image of 85°C wound at superficial layer of dermis. Gray arrow: no re-epithelisation. Black arrow: blood vessels. Red boxes indicate zoomed region of interests (e) & (f). (f) Zoomed image of 55°C burn wound taken from centre of dermis. Purple arrow: Presence of leukocytes. Scale bar: 100μm.

3.2.3 Inflammatory score in rat burn injury

To understand the presence of inflammatory cells in rat burn injury, I performed the following a scoring analysis based on histological analysis of rat burn wounds. An in-house scoring criteria was determined based on the histology obtained from the various burn temperature (50, 55, 60, 65, 70, 75, 80 and 85°C) testing conducted on rat burn. **Score 0**: Little/no recruitment of leukocytes. **Score 1**: Some recruitment of leukocytes to burn area. **Score 2**: Moderate recruitment of leukocytes to dermis within burn area. **Score 3**: Large recruitment of leukocytes (focal accumulation around hair follicles and adipocyte). **Score 4**: Extensive recruitment of leukocytes from deep dermis to upper dermis. By scoring I found that on PBD 1, there was no difference in immune cell infiltration between 55°C and 85°C burn condition. On PBD 4, there were significantly more immune cell infiltration into the dermis of 85°C burn than 55°C burn. However, there was no difference on PBD 7 (Figure 3.7).

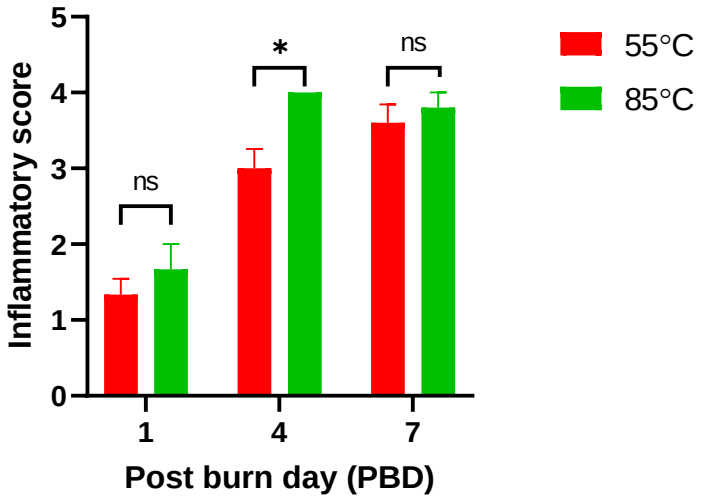

Figure 3.7 Comparing immune cell penetration using inflammatory score.
Graph showing comparison in immune cell recruitment to rat burn injury on PBD 1, 4 & 7. Score 0: Little/no recruitment of leukocytes. Score 1: Some recruitment of leukocytes to burn area. Score 2: Moderate recruitment of leukocytes. Score 3: Large recruitment of leukocytes (focal accumulation around hair follicles and adipocyte). Score 4: Extensive recruitment from

deep dermis to upper dermis. Data is presented as mean value ± S.E.M. Statistical comparisons were made using a One-way ANOVA, post-hoc Tukey. (*p<0.05, ns: not significant, n=6 burn wounds for each burn condition on PBD 1 & 4, n=5 burn wounds for each burn condition on PBD 7).

3.2.4 Elevated expression of Cx43 in rat burn injury

3.2.4.1 Epidermis

To understand the Cx43 expression within the rat burn injury, I performed Cx43 immunostaining analysis on PBD 4. Here I studied the expression of Cx43 in various parts of epidermis comprising the leading edge of the epidermis as well as the hyper-thickened epidermis that is located at the wound edge of the rat burn, and the intact far edge epidermis. I observed a significant increase in Cx43 expression in the leading edge epidermis of 55°C and 85°C as compared to normal skin ($p<0.01$) (Figure 3.8 a, b & g). In hyper-thickened wound edge epidermis, I observed significantly elevated expression of Cx43 in 55°C and 85°C compared to normal skin ($p<0.0001$) (Figure 3.8 c, d & g). As Cx43 expression is involved in cell-to-cell communication, we wanted to understand if the distal far edge epidermis had elevated expression of Cx43. I noted significant increases of Cx43 in far edge epidermis of 55°C and 85°C burn condition as compared to normal skin ($p<0.01$ and $p<0.001$, respectively) (Figure 3.8 e, f & g).

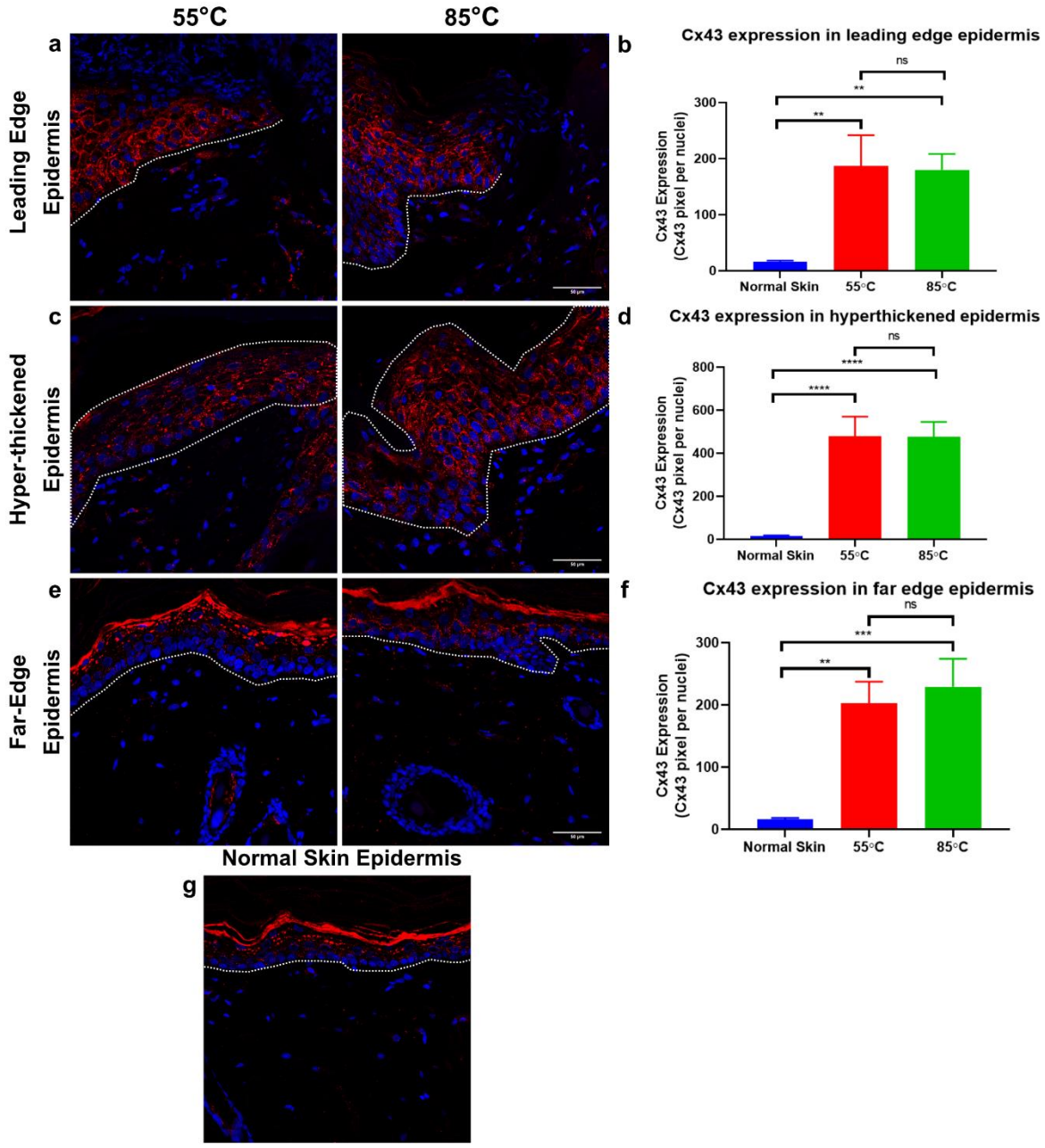

Figure 3.8 Cx43 expression in epidermis of rat burn injury on PBD 4.
(a) Representative immunofluorescence image of Cx43 expression in leading edge epidermis of 55°C and 85°C burn condition. White dotted line represents demarcation of leading edge epidermis from dermis. (b) Image analysis graph represents Cx43 expression in leading edge epidermis of normal skin, 55°C and 85°C burn condition. (c). Representative immunofluorescence image of Cx43 expression in hyper-thickened epidermis of 55°C and 85°C burn condition. White dotted line represents demarcation of hyper-thickened epidermis from dermis. (d) Image analysis graph represents Cx43 expression hyper-thickened epidermis of normal skin, 55°C and 85°C burn condition. (e) Representative immunofluorescence image of Cx43 expression in far edge epidermis of 55°C and 85°C burn condition. White dotted line

represents demarcation of far edge epidermis from dermis. (f) Image analysis graph represents Cx43 expression far edge epidermis of normal skin, 55°C and 85°C burn condition. (g) Representative immunofluorescence image of Cx43 expression in normal skin epidermis. Magnification: 40x. Data is presented as mean value ± S.E.M. Statistical comparisons were made using a One-way ANOVA, post-hoc Tukey (*p<0.05, **p<0.01, ***p<0.001, ****p<0.0001, ns: not significant, n=5 animals per condition). Scale bar: 50µm.

3.2.4.2 Dermis

I performed Cx43 expression analysis on rat burn injury and studied the expression pattern in various parts of the dermis such as the zone of stasis (ZOS) within burn dermis, the far edge dermis and the deep dermis of rat burn 55°C and 85°C on PBD 4. I observed that there was a significant increase in Cx43 expression zone of stasis of 55°C and 85°C ($p<0.01$) compared to normal skin (Figure 3.9 a, b & g). As Cx43 is involved in cell-to-cell communication, I wanted to understand if there is a transient effect of burn injury in distal far edge dermis. No increase in Cx43 expression in 55°C and 85°C burn was observed as compared to normal skin ($p=0.8400$ and $p=0.2206$, respectively) (Figure 3.9 c, d & g). I also looked at the expression of Cx43 in deep dermis of rat burn injury and have found that 55°C and 85°C burn condition did not change in Cx43 expression compared to normal skin ($p=0.3133$ and $p=0.7084$, respectively (Figure 3.9 e, f & g). In summary, an elevated Cx43 expression was observed in wound edge dermis upon rat burn injury.

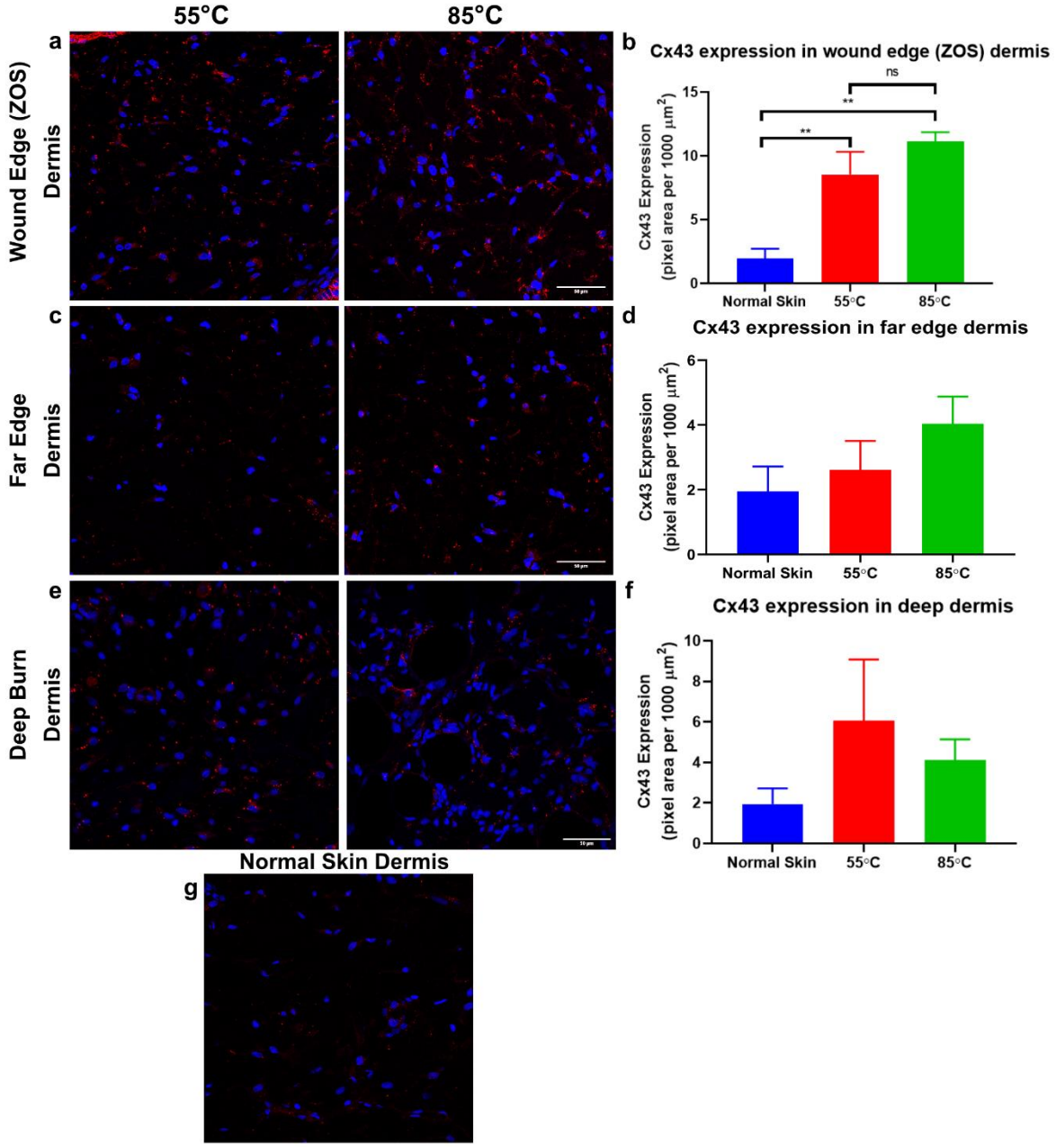

Figure 3.9 Cx43 expression in the dermis of a rat burn injury on PBD 4.
(a) Representative immunofluorescence images of Cx43 expression in the zone of stasis (ZOS) at the wound edge dermis of 55°C and 85°C burn conditions. (b) Image analysis graph represents Cx43 expression in the zone of stasis (ZOS) at the wound edge dermis of 55°C, 85°C burn condition and normal skin. (c) Representative immunofluorescence image of Cx43 expression in far edge dermis of 55°C and 85°C burn condition. (d) Image analysis graph represents Cx43 expression in normal skin, far edge dermis 55°C and 85°C burn condition. (e) Representative immunofluorescence image of Cx43 expression in deep dermis of 55°C and 85°C burn condition. (f) Image analysis graph represents Cx43 expression of normal skin, deep dermis 55°C and 85°C burn condition. (g) Representative immunofluorescence image of Cx43 expression in normal skin dermis. Magnification: 40x. Data is presented as mean value ±

S.E.M. Statistical comparisons were made using a One-way ANOVA, post-hoc Tukey (**p<0.01, ns: not significant, n=5 animals per condition). Scale bar: 50µm.

3.2.5 Elevated percentage of MPO positive cells in rat burn injury

To assess the inflitration of immune cells, I perform immunofluorescence staining to stain for MPO positive cells. I observed significant increase in MPO positive cells in 55°C and 85°C burn condition as compared to normal skin in the wound edge dermis of rat burn injury on PBD 4 ($p<0.0001$). However, there was no difference in percentage of MPO positive cells between the two burn conditions ($p=0.900$) (Figure 3.10).

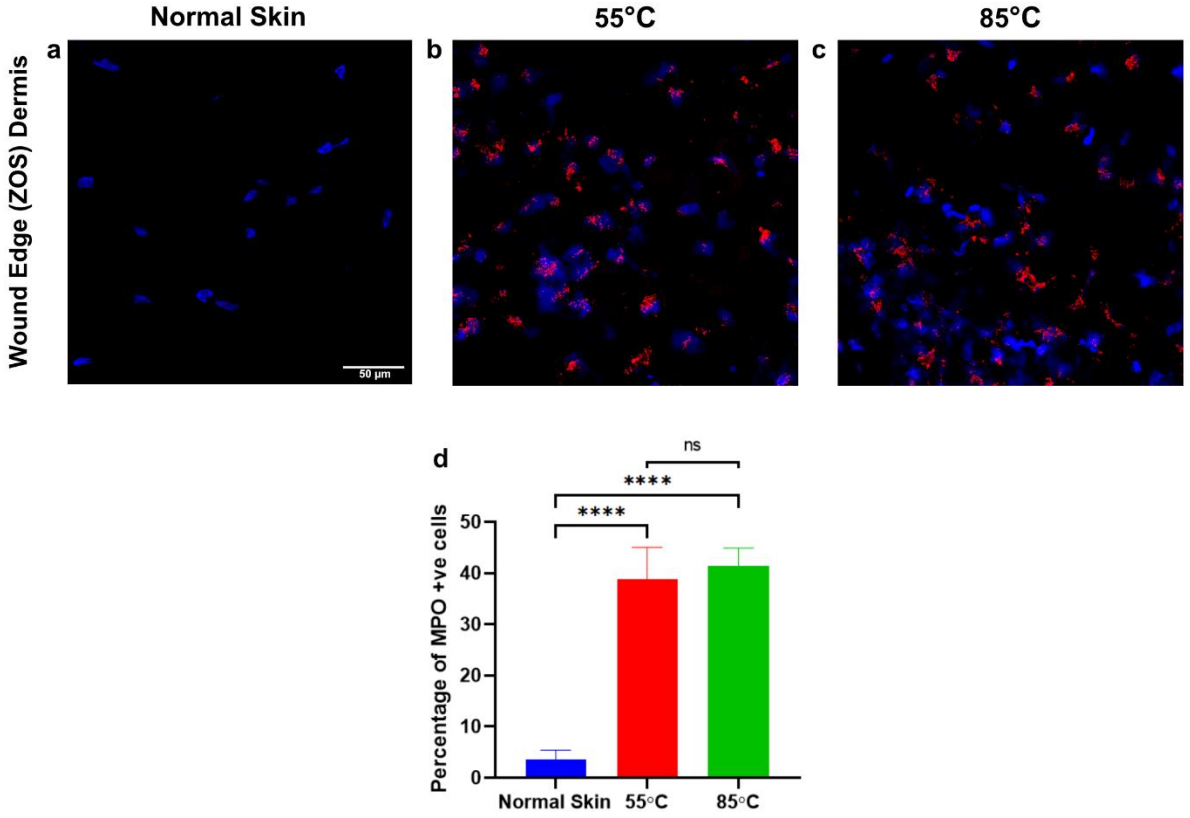

Figure 3.10 Percentage of MPO positive cells in the dermis of a rat burn injury on PBD 4.
(a) Representative immunofluorescence images of Cx43 expression in the zone of stasis (ZOS) at the wound edge dermis of normal skin, (b) 55°C,(c) 85°C burn conditions. (d) Image analysis

graph represents perecentage of MPO positive cells in the zone of stasis (ZOS) at the wound edge dermis of 55°C, 85°C burn condition and normal skin. Magnification: 40x. Data is presented as mean value ± S.E.M. Statistical comparisons were made using a One-way ANOVA, post-hoc Tukey (****$p<0.0001$, ns: not significant, n=5 animals per condition). Scale bar: 50µm.

3.3 Discussion

The purpose of this chapter was to create a rodent model of burn injury that was simple, reproducible, predictable, and quantifiable. I characterised the rat burn model in two parts. In the first part, I studied the histological changes in the rat burn using various temperatures and kept the duration constant at 10 s. Using a scoring system adopted from Medina et al 2018, I scored the injuries (Medina et al., 2018). Although in their paper, they described the histological features using a mouse burn model to score the depth of burn, it was closely related to the burn features that were found in the rat burn injury. Furthermore, the description of the scoring matrix closely resembled human burn classification (Vaughn & Beckel, 2012). As a result, I applied this scoring matrix to the rat burn wounds and discovered that a 55°C for 10 s burn was sufficient to produce deep partial thickness burns on PBD 4. The 60°C burn condition showed differing histological evidences between animals as compared to 55°C burn condition hence 55°C was chosen to study the burn burn progression. I also compared this temperature to an 85°C 10 s burn wound. This confirmed there were distinct differences in the depth of burn and histological features to indicate that the burn creation method successfully delivers progressive depths of burn with increasing temperature settings. These histological features of 55°C 10 s burn include immediate damage to epidermis, and coagulated dermis. In addition, infiltration of neutrophils into the burn area that demarcates the necrotic tissue area and possibly surviving area with large and round adipocytes in dermis depicts zone of stasis. In 85°C 10 s burn dermis, increased number of adipocytes larger in size were seen in the centre of dermal layer of the burn area. Additionally, increased number of inflammatory cells were present along with fibroblasts in the burn edge region of 85°C 10 s burn. In the second part, I studied the burn progression of 55°C and 85°C burn conditions and have found that the 55°C 10 s burn that was initially a partial thickness burn progressed into a deep partial thickness burn

on PBD 4. Subsequently, the burn conditions progressed into deeper dermis on PBD 7 without turning into a full thickness burn. However, the 85°C burn condition resulted into a full thickness burn by PBD 4. My research has shown that it is not possible to identify the depth of burn on PBD 1, and that this information must be obtained at a later timepoint, such as PBD 4. Early burn depth assessment is difficult and may not be reliable, according to some research (Karim et al., 2020).

3.3.1 Histological changes in burn injury

The depth of a burn impacts the likelihood of successful wound healing because the skin appendages in the reticular dermis contain keratinocyte reservoirs with the capacity to repopulate the epidermis (Shakespeare, 2001). Thermal injury causes complete damage to the epidermis. In superficial and partial thickness wounds, the intact hair follicles, sweat glands, and sebaceous glands produce a plentiful supply of new epithelium throughout the injured area. The destruction of the deep structures and extracellular matrix (ECM) causes the loss of stem cells and requires clearance and replacement of the ECM in deep partial thickness and full thickness burn wounds (Shakespeare, 2001). As a result, the supply of new epithelium will effectively be restricted to the edges of the wound and take more time for wound healing to take place (Shakespeare, 2001). Hence, it is critical to structure the wound care and management regimen required for each patient based on an estimate of the time required for re-epithelialization based on the depth of the wound (Tenenhaus et al., 2007).

I observed nuclear condensation in hair follicles, sebaceous glands, blood vessels, and fibroblasts as an indication of cell death. Gravante and colleagues have reported positive staining of deoxynucleotide transferase-mediated dUTP nick-end labelling (TUNEL) and FasL, with 44% of dermal cells undergoing apoptosis and the presence of apoptotic cells

persisting up to 13 days after injury in deep partial thickness burn wounds of humans (Gravante et al., 2007). In another study of theirs, a comparison between superficial partial thickness burns and deep partial thickness burns revealed 5.6% and 44.5% apoptotic cells, respectively. In contrast 0% apoptotic cells were reported in full thickness burns as thermal injury killed all the cells, suggesting that deep burns sustain an ischaemic damage that forces cells to undergo apoptosis and may serve as the strong basis for conversion into full-thickness burns (Gravante et al., 2006). Utilizing a rat comb burn model, Singer and colleagues carried out immunostaining of cleaved caspase-3 to mark for apoptosis and high mobility group box 1 (HMGB1) to mark for necrosis. At 30 min after burn injury, they reported cleaved caspase-3 positive cells in the epidermis, dermal fibroblasts, dermal follicles, and dermal sebaceous glands. Additionally, at 24 and 48 hours, HMGB1-positive cells were discovered in the epidermis, sebaceous glands, and follicles, indicating that early apoptosis and delayed necrosis are present in the zone of stasis and are contributing to burn progression (Singer et al., 2008). Although cleaved caspase-3 and HMGB1 immunostaining were not carried out in the current investigation, H&E observations show cellular death in the zone of stasis after burn injury.

Cell death is a common and effective promoter of sterile inflammation. *In vivo* cell death results in the fast infiltration of the tissue by leukocytes, initially composed of neutrophils and thereafter accumulating as monocytes (Rock & Kono, 2008). I observed leukocyte infiltration in the rat burn models from PBD 1 to PBD 14. Even though, inflammation is a key element in promoting wound healing, it can also slow down the recovery time. Local inflammation has advantageous consequences such as cellular debris removal and antimicrobial defence in burn injuries (Chitnis et al., 1996). However, a prolonged inflammatory response can result in persistently elevated levels of proinflammatory cytokines such as TNFα and IL-6 (Summer et al., 2008), which can cause cell death in keratinocytes and bring about collagen degradation

(Zhang et al., 2022). In addition, neutrophil adhesion to the venular endothelium can compromise microvascular function, and the production of oxygen-derived free radicals can damage plasma membranes (Parihar et al., 2008; Wang et al., 2021). Although, I did not quantify the rat burn wounds with specific markers for macrophages in this chapter, I can recognise the presence of these cells in H&E stained tissues. In addition, there was a significant increase in MPO positive cells that marks for neutrophils in the wound edge dermis of burn wound conditions on PBD 4. In particular, using the inflammatory scoring system, there was significantly more leukocyte inflitration in the dermis of 85°C than 55°C burn condition which may be contributed by the influx of various immune cell types in a temperature dependent manner. Unfortunately, one limitation of this study is that a single marker (MPO) was used for leukocyte infiltration and requires additional marker for further validation of the leukocyte infiltration. In the upcoming chapters, I will investigate and discuss in depth in relation to the inflammatory response in rat burn wounds with and without treatment with Cx43asODN or Tonabersat as potential therapeutics. As burn injuries are accompanied by cellular damage and increased inflammatory mediators, changes in histamine, bradykinin, and platelet-activating factor (PAF), cytokines such as vascular endothelial growth factor (VEGF), metabolic factors such as ATP, and activated neutrophils can affect vascular permeability (Alves et al., 2018). A compromised vascular endothelial barrier increased permeability after burn injury, resulting in the release of red blood cells from damaged blood vessels (Clark et al., 2018). In addition, accumulation of albumin and plasma results in swelling or edema in burn wounds. This causes the inflammatory response to become more aggravated and increase permeability of blood vessels, which causes more tissue damage and organ failure (Chi et al., 2021). Increased microvascular hyperpermeability, or the excessive leaking of proteins and fluids from the intravascular area to the extravascular space, has been seen in several rat burn investigations (Goto et al., 2006; Wiggins-Dohlvik & Tharakan, 2018). In addition, increased vascular hyper-

permeability following ischaemia-reperfusion injury has caused loss of function in heart endothelial cells (Hastie et al., 1997). These findings are consistent with the observations of blood vessel occlusion and leaky blood vessels in rat burn injury.

3.3.2 Cx43 in rat burn injury

Elevated Cx43 gap junctional protein expression has been reported in chronic wounds such as diabetic foot ulcers, venous leg ulcers and pressure ulcers (Kanapathy et al., 2018; Kwek et al., 2021; Sutcliffe et al., 2015). Moreover, studies have shown that Cx43 plays a role in cell migration, proliferation, inflammation and wound contraction, all events that are crucial for the wound healing processes (D'Hondt et al., 2014; Saitoh et al., 1997; Wan et al., 2021; Yin et al., 2018). In human burns, Cx43 expression was found to be elevated in dermal fibroblasts within the zone of stasis (Feng et al., 2020). Moreover, they also found increased expression of cleaved caspase-3 in the zone of stasis, suggesting that Cx43 may play an active role in burn conversion (Feng et al., 2020). In addition, Cx43 is elevated in a mouse burn model (Coutinho et al., 2005). Hence, I hypothesized that Cx43 is upregulated in rat burn injury and plays a role in burn progression. In this study, I observed a significant increase in Cx43 in 55°C and 85°C burn conditions compared to normal skin on PBD 4, however, Cx43 expression was not significantly different between 55°C and 85°C burn conditions (Figure 3.8 & Figure 3.9). Histological evidence has shown that burn progression occurs in the early phases of burn injury, and this could possibly occur via Cx43 gap junctions and hemichannels. Hence, downregulating Cx43 could be a potential therapeutic option to prevent burn progression in rat burn injury.

3.3.3 Model selection

Choosing the right depth of burn for the type of treatment is crucial. Using a full thickness burn model is not ideal for topical application as the cell and tissue viability is compromised, and

the uptake of treatment might not be successful because of cell death. Full thickness burn models are ideal for testing of full thickness scaffolds (Ramakrishnan et al., 2022). For preliminary testing of topical agents, it is best to use partial or deep partial thickness burn models (Becic et al., 2005). The findings of 55°C burn condition reveals that the initial partial thickness burn has progressed in to a deep partial thickness burn. Therefore, using a 55°C burn condition would be ideal to test topical application of Cx43 targetted therapeutics rather than 85°C burn that resulted in full thickness burn. Furthermore, 55°C temperature is a safe temperature for operators to work with when creating burns on rats. Rats have been used widely to investigate burn injury because they can be handled easily and can be studied with a large sample size. Moreover, they are inexpensive, and have a faster rate of wound healing (Abdullahi et al., 2014). Additionally, rats are less susceptible to systemic infections and immunosuppression than larger animals (Dahiya, 2009). These factors make the rat model of burn wound healing appealing for experimentation.

3.3.4 Challenges with rat burn injury

Although, there are notable differences in the structure and anatomy of skin of humans and rats, years of research have shown that experimentation using rat models for burn wound healing have provided great insights into the cause and progression of burn injury and has been shown to be a valuable tool for the development of therapeutic agents. The arrangement and number of hair follicles and the presence of the panniculus carnosus muscle layer distinguish rat skin from human skin in a pronounced way. Instead of re-epithelialization as seen in humans, the panniculus carnosus would make the wounds heal mostly through contraction (Cross et al., 1995). It is important to note that the rat skin undergoes hair follicle cyclic changes. This consists of a growing (anagen) phase and a resting (telogen) phase (Plikus & Chuong, 2008). Using a standardized burn technique, skin undergoing the anagenic phase

might sustain a more superficial burn with an increased percentage of hair survival than skin undergoing the telogenic phase that results in damage to the deeper layers of skin (Zawacki & Jones, 1967). Meyerholz and colleagues have reported that the detection of injury in deep burns was hindered by hair follicle cell injury in a variety of anagen to telogen hair follicles among animals (Meyerholz, Piester, Sokolich, et al., 2009). Hence, it is important to use a guide of the anagen and telogen phases of rat skin to achieve consistent burn creation and reduce variability in the depth of burn within an experiment (Morisaki et al., 2013). Prior to burn creation, a hair removal technique should ensure complete removal of hair shafts, which resets the hair follicle cycle (Cai et al., 2014). This will reduce any variability induced by hair follicle cycle. In this study, I performed experiments while the hair follicle was in the telogen phase and ensured the hair was removed completely before burn creation.

I employed a corrosion and rust resistant soldering iron metal rod in this study. Rust and corrosion may begin to accumulate after a number of experiments, leaving the metal rod with uneven surfaces. Care should be taken and irregular surface on rod should be checked to ensure a uniform burn creation is achieved. In addition, during burn creation, the soldering iron rod should be allowed to rest on its own weight (Tavares Pereira Ddos et al., 2012; Upadhyay et al., 2009). This is the most practical and precise approach for standardizing the pressure that the rod applies to the skin. Furthermore, no additional pressure should be applied on skin as described by some studies (Gurung & Skalko-Basnet, 2009; Pessolato et al., 2011) as this will introduce variable pressure exerted to each burn created. In addition, I limited burn creation to the dorsal skin and loin area, as skin closer to the head and forelimbs was thinner and loose and introduces variability (Zohdi et al., 2011). These steps should be taken when creating burn injury rat models to minimize variations and achieve reproducible burn wounds.

3.4 Conclusion

The rat burn model was selected based on burn creation reproducibility and the depth of burn created to cause a significant increase in Cx43 expression. Particularly on PBD 4, I have shown the histological changes that occur in a rat burn injury, such as immediate damage to the epidermis, and coagulated dermis. In addition, infiltration of neutrophils into the burn area that demarcates the necrotic tissue area and possibly the surviving area with large and round adipocytes in the dermis depicts the zone of stasis. Furthermore, the results show that using our burn creation setup, the 55°C 10 s burn condition reveals an initial partial thickness burn injury that progresses to a deep partial thickness burn, suggesting that the initial zone of stasis is converted into a zone of necrosis. In addition, elevated Cx43 in the rat burn injury suggests that Cx43 may play a role in rat burn progression. Targeting Cx43 expression in rat burn injury could be a future therapeutic target for burn progression prevention. In the following chapter, topical application of Cx43 targeted therapeutics of Cx43asODN and Tonabersat will be carried out using the selected burn model.

Chapter 4: Targeted Cx43 therapeutics reduce inflammasome activation in rat burn injury

4.1 Introduction

The impact of a major burn injury can give rise to serious complications , such as sepsis due to bacterial infection (Zhang et al., 2021), shock caused by hypovolemia (a condition when the body loses excess fluids like water or blood) (Rae et al., 2016), or deep tissue scarring after improper wound healing that could affect quality of life (Chiang et al., 2016). A series of overlapping steps occurs to achieve normal wound healing; homeostasis, inflammation at the site of injury, cell migration, proliferation, differentiation, angiogenesis, re-epithelialisation, collagen synthesis and remodelling of extracellular matrix (ECM) (Table 4.1) (Chiang et al., 2016; Guo & Dipietro, 2010).

It is important to note that these wound healing events, such as inflammation, proliferation and remodelling occur in all types of burn injuries. However, the period of each stage differs and carries variable downstream effects depending on the condition, depth and extent of the burn injury (Sakallioglu et al., 2006). In superficial burns, the time taken for recovery with minimal scarring is within 14 days of injury. In partial thickness burn injuries, re-epithelialisation occurs via migration of keratinocytes from viable skin appendages within the burn region (Shpichka et al., 2019). In deeper burns where skin appendages are mostly damaged, healing therefore generally takes place from the edges rather than from the centre of the wound, resulting in wound contraction that helps wound closure be achieved (Mokos et al., 2017). Angiogenesis occurs in burn injury and is induced by hypoxia-inducible-factor-1 and angiogenic cytokines such as VEGF and CXCL12, as well as neovascularisation of endothelial progenitor cells. In

addition to this phenomena, continuous activation of transforming growth factor beta (TGFβ1), stalls the remodelling phase and leads to hypertrophic scar formation (Chiang et al., 2016; Sakallioglu et al., 2006).

Table 4.1 Cellular events in wound healing.

Phase	Cellular events
Homeostasis	Vascular constriction Platelet aggregation, degranulation, and fibrin formation
Inflammation	Neutrophil infiltration Monocyte infiltration and macrophage differentiation Lymphocyte infiltration
Proliferation	Re-epithelialisation Angiogenesis Collagen synthesis ECM formation
Remodelling	Collagen remodelling Vascular maturation and regression Scar contraction

Adapted from (Guo & Dipietro, 2010).

Burn injury is dominated by the immune response. Immediately after burn injury, immune cells at the site of injury release cytokines, chemokines, adipocytokines, as well as reactive oxygen species (ROS), cortisol, and catecholamines that mediate a strong local inflammatory response and systemic inflammation (Poranki et al., 2016; Strudwick & Cowin, 2017).

The inflammasome is a family of multiprotein complexes that accumulate in the cytosol upon detection of pathogen-associated molecular patterns (PAMPs) such as irritants, peptidoglycans, or bacterial LPS, and damage-associated molecular patterns (DAMPs) like inflammatory cytokines or chemokines. The inflammaomse are mainly composed of nucleotide-binding and oligomerization domain-like receptor (NLR), with apoptosis-associated speck like proteins containing a C-terminal caspase recruitment domain (CARD) (D'Arpa & Leung, 2017). They have a key role in innate immunity and are activated in response to stress, cell damage, tissue injury and infection (Sierawska et al., 2022). Recently, it has been shown that NLRP3 upregulation is positively correlated with mortality in burns, suggesting that NLRP3 could have an important function during the acute phase of burn injury (Stanojcic et al., 2014; Vinaik et al., 2018). Severe burns not only cause inflammation but also induce metabolic changes such as hyperglycaemia, hyperinsulinemia, and hyperlipidaemia that stimulate the NLRP3 inflammasome (Stanojcic et al., 2014). NLRP3 oligomerization recruits ASC and pro-caspase-1, part of the cysteine protease family to form a complex. The cleavage of active caspase-1 transforms pro-IL-1β and pro-IL-18 to their mature and biologically active forms (Artlett, 2012; Sayan & Mossman, 2016). The production of circulatory IL-1β affects the metabolic state of the tissues and increases insulin signalling and insulin resistance in stress-induced diabetes patients with burn injuries, which results in increased mortality (Stanojcic et al., 2014). Moreover, IL-1β is involved in extracellular matrix remodelling and fibrogenesis. Notably, IL-1β is overexpressed in the early inflammatory phase of wound healing and increased in impaired wound repair and hypertrophic scar formation (Salgado et al., 2012; Sierawska et al., 2022). It has been reported that classically activated macrophages secrete NLRP3 and induce the release of proinflammatory cytokine IL-1β, chemokine CCL2 and growth factors VEGF, FGF2, and TGFβ1, leading to the activation of the proliferative healing phase of burn wounds (Vinaik et al., 2020). These cellular events and processes are known to happen at least in part

via Cx43 and its associated hemichannels (Coutinho et al., 2020; Coutinho et al., 2005; Delvaeye et al., 2019; Feng et al., 2020; Gilmartin et al., 2016; Mugisho, Green, et al., 2019). Downregulating Cx43 in the mouse burn model has been shown to reduce neutrophil accumulation, improve wound closure rate and prevent burn progression (Coutinho et al., 2005). In brain injury, radiation injury, and heart ischaemia, it has been demonstrated that downregulating Cx43 or blocking these channels can slow the spread of the death signals and stop healthy neighbouring cells from undergoing apoptosis (Du et al., 2017; Frantseva et al., 2002; Lin et al., 1998; Mancuso et al., 2011). Moreover, blocking of hemichannels with mimetic peptides has been shown to accelerate wound healing and enhance cell proliferation in *in vitro* skin models (Faniku et al., 2018), *ex vivo* skin models (Pollok et al., 2011) and human dermal fibroblasts *in vitro* under hyperglycaemic/hyperinsulinemia conditions (Wright et al., 2012). Furthermore, release of extracellular ATP from Cx43 hemichannels triggers P2X7 activation in tubular epithelial cells, which was shown to be blocked with Cx43 mimetic peptides (Xu et al., 2022). Blocking Cx43 hemichannels with Tonabersat has the potential to reduce inflammation, restore and improve overall functionality in retinal eye disease (Kim, Griffin, Nor, et al., 2017; Louie et al., 2021; Mat Nor et al., 2020; Mugisho, Rupenthal, et al., 2019). In light of this, early downregulation of Cx43 function or expression may be beneficial for the prevention of burn progression and improving wound healing.

4.1.1 Hypothesis

My hypothesis is that: Early intervention by reducing burn injury induced Cx43 expression in zone of stasis with Cx43asODN or Tonabersat prevents burn progression and improves rat burn wound healing.Aims

To test my hypothesis, I characterised a rat burn model (55°C, 10 s burn exposure) and treated it with Cx43 targeted therapeutics, Cx43asODN or Tonabersat. The latter is a small molecule drug that has been previously demonstrated to target Cx43 gap junction and hemichannels. The effect of Cx43asODN or Tonabersat were analysed by investigating two broad components of the response:

1. Immunostaining analysis was conducted to assess the Cx43 and protein hemichannel expression along with P2X7 and markers of NLRP3 inflammasome complex and inflammatory response in zone of stasis during the early phase of burn wound healing,

2. Analysis of skin fibrosis markers and histological analysis of collagen content and nascent epidermal thickness in rat burn injury.

4.2 Results

4.2.1 Cx43 Targeted therapeutics reduced the macroscopic burn wound size

As the burn wound heals, a scab forms on top of the wound region and obscures the actual size of the wound. Hence, it is difficult to determine the size of wound for analysis from macroscopic images. However, from gross observation, I observed a reduced red ring of inflammation in wounds treated with either AS-300 or Tona-100 on PBD 7. At PBD 21, I observed that the scab formation in wounds treated with AS-300 or Tona-100 was smaller compared to UN and Veh wounds (Figure 4.1).

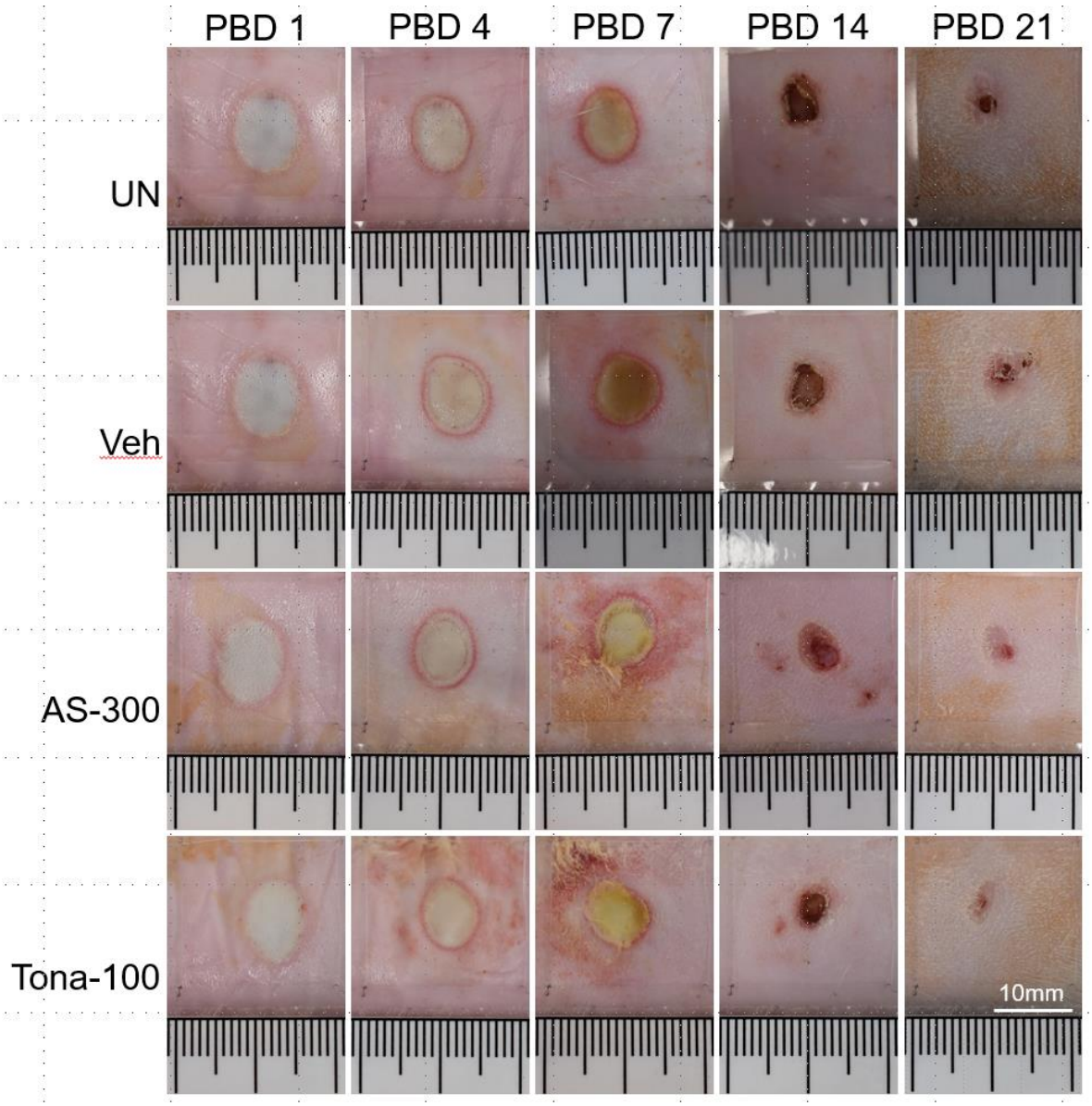

Figure 4.1 Cx43 targeted therapeutics reduced burn injury in the rat burn model.
Representative macroscopic images of burn injury on the rat burn model on PBD 1, 4, 7, 14 & 21. UN – untreated wound, Veh – Vehicle control wound, AS-300 – Cx43asODN 300µm treated wounds, Tona-100 – Tonabersat 100µm treated wounds. Scale bar: 10mm

4.2.2 Cx43 targeted therapeutics reduced Cx43 protein expression in the zone of stasis

First, I confirmed there was an increase in Cx43 protein expression in the zone of stasis as a pathological response to rat burn injury. Then the use of Cx43asODN 300μM (AS-300) or Tonabersat 100μM (Tona-100) as a topical treatment was explored to investigate the role of Cx43 in the zone of stasis.

Upon burn wound injury, there was a significant increase in Cx43 protein levels compared to normal skin (NS) ($p<0.001$) on PBD 1 and it remained elevated on PBD 4 ($p<0.0001$) and 7 ($p<0.0001$) (Figure 4.2). Cx43 appears as puncta in the plasma membrane. At PBD 1, I observed that Cx43 protein levels were significantly reduced in the zone of stasis of wounds that were treated with AS-300 ($p<0.01$) or Tona-100 ($p<0.05$) compared to Veh control (Figure 4.2 b & e). On PBD 4, we observed a significant reduction in Cx43 protein level in AS-300 and Tona-100 treated groups compared to UN wounds ($p<0.001$). Even though there is no significant difference between the Veh and treated wounds, it important to note that the reduction in Cx43 protein expression levels were maintained on PBD 4 (Figure 4.2 c & e). In addition, the sustained delivery of topical application of either AS-300 or Tona-100, significantly reduced Cx43 protein expression on PBD 7 when compared with UN and Veh ($p<0.01$) (Figure 4.2d & e). The reduction of Cx43 protein level was observed in both immune cells and fibroblasts in the zone of stasis with treatment in AS-300 or Tona-100.

In summary, these observations indicate that the treatment with either AS-300 or Tona-100 can reduce the pathological increase of Cx43 protein levels in the zone of stasis.

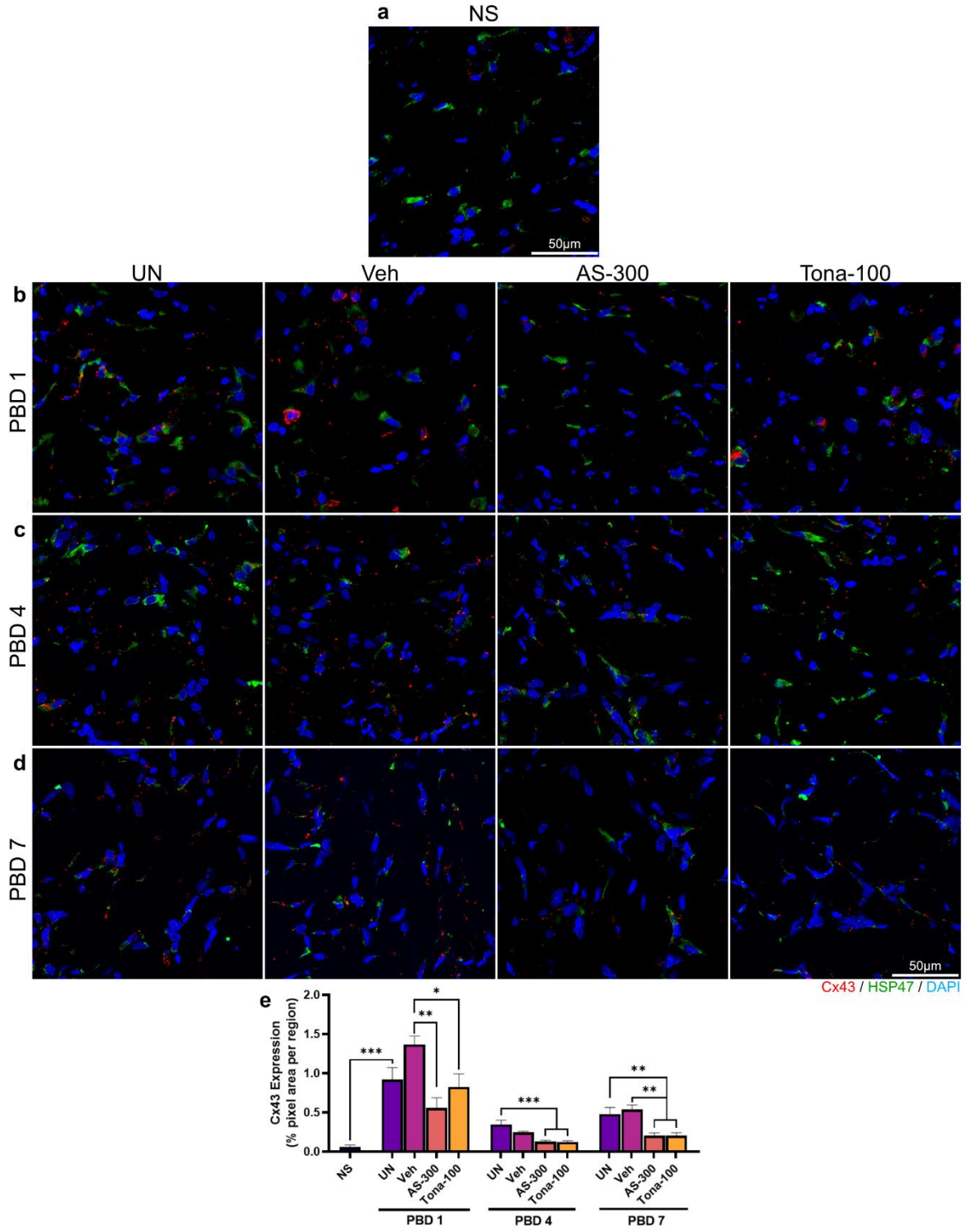

Figure 4.2 Cx43 targeted therapeutics significantly reduced Cx43 protein expression in zone of stasis on PBD 1, 4 & 7.

(a) Representative immunofluorescence images of Cx43 expression in normal skin (NS) Cx43 labelled in red and dermal fibroblasts labelled with HSP47 in green. (b) The panel shows representative immunofluorescence images of Cx43 protein expression in cells in zone of stasis at PBD 1 (NS: n=6, UN: n=5, Veh: n=6, AS-300: n=5, Tona-100: n=6). (c) The panel shows representative immunofluorescence images of Cx43 protein expression in zone of stasis at PBD

4 (n=6 animals per group). (d) The panel shows representative immunofluorescence images of Cx43 protein expression in zone of stasis at PBD 7 (n=6 animals per group). Magnification used: 63X. Scale bar: 50µm. UN – untreated wound, Veh – Vehicle control wound, AS-300 – Cx43asODN 300µM treated wounds, Tona-100 – Tonabersat 100µM treated wounds. (e) Image analysis graph shows an increased expression between NS vs UN on PBD 1, 4, & 7. Image analysis reveals lower Cx43 protein expression in the zone of stasis of treated (AS-300, Tona-100) compared to the UN and Veh control groups on PBD 1, 4 & 7. Data is presented as mean value ± S.E.M. Statistical comparisons were made using a One-way ANOVA. (*$p<0.05$, **$p<0.01$ & ***$p<0.001$).

4.2.3 Reduced hemichannel expression in zone of stasis observed on PBD 7

After confirming that the AS-300 and Tona-100 were able to reduce Cx43 expression in the zone of stasis, I then explored hemichannel expression in the zone of stasis on PBD 1, 4 & 7 (Figure 4.3). The hemichannel antibody (AB3000, Table 2.5) is custom made generated from peptides covering the extracellular loop region, E1 of Cx43 between amino acid residues 42 and 61, sequence: ESAWGDEQSAFRCNTQQPGC (Glass, 2014). As gap junctions are tightly regulated channels with a limited interchannel space, the hemichannel antibody cannot get access to epitopes located in the gap junctional plaques (Riquelme et al., 2013). Hemichannel antibody gives strong perinuclear reactivity with vesicular, fine intracellular punctate staining that appears to be a dust-like feature compared to the larger puncta of Cx43 gap junctions recognized with Cx43 antibody (Siller-Jackson et al., 2008). Upon wound injury on PBD 1, hemichannel expression in the zone of stasis of UN treated wounds did not reduce as compared to NS ($p=0.1542$). However, the hemichannel expression was significantly elevated on PBD 4 & 7 ($p<0.0001$ & $p<0.001$, respectively) (Figure 4.3 a, c, d & e). On PBD 1 and 4, there was no difference between treatment and controls (Figure 4.3 c & e). On PBD 7, there was a significant reduction in hemichannel expression in the wounds treated with AS-300 and Tona-100 compared to UN in the zone of stasis ($p<0.01$). However, there was no difference between

the Veh and AS-300 or Tona-100 in the zone of stasis was ($p=0.9215$ & $p=0.9108$, respectively) (Figure 4.3 d & e). Overall, these observations suggest that the treatment with AS-300 and Tona-100 has reduced the pathological increase in hemichannel expression in the zone of stasis.

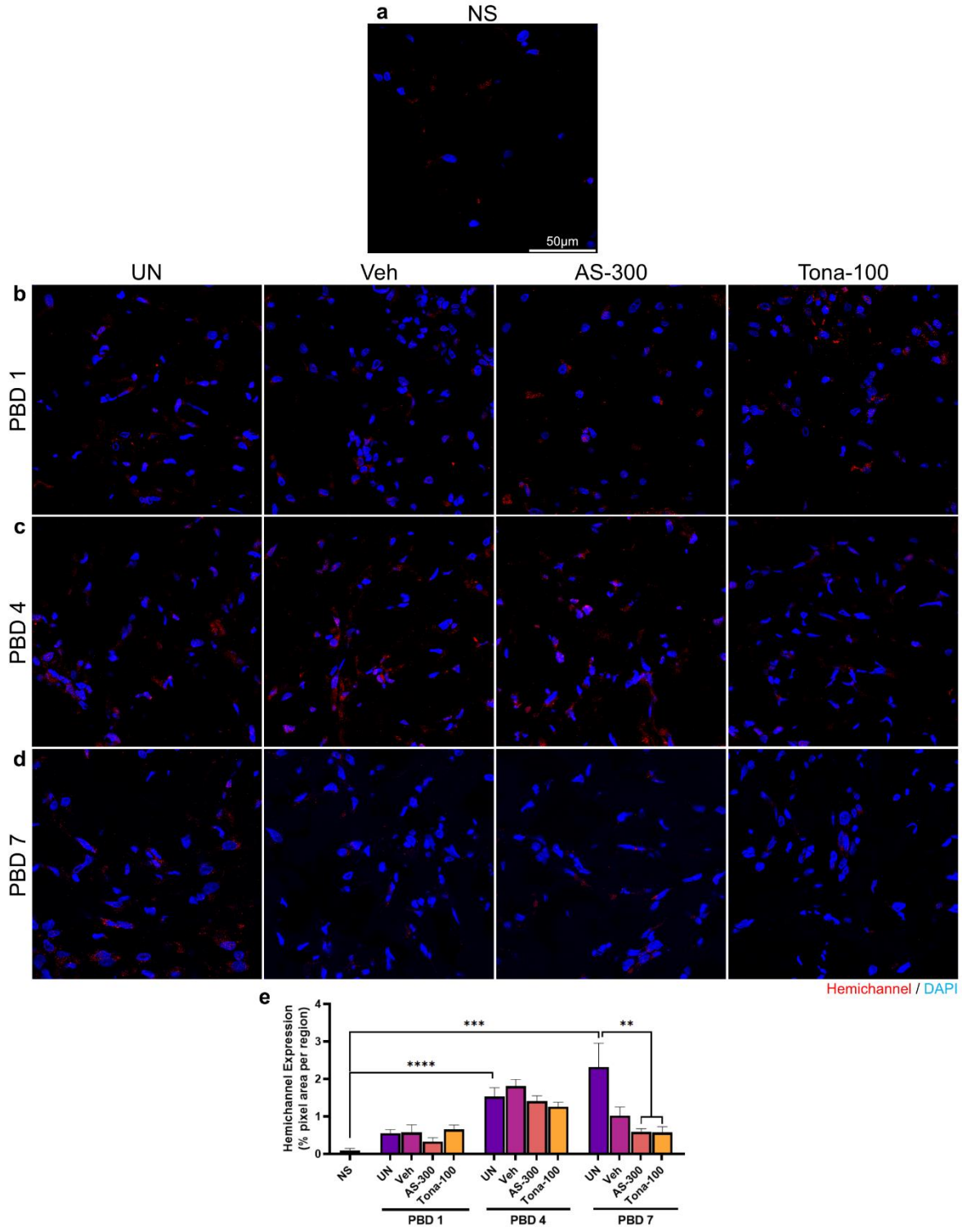

Figure 4.3 Cx43 targeted therapeutics significantly reduced hemichannel protein expression in zone of stasis on PBD 7.

(a) Representative immunofluorescence image of hemichannel expression in normal skin (NS). (b) The panel shows representative immunofluorescence images of hemichannel protein expression in cells in zone of stasis at PBD 1 (NS: n=5, UN: n=6, Veh: n=6, AS-300: n=6, Tona-100: n=6 animals per group) . (c) The panel shows representative immunofluorescence

images of hemichannel protein expression in zone of stasis at PBD 4 (UN: n=5, Veh: n=6, AS-300: n=6, Tona-100: n=6 animals per group). (d) The panel shows representative immunofluorescence images of hemichannel protein expression in zone of stasis at PBD 7 (n=6 animals per group). Magnification used: 63X. Scale bar: 50µm. UN – untreated wound, Veh – Vehicle control wound, AS-300 – Cx43asODN 300µM treated wounds, Tona-100 – Tonabersat 100µM treated wounds. (e) Image analysis graph shows an increased expression between NS vs UN on PBD 1, 4, & 7. Image analysis reveals lower Cx43 protein expression in the zone of stasis of treated (AS-300, Tona-100) compared to the UN and Veh control groups on PBD 1, 4, & 7. Data is presented as mean value ± S.E.M. Statistical comparisons were made using a One-way ANOVA. (*$p<0.05$, **$p<0.01$, ***$p<0.001$ & ****$p<0.0001$).

4.2.4 NLRP3 inflammasome complex activation significantly reduced on PBD 4 in treated wounds with Cx43 targeted therapeutics

To investigate if the NLRP3 inflammasome complex is activated and Cx43 targeted therapeutics have an effect on targeting the inflammasome complex, I investigated the expression of NLRP3, Cas-1 and IL-1β in the zone of stasis (Figure 4.4, Figure 4.5 & Figure 4.6). Upon activation of NLRP3, it exits the endoplasmic reticulum and enters the cytoplasm to form the inflammasome complex. I analysed the cytoplasmic NLRP3 expression in the zone of stasis. Upon rat burn injury, I observed that there was slightly increased in NLRP3 expression in UN wounds as compared to NS on PBD1, 4 and 7, though it was not significant ($p=0.6595$, $p=0.8239$ and $p=0.3284$, respectively) (Figure 4.4 a, b, c & e). I then analysed the expression of NLRP3 between the control group and treatments. I observed that there was slight but insignificant decrease in NLRP3 expression in the zone of stasis of wounds treated with AS-300 as compared to UN and Veh controls on PBD 1 ($p=0.5034$ and $p=0.3233$, respectively) (Figure 4.4 b & e). This pattern was also observed on PBD 4 AS-300 treated group as compared to UN ($p=0.7876$). However, AS-300 was significantly reduced than Veh ($p<0.05$) (Figure 4.4 c & e). On PBD 7, there was no significant difference between the AS-300 and control groups on PBD 7 (Figure 4.4 d & e). Wounds treated with Tona-100 did not appear to affect NLRP3 expression when compared to UN ($p=0.9868$) and Veh ($p=0.9239$) on PBD 1 (Figure 4.4 b & e). On PBD 4, there was a significant reduction between Tona-100 treated wounds than Veh control ($p<0.05$) (Figure 4.4c & e). On PBD 7, Tona-100 treated wounds had a significant decrease in NLRP3 expression as compared to UN wounds ($p<0.05$). However, there was no difference between Tona-100 treated wounds and Veh control wounds (Figure 4.4 d & e).

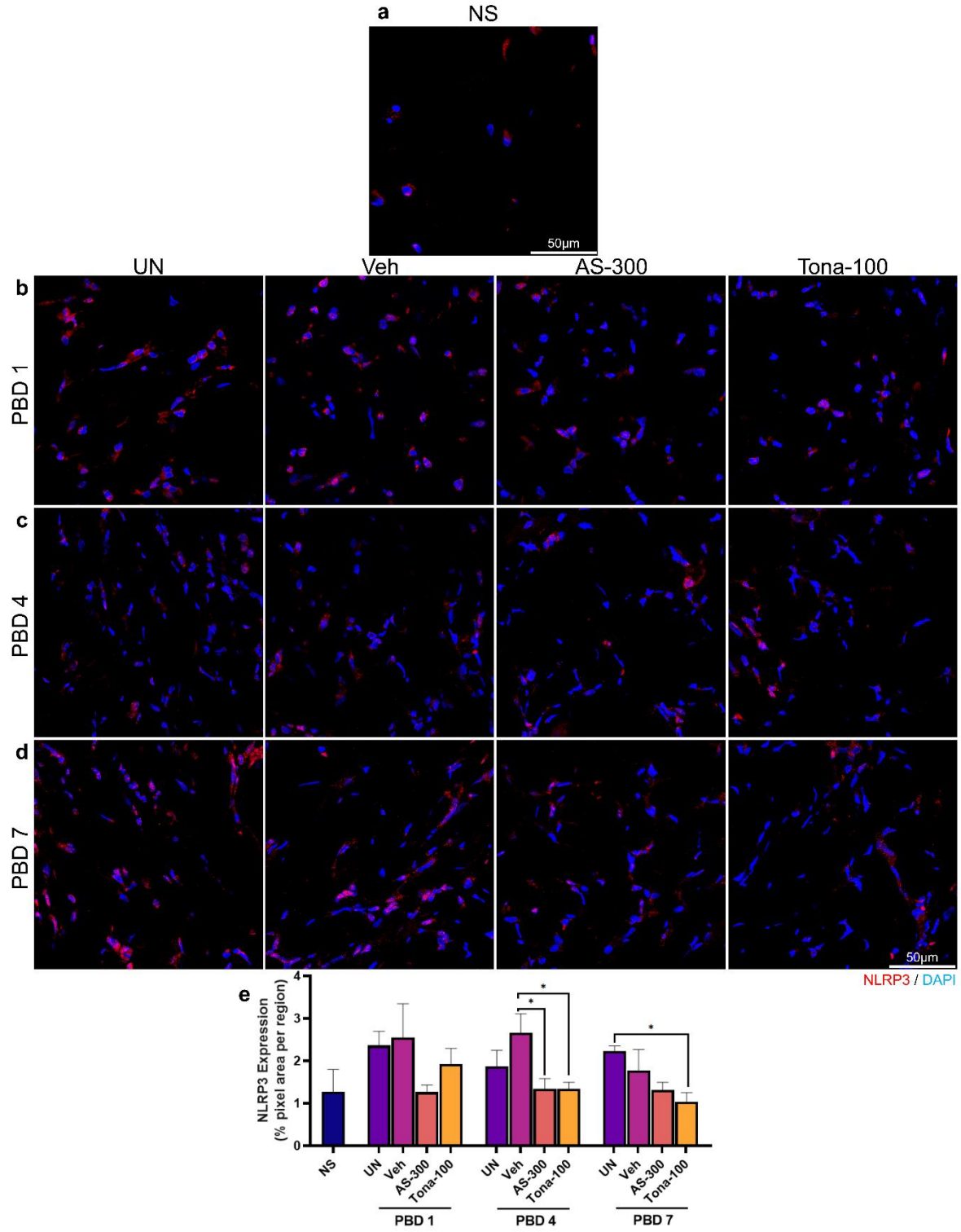

Figure 4.4 Cx43 targeted therapeutics significantly reduced NLRP3 protein expression in zone of stasis on PBD 1, 4 & 7.

(a) Representative immunofluorescence image of NLRP3 expression in normal skin (NS). (b) The panel shows representative immunofluorescence images of NLRP3 expression in cells in zone of stasis at PBD 1 (n=6 animals per group). (c) The panel shows representative immunofluorescence images of NLRP3 expression in zone of stasis at PBD 4 (n=6 animals per

group). (d) The panel shows representative immunofluorescence of NLRP3 in zone of stasis at PBD 7 (n=6 animals per group). Magnification used: 63X. Scale bar: 50µm. UN – untreated wound, Veh – Vehicle control wound, AS-300 – Cx43asODN 300µM treated wounds, Tona-100 – Tonabersat 100µM treated wounds. (e) Image analysis graph represents cytoplasmic NLRP3 expression on PBD 1, 4, & 7 is reduced in AS-300 and Tona-100 treated wounds in the zone of stasis as compared to UN and Veh. Data is presented as mean value ± S.E.M. Statistical comparisons were made using a One-way ANOVA. (*$p<0.05$).

During the NLRP3 inflammasome complex formation, Cas-1 is recruited and tightly regulated and subsequently result in secretion of mature IL-1β. Here I observed that upon rat burn injury, there was an increase in Cas-1 expression in UN wounds as compared to NS on PBD 1, though it was not significant ($p=0.1068$) (Figure 4.5 a, b & e). In addition, no difference in Cas-1 expression was observed between control and treated groups on PBD 1 (Figure 4.5 b & e). On PBD 4, there was a significant increase in Cas-1 expression in the zone of stasis in UN wounds ($p<0.01$) (Figure 4.5 c & e). On PBD 4, AS-300 and Tona-100 had a significant decrease in Cas-1 expression as compared to UN ($p<0.05$ & $p<0.001$, respectively) and Veh control ($p<0.05$ & $p<0.01$, respectively) (Figure 4.5 c & e). On PBD 7, there was no difference between treated and control groups (Figure 4.5 d & e).

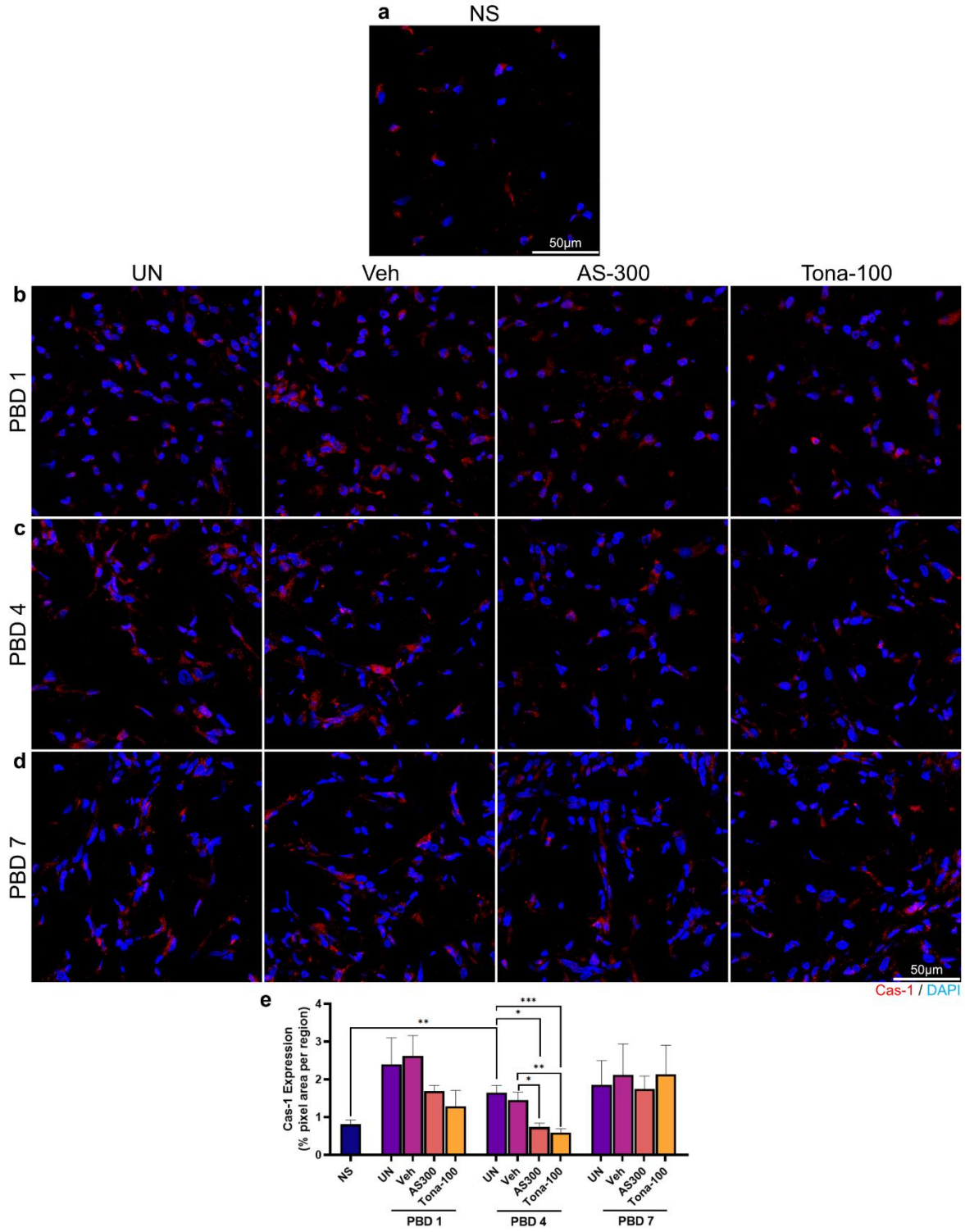

Figure 4.5 Cx43 targeted therapeutics significantly reduced Cas-1 protein expression in zone of stasis on PBD 1, 4 & 7.

(a) The panel shows a representative immunofluorescence image of Cx43 expression in cells of normal skin (NS). (b) The panel shows representative immunofluorescence images of Cas-1 expression in zone of stasis at PBD 1 (n=6 animals per group). (c) The panel shows

representative immunofluorescence images of Cas-1 expression in zone of stasis at PBD 4 (n=6 animals per group). (d) The panel shows representative immunofluorescence of Cas-1 in zone of stasis at PBD 7 (n=6 animals per group). Magnification used: 63X. Scale bar: 50µm. UN – untreated wound, Veh – Vehicle control wound, AS-300 – Cx43asODN 300µM treated wounds, Tona-100 – Tonabersat 100µM treated wounds. (e) Image analysis graph represents Cas-1 expression on PBD 1, 4, & 7 is reduced in AS-300 and Tona-100 treated wounds in the zone of stasis as compared to UN and Veh. Data is presented as mean value ± S.E.M. Statistical comparisons were made using a One-way ANOVA. (*$p<0.05$, **$p<0.01$ & ***$p<0.001$).

Following the activation of Cas-1, I investigated the release of mature forms of IL-1β. Here, I observed that upon rat burn injury, there was significant increase in IL-1β expression in UN wounds as compared to NS on PBD 1, 4 & 7 ($p<0.01$, 0.01 & 0.05, respectively) (Figure 4.6). However, no changes in IL-1β expression was observed between control and treated groups on PBD 1 (Figure 4.6 b & e). On PBD 4, AS-300 had a significant reduction compared to UN and Veh wounds ($p<0.05$) and Tona-100 had slightreduction in IL-1β was observed from control groups ($p=0.1010$ and $p= 0.0631$) (Figure 4.6 c & e). On PBD 7, AS-300 treatment has a slight reduction in IL-1β than UN ($p=0.3471$) (Figure 4.6 d & e). However, Tona-100 did not have an effect on IL-1β on PBD 7 as compared to UN and Veh (Figure 4.6 d & e).

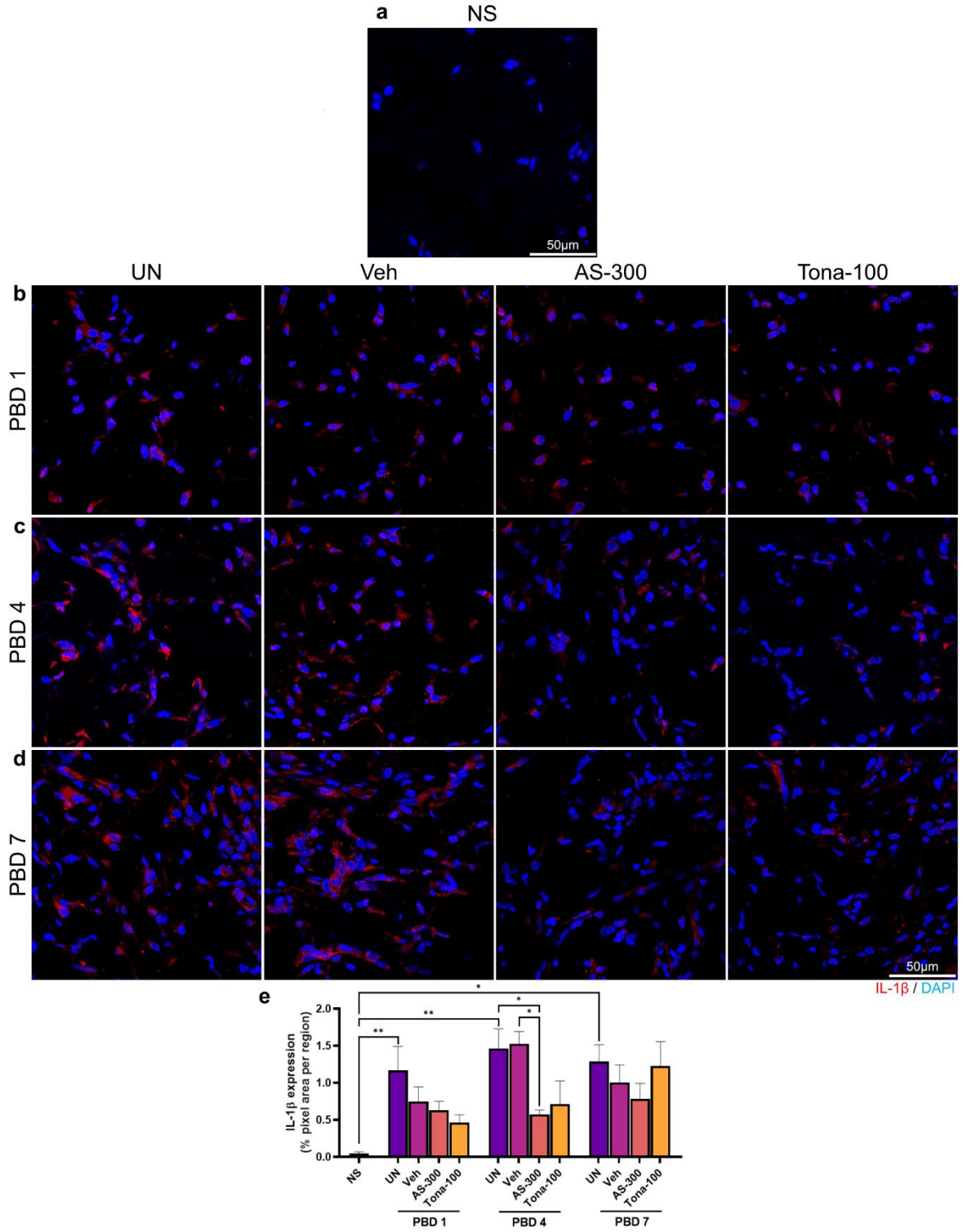

Figure 4.6 Cx43 targeted therapeutics significantly reduced IL-1β protein expression in zone of stasis on PBD 1, 4 & 7.

(a) The panel shows representative immunofluorescence image of IL-1β expression in cells in normal skin (NS) (b) The panel shows representative immunofluorescence images of IL-1β expression in cells in zone of stasis at PBD 1(NS: n=4, UN: n=6, Veh: n=6, AS-300: n=6,

Tona-100: n=6 animals per group). (c) The panel shows representative immunofluorescence images of IL-1β expression in zone of stasis at PBD 4 (n=6 animals per group). (d) The panel shows representative immunofluorescence of IL-1β in zone of stasis at PBD 7 (n=6 animals per group). Magnification used: 63X. Scale bar: 50µm. UN – untreated wound, Veh – Vehicle control wound, AS-300 – Cx43asODN 300µM treated wounds, Tona-100 – Tonabersat 100µM treated wounds. (e) Image analysis graph represents IL-1β expression on PBD 1, 4, & 7 is reduced in AS-300 and Tona-100 treated wounds in the zone of stasis as compared to UN and Veh. Data is presented as mean value ± S.E.M. Statistical comparisons were made using a One-way ANOVA. (*$p<0.05$, **$p<0.01$).

4.2.5 Significant increase in P2X7 expression in the zone of stasis upon burn injury

ATP release via Cx43 binds to P2X7 purinergic receptors and activates the NLRP3 inflammasome complex. I investigated whether Cx43 might have a direct link to P2X7. Immunofluorescence analysis showed that there was a significant increase of P2X7 expression in the zone of stasis following rat burn injury ($p<0.001$) on PBD 1 and 4 (Figure 4.7 a, b & e). Treatment with AS-300 marginally reduced P2X7 expression in the zone of stasis as compared to UN and Veh controls on PBD 1 ($p=0.6939$ and $p=0.6589$, respectively). Similarly, treatment with Tona-100 appear to marginally reduce the P2X7 expression in the zone of stasis as compared to UN and Veh controls on PBD 1 ($p=0.5342$ and $p=0.4990$, respectively). On PBD 4 and 7, there was no significant difference between the treated and control groups (Figure 4.7).

In summary, these results indicate that there is involvement of the activation of NLRP3 inflammasome complex in rat burn injury and this is abolished during early phase of wound treatment with Cx43 antisense oligodeoxynucleotide or Tonabersat treated wounds.

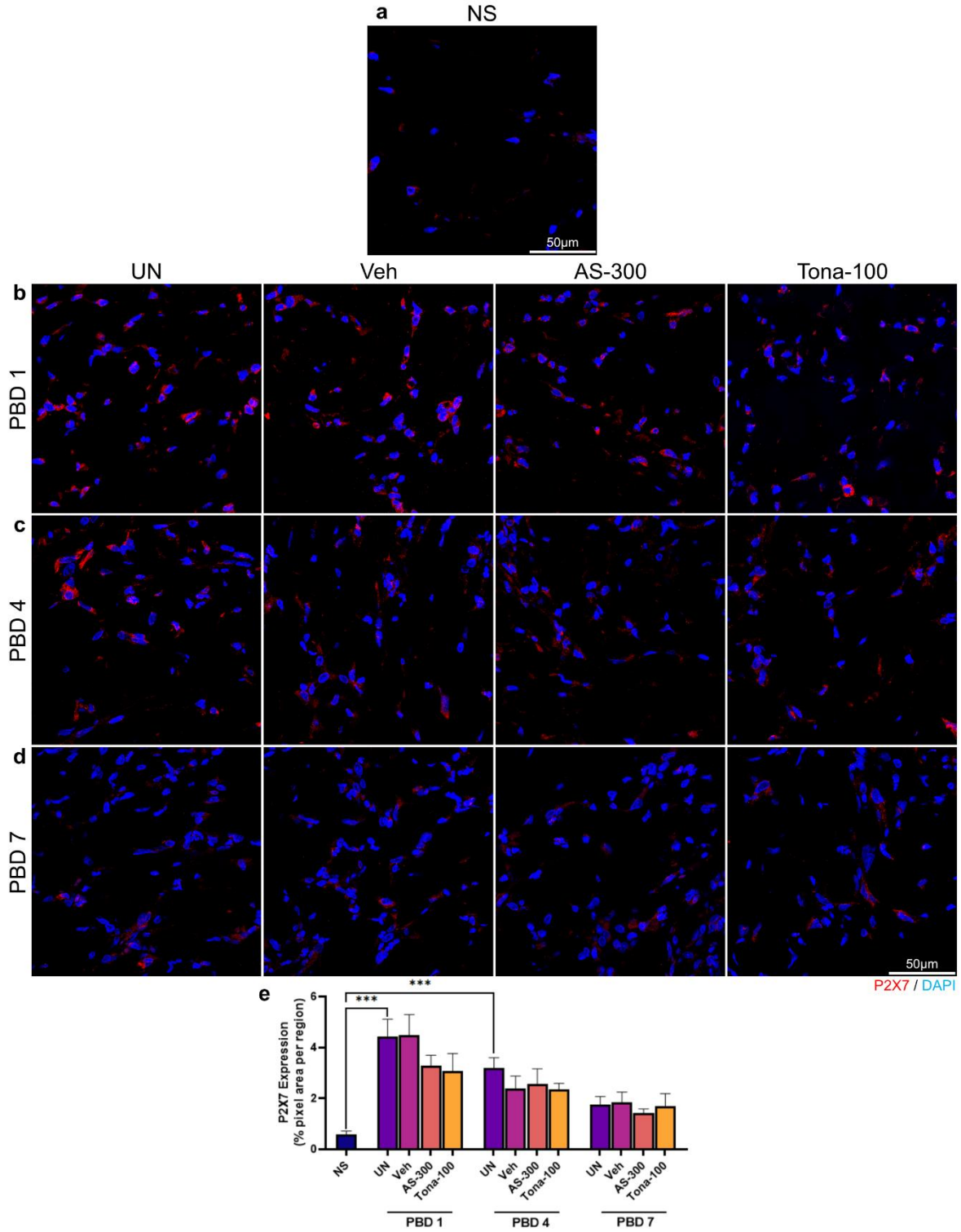

Figure 4.7 Cx43 targeted therapeutics marginally reduced P2X7 protein expression in zone of stasison PBD 1, and subsequently did not change protein expression on PBD 4 & 7.

(a) The panel shows representative immunofluorescence image of P2X7 expression in cells in normal skin (NS) (b) The panel shows representative immunofluorescence images of P2X7

expression in cells in zone of stasis at PBD 1 (n=6 animals per group). (c) The panel shows representative immunofluorescence images of P2X7 expression in zone of stasis at PBD 4 (n=6 animals per group). (d) The panel shows representative immunofluorescence of P2X7 in zone of stasis at PBD 7 (n=6 animals per group). Magnification used: 63X. Scale bar: 50µm. UN – untreated wound, Veh – Vehicle control wound, AS-300 – Cx43asODN 300µM treated wounds, Tona-100 – Tonabersat 100µM treated wounds. (e) Image analysis graph represents P2X7expression on PBD 1, 4, & 7 is reduced in AS-300 and Tona-100 treated wounds in the zone of stasis as compared to UN and Veh. Data is presented as mean value ± S.E.M. Statistical comparisons were made using a One-way ANOVA. (***$p<0.001$).

4.2.6 Cx43 Targeted therapeutics reduced inflammation in the zone of stasis

To investigate the infiltration of leukocytes in the zone of stasis, MPO and CD68 were used as markers for neutrophils and macrophages respectively. Upon wound injury, there was the significant increase in percentage of MPO positive cells in the zone of stasis in UN wounds when compared to NS at PBD 1 ($p<0.0001$) and this remained elevated on PBD 4 ($p<0.0001$) and 7 ($p<0.0001$) (Figure 4.8). Following treatment with AS-300 or Tona-100, the percentage of MPO positive cells were significantly reduced compared to Veh control on PBD 1 ($p<0.05$ and $p<0.01$, respectively) (Figure 4.8 b & e). On PBD 4, the percentage of MPO positive cells in AS-300 and Tona-100 was sustained when compared to Veh ($p<0.01$ and $p<0.05$, respectively), but this was insignificant when compared with UN control (Figure 4.8 c & e). Moreover, on PBD 7, the percentage of MPO positive cells were reduced in AS-300 and Tona-100 when compared with Veh control ($p<0.001$ and $p<0.01$, respectively) (Figure 4.8 d & e). In addition, on PBD 7, the number of MPO cells for AS-300 and Tona-100 were significantly reduced compared to UN control ($p<0.05$ and $p<0.001$ respectively) (Figure 4.8 d & e). I quantified the percentage of CD68 positive macrophages and observed that there was a significant increase upon burn wound injury (UN) when compared to NS on PBD 1 ($p<0.05$) and a persistent increase on PBD 4 and 7 ($p<0.0001$ and $p<0.001$, respectively) (Figure 4.8). Interestingly, I observed that there was an increase in the percentage of CD68 positive macrophages in AS-300 from UN and Veh controls and there was a significant increase in CD68 positive macrophages in Tona-100 treated wounds than UN ($p<0.001$) (Figure 4.8 b & e). On PBD 4, AS-300 and Tona-100 treated wounds had significantly increased CD68 positive macrophages as compared to Veh control ($p<0.001$) (Figure 4.8 c & e). However, on PBD 7, there was no significant difference between the treated groups and controls (Figure 4.8 d & e).

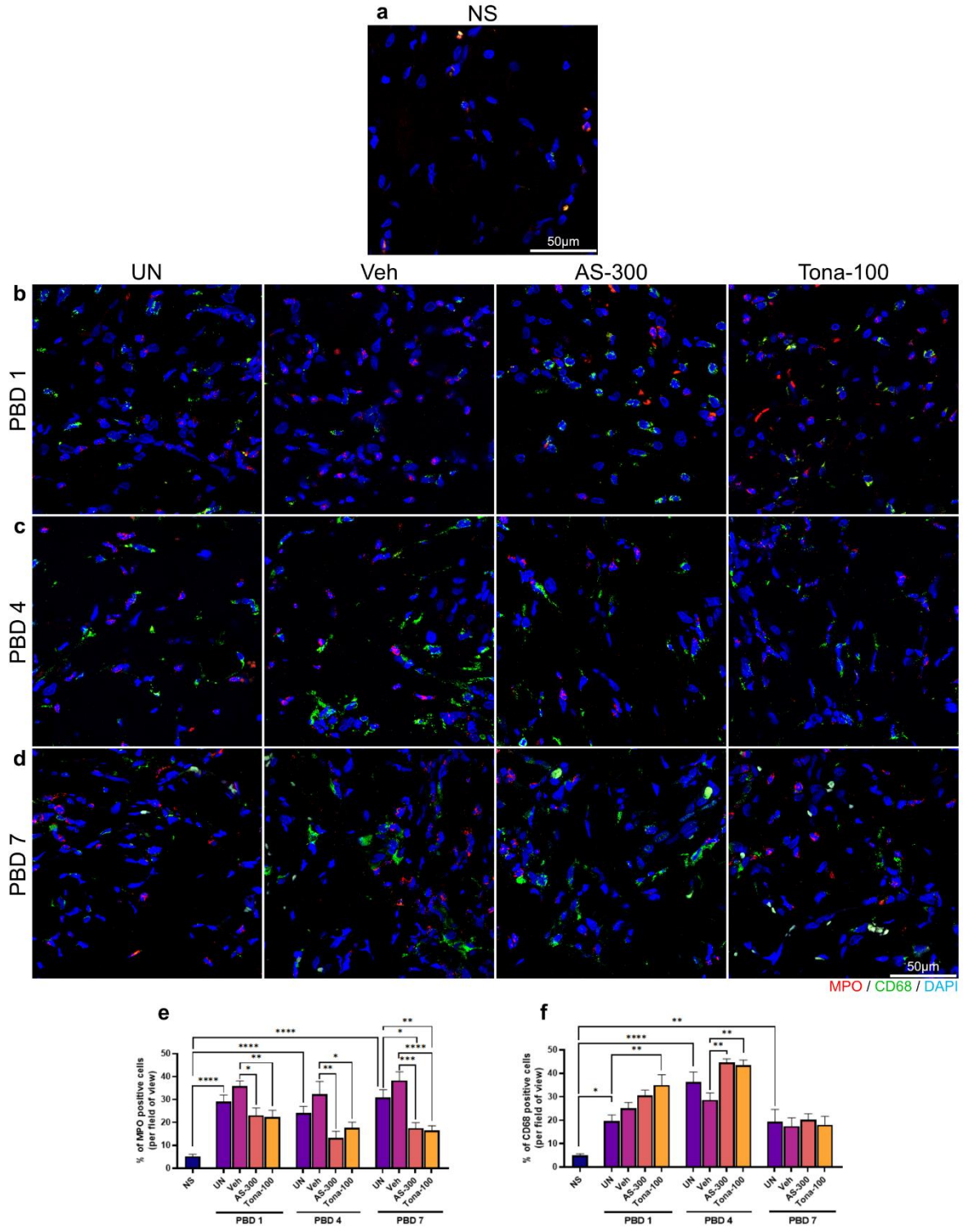

Figure 4.8 Cx43 targeted therapeutics significantly reduced inflammatory response in zone of stasis on PBD 1, 4 & 7.

(a) Representative image of MPO (red) & CD68 (green) positive cells in normal skin (NS). (b) The panel shows representative immunofluorescence images of MPO and CD68 positive cells in cells in zone of stasis at PBD 1 (n=6 animals per group). (c) The panel shows representative

immunofluorescence images of MPO and CD68 positive cells in zone of stasis at PBD 4 (n=6 animals per group). (d) The panel shows representative immunofluorescence of MPO and CD68 positive cells in zone of stasis at PBD 7 (n=6 animals per group). Magnification used: 63X. Scale bar: 50µm. UN – untreated wound, Veh – Vehicle control wound, AS-300 – Cx43asODN 300µM treated wounds, Tona-100 – Tonabersat 100µM treated wounds. (e) Image analysis graph shows an increased percentage of MPO positive cells between NS vs UN on PBD 1, 4, & 7. Image analysis reveals lower percentage of MPO positive cells in the zone of stasis of treated (AS-300, Tona-100) (n=6) compared to the UN and Veh control groups (n=6) on PBD 1, 4, & 7. (f) Image analysis graph shows an increase in the percentage of CD68 positive cells on PBD 1 & 4 in AS-300 and Tona-100 treated wounds in the zone of stasis. On PBD 7, there was no difference in the percentage of CD68 positive cells between control groups (UN & Veh) and treated groups (AS-300 & Tona-100). Data is presented as mean value ± S.E.M. Statistical comparisons were made using a One-way ANOVA. (*$p<0.05$, **$p<0.01$, ***$p<0.001$ & ****$p<0.0001$).

4.2.7 Skin fibrosis and ECM degradation markers were reduced in Cx43asODN and Tonabersat treated wounds

Increased NLRP3 inflammasome activation results in fibrosis in kidney disease. To determine whether skin fibrosis is increased in rat burn injury, αSMA, HSP47 & MMP-9 were investigated (Figure 4.9 & Figure 4.10). Three ROIs from the centre of a burn wound were analysed as shown on Figure 2.10. On PBD 14, I observed that there was increased αSMA expression in rat burn injury as shown in UN wounds compared to NS ($p<0.05$, Figure 4.9 a & b). After treatment with AS-300 the expression of αSMA was slightly reduced on PBD 14 when compared to Veh ($p=0.2990$) (Figure 4.9 a & b). On PBD 21, there was a significant reduction in αSMA expression in wounds treated with AS-300 compared to Veh control ($p<0.001$) (Figure 4.9 a & d). Similarly, this pattern in αSMA expression was observed in wounds treated with Tona-100 on PBD 14 and PBD 21 ($p<0.05$) (Figure 4.9 b & d).

When I assessed for HSP47 expression, I observed that wounds treated with AS-300 had slight reduction in HSP47 expression on PBD 14 compared with UN and Veh controls ($p=0.2491$ and $p=0.3000$, respectively) (Figure 4.9 a & c). On PBD 21, there was a slight reductionn in HSP47 expression in wounds treated with AS-300 as compared to UN ($p=0.1153$) and a significant reduction when compared to Veh ($p<0.0001$) (Figure 4.9 e). In contrast, there was no difference in HSP47 expression in wounds treated with Tona-100 on PBD 14 and PBD 21 as compared to UN or Veh (Figure 4.9 a, c & e).

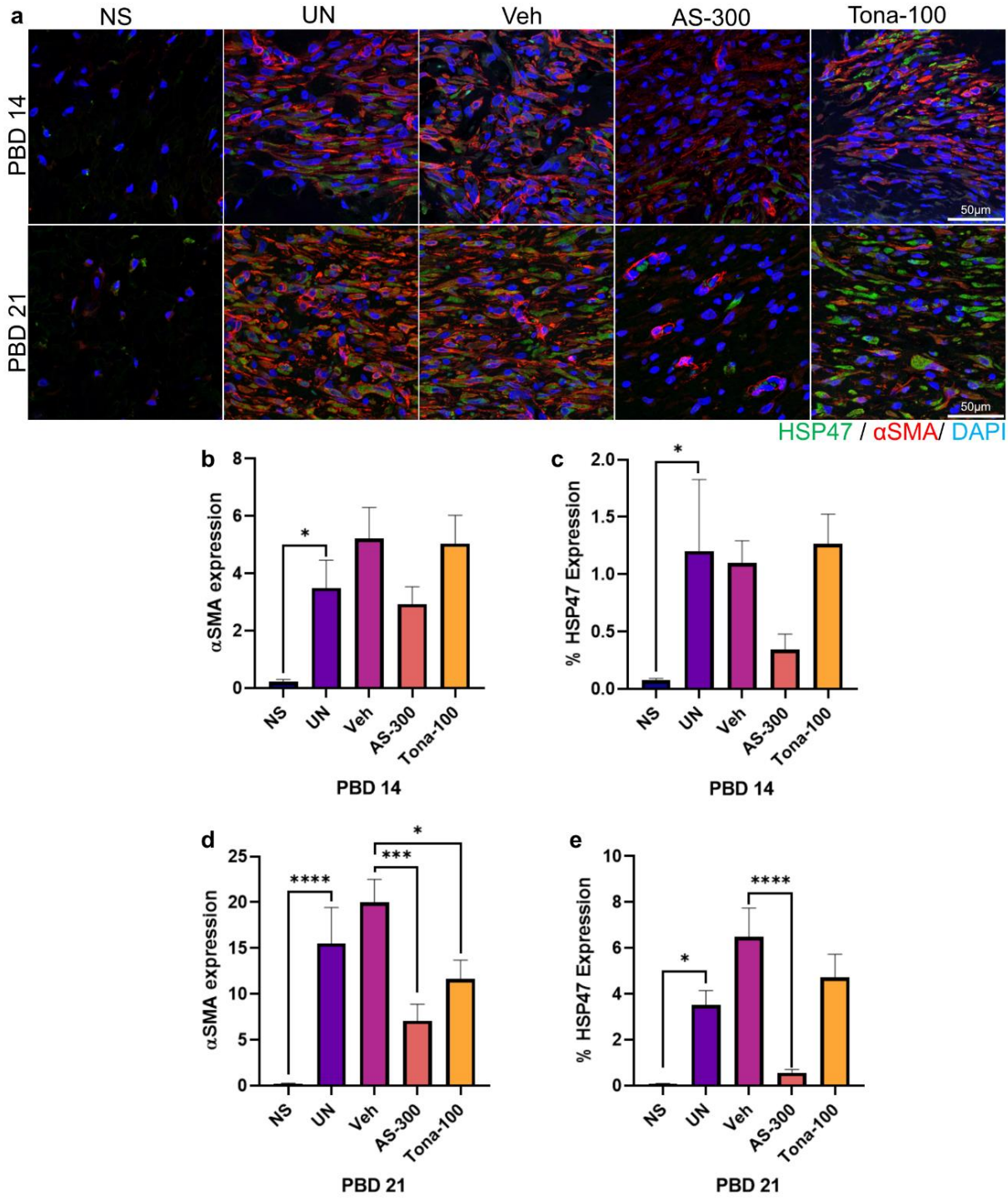

Figure 4.9 Cx43 targeted therapeutics mildly reduced skin fibrosis markers αSMA and HSP47 expression in zone of stasis on PBD 14 and PBD 21.

(a) The panel shows representative immunofluorescence images of co-immunofluorescence protein expression of αSMA (red) and HSP47 (green) expression in cells located in the centre of wound bed on PBD 14 & PBD 21 (n=6) Magnification used: 63X. Scale bar: 50µm. UN – untreated wound, Veh – Vehicle control wound, AS-300 – Cx43asODN 300µM treated wounds, Tona-100 – Tonabersat 100µM treated wounds. (b) Image analysis graph represents

expression of αSMA on PBD 14 in UN, Veh, AS-300 and Tona-100 treated wounds (n=6). (c) Image analysis graph represents expression of HSP47 on PBD 14 in UN, Veh, AS-300 and Tona-100 treated wounds (n=6). (d) Image analysis graph represents expression of αSMA on PBD 21 in UN, Veh, AS-300 and Tona-100 treated wounds (n=6). (e) Image analysis graph represents expression of HSP47 on PBD 21 in UN, Veh, AS-300 and Tona-100 treated wounds (n=6). Data is presented as mean value ± S.E.M. Statistical comparisons were made using a One-way ANOVA. (*$p<0.05$, **$p<0.01$, ***$p<0.001$ & ****$p<0.0001$).

Overexpression of MMP-9 results in degradation of extracellular matrix. When I assessed MMP-9 expression, I observed that on PBD 14, MMP-9 protein levels in wounds treated with AS-300 and Tona-100 did not alter as compared to UN and Veh controls (Figure 4.10 a, b & d). On PBD 21, AS-300 and Tona-100 had slight reduction in MMP-9 expression as compared to Veh group ($p=0.1542$ and $p=0.7480$, respectively) (Figure 4.10 a, c & e).

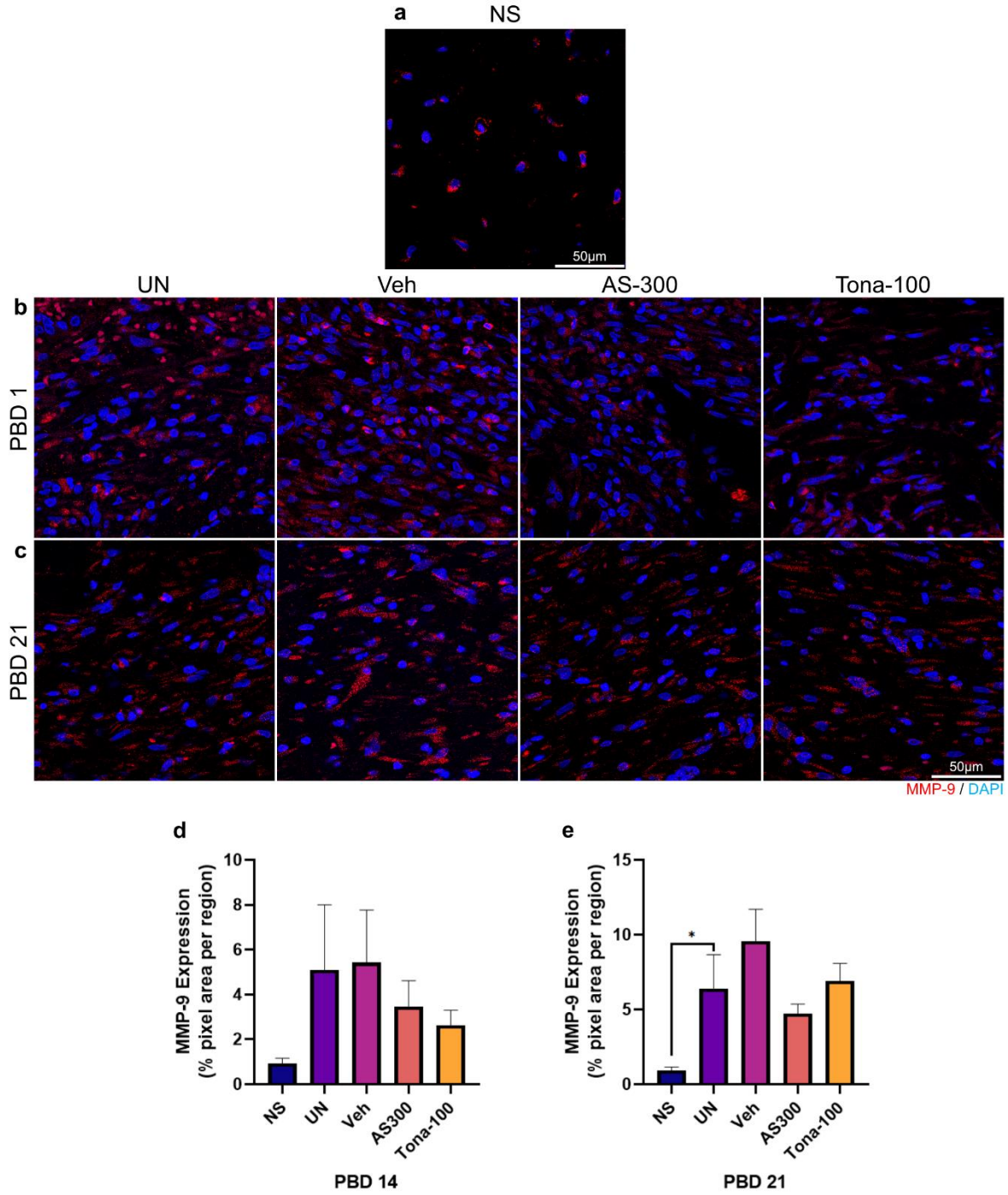

Figure 4.10 Cx43 targeted therapeutics significantly MMP-9 expression in zone of stasis on PBD 14 and PBD 21.

(a) Representative image of MMP-9 expression in normal skin (NS) (b) The panel shows representative immunofluorescence images immunofluorescence protein expression MMP-9 expression in cells located in the centre of wound bed on PBD 14. (c) The panel shows representative immunofluorescence images immunofluorescence protein expression MMP-9

expression in cells located in the centre of wound bed on PBD 21 (n=6) Magnification used: 63X. Scale bar: 50µm. UN – untreated wound, Veh – Vehicle control wound, AS-300 – Cx43asODN 300µM treated wounds, Tona-100 – Tonabersat 100µM treated wounds. (d) Image analysis graph represents expression of MMP-9 on PBD 14 in UN, Veh, AS-300 and Tona-100 treated wounds (n=6). (e) Image analysis graph represents expression of MMP-9 on PBD 21 in UN, Veh, AS-300 and Tona-100 treated wounds (n=6). Data is presented as mean value ± S.E.M. Statistical comparisons were made using a One-way ANOVA. (*$p<0.05$).

4.2.8 Increase in collagen content was observed in rat burn wounds treated with Cx43 therapeutics

To assess the quality of collagen content in rat burn wounds, I performed H&E, Masson's Trichrome, and Picrosirius Red staining on PBD 21 burn wounds (Figure 4.11 & Figure 4.12). Histological observations of Masson's Trichrome and Picrosirius red staining revealed increased dense collagen deposition in wounds treated with AS-300 and Tona-100 as compared to UN and Veh control groups (Figure 4.11 & Figure 4.12). In addition, number of cells in the region of interest dropped significantly on PBD21 in wounds treated with AS-300 and Tona-100 showing more mature granulation tissue (Figure 4.11 & Figure 4.12). Quantification of percentage area of collagen content using Masson's Trichrome stained tissues in the upper dermis that received thermal injury. I observed that the wounds treated with AS-300 and Tona-100 had a significantly increased percentage area of collagen when compared to Veh control ($p<0.001$ and $p<0.05$, respectively). AS-300 treated wounds had a significant increase in percentage of collagen content compared to UN wounds on PBD 21 ($p<0.001$) (Figure 4.12 b, c & d). Studies have reported that collagen I:III is lower in wounds compared to normal skin (Xue & Jackson, 2015). The collagen I:III ratio is dramatically reduced by the biofilm-mediated collagenolytic environment in the wound, which also impairs the biomechanical qualities of the regenerated skin and may make it more susceptible to subsequent wounds (Roy et al., 2020). Type III collagen is expressed in early granulation tissues in cutaneous wound repair which is replaced with Type I collagen later. Using this ratio, we can understand that the amount of Collagen I to Collagen III in wounds. Poor formation of collagen structures during wound repair is evaluated based on the decrease in collagen I:III ratio. I performed qPCR to analyse mRNA level of Collagen I:III ratio normalised to normal skin. I observed that there was an increase in collagen I:III ratio in wounds treated with AS-300 and Tona-100 as compared to UN and Veh control wounds (Figure 4.12 e).

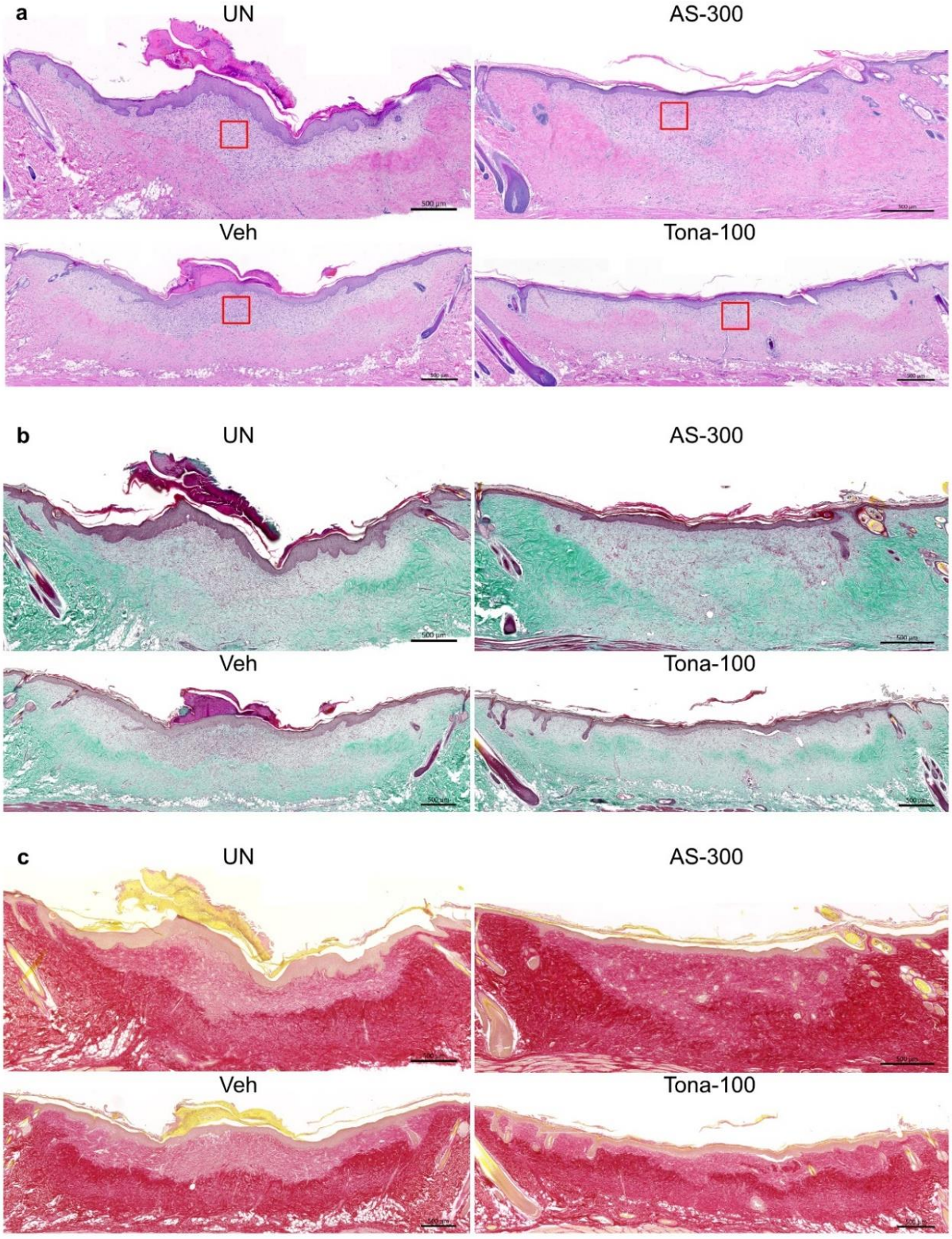

Figure 4.11 Cx43 targeted therapeutics improved collagen content in rat burn injury on PBD 21.

(a) The panel shows representative H&E images of rat burn injury on PBD 21 of UN – untreated wound, Veh – Vehicle control wound, AS-300 – Cx43asODN 300µM treated wounds, Tona-100 – Tonabersat 100µM treated wounds. Red box indicates area of zoomed

images of centre of wound bed in Figure 4.12. (b) The panel shows representative images of Masson's Trichrome staining of UN, Veh, AS-300 & Tona-100 sister sections on PBD 21. (c) The panel shows representative images of Picrosirius Red staining of UN, Veh, AS-300 & Tona-100 sister sections on PBD 21. Scale bar: 500μm.

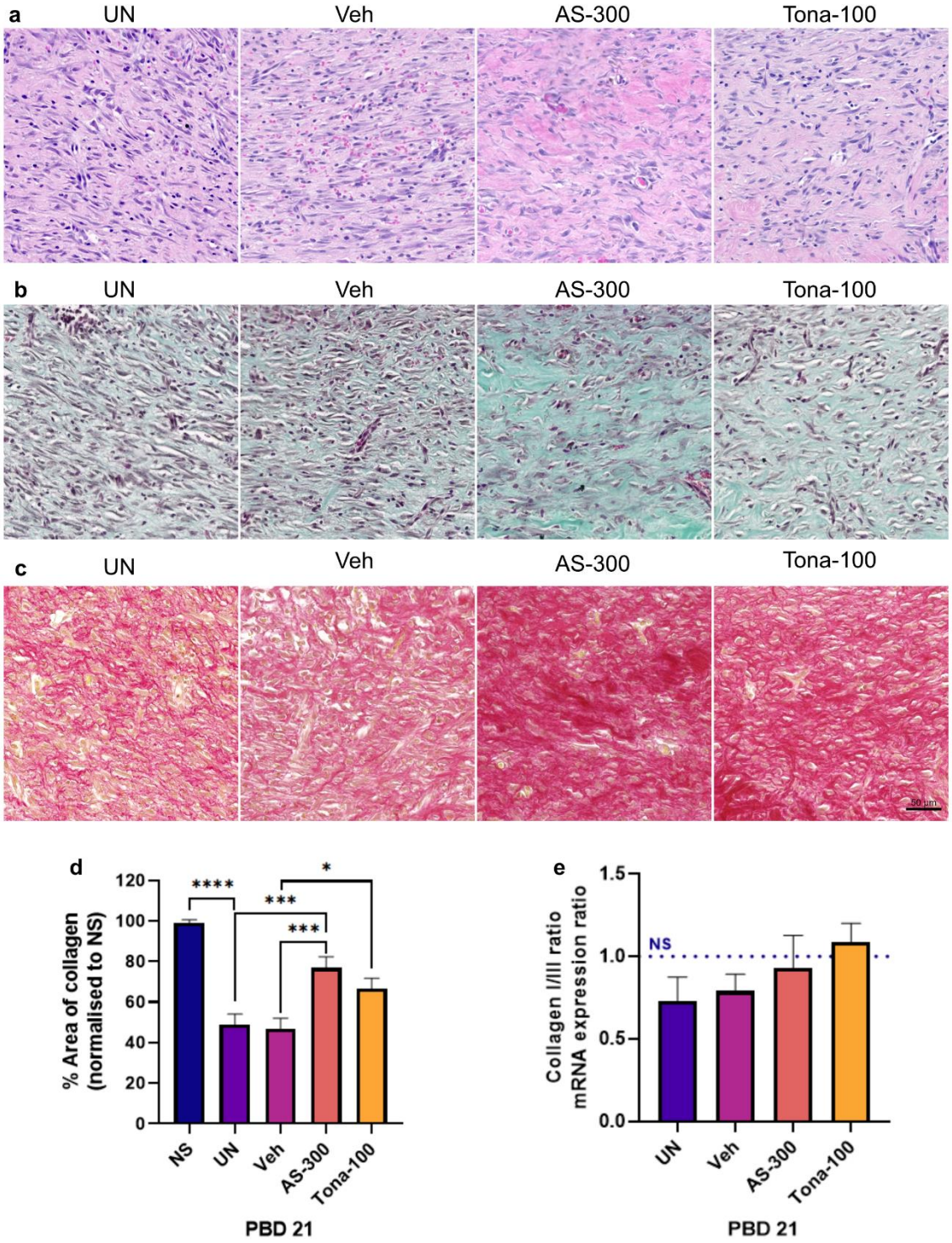

Figure 4.12 Histological evaluation of Cx43 targeted therapeutics improved collagen content in rat burn injury on PBD 21.

(a) H&E images of zoomed images taken from centre of wound bed (b) Masson's Trichrome images of zoomed images taken from centre of wound bed. Staining: Collagen—green; nuclei—black; muscle fibres and cytoplasm—red. (c) Picrosirius Red images of zoomed

images taken from centre of wound bed. Staining: Collagen – red. (d) Image analysis graph represents percentage area of collagen content of NS and wounds of UN, Veh, AS-300 and Tona-100 on PBD 21. (e) qPCR analysis of ratio of collagen I:III UN, Veh, AS-300 and Tona-100 treated wounds. NS is represented as normalised dotted line in blue (n=6). Data is presented as mean value ± S.E.M. Statistical comparisons were made using a One-way ANOVA. (*p<0.05, **p<0.01, ***p<0.001 & ****p<0.0001).

4.2.9 Significant reduction in nascent epidermal thickness in treated burn wounds at PBD 21

When I assessed the rate of re-epithelialisation, I observed that there was no significant difference between controls and treatment groups on both PBD 14 and 21 (Figure 4.13 b). Here I measured the thickness of nascent epidermis (Figure 4.13 c). I observed that there is a significant decrease in nascent epidermal thickness in wounds treated with AS-300 and Tona-100 when compared to UN ($p<0.0001$). This was also observed when the treatment groups were assessed with Veh ($p<0.001$ and $p<0.0001$, respectively) (Figure 4.13 a & c).

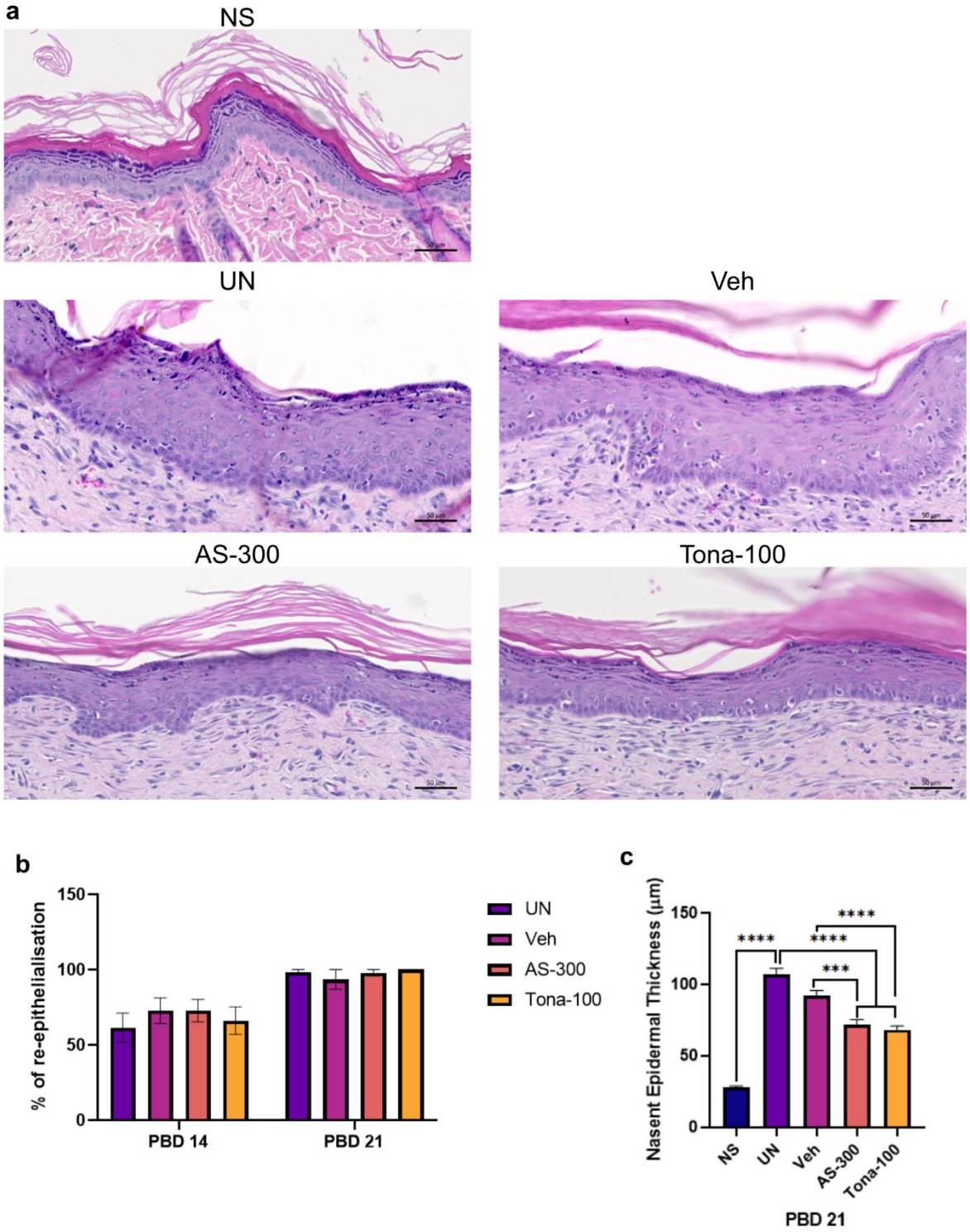

Figure 4.13 Cx43 targeted therapeutics reduced nascent epidermal thickness in rat burn injury on PBD 21.

(a) The panel shows representative H&E images normal skin (NS) epidermis and nascent epidermis UN – untreated wound, Veh – Vehicle control wound, AS-300 – Cx43asODN 300µM treated wounds, Tona-100 – Tonabersat 100µM treated wounds. on PBD 21. (n=6) Scale bar: 50µm. (b) Image analysis of rate of re-epithelialisation in rat burn injury of UN, Veh, AS-300 and Tona-100 (n=6). (c) Image analysis of normal skin epidermis thickness (NS)

and nascent epidermis thickness of wound of UN, Veh, AS-300 and Tona-100 on PBD 21. Ten regions of interest across the epidermis were quantified (n=10, N=6). Data is presented as mean value ± S.E.M. Statistical comparisons were made using a One-way ANOVA. (*p<0.05, **p<0.01, ***p<0.001 & ****p<0.0001).

4.3 Discussion

4.3.1 Summary of key findings:

Four consecutive days of treatment with either AS-300 or Tona-100 topical application, resulted in the prevention of 1) increase in Cx43 and hemichannel protein expression, 2) reduction in immune cell infiltration, 3) reduction of NLRP3, Cas-1 & IL-1β inflammasome complex protein expression, 4) reduced αSMA, HSP47 & MMP-9, 5) improved collagen content, faster maturation of the wounds as shown by reduced cellularity in granulation tissues and reduced nascent epidermal thickness.

In this chapter, I explored the use of the therapeutics AS-300 or Tona-100 in the rat burn model. The results will be discussed in two main parts: 1) prevention of upregulated Cx43 and hemichannels in the zone of stasis in the early phase of burn wound healing, 2) effect of Cx43 downregulation on NLRP3 inflammasome activation and histological observations.

4.3.2 Connexins in burn injury

During the early phases of burn wound healing, pathological increase in Cx43 protein levels in the zone of stasis were evident. At one day post burn, the highest Cx43 protein levels were observed in the zone of stasis. Subsequently, these elevated Cx43 levels were slightly dampened on PBD 4 and 7. Using a marker for dermal fibroblasts (Kuroda & Tajima, 2004), I was able to tease out that the expression of Cx43 was localised in dermal fibroblasts and inflammatory cells, but predominantly in the latter. This is consistent with our previous work on Cx43 expression in the human burn zone of stasis (Feng et al., 2020). Visualization of co-stained sections of MPO/CD68 inflammatory cells and H&E sister sections allowed me to speculate that Cx43 expression is predominantly in inflammatory cells in the stasis zone (Figure 4.2). Similar results have been reported in other studies of Cx43 expression in

neutrophils and macrophages (Brandner et al., 2004; Cogliati et al., 2015; Kameritsch & Pogoda, 2020; Rodjakovic et al., 2021).

Increased Cx43 expression has been reported in cutaneous injuries such as chronic wounds (Becker et al., 2012; Sutcliffe et al., 2015), pressure ulcers (Kwek et al., 2021), *ex vivo* diabetic skin (Pollok et al., 2011), and burns (Coutinho et al., 2005; Feng et al., 2020). These studies, however, did not distinguish hemichannels and Cx43 gap junctions. In this study, I specifically examine the expression of hemichannels in burn injuries with the aid of the Cx43 hemichannel antibody that detects the E1 domain of Cx43, amino acid between 42 and 61 (Figure 4.3) (Glass, 2014). The localisation of hemichannels appears to be a dust-like feature (Figure 4.3) compared to the larger puncta of Cx43 gap junctions (Figure 4.2). These findings demonstrate that the hemichannel expression was increased in the zone of stasis during the early phase of burn wound injury, with significantly elevated expression on PBD 4 and 7. Similar to Cx43 expression, hemichannel expression appeared to be predominantly in inflammatory cells and slightly lower in dermal fibroblasts. An increase in Cx43 hemichannel expression is reported in *in vitro* and *in vivo* models of amyotrophic lateral sclerosis (ALS) (Almad et al., 2022).

Four consecutive days of treatment with Cx43asODN or Tonabersat markedly reduced Cx43 and hemichannel expression in the zone of stasis during the early phase of wound healing. Comparable results were reported in a mouse model of partial thickness burn injury treated with single application of Cx43asODN (Coutinho et al., 2005) and skin ischaemia reperfusion in murine model (Glass, 2014) which correlated with reduced extent of tissue damage and reduced inflammatory response. Tonabersat was first used in animal models of migraine with aura, in which Cx26 expression was inhibited in the brain via activating the p38-mitogen-activated protein kinase pathway and antagonizing transient neuronal hyperexcitability linked

to cortical spreading depression (Damodaram et al., 2009). However, later it was discovered that Tonabersat is not Cx26 specific and could inhibit Cx43 hemichannel pathological opening (Kim, Griffin, Nor, et al., 2017). Treatment with Tonabersat in low doses blocked hemichannels and inhibited ATP release, while higher doses of Tonabersat reduced Cx43 gap junctional coupling via the lysosomal pathway in central nervous system injuries (Kim, Griffin, Nor, et al., 2017). This was evident in these findings whereby hemichannel expression was not altered on PBD 1 and 4. However, gap junctional Cx43 expression was reduced in Tonabersat treated group. In addition, similar findings were also reported in Tonabersat treated human induced pluripotent stem cell–derived astrocytes from both familial and sporadic ALS (Almad et al., 2022). Administration of Tonabersat to ALS mice model protected motor neurons while reactive astrocytosis and microgliosis were decreased. (Almad et al., 2022). Furthermore, a study conducted by Louie and colleagues, demonstrated that Tonabersat Cx43 hemichannels in a human *ex vivo* model of diabetic retinopathy and inhibited NLRP3 inflammasome activation (Louie et al., 2021). These findings support the hypothesis that Cx43 gap junction and hemichannel expression is elevated in zone of stasis and upon treatment with Cx43 targeted therapeutics the protein levels are downregulated. Kim and colleagues showed that low concentrations of Tonabersat acts primarily and directly on connexin hemichannel to reduce channel opening and inhibit ATP release without altering the protein levels of Cx43, while higher doses of Tonabersat reduced Cx43 gap junctional coupling (Kim, Griffin, Nor, et al., 2017). Although, I did not observe a change in hemichannel expression during early burn wound healing, blocking Cx43 hemichannels with Tonabersat may have inhibited ATP release. In addition, reduced Cx43 protein expression in Tonabersat treated rat burn wounds may suggest decoupling of Cx43 gap junctions via lysosomal pathway and improved wound healing outcomes as proposed by Kim and colleagues (Kim, Griffin, Nor, et al., 2017).

4.3.3 P2X7 and NLRP3 Inflammasome activation in rat burn injury

Our data demonstrate that upregulation of Cx43 expression in a rat burn injury triggers the NLRP3 inflammasome complex activation via the P2X7 receptor. First, I observed an increase in P2X7 expression during the early phase of burn injury, as expressed in the zone of stasis (Figure 4.7). Following this, NLRP3, Cas-1 and IL-1β expression also increased in the zone of stasis (Figure 4.4, Figure 4.5 & Figure 4.6). These findings may suggest that the Cx43/P2X7 mediated NLRP3 pathway is activated in the zone of stasis. Treatment with Cx43asODN or Tonabersat in our rat burn injury, revealed that P2X7 expression was marginally decreased on PBD 1, and subsequently, there was no difference in controls and treatments on PBD 4 & 7. However, NLRP3, Cas-1 and IL-1β expression were reduced on PBD 1 and 4, with no effect on PBD 7.

The persistent opening of pathological hemichannels mediates the release of extracellular ATP. Numerous studies have demonstrated that extracellular ATP triggers the P2 purinergic receptors such as P2X4, P2X7 and P2Y 12, as a physiological cellular communication resulting in a flux of Na^{+}, Ca^{2+} and K^{+} ions across the pore (Acosta et al., 2021; Lohman & Isakson, 2014; Mugisho, Rupenthal, et al., 2019). More commonly, a strong association has been established between Cx43 hemichannels and P2X7 receptors (Xu et al., 2022; Zhu et al., 2021). However, no studies that I am aware of, have shown this link in burn injury. Although, I did not measure ATP release from our rat burn wounds specifically, studies have shown that ATP is elevated during the early hours of burn injury and contributes to burn progression (Bayliss et al., 2014). In this study, I demonstrated that increased Cx43 hemichannel and P2X7 protein levels were found in the zone of stasis upon burn wound injury. This may suggest the possibility of change in P2X7 activity with altered ATP release from Cx43 hemichannels. Treatment with Cx43asODN or Tonabersat, reduced the expression of Cx43 hemichannels in the zone of stasis.

However, P2X7 expression was marginally reduced during early burn wound healing and subsequently did not reduce with Cx43 targeted therapeutics in the zone of stasis on PBD 4 & 7. Cx43asODN prevents the gap junctional channels from forming in the first place as less protein translation occurs. By doing so, it distrupts the direct cell to cell communcation. Where as, Tonabersat blocks ATP release from hemichannels, and from already formed channels. Xu and colleagues reported that the release of extracellular ATP from Cx43 hemichannels triggers P2X7 activation in tubular epithelial cells (Xu et al., 2022). Additionally, blockade of the Cx43 hemichannel using a mimetic peptide Gap26 reduced ATP release (Pearson et al., 2005). This suggests that downregulating hemichannel expression reduced P2X7 activation. It is important to note that the expression of the P2X7 protein levels alone may not be a reliable proxy to determine its activity. Functional assays are required such as calcium influx assays or fluorescent dye uptake assays to measure specific cellular responses or events triggered by P2X7 receptor. However, it is generally more challenging to perform these assays directly in tissues or in vivo due to the complexities and limitations of working with whole organisms. Immunohistochemistry or immunofluorescence are useful techniques to detect the presence of P2X7 receptors in tissue sections. While these techniques do not directly measure activity, they provide information about receptor expression and localization within tissues.

Increasing evidence has indicated that P2X7 activation leads to NLRP3 inflammasome complex activation via ASC and caspase-1 recruitment and activation, producing increased levels of mature IL-1β in models of diabetic retinopathy, liver fibrosis and neuroinflammation (Albalawi et al., 2017; Kong et al., 2022; Tao et al., 2020). In addition, Lu and colleagues have demonstrated that ATP can be released from Cx43 hemichannels in cardiac fibroblasts and can activate P2Y2 and subsequent profibrotic genes (Lu et al., 2012) and trigger the NLRP3 inflammasome complex in retinal pigment epithelial cells during hypoxic conditions (Doktor

et al., 2018). Similarly, another report demonstrated elevated Cx43 increased ATP-sensitive P2Y1 receptor expression levels in mouse spinal cord astrocytes (Suadicani et al., 2003). In this study, I demonstrated that P2X7 protein levels was mostly increased on PBD 1 and marginally downregulated with Cx43 targeted therapeutics, and subsequently no difference was observed between treated and control groups. Treatment also reduced NLRP3 and its components in the zone of stasis. However, elevated NLRP3, Cas-1 and IL-1β on PBD 4 could suggest that other P2 purinergic family members may play a role in the inflammasome activation via Cx43.

Burn injuries cause immediate cell death by necrosis, apoptosis, or necroptosis, which causes ATP release and intracellular damage associated molecular patterns (DAMPs) to be secreted (McNamara et al., 2010; Reddy et al., 2015; Singer et al., 2008). Many studies have shown that Cx43 gap junctions and hemichannel are involved in the cell death processes (Contreras et al., 2004; Decrock et al., 2009; Rodriguez-Sinovas et al., 2007). DAMPs from various intracellular compartments may be released during these kinds of cell death and enter the extracellular space (Pantalone et al., 2021). The production of DAMPs can activate Toll-receptors and upregulate the transcription of NLRP3 inflammasome elements by activating nuclear factor-kappa B (NF-κB). DAMPs can also cause the synthesis of ROS, which in turn can cause the NLRP3 inflammasome to become active and produce IL-1β (Q. Ye et al., 2021). Xu and colleagues reported that depletion of Cx43 or using Cx43 inhibitors reduced fibrosis and inflammation in tubular epithelial cells from mice with unilateral ureteral obstruction (UUO) induced renal injury. The release of extracellular ATP, which serves as DAMPs, from tubular epithelial cells drives the development of macrophage inflammasomes and kickstarts pyroptosis via the P2X7 receptors after UUO. In addition, the macrophage pyroptosis induced fibrosis related chemokine CXCL10 expression and aggravated the progression of UUO-induced renal fibrosis

(Xu et al., 2022). Blocking Cx43 hemichannels with Gap26 peptide, attenuated αSMA positive cells in the treated UUO group and prevented renal interstitial fibrosis (Xu et al., 2022). The cell death pathways in this study were not investigated, but it can be postulated that these processes may have contributed to the continued activation of the NLRP3 inflammasome via the Cx43 hemichannels or gap junctions.

Burn injury causes increased production of Ca^{2+} leading to mitochondrial stress and ROS production (Parihar et al., 2008).This process is known to be regulated by Cx43 gap junction intercellular communication (Roger et al., 2022). In a study using rat alveolar epithelial cells, it was shown that Ca^{2+} waves propagating through gap junctions were increased when the cells were stimulated mechanically or with ATP (Isakson et al., 2001). Increase in intracellular Ca^{2+} influx or ER calcium was shown to activate the NLRP3 inflammasome and increase production of IL-1β (Zhong et al., 2013). Here it can be speculated that there is a possibility of the NLRP3 inflammasome activation being triggered via gap junctional communication.

In this study, it was shown that with Cx43asODN treatment both gap junctional Cx43 expressionand hemichannel expression was downregulated in rat burn injury. There is a possibility that Cx43asODN could be effective at reducing both the Cx43 hemichannel ATP release mediated NLRP3 inflammation and Cx43 gap junctional intercellular communication medicated NLRP3 inflammasome activation in rat burn injury. Tonabersat treatment reduced hemichannel and P2X7 expression in rat burn injury. In addition, 100μM Tonabersat has been shown to reduce Cx43 gap junctional protein. This finding is consistent with Kim et al., whereby prolonged treatment with higher concentration of Tonabersat (> 100 μM) uncoupled gap junctions with junctional plaques internalized and degraded via the lysosomal pathway (Kim, Griffin, Nor, et al., 2017). Furthermore, Tonabersat could be effective at reducing Cx43

hemichannel ATP mediated NLRP3 inflammasome activation in rat burn injury as shown by decreased, NLRP3, Cas-1 and IL-1β expression. The results of this study are consistent with those of Xiao et al, who found that an intraperitoneal injection of 3,4-Methylenedioxy-nitrostyrene inhibited NLRP3 inflammasome activation as shown by decreased Cas-1 and maturation of 1L-1β (Xiao et al., 2016). Consequently, this resulted in a significant reduction of inflammatory cytokine production and amelioration of burn wound progression in deep partial thickness rat burns (Xiao et al., 2016). Vinaik et al., have found that prolonged NLRP3 inflammasome activation resulted in poor outcomes in wound healing after burn injury (Vinaik et al., 2020; Vinaik et al., 2018). They reported that NLRP3 knockout mice had decreased expression of pro-inflammatory cytokines, chemokines, inflammatory markers, growth factors, and collagen deposition compared to wild-type mice (Vinaik et al., 2020; Vinaik et al., 2018). These results support the hypothesis that targeting Cx43 reduces NLRP3 inflammasome activation via P2X7 receptor in rat burn injury.

4.3.4 Inflammatory response during burn injury

I demonstrated that the inflammatory response was increased in the zone of stasis as indicated by the increased percentage of MPO and CD68 positive cells in the early phases of burn wound healing (Figure 4.8). I also observed that in the rat burn, Cx43 was predominantly expressed in inflammatory cells. This result is in line with prior research that found that neutrophils and macrophages had higher levels of the Cx43 protein (Branes et al., 2002; Eugenin et al., 2003). Moreover, previous studies have reported that downregulation of Cx43 with Cx43asODN reduced neutrophil infiltration (Qiu et al., 2003) and pro-inflammatory C-C motif chemokine ligand 2 and TNFα in the wound bed of excisional wounds in mice, leading to improved wound healing (Mori et al., 2006). Furthermore, a study exploring *in vitro* interactions between mouse endothelial cells and neutrophils were found to be dramatically decreased in the presence of

Gap26 peptide (Sarieddine et al., 2009) which is known to block both connexin hemichannels and gap junctional intercellular communication (Desplantez et al., 2012). Eltzschig et al., have demonstrated that activated neutrophils in heterozygous Cx43 knockout mice release 15% less ATP via Cx43 hemichannels (Eltzschig et al., 2006). Moreover, neutrophil chemoattractant synthesis is initiated by a persistent calcium flux upon contact with necrotic tissue in zebrafish. Through Cx43 hemichannels, which are potent ATP release mediators, this "calcium alarm" signal spreads quickly in the developing neutrophil cluster (Poplimont et al., 2020). Blocking neutrophil Cx43 hemichannels with mimetic peptide Gap27 inhibited ATP release in a concentration dependent manner (Eltzschig et al., 2006). , In this study, I have shown reduced neutrophil infiltration in the zone of stasis of wounds treated with Cx43asODN or Tonabersat as well as reduced Cx43 and hemichannel expression, suggesting that neutrophilic gap junction communication and hemichannel action have been reduced.

Xiao and colleagues reported that inhibition of NLRP3 inflammasome activation in the zone of stasis via intraperitoneal injection of 3,4-Methylenedioxy-nitrostyrene reduced neutrophil infiltration, leading to the prevention of burn progression (Xiao et al., 2016). Emerging evidence indicates that neutrophils can assemble inflammasomes and secrete NLRP3-dependent IL-1β in autoimmune diseases (Stackowicz et al., 2021) or during immune responses in the presence of infection (Hassane et al., 2017). The neutrophilic NLRP3 inflammasome has been proposed as a crucial source of IL-1β, contributing to increased inflammation and pain in a rat model of experimental gout (Goldberg et al., 2017). Using the selective NLRP3 inhibitor MCC950 on purified neutrophils from patient donors stimulated with TNFα/bacterialPly abrogated IL-1β production (Hassane et al., 2017). This effect was also observed in the *S.pneumoniae*-infected mice. In this investigation, it was discovered that early stages of burn injury had elevated P2X7/NLRP3/Cas-1/IL-1β expression in the zone of stasis, which was

dominated by MPO-positive neutrophils. However, treatment with Cx43asODN or Tonabersat reduced this expression in these cells, suggesting that targeting NLRP3 via the Cx43/P2X7/NLRP3 pathway has reduced the neutrophil response in the zone of stasis. It is important the limitation of studying interleukin-1 beta (IL-1β) in tissues is the potential for the secreted IL-1β to be washed away or diluted within the tissue microenvironment. Although I observed a reduction in IL-1β expression with Cx43 treatment therapeutics, the localized secretion of IL-1β may be quickly dispersed or transported away by interstitial fluids, limiting its accumulation and detection in the tissue of interest. Hence, future work could employ specialized techniques to overcome this limitation, such as ELISA from tissue homogenates, to better understand the role of IL-1β in specific tissue microenvironments and its contributions to inflammation and immune responses.

Cellular ATP release via Cx43 hemichannels can regulate macrophage autocrine activation via ATP signalling (Choi et al., 2022; Dosch et al., 2019). In co-cultured fibroblasts, Cx43 deletion in lung macrophages generated a decrease in cytosolic calcium response and lowered extracellular ATP (Bhattacharyya et al., 2022). Additionally, after bleomycin-induced damage, heterozygous Cx43 knockout mice also showed lower lung fibrosis, indicating that Cx43-dependent fibrosis may be mediated via macrophage activation (Bhattacharyya et al., 2022). Interestingly, I observed that there was an increased number of CD68 positive macrophages in the treated groups as compared to the control groups. Macrophages emerge as one of the key players in the progression of burn wounds and play a critical role in burn wound conversion. They are classified as M1 pro-inflammatory macrophages and M2 anti-inflammatory macrophages. The M1 macrophages are predominantly involved in inflammation and recruitment to the wound area. Whereas the M2 macrophages are associated with proliferation and tissue repair (Jing et al., 2018). In a study, it was found that pre-treating macrophages with

the mimetic peptides Gap26 and Gap19 decreased the mRNA and protein expression levels of M1 type macrophage polarization markers. Gap19 was more successful than Gap26 in lowering the M1-type polarization index (Wu et al., 2020), suggesting that the pro-inflammatory phenotype was reduced.

In a mouse model of metabolic dysfunction, Cx43-knockout specific to macrophages (Cx43-MKO) expressed a decrease in pro-inflammatory markers and increased expression of genes involved in anti-inflammatory responses of M2 macrophage markers (Choi et al., 2022). In addition, another study suggested the possibility of M2 macrophage polarization in an *in vivo* macrophage specific Cx43 knockout mouse model, leading to alleviated adipose inflammation and restoration of mitochondrial function (Q. Zhou et al., 2022). M2 macrophage polarization was shown to be mediated by AMPK/mTOR/NLRP3 and AMP-NF/κB pathway. Treatment with Metformin regulated the AMPK/mTOR pathway to inhibit the NLRP3 inflammasome activation, which boosted M2 macrophage polarization and accelerated wound healing in rat excisional skin wounds (Qing et al., 2019). This information suggests that reducing NLRP3 activation could increase anti-inflammatory M2 macrophage production to reduce inflammation and promote functionality in disease conditions.

In this study, I have used the CD68 macrophage marker that recognizes both M1 and M2 phenotypes. Interestingly, at PBD 1 and 4, a rise in CD68 positive cells in the zone of stasis may suggest that M2 macrophage polarization could be occurring to begin proliferation and burn tissue repair in wounds treated with Cx43asODN or Tonabersat. In addition, this could be a consequence of Cx43/P2X7 mediated NLRP3 inflammasome inhibition altering the inflammatory response during the early phase of burn injury to speed wound healing. In order to establish a firm connection between macrophages and the Cx43/P2X7/NLRP3 pathway,

future research could look for CD206 positive macrophages that particularly mark the M2 phenotype.

4.3.5 Reduced skin fibrosis and MMP-9 improved collagen content and epidermal thickness in rat burn injury

Burn injuries can lead to fibrosis depending on the size, depth of burn and general conditions of the wounds (Shpichka et al., 2019). In response to profibrotic cytokines, fibroblasts differentiate into myofibroblasts, which are characterized by the acquisition of de novo expression of αSMA, which is crucial for tissue regeneration and wound healing. Through the competing binding of endogenous Smads and Cx43 to microtubules, it has been demonstrated that TGF profibrotic mediator drives αSMA expression in myofibroblastic phenoconversion (Asazuma-Nakamura et al., 2009). However, downregulating Cx43 with Cx43asODN reversed this phenomenon in cardiac fibroblasts (Asazuma-Nakamura et al., 2009). In addition, another study showed that Smad2 activation and myofibroblast production caused by TGFβ1 were reduced by transient Cx43 silencing in asthmatic fibroblasts treated with Cx43 small interfering RNA (Mori et al., 2006; Paw et al., 2017). Moreover, downregulation of Cx43 with a single application of Cx43asODN reduced PAI-1 and αSMA expression in peritoneal adhesion mouse model (Chua et al., 2022). In addition, in an ERK-dependent manner, ATP binding to P2Y2 receptors increased αSMA production and collagen accumulation by 60% and the mRNA expression of profibrotic markers, plasminogen activator inhibitor-1 (PAI-1) and monocyte chemotactic protein-1, by 4.5 and 4.0 fold, respectively in cardiac fibroblasts. However, this was abolished with the treatment of Apyrase (Lu et al., 2012). According to Inzaugarat and colleagues, LPS and ATP stimulation in hepatic stellate cells (HSCs) grown from WT mice produced more NLRP3-mediated ROS and more profibrotic myofibroblastic phenotype expressing αSMA than NLRP3-/- mice (Inzaugarat et al., 2019).

Excessive collagen accumulation is a hallmark for fibrosis. Upregulation of HSP47 correlates with collagen expression in several fibrotic conditions of lung, kidney, peritoneal, skin and intestine (Chen et al., 2007; Kitamura et al., 2011; Mishima et al., 2003; Otsuka et al., 2017; Xiao et al., 2012). Kakugawa et al., have shown that HSP47 mRNA was also upregulated in myofibroblasts, in type II pneumocytes and in macrophages present in fibrotic lungs (Kakugawa et al., 2010). In a study of liver fibrosis, *in vitro* and *in vivo* stimulation with arsenic induced NLRP3 and HSP47 expression. Inhibition of NLRP3 with specific inhibitor MCC950 significantly mitigated the activation of the NLRP3 inflammasome, decreased the expression of HSP47 and profibrotic markers collagen type I and αSMA thereby attenuating the arsenic-induced hepatic stellate cells (HSCs) activation (Yuan et al., 2022). Similarly, in a previous study on dermal fibrosis, delivery of HSP47 siRNA using a nanoparticle platform was shown to reduce HSP47 protein expression and profibrotic markers NOX4, collagen type I and αSMA (Morry et al., 2015). This evidence would support the involvement of NLRP3 inflammasome activation and association with profibrotic markers HSP47 and αSMA leading to fibrosis. Co-expression of HSP47 and αSMA in rat burn injury could suggest that fibrotic expression is reduced via the NLRP3 inflammasome pathway with Cx43asODN or Tonabersat. However, it is important to note that, Ruigrok et al. discovered contrasting findings in fibrogenic lung, where neither the expression of fibrogenesis-related genes nor αSMA was impacted by HSP47 knockdown (Ruigrok et al., 2021).

MMP-9 is the main metalloproteinase enzyme responsible for the degradation of ECM. Various inflammatory cytokines such as TGFβ1, TNFα, IL-6 and IL-1β play a pivotal role in the production of MMP-9 and secretion, contributing to fibrogenic remodelling (Brandner et al., 2008; H. Luo et al., 2020; Razzaque et al., 2003; Xiao et al., 2012). In a mouse study, it was discovered that alkali burn injury to the cornea results in increased IL-1β and MMP-9 mRNA

levels. However, this pattern was reversed in alkali burn injury inflicted on NLRP3 knockout animals, which also had reduced corneal opacity. Additionally, LPS-treated NLRP3 deletion animals showed less neutrophil infiltration, suggesting that the NLRP3 inflammasome plays a strong role in corneal sterile inflammation (Shimizu et al., 2019). Moreover, degradation of collagen in the corneal stroma by activating corneal fibroblasts, increased secretion of MMP by these fibroblasts, are postulated to be driven by neutrophil-derived IL-1 (Li et al., 2003). In the dysfunction of aortic disease, *in vitro* palmitic acid treated smooth muscle cells were treated with siRNA targeting NLRP3 inflammasome components and were shown to have reduced NLRP3-ASC-Cas-1 inflammasome activation, reduced MMP-9 production, and improved smooth muscle cell functions (Wu et al., 2013).

Burn injury and impaired wound healing or suboptimal wound care intervention can lead to hypertrophic scars (Tredget et al., 2014). Some of the notable features of hypertrophic scars is increased epidermal thickness and increased keratinocyte proliferation (Hakvoort et al., 1999). In addition, increase in pro-inflammatory cytokines, fibrogenic and growth factors, as well as the increase of keratin markers 5, 6, and 17 influence the development of hypertrophic scars (Hakvoort et al., 1999). In diabetic ulcers and venous leg ulcers, hyper-thickened epidermis is correlated with increasing Cx43 expression (Becker et al., 2012). Downregulation of Cx43 with Cx43asODN has been shown to enhance epidermal keratinocyte migration and fibroblast migration from wound edges of excisional and incisional mouse skin wound models (Mori et al., 2006). In another study, nitrogen mustard (NM) injured SKH-1 hairless mouse dorsal skin treated with Cx43asODN reduced levels of Cx43 and phosphorylated Cx43 with minimal keratin 17 expression leading to improved re-epithelisation and reduced keratinocyte hyperproliferation (Chang et al., 2015). In summary, these studies support the hypothesis that targeting Cx43 reduces skin fibrogenic factors, keratinocyte hyperproliferation, and reduces

epidermal thickness. These findings are consistent with reports suggesting that targeting Cx43 and hemichannels with Cx43asODN or Tonabersat in rat burn injury reduced αSMA, HSP47 and MMP-9 production. Consequently, this leads to reduced ECM degradation and improved collagen formation as indicated by Picrosirius Red and Masson's Trichrome histological analysis. Although, I did not observe a difference in the rate of re-epithelialisation, it is notable that keratinocyte hyperproliferation, as indicated by nascent epidermal thickness, had thinned down in the wounds treated with Cx43asODN or Tonabersat compared to the controls. Furthermore, this study suggests that burn progression in rat burn injury is prevented and skin fibrosis is reduced via the modulation of Cx43/P2X7/NLRP3 inflammasome pathway with a possibility of other P2 purinergic family members being involved. To the best of my knowledge, this is the first study to test Tonabersat topically in burn injury. Although, results from this chapter show the potential use of Tonabersat for burn injury, wound healing outcomes from Cx43asODN supersede those from Tonabersat therapeutic application in rat burn injury as indicated by better collagen content and reduced epidermal thickness. Suggesting that targeting the Cx43 gap junction and hemichannels simultaneously is more effective than targeting the hemichannels alone.

4.4 Conclusion

In this chapter, I have established the role of Cx43 in rat burn injury. I found an increase in Cx43 expression and hemichannel expression in the zone of stasis in the early phases of burn wound healing that was accompanied by an increased inflammatory response, and prevented burn progression, and kickstarted early wound repair. The significance of Cx43 was further established with the use of topical application of Cx43asODN that targets the mRNA of Cx43 reduced Cx43 gap junctional and hemichannel protein levels. Additionally, Tonabersat a

hemichannel blocker, has been shown to significantly reduce Cx43 hemichannel protein levels in the zone of stasis via immunolabeling. Protein quantification with western blotting may have provided further evidence to support the conclusion that Tonabersat can reduce hemichannel protein levels rather than just blocking pathologic Cx43 hemichannel opening. However, western blotting technique will not be able to differentiate the zone of stasis within the burn that is the region of interest in this study. However, the reduction in Cx43 concomitantly marginally and tranisently reduced P2X7 and NLRP3 expression leading to reduced IL-1β production in rat burn injury. Early assessment of macroscopic images has shown reduced wound size in injuries treated with either Cx43asODN or Tonabersat. Furthermore, there was a notable reduction in αSMA and HSP47 skin fibrosis markers, along with MMP-9. Histological observations of rat burn injury revealed better collagen formation and reduced nascent epidermal thickness in Cx43asODN and Tonabersat treated wounds. Using a rat burn model is cost-effective and provides a basis for preliminary testing of drugs. Though the skin healing mechanism is predominantly through wound contraction, the results obtained sets the stage for preclinical evaluation. Collectively, these findings suggest a possible involvement the of Cx43 mediated NLRP3 inflammasome pathway via P2X7 activation in early burn wound healing. This indicates that downregulating the Cx43 hemichannel may have a potential therapeutic target effect to prevent burn progression and improve healing outcomes.

Chapter 5: Preliminary study of role of Targeted Cx43 therapeutics in porcine burn injury

5.1 Introduction

5.1.1 Porcine skin

Pigs have gained popularity in recent years as research animals for pharmacological and cutaneous biology experiments. Porcine skin closely resembles human skin in both anatomical and physiological aspects. Some of the characteristics include a sparse and dense layer of hair, epidermal thickness with well-defined rete pegs, dynamics of epidermal tissue turnover, the amount and complexity of dermal collagen and elastin fibers, and lipid composition (Sullivan et al., 2001). Pig epidermis and dermis are similar in thickness to those of humans. The human epidermis has a thickness range of 50 to 120 µm, whereas the pig epidermis spans from 30 to 140 µm (Meyer et al., 1978). Pig skin is also tightly connected to the underlying structures, which are identical to those in humans. Additionally, the panniculus carnosus, which is a muscle layer tightly attached to skin and fascia in rodents, is absent from both pig and human skin (Schneider & Wolf, 2016). However, there are certain differences between pig and human skin. Pig skin has a higher pH, a fatty subcutis, more apocrine sweat glands, and eccrine sweat glands that are only found in specific areas. Although the microvascular structure of humans and pigs is the same, human skin has a richer dermal skin vasculature. The evidence for the increasing use of pig models for cutaneous research is illustrated by the diversity of applications that undergo study, including: radiobiology (Aghdam et al., 2020), contact dermatitis (Nadworny et al., 2008), prediction of percutaneous drug absorption or penetration (Alsaab et al., 2016), acne cryotherapy (Ray Jalian et al., 2015), and studies on the healing of

partial or full thickness excisional wounds, incisional wounds, laser-induced wounds, ischaemic wounds, and burn injuries of various degrees (Seaton et al., 2015).

5.1.2 Porcine burn injury

Burn injuries are a common and destructive injury that frequently result in significant morbidity and extended suffering. It is necessary to use an adequate animal model that mimics human burn features and burn wound progression in order to discover viable therapeutics for burn injuries (Sullivan et al., 2001). Two commonly used methods to study burn injury are: (1) contact burns, (2) scald burns. Contact burns are created using a metal rod burn device made of varying materials such as brass (Brans et al., 1994), aluminium (Menon et al., 2016), stainless steel (J. Y. Kim et al., 2016), and iron (Brink et al., 1986). Generally, these materials require a heat source, either a metal rod heated in a water bath or connected to an electrical supply. Additionally, the thermodynamics of each material have a different heating capacity, and the capacity to transfer heat to the skin has an impact on the severity of burn damage (Andrews & Cuttle, 2017; Singh et al., 2016). On the other hand, emphasis on scald injuries was mostly obtained using a glass cup filled with heated water, which behaves more like a contact burn and is not a true scald injury (Cuttle et al., 2006).

A model created by Moritz and Henriques, that lacked quantitative histological evaluation of burns created in their study (Moritz & Henriques, 1947), inspired Andrews and colleagues to develop a porcine scald model in a similar manner to allow continuous application of hot water to the skin for burn creation (Andrews et al., 2016). This technique shows how immersion injuries result from prolonged exposure as opposed to splatter injuries from brief and rapid exposure (Singer et al., 2020). Additionally, using various time and temperature conditions, this method of scald burn injury is capable of producing various depths of burn and allows the

pathophysiology of scald burn progression to be examined (Andrews et al., 2016). For example, histological analysis of skin after 50°C water temperature with a 10 min exposure on skin resulted in deep tissue injury 24 h after burn creation. Increased damage was seen 3 days after burn creation from 5 s of exposure to 80°C and 90°C water, which resulted in significantly deeper tissue damage than 70°C water (Andrews et al., 2016).

In a study conducted by Brans and team, it was found that histological evaluation of contact burns showed clear demarcation of infiltrating neutrophils between the viable and necrotic tissues in the first 72 h, after burn injury (Brans et al., 1994). In contrast, in scald burns, an intermingled pattern of damaged and intact collagen fibers with delayed and progressive vascularity was noted over the first 72 h and it was suggested that studies focusing on burn progression should use the scalding method to create burns (Brans et al., 1994).

Health and safety concerns over an elevated risk of burn injuries to researchers compared to contact burns are one of the commonly highlighted drawbacks of using the scald infliction technique. However, the method put forth by Andrews and team was made in such a way that there was never more than a tiny amount of hot water available to contact the pig skin. In addition, this method reduces the amount of hot water that is handled by pumping water directly from the water bath rather than manually moving it from one source to another (Andrews et al., 2016). Hence, for consistent creation of scald burn wounds and the safety of the researchers, we adopted the porcine scald burn model demonstrated by Andrews and team (Andrews et al., 2016) using 60°C water for 1 min.

5.1.3 Porcine Cx43

Cx43 is expressed in pig skin (Tarzemany et al., 2017). In a model of Duchenne muscular dystrophy (DMD), heterozygous $DMD^{+/-}$ porcine litter showed increasing myocardial fibrosis

and increased expression of Cx43 in the heart at 3 months of age, which were linked to a considerably worse left ventricular ejection fraction. Additionally, behavioural testing showed signs of cognitive impairment (Stirm et al., 2021). In a cutaneous injury pig model, full thickness excisional wounds have been shown to have increased Cx43 via western blot. This increase was abolished with the treatment of ACT1 peptide, and histological analysis revealed reduced neutrophil recruitment, better vascularization, and reduced scarring and wound area as compared to controls (Ghatnekar et al., 2009). Endogenous Cx43 expression was elevated in *in vitro* pig cardiomyocytes stimulated with Ca^{2+}, and this was inhibited by 50% with siRNA targeting Cx43 (N. Wang et al., 2012). The ischaemic condition in pig hearts enhanced the permeability of Cx43 gap junctions and hemichannels (Schulz et al., 2003), and this has been linked to the swelling of cardiomyocytes in response to simulated ischaemia (Schulz et al., 2007). Treatment with the mimetic peptide Gap26 or Gap27 inhibited functional Cx43 hemichannels and hemichannel currents promoted by Ca^{2+} elevation ((N. Wang et al., 2012) . Furthermore, Gap19 also inhibited Cx43 hemichannels present in *in vivo* pig ventricular cardiomyocytes (D'Hondt et al., 2014).

5.1.4 Porcine NLRP3 inflammasome activation

Multiple molecular and cellular events, such as ionic flux, mitochondrial malfunction, ROS generation, and lysosomal degradation, occur in response to a variety of stressors that trigger the inactive NLRP3 to interact with ASC and procaspase-1 to form the NLRP3 inflammasome complex. This triggers automatic cleavage of procaspase-1 to its active form caspase-1 which subsequently cleaves IL-1β and IL-18 to their mature forms (Gombault et al., 2012; Kelley et al., 2019). As described in Chapter 4, the activation of the NLRP3 inflammasome has been extensively studied in mouse and rat models of various disease conditions. However, there is little information on porcine NLRP3 inflammasome activation. It is noteworthy that Tohno and

colleagues reported that 83.9% nucleotide sequence of porcine NLRP3 open reading frame was similar to human NLRP3, and an 84% amino acid similarity to human NLRP3, compared to 79.1% nucleotide sequence and 79.6% amino acid similarity to mouse NLRP3 (Tohno et al., 2011). Consequently, because of the greater similarities between NLRP3 in porcine and humans, research employing porcine models may help us understand NLRP3 forming inflammasomes and regulating the innate immune response is activated in humans.

In a model of lung injury in neonatal pigs exposed to asphyxia and hemorrhage, elevated MPO and Cx43 contributed to increased vascular permeability, which in turn caused decreased function and lung edema. In addition, C5aR2 was elevated in these lung tissues (Weber et al., 2019). In murine pyelonephritis disease, increased C5aR2 expression has been shown to activate the NLRP3 inflammasome complex via induced MAPK and AKT signaling and contribute to the production of IL-1β (Zhang et al., 2020). In a study of myocardial infarction, *in vitro* porcine peripheral blood mononuclear cells stimulated with both LPS and ATP have been shown to have significantly increased IL-1β production. Furthermore, pigs that received transluminal balloon occlusion have been shown to have increased production of NLRP3 mediated IL-1β and neutrophil infiltration in infarcted hearts, contributing to increased infarct size and poor cardiac function (van Hout et al., 2017). It has been demonstrated that exposing piglets to cadmium chloride causes neurotoxicity and neuroinflammation. Additionally, these events have been shown to take place when the NLRP3 inflammasome is activated, causing pyroptotic cell death to exacerbate the inflammatory responses via IL-1β/IκB-α-NF-κB-NLRP3 inflammasome feedback loop in the pig brain (Cai et al., 2021).

5.1.5 Targeted therapeutics of Cx43

It is well established that burn injuries are dominated by inflammatory responses contributing to burn wound progression, e.g., an initial partial thickness burn can convert to a deep partial or full thickness burn due to apoptotic cell death leading to progressive tissue damage (Gravante et al., 2007) or other contributing factors such as infection (Johnson & Richard, 2003). The ability of Cx43 gap junctions and hemichannels to regulate these cellular events and processes make them attractive as therapeutic targets (Coutinho et al., 2020; Coutinho et al., 2005; Delvaeye et al., 2019; Feng et al., 2020; Gilmartin et al., 2016; Mugisho, Green, et al., 2019). Human burns show increased expression of the Cx43 gap junction protein, indicating that it may play a significant role in burn conversion (Feng et al., 2020). In a mouse burn model, it has been demonstrated that downregulating Cx43 lowers neutrophil aggregation, speeds up wound healing, and prevents burn progression (Coutinho et al., 2005). In brain injury, radiation injury, and heart ischaemia, it has been demonstrated that downregulating Cx43 or blocking these channels can slow the spread of the death signals and stop healthy neighbouring cells from undergoing apoptosis (Du et al., 2017; Frantseva et al., 2002; Lin et al., 1998; Mancuso et al., 2011). Additionally, it has been demonstrated that using mimetic peptides to block hemichannels speeds up scrape wound closure and promotes cell proliferation in *in vitro* skin models (Faniku et al., 2018), *ex vivo* skin models (Pollok et al., 2011), and human dermal fibroblasts *in vitro* under hyperglycaemic/hyperinsulinemia conditions (Wright et al., 2012). Furthermore, it was discovered that Cx43 mimetic peptides can prevent the activation of P2X7, in tubular epithelial cells, which is caused by extracellular ATP release from Cx43 hemichannels (Xu et al., 2022). The ability of Tonabersat to block Cx43 hemichannels has been demonstrated to reduce inflammation, restore, and enhance overall functionality in retinal eye disease (Kim, Griffin, Nor, et al., 2017; Louie et al., 2021; Mat Nor et al., 2020; Mugisho, Rupenthal, et al., 2019). In light of this, it may be beneficial to block Cx43 hemichannels or

downregulate Cx43 function or expression early, in order to prevent the progression of burn injury and enhance wound healing in a porcine burn model.

5.1.6 Hypothesis

That the Cx43 gap junctions and hemichannels play a vital role in porcine burn injury and that downregulating Cx43 gap junctions and hemichannels with topical application of either Cx43asODN or Tonabersat would reduce inflammation and NLRP3 inflammasome activation in porcine burn injury to reduce burn severity.

5.1.7 Aims

The main is to investigate the role of Cx43 in porcine burn injury. To address this, I adopted and optimised the porcine scald burn creation methodology from Andrews et al., 2016. To explore the therapeutic effect of Cx43 and hemichannels, topical application of low and high concentrations of Cx43asODN or Tonabersat were delivered for four consecutive days and tissues were harvested for immunofluorescence and histological analysis.

1. Quantifying Cx43 and hemichannnel expression in porcine burn injury.
2. Quantifying the expression of NLRP3 inflammasome markers and skin fibrosis makers.
3. Qualitative observations of collagen content and nascent epidermal thickness in porcine burn injury treated with Cx43 targeted therapeutics.

5.2 Results

5.2.1 Consistent porcine scald burn creation

I created deep partial thickness scald burns using 60°C water for 1 min (Andrews et al., 2016; Andrews et al., 2017) (Figure 5.1). I refined the burn device by using a stainless pipe that had an aperture 45mm whereas Andrews et al., used 50mm aperture (Andrews et al., 2016). In addition, the flow rate of water pumped into our scald device using a submersible water pump was approximately 2 litres per min whereas Andrews et al., reported 1.3 litres per min in their set up (Andrews et al., 2016). Water temperature within the scald burn device was recorded every second by using a hand-held digital type-K thermocouple probe thermometer (Fluke Australia Pty Ltd., Australia). Temperatures logged from the probe within the scald device fluctuated in the first 5–10 s before stabilising, at which point a more consistent and accurate reading of the water temperature was obtained 60.3°C ± 3.13°C.

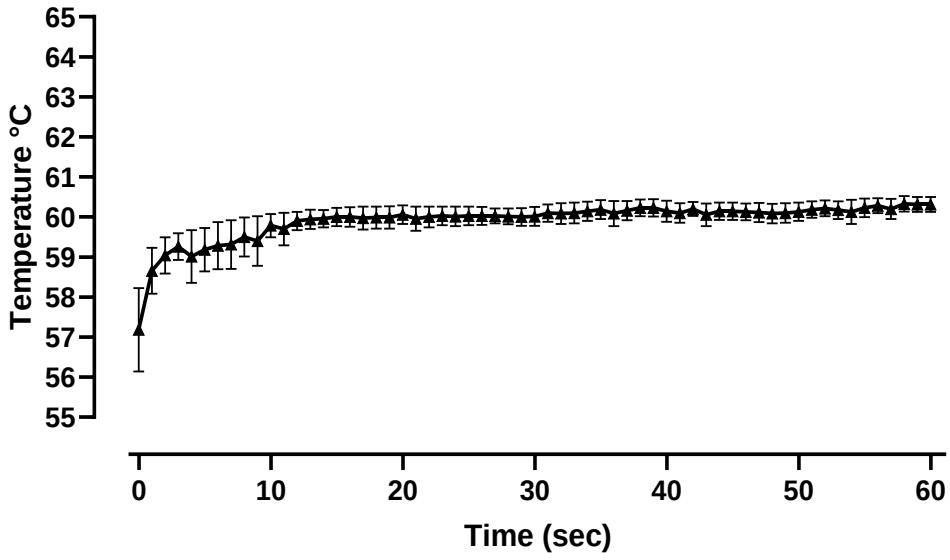

Figure 5.1 Temperature of water in the device during burn creation.
60°C for 1 min exposure (n=8 wounds). Mean ± SEM.

5.2.2 Topical gel application of Cx43 targeted therapeutics reduced ring of inflammation and preserved hair follicles in the porcine scald burn injury

Topical application of high doses and low doses of Cx43asODN and Tonabersat were tested on pilot scald burn porcine as listed in Table 2.2. Wounds underwent four consecutive days of Cx43asODN or Tonabersat topical treatment, wound healing progression was monitored by macroscopic photography of the wounds of PBD 1, 4, 7, 14 & 21.

The red ring of inflammation around the wound and visible on PBD 1 was reduced by PBD 4 in wounds that were treated with a high dose of Cx43asODN or Tonabersat. On PBD 7, 14 and 21, there was a similar trend toward smaller wound size in the Cx43asODN and Tonabersat treated groups. Although statistically not significant, overall burn wound size was reduced in the treated groups compared to control groups (Figure 5.2 & Figure 5.3a). Interestingly, wounds treated with 300µM Cx43asODN (AS-300) and 100µM Tonabersat (Tona-100) treated groups had visibly higher numbers of hair follicles preserved in the wound area on PBD 21 (Figure 5.2 & Figure 5.3b). In summary, wound healing outcomes were improved, and hair follicles were better preserved in treated wounds.

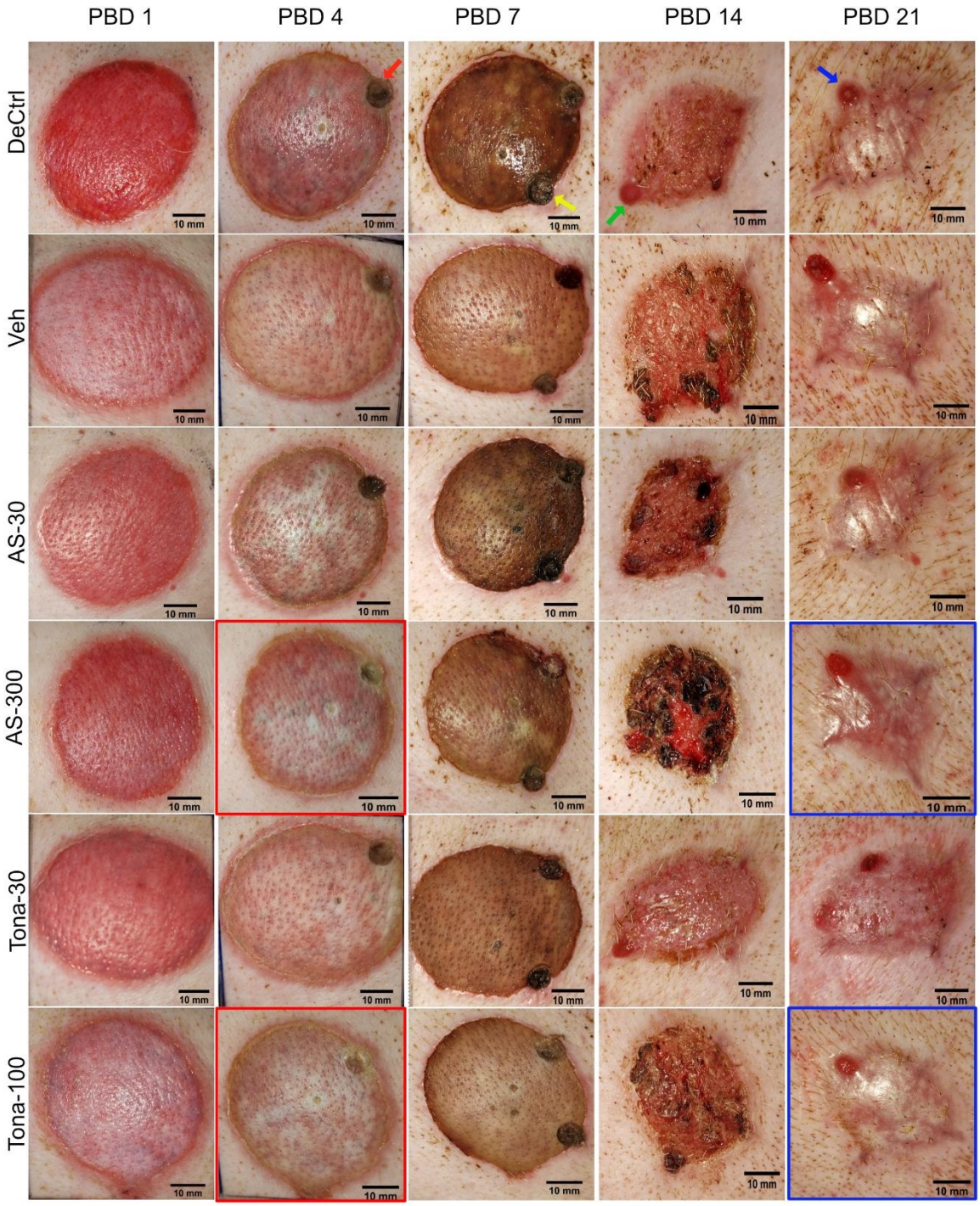

Figure 5.2 Macroscopic images of wound healing process of topically treated porcine burn wounds.

DeCtrl: Debrided Control (n=3 animals); Veh: 30% Pluronic (n=2 animals), AS-30: Cx43asODN, 30µM (n=3 animals); AS-300: Cx43asODN (n=3 animals), 300µM; Tona-30: Tonabersat, 30µM (n=2 animals); Tona-100: Tonabersat 100µM (n=3 animals). Red arrow: biopsy excision of PBD 1, yellow arrow: biopsy excision of PBD 4, green arrow: biopsy excision of PBD 7, blue arrow: biopsy excision of PBD 14. Red box shows, reduced red ring of inflammation around wound. Blue box indicates hair follicle preservations in wounds. Scale bar: 10mm.

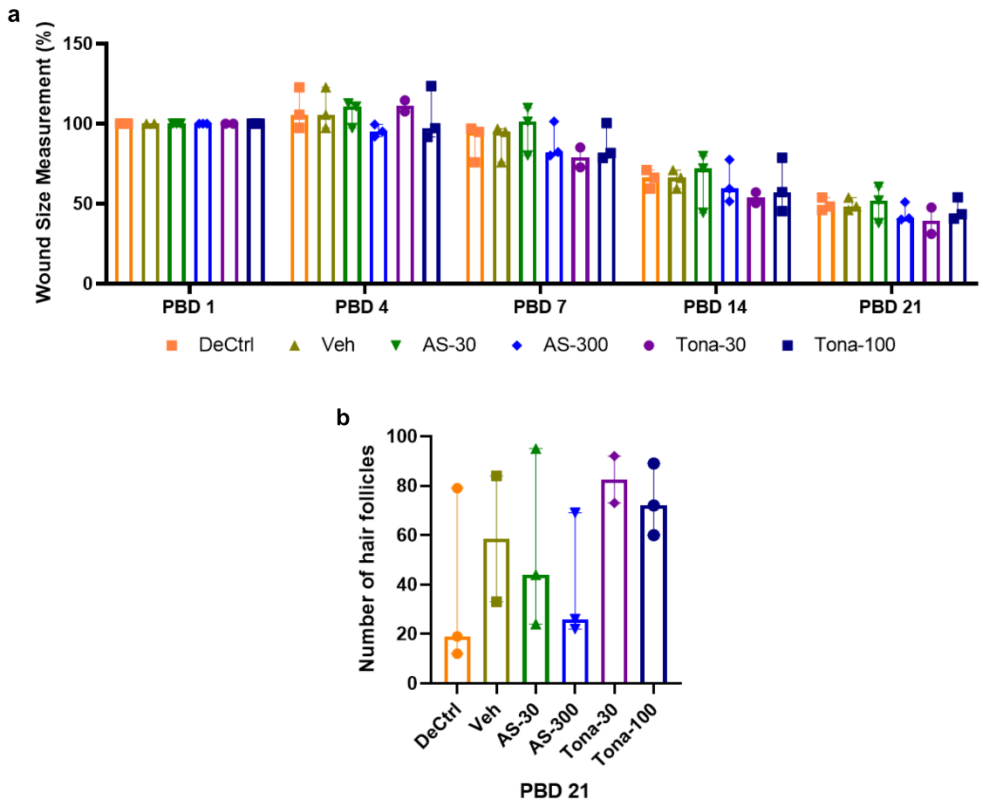

Figure 5.3 Marginally reduced wound size and increase in number of hair follicles in Cx43asODN and Tonabersat treated porcine burn wounds.
(a) Wound size measurement of porcine burn wounds treated with Cx43asODN and Tonabersat treated burn wounds on PBD 1, 4, 7, 14 & 21. Debrided Ctrl: DeCtrl (n=3 animals); Veh: 30% Pluronic (n=2 animals); AS-30: Cx43asODN, 30µM (n=3 animals), AS-300: Cx43asODN (n=3 animals); Tona-30: Tonabersat, 30µM (n=2 animals); Tona-100: Tonabersat 100µM (n=3 animals). (b) Number of hair follicles present on burn wounds on PBD 21. Data are presented as median and interquartile range (IQR). Statistical comparisons were made using Kruskal-Wallis Test. ***Cx43 targeted therapeutics prevents upregulation of Cx43 protein expression in the porcine burn zone of stasis***

I first wanted to investigate if there is a change in the pathological Cx43 expression in porcine burn injury. I performed immunostaining analysis and ROIs were taken from zone of stasis as shown in Figure 5.4. Upon wound injury, there was a significant increase in Cx43 protein levels compared to normal skin (NS) ($p<0.05$) on PBD 4 and PBD 7 (Figure 5.5 a, b & d). I then explored the use of Cx43asODN (low concentration: AS-30 µM & high concentration: AS-300 µM) and Tonabersat (low concentration: Tona-30 µM & high concentration: Tona-100 µM) as topical treatment in porcine burn injury. On PBD 4, I observed that Cx43 protein levels were

reduced in wounds treated groups as compared to control wounds, but this was not significant (p>0.99) (Figure 5.5 b & d). However, on PBD 7, wounds treated with AS-300, Tona-30 and Tona-100 µM had lower Cx43 protein expression as compared to DeCtrl (p=0.4512, p= 0.6692 and p=0.8568, respectively), but no difference was observed when compared with Veh control (>0.9999) (Figure 5.5 e). These results may indicate that topical application with Cx43asODNor Tonabersat, reduces the expression of Cx43 at early timepoints after burn wounds.

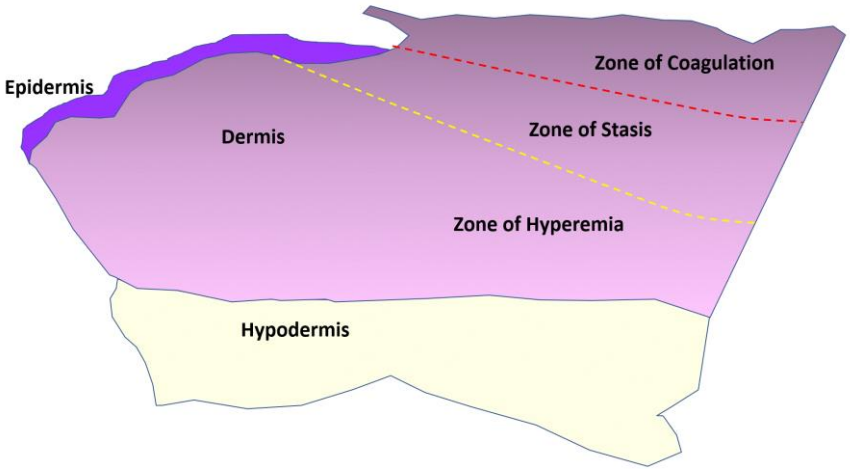

Figure 5.4 Schematic diagram of zone of stasis in porcine burn injury.
Diagram depicts zone of coagulation, stasis and hyperemia in porcine burn injury.

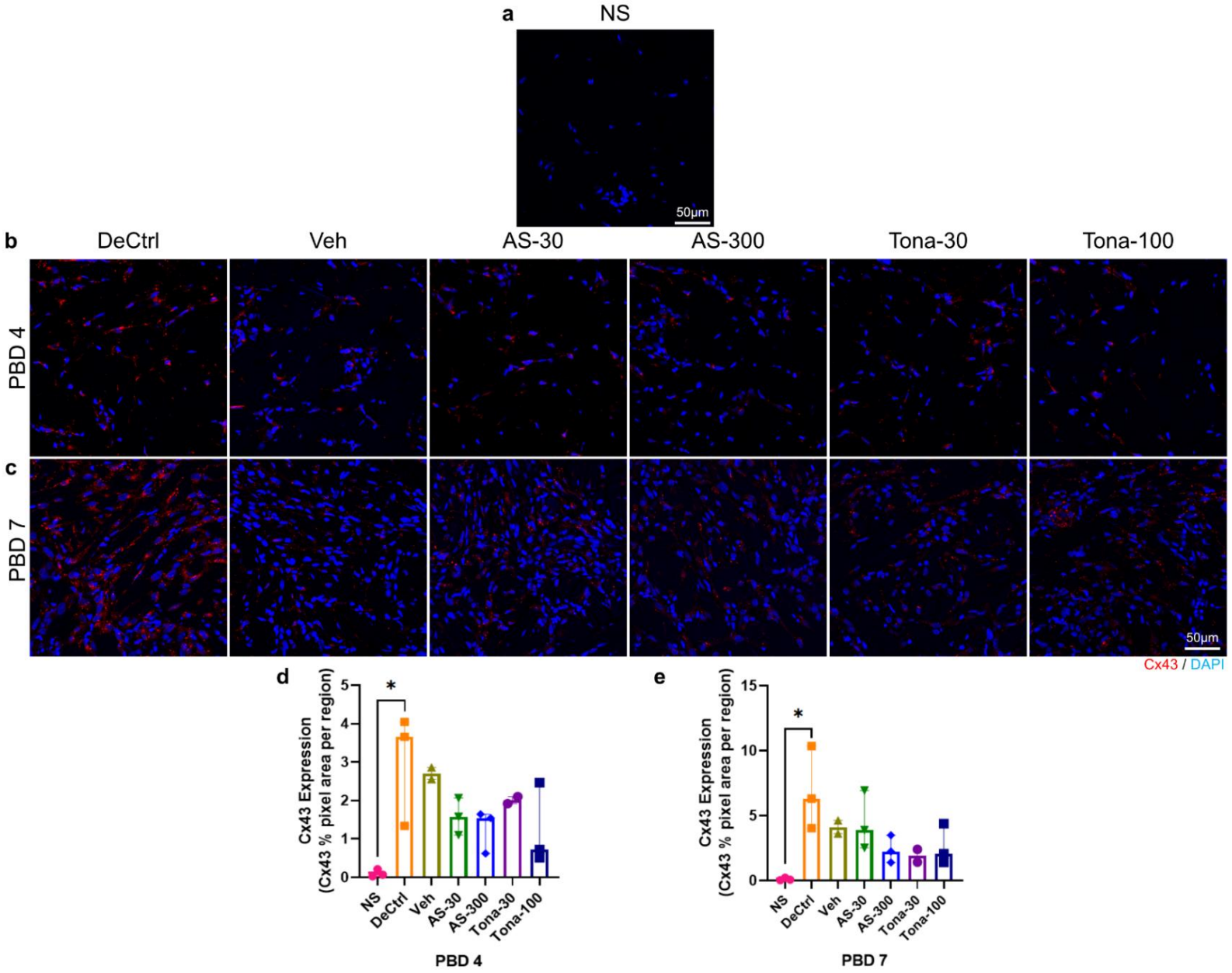
a
NS
50μm
b
DeCtrl
Veh
AS-30
AS-300
Tona-30
Tona-100
PBD 4
c
PBD 7
50μm
Cx43 / DAPI
d
Cx43 Expression
(Cx43 % pixel area per region)
*
NS
DeCtrl
Veh
AS-30
AS-300
Tona-30
Tona-100
PBD 4
e
Cx43 Expression
(Cx43 % pixel area per region)
*
NS
DeCtrl
Veh
AS-30
AS-300
Tona-30
Tona-100
PBD 7

Figure 5.5 Topical application of Cx43 targeted therapeutics reduced Cx43 protein expression in the zone of stasis on PBD 4 & 7.
Representative immunofluorescence image of Cx43 expression in (a) normal skin (NS), (b) zone of stasis at PBD 4 and (c) PBD 7. Debrided Ctrl: DeCtrl, Vehicle control: Veh, Cx43asODN 30µM: AS-30, Cx43asODN 300µM: AS-300, Tonabersat 30µM: Tona-30, Tonabersat 100µM: Tona-100. Magnification: 40x. Scale bar: 50µm. (d) Image analysis graph of Cx43 expression on PBD 4 and (e) PBD 7. Image analysis graph shows an increased expression between NS vs DeCtrl (n=3 animals per group) on PBD 4 & 7. Image analysis reveals lower Cx43 protein expression in the zone of stasis of treated (AS-30, AS-300, Tona-30 & Tona-100, n=3, 3, 2 & 3 animals, respectively) compared to DeCtrl & Veh (n=3 & 2 animals, respectively) on PBD 4 & 7. Data are presented as median and interquartile range (IQR). Statistical comparisons were made using Kruskal-Wallis Test. (*$p<0.05$).

5.2.4 Hemichannel expression in did not alter with treatment in the zone of stasis

After establishing that Cx43 targeted therapeutics were able to reduce Cx43 gap junction protein expression, I then explored the hemichannel expression in the zone of stasis (Figure 5.6. I observed that there is an increased expression of hemichannels upon burn wound injury in DeCtrl in comparison to NS on PBD 4 ($p=0.1364$) (Figure 5.6 a, b & d). However, treatment with Cx43asODN or Tonabersat did not make a difference to hemichannel expression on PBD 4 ($p=0.9999$) (Figure 5.6 b & d). Similarly, on PBD 7, there was an increased expression of hemichannels in DeCtrl as compared to NS ($p=0.0811$). However, Cx43asODN did not have any effect on hemichannel expression as compared to DeCtrl and Veh control.Tona-30 µM treated wounds had slight reduction in hemichannel expression compared to DeCtrl and Veh control, however this was not significant ($p=0.7180$ and $p=0.68$, respectively). Tona-100 µM treated wounds had no difference in comparison to DeCtrl and Veh control wounds ($p=0.9999$) (Figure 5.6 c & e).

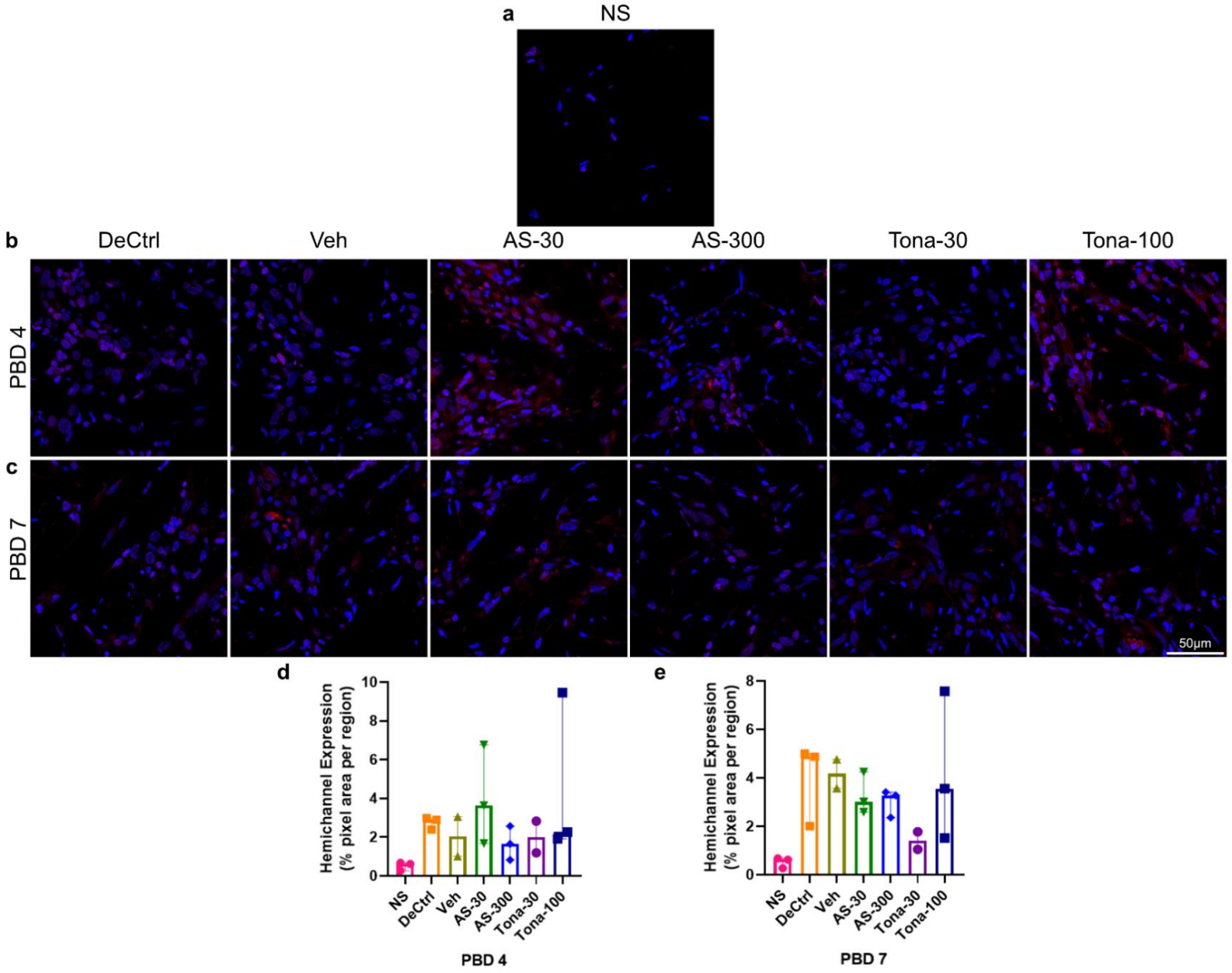
a
NS
b
DeCtrl
Veh
AS-30
AS-300
Tona-30
Tona-100
PBD 4
c
PBD 7
50μm
d
Hemichannel Expression
(% pixel area per region)
NS
DeCtrl
Veh
AS-30
AS-300
Tona-30
Tona-100
PBD 4
e
Hemichannel Expression
(% pixel area per region)
NS
DeCtrl
Veh
AS-30
AS-300
Tona-30
Tona-100
PBD 7

Figure 5.6 Topical application of Cx43 targeted therapeutics did not reduce Hemichannel protein expression in zone of stasis on PBD 4 & 7.
Representative immunofluorescence image of Hemichannel expression in (a) normal skin (NS), (b) zone of stasis at PBD 4 and (c) PBD 7. Debrided Ctrl: DeCtrl, Vehicle control: Veh, Cx43asODN 30µM: AS-30, Cx43asODN 300µM: AS-300, Tonabersat 30µM: Tona-30, Tonabersat 100µM: Tona-100. Magnification: 63x. Scale bar: 50µm. (d) Image analysis graph of Hemichannel expression on PBD 4. (e) Image analysis graph of Hemichannel expression on PBD 7. Image analysis graph shows an increased expression between NS vs DeCtrl (n=3 animals per group) on PBD 4 & 7. Image analysis reveals Hemichannel expression comparison of treated (AS-30, AS-300, Tona-30 & Tona-100, n=3, 3, 2 & 3 animals, respectively) to DeCtrl & Veh (n=3 & 2 animals, respectively) on PBD 4 & 7. Data are presented as median and interquartile range (IQR). Statistical comparisons were made using Kruskal-Wallis Test. (*$p<0.05$).

5.2.5 Topical application of Cx43 targeted therapeutics did not reduce inflammation in the zone of stasis

In burn injury, inflammation plays a significant role in removing cells but also could lead to systemic inflammatory responses and to further damage inducing hypertrophic scarring. Infiltration of neutrophils to the dermis following porcine burn injury was observed. It was important to determine if topical treatment with Cx43asODNor Tonabersat was able to reduce neutrophil infiltration in the zone of stasis. On PBD 4, MPO positive neutrophils were observed after scald burn injury ($p=0.1804$) (Figure 5.7 a, b & d). However, treatment with either Cx4asODN or Tonabersat did not reduce MPO positive neutrophils in the zone of stasis ($p>0.9999$) (Figure 5.7 b & d). Wounds treated with AS-30 µM and Tona-30 µM had increased MPO positive neutrophils in the zone of stasis ($p>0.9999$) (Figure 5.7 b & d). On PBD 7, surprisingly, Veh control had the lowest MPO positive neutrophils as compared to DeCtrl and wounds treated with Cx43 antisense oligodeoxynucleotides or Tonabersat. However, wounds treated with AS-30 µM, AS-300 µM, Tona-30 µM and Tona-100 µM had had no difference compared to control wounds ($p>0.9999$) (Figure 5.7 c & e).

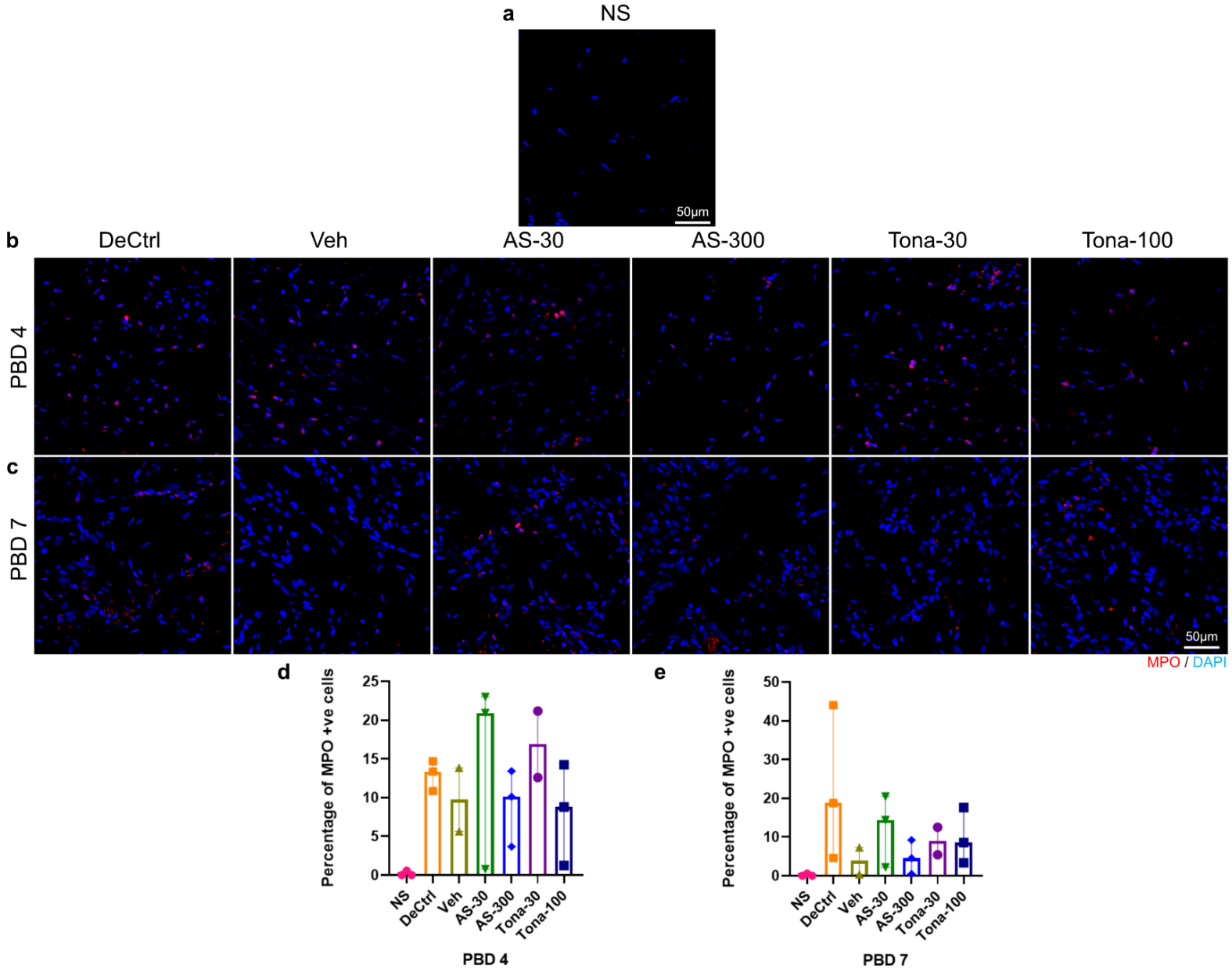
a
NS
50μm
b
DeCtrl
Veh
AS-30
AS-300
Tona-30
Tona-100
PBD 4
c
PBD 7
50μm
MPO / DAPI
d
Percentage of MPO +ve cells
25
20
15
10
5
0
NS
DeCtrl
Veh
AS-30
AS-300
Tona-30
Tona-100
PBD 4
e
Percentage of MPO +ve cells
50
40
30
20
10
0
NS
DeCtrl
Veh
AS-30
AS-300
Tona-30
Tona-100
PBD 7

Figure 5.7 Topical application of Cx43 targeted therapeutics did not reduce percentage of MPO positive cells in zone of stasis on PBD 4 & 7.
Representative immunofluorescence image of percentage of MPO positive cells in (a) normal skin (NS), (b) zone of stasis at PBD 4 and (c) PBD 7. Debrided Ctrl: DeCtrl, Vehicle control: Veh, Cx43asODN 30µM: AS-30, Cx43asODN 300µM: AS-300, Tonabersat 30µM: Tona-30, Tonabersat 100µM: Tona-100. Magnification: 40x. Scale bar: 50µm. (d) Image analysis graph of percentage of MPO positive cells on PBD 4 and (e) PBD 7. Image analysis graph shows increased percentage of MPO positive cells between NS vs DeCtrl (n=3 animals per group) on PBD 4 & 7. Image analysis reveals percentage of MPO positive cells comparison of treated (AS-30, AS-300, Tona-30 & Tona-100, n=3, 3, 2 & 3 animals, respectively) to DeCtrl & Veh (n=3 & 2 animals, respectively) on PBD 4 & 7. Data are presented as median and interquartile range (IQR). Statistical comparisons were made using Kruskal-Wallis Test. (*$p<0.05$).

5.2.6 Significant increase P2X7 receptor expression was observed in porcine burn injury

Cx43 hemichannels regulate the release of ATP into the extracellular space and activate P2X7 receptors to regulate its function and induce inflammatory response. To further understand the relationship between Cx43 and P2X7 receptors, pig burn tissues were immunostained with P2X7. On PBD 4, there was an increase in P2X7 protein expression as shown in DeCtrl compared to NS ($p<0.05$) (Figure 5.8 a, b & d). Upon treatment with Cx43asODN or Tonabersat, there was no difference treated wounds compared to DeCtrl or Veh control on PBD 4. On PBD 7, there was no difference in P2X7 expression across all treatments (Figure 5.8 c & e).

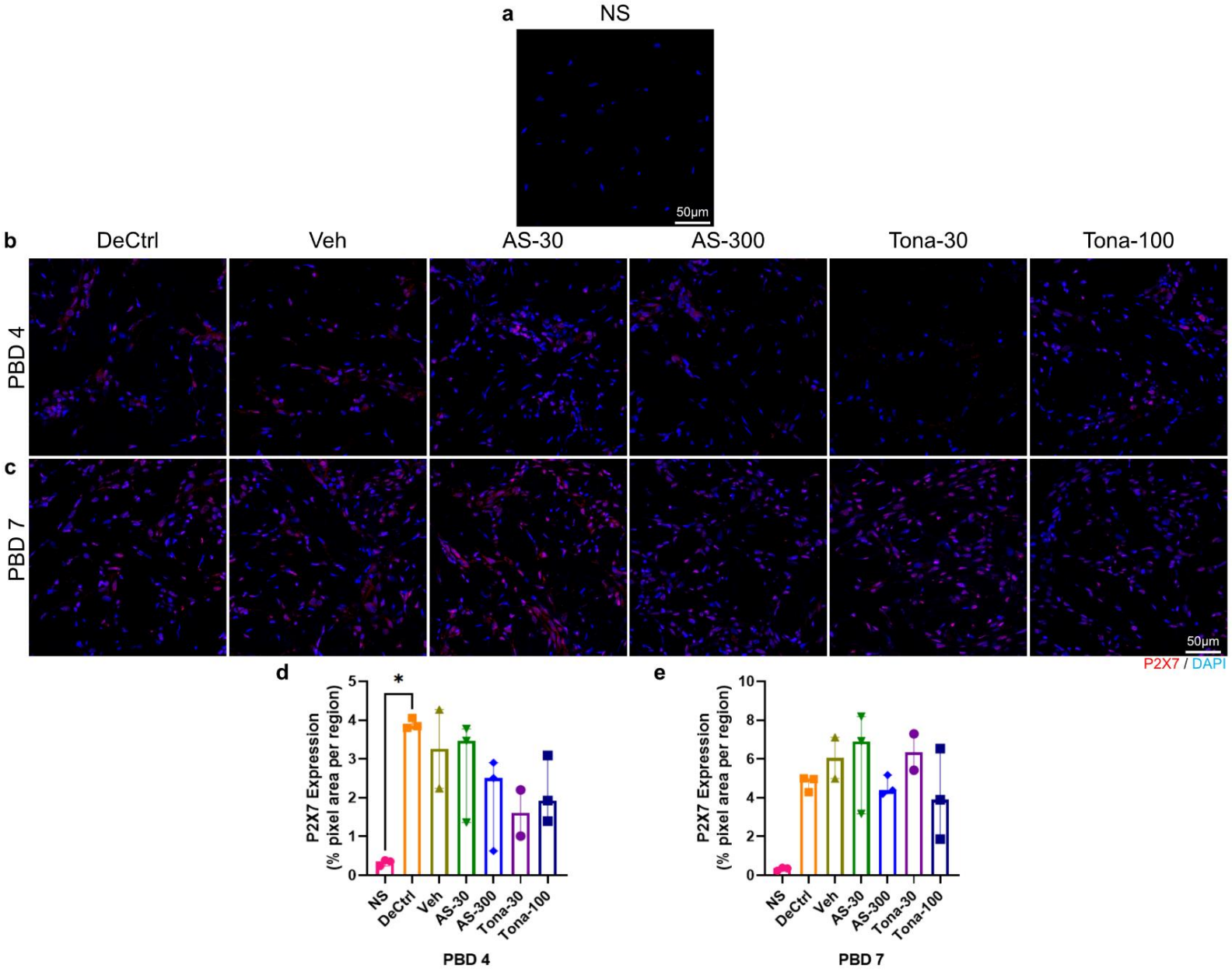
a
NS
50μm
b
DeCtrl
Veh
AS-30
AS-300
Tona-30
Tona-100
PBD 4
c
PBD 7
50μm
P2X7 / DAPI
d
P2X7 Expression
(% pixel area per region)
*
NS
DeCtrl
Veh
AS-30
AS-300
Tona-30
Tona-100
PBD 4
e
P2X7 Expression
(% pixel area per region)
NS
DeCtrl
Veh
AS-30
AS-300
Tona-30
Tona-100
PBD 7

Figure 5.8 Topical application of Cx43 targeted therapeutics did not reduce P2X7 expression in zone of stasis on PBD 4.

Representative immunofluorescence image of P2X7 expression in (a) normal skin (NS), (b) zone of stasis at PBD 4 and (c) PBD 7. Debrided Ctrl: DeCtrl, Vehicle control: Veh, Cx43asODN 30µM: AS-30, Cx43asODN 300µM: AS-300, Tonabersat 30µM: Tona-30, Tonabersat 100µM: Tona-100. Magnification: 40x. Scale bar: 50µm. (d) Image analysis graph of P2X7 expression on PBD 4 and (e) PBD 7. Image analysis graph shows an increased P2X7 expression between NS vs DeCtrl (n=3 animals per group) on PBD 4 & 7. Image analysis reveals P2X7 expression comparison of treated (AS-30, AS-300, Tona-30 & Tona-100, n=3, 3, 2 & 3 animals, respectively) to DeCtrl & Veh (n=3 & 2 animals, respectively) on PBD 4 & 7. Data are presented as median and interquartile range (IQR). Statistical comparisons were made using Kruskal-Wallis Test. (*$p<0.05$).

5.2.7 Reduction in NLRP3 and Cas-1 expression observed in treated burn wounds

P2X7 receptor activation triggers the formation of NLRP3 inflammasome complex, comprising of apoptosis-associated ASC and Caspase-1 (Cas-1) (Figure 5.9 & Figure 5.10). On PBD 4, there was an increase in NLRP3 expression in the zone of stasis following burn wound injury compared to NS ($p<0.05$) (Figure 5.9 a, b & d). Treatment with Cx4asODN, had slight reduction in NLRP3 expression in AS-300 µM treated wounds compared to DeCtrl and Veh control wounds ($p=0.3800$ and $p=0.9428$, respectively). Wounds treated with Tona-100 µM had slight reduction in NLRP3 expression compared to DeCtrl ($p=0.6275$) (Figure 5.9 b & d). However, there was no difference between the treated groups and Veh control groups. On PBD 7, NLRP3 expression remained significantly increased in DeCtrl control wound compared to NS ($p<0.05$). Treatment with Cx43asODN or Tonabersat did not have any effect on PBD 7 when compared to DeCtrl and Veh controls (Figure 5.9 c & e).

On PBD 4, there was an increase in Cas-1 expression in the zone of stasis, following burn wound injury as compared to NS ($p<0.05$) (Figure 5.10 a, b & d). Wounds treated with Cx43asODN slightly reduced Cas-1 expression in AS-300 µM treated wounds was observed compared to DeCtrl ($p=0.8166$). Wounds treated with Tona-30 µM and Tona-100 µM had slight reduction Cas-1 expression than DeCtrl ($p=0.8551$ and $p=0.3539$, respectively) (Figure 5.10 b & d). On PBD 7, no difference in the treated groups and DeCtrl. AS-300 µM and Tona-100 µM had slight reduction in Cas-1 expression as compared to Veh ($p=0.5559$ and $p=0.8551$, respectively) (Figure 5.10 c & e).

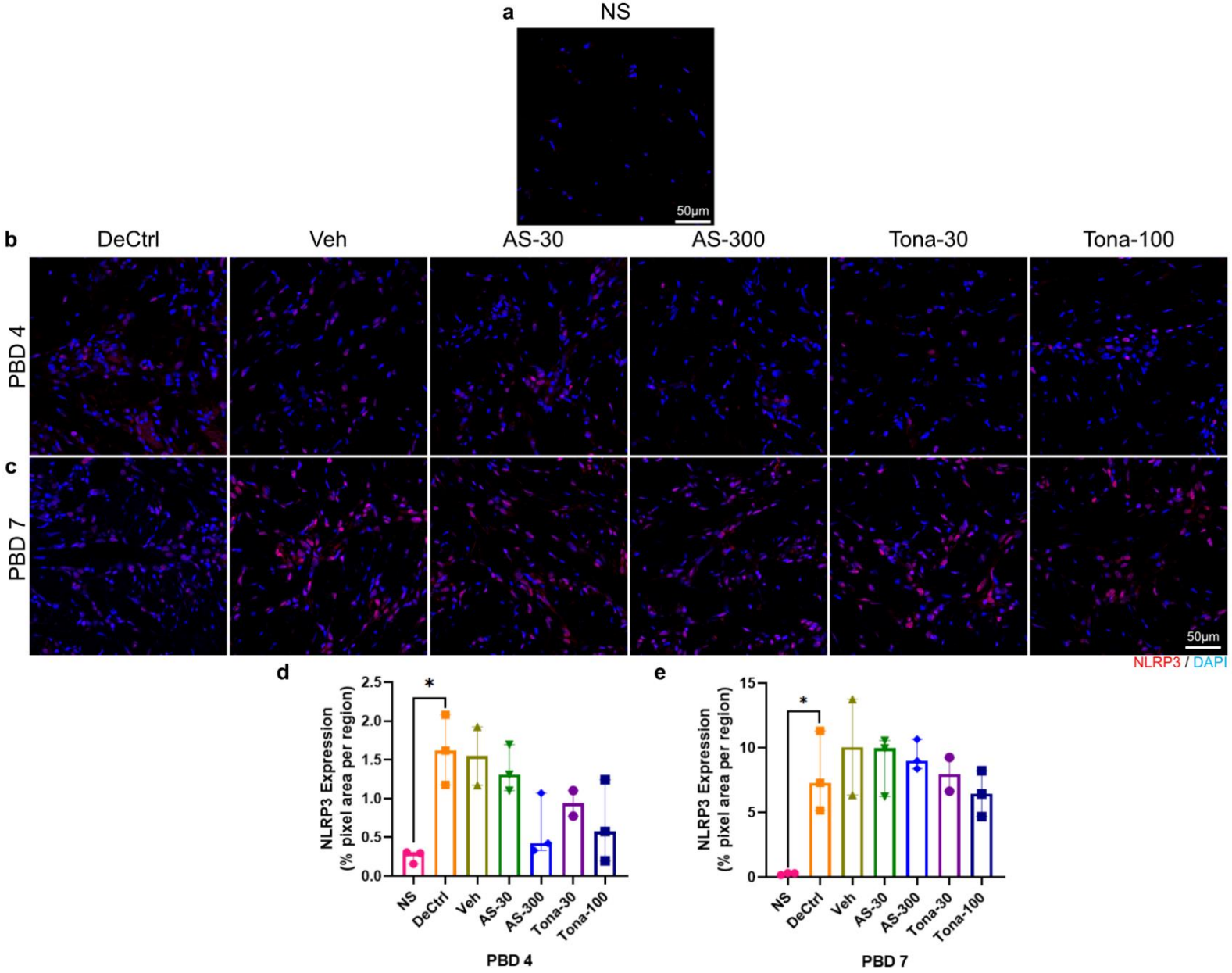
a
NS
50μm
b
DeCtrl
Veh
AS-30
AS-300
Tona-30
Tona-100
PBD 4
c
PBD 7
50μm
NLRP3 / DAPI
d
NLRP3 Expression
(% pixel area per region)
2.5
2.0
1.5
1.0
0.5
0.0
*
NS
DeCtrl
Veh
AS-30
AS-300
Tona-30
Tona-100
PBD 4
e
NLRP3 Expression
(% pixel area per region)
15
10
5
0
*
NS
DeCtrl
Veh
AS-30
AS-300
Tona-30
Tona-100
PBD 7

Figure 5.9 Topical application of Cx43 targeted therapeutics marginally reduced NLRP3 expression in zone of stasis on PBD 4.

Representative immunofluorescence images of NLRP3 expression in (a) normal skin (NS), (b) zone of stasis at PBD 4 and (c) PBD 7. Debrided Ctrl: DeCtrl, Vehicle control: Veh, Cx43asODN 30µM: AS-30, Cx43asODN 300µM: AS-300, Tonabersat 30µM: Tona-30, Tonabersat 100µM: Tona-100. Magnification: 40x. Scale bar: 50µm. (d) Image analysis graph of NLRP3 expression on PBD 4 and (e) PBD 7. Image analysis graph shows an increased NLRP3 expression between NS vs DeCtrl (n=3 animals per group) on PBD 4 & 7. Image analysis reveals NLRP3 expression comparison of treated (AS-30, AS-300, Tona-30 & Tona-100, n=3, 3, 2 & 3 animals, respectively) to DeCtrl & Veh (n=3 & 2 animals, respectively) on PBD 4. Data are presented as median and interquartile range (IQR). Statistical comparisons were made using Kruskal-Wallis Test. (*$p<0.05$).

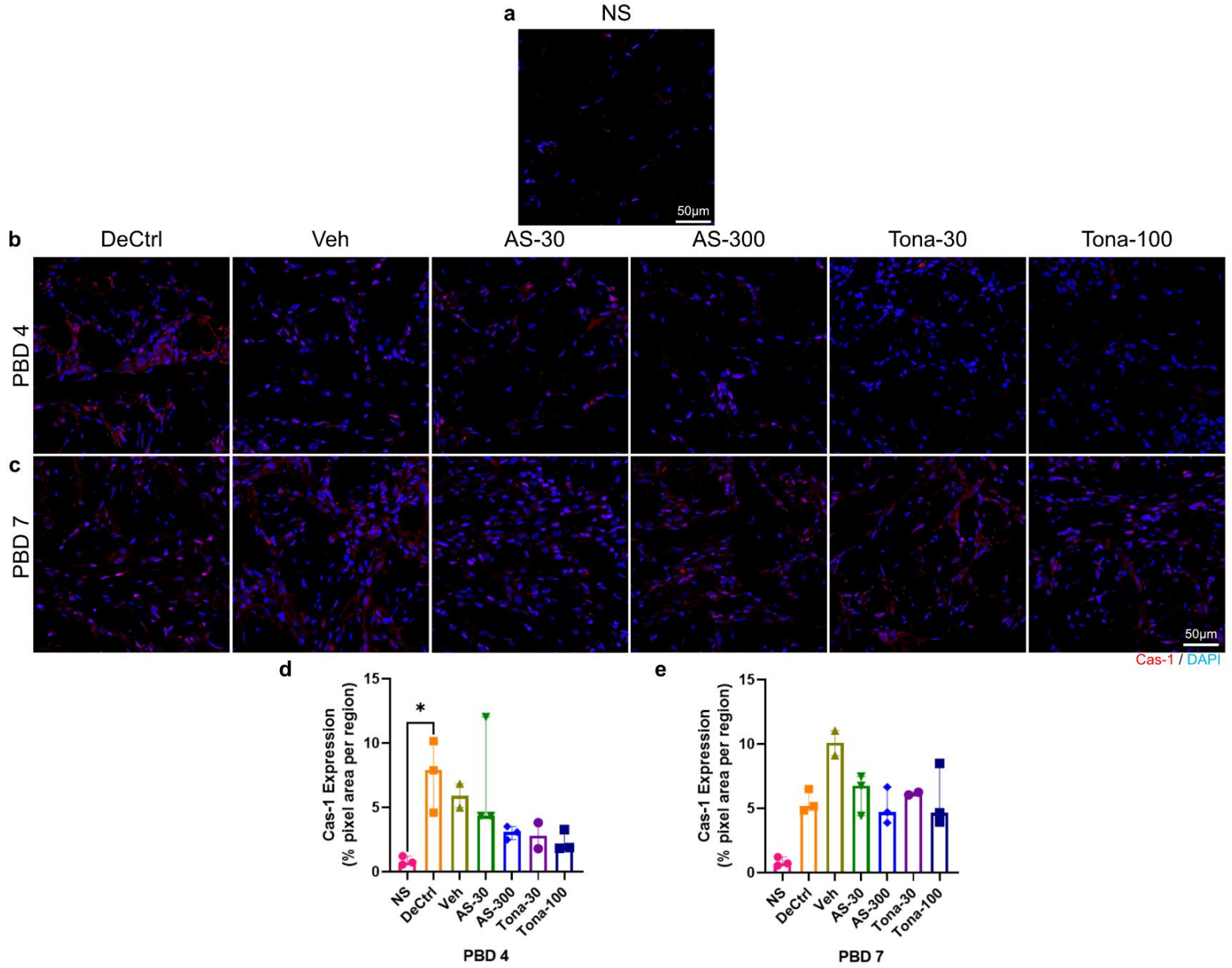
a
NS
50μm
b
DeCtrl
Veh
AS-30
AS-300
Tona-30
Tona-100
PBD 4
c
PBD 7
50μm
Cas-1 / DAPI
d
Cas-1 Expression
(% pixel area per region)
15
10
5
0
*
NS
DeCtrl
Veh
AS-30
AS-300
Tona-30
Tona-100
PBD 4
e
Cas-1 Expression
(% pixel area per region)
15
10
5
0
NS
DeCtrl
Veh
AS-30
AS-300
Tona-30
Tona-100
PBD 7

Figure 5.10 Topical application of Cx43 targeted therapeutics marginally reduced Cas-1 expression in zone of stasis on PBD 4.

Representative immunofluorescence images of Cas-1 expression in (a) normal skin (NS), (b) zone of stasis at PBD 4 and (c) PBD 7. Debrided Ctrl: DeCtrl, Vehicle control: Veh, Cx43asODN 30µM: AS-30, Cx43asODN 300µM: AS-300, Tonabersat 30µM: Tona-30, Tonabersat 100µM: Tona-100.Magnification: 40x. Scale bar: 50µm. (d) Image analysis graph of Cas-1 expression on PBD 4 and (e) PBD 7. Image analysis graph shows an increased NLRP3 expression between NS vs DeCtrl (n=3 animals per group) on PBD 4 & 7. Image analysis reveals Cas-1 expression comparison of treated (AS-30, AS-300, Tona-30 & Tona-100, n=3, 3, 2 & 3 animals, respectively) to DeCtrl & Veh (n=3 & 2 animals, respectively) on PBD 4 & 7. Data are presented as median and interquartile range (IQR). Statistical comparisons were made using Kruskal-Wallis Test. (*$p<0.05$).

5.2.8 Topical application of Cx43 targeted therapeutics marginally reduced skin fibrosis markers in porcine burn injury

Increased NLRP3 inflammasome activation results in fibrosis in kidney disease (Song et al., 2018; W. Wang et al., 2013). To determine whether skin fibrosis is increased in porcine scald burn injury, αSMA & HSP47 were investigated (Figure 5.11). On PBD 14, there was an increase in αSMA in DeCtrl control and Veh control compared to NS (p=0.2228 and, 0.1252, respectively) (Figure 5.11 a, b & d). Treatment with either Cx43asODN or Tonabersat did not alter αSMA expression on PBD 14 (Figure 5.11 b & d). On PBD 21, there was a significant increase in αSMA in DeCtrl wounds compared to NS (p<0.01). Wounds treated with AS-300 µM had mildly reduced αSMA compared to DeCtrl and Veh control (p=0.4222 and p=0.6924, resepctively). Wounds treated with Tona-100 µM slightly reduced αSMA compared to DeCtrl and Veh control (p=0.5926 and p=0.9158, resepctively). AS-30 µM and Tona-30 µM did not have any difference from DeCtrl and Veh control (p>0.9999) (Figure 5.11 c & e).

On PBD 14, there was an slight increase in HSP47 expression in DeCtrl compared to NS (p=0.422) (Figure 5.11 a, b & f). However, treatment with Cx43asODN or Tonabersat did not reduce HSP47 (Figure 5.11 b & f). On PBD 21, the expression of HSP47 remained slightly elevated in DeCtrl compared to NS (p=0.1111) (Figure 5.11 a, c & g). AS-300 µM treated wounds had lower expression compared to DeCtrl (p=0.5926). However, HSP47 expression on AS-30 µM, Tona-30 µM and Tona-100 µM treated wounds remained unchanged compared to DeCtrl and Veh control on PBD 21 (p>0.9999) (Figure 5.11 c & g).

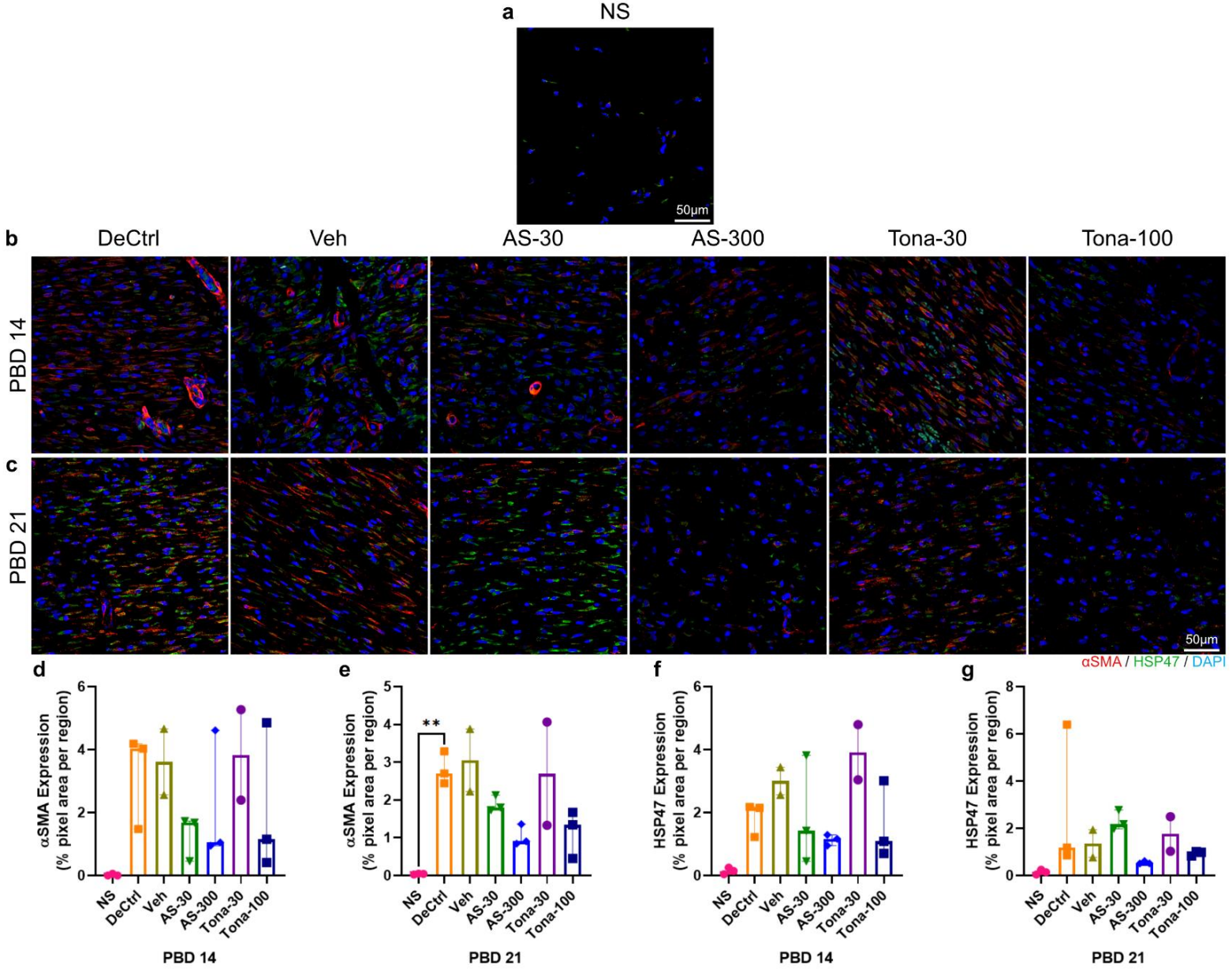
a
NS
50μm
b
DeCtrl
Veh
AS-30
AS-300
Tona-30
Tona-100
PBD 14
c
PBD 21
50μm
αSMA / HSP47 / DAPI
d
αSMA Expression (% pixel area per region)
NS
DeCtrl
Veh
AS-30
AS-300
Tona-30
Tona-100
PBD 14
e
αSMA Expression (% pixel area per region)
**
PBD 21
f
HSP47 Expression (% pixel area per region)
PBD 14
g
HSP47 Expression (% pixel area per region)
PBD 21

Figure 5.11 Topical application of Cx43 targeted therapeutics reduced αSMA and HSP47 expression in zone of stasis on PBD 14 & 21.
Representative immunofluorescence images of co-labelled αSMA (red) and HSP47 (green) expression in (a) normal skin (NS), (b) Debrided Ctrl: DeCtrl, Vehicle control: Veh, Cx43asODN 30µM: AS-30, Cx43asODN 300µM: AS-300, Tonabersat 30µM: Tona-30, Tonabersat 100µM: Tona-100 at PBD 14 and (c) PBD 21. Magnification: 40x. Scale bar: 50µm. (d) Image analysis graph of αSMA expression on PBD 14 and (e) PBD 21. (f) Image analysis graph of HSP47 expression on PBD 14 and (g) PBD 21. Comparisons were made between NS vs DeCtrl (n=3 animals per group) on PBD 14 & 21. Comparison of treated (AS-30, AS-300, Tona-30 & Tona-100, n=3, 3, 2 & 3 animals, respectively) to DeCtrl & Veh (n=3 & 2, respectively) on PBD 14 & 21. Data are presented as median and interquartile range (IQR). Statistical comparisons were made using Kruskal-Wallis Test. (**$p<0.01$).

5.2.1 Topical application of Cx43 targeted preserved normal collagen content in the deep dermis of porcine burn injury

To quantify total percentage of collagen content in porcine burn injury, I analysed tissues stained with Masson's Trichrome. I divided the tissues into three portions, namely, upper dermis, mid dermis and deep dermis (Figure 5.12). In upper dermis, DeCtrl wounds and Veh control wounds had the least collagen deposition compared to the AS-30 µM, AS-300 µM, Tona-30 µM and Tona-100 µM treated groups (Figure 5.12 a & d). In the mid dermis, wounds treated with AS-30 µM, AS-300 µM and Tona-100 µM had better collagen preservation compared to DeCtrl and Veh control (Figure 5.12 a & d). Wounds treated with Tona-30 µM had similar collagen preservation pattern to DeCtrl and Veh control in mid dermis and deep dermis (Figure 5.12 b, c & d). Whereas wounds treated with AS-30 µM, AS-300 µM and Tona-100 µM displays normal collagen pattern in deep dermis (Figure 5.12 c & d).

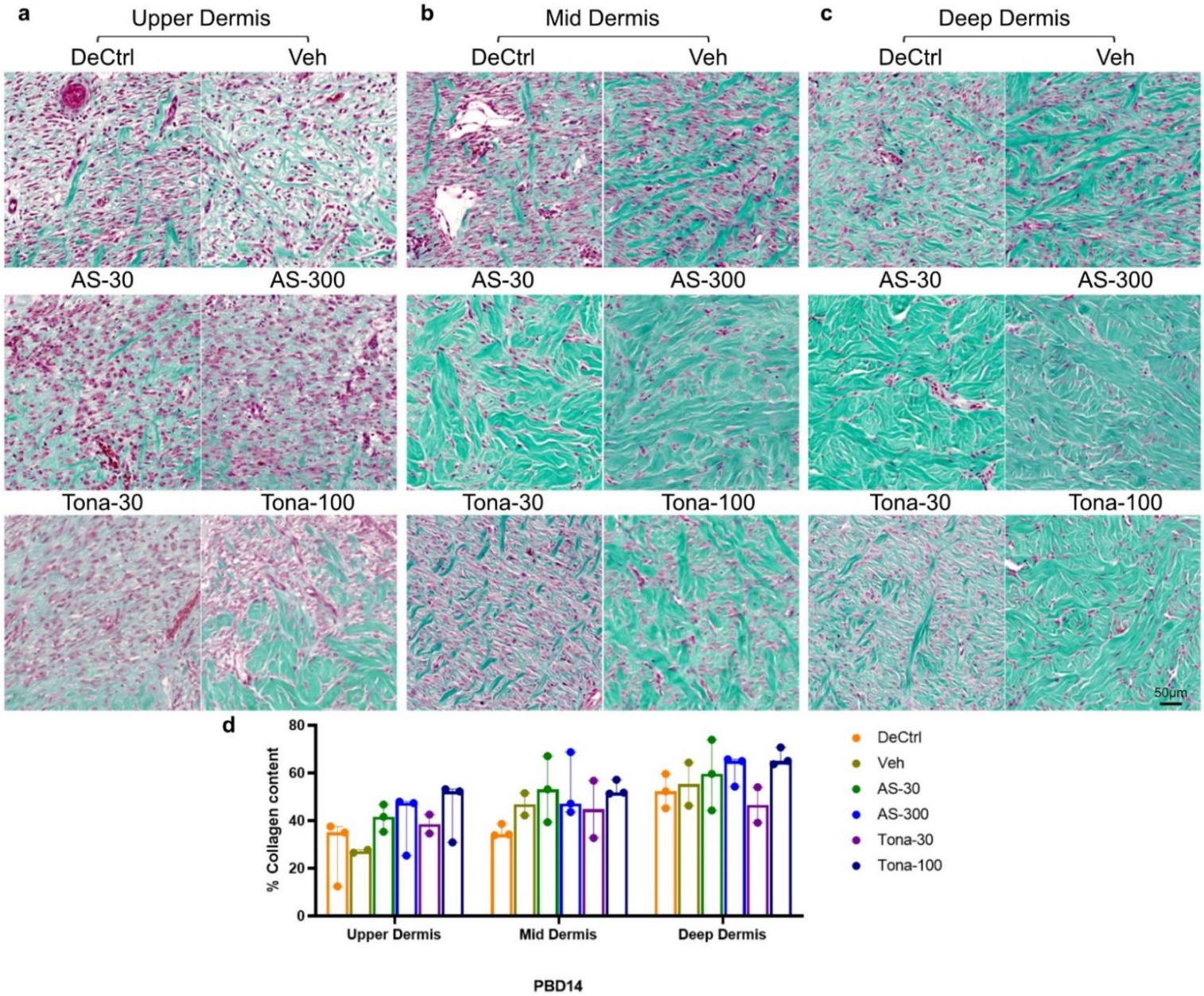
a
Upper Dermis
DeCtrl
Veh
b
Mid Dermis
DeCtrl
Veh
c
Deep Dermis
DeCtrl
Veh
AS-30
AS-300
AS-30
AS-300
AS-30
AS-300
Tona-30
Tona-100
Tona-30
Tona-100
Tona-30
Tona-100
50μm
d
% Collagen content
80
60
40
20
0
Upper Dermis
Mid Dermis
Deep Dermis
PBD14
DeCtrl
Veh
AS-30
AS-300
Tona-30
Tona-100

Figure 5.12 Cx43 targeted therapeutics improved collagen content in pig burn on PBD 14.
(a) The panel shows representative Masson's Trichrome stained images of (a) upper dermis, (b) mid dermis and (c) deep dermis of porcine burn injury on PBD 14. DeCtrl: Debrided control, Veh: Vehicle control, Cx43asODN 30µM: AS-30, Cx43asODN 300µM: AS-300, Tonabersat 30µM: Tona-30, Tonabersat 100µM: Tona-100. Staining: Collagen—green; nuclei—black; muscle fibres and cytoplasm—red. (d) Image analysis of collagen content from Masson's Trichrome stained images of upper dermis, mid dermis & deep dermis (DeCtrl, Veh, AS-30, AS-300, Tona-30 and Tona-100; n=3, 2, 3, 3, 2 & 3 animals, respectively). Data are presented as median and interquartile range (IQR). Statistical comparisons were made using Kruskal-Wallis Test – not significant. Scale bar: 50µm.

5.2.2 Reduction in nascent epidermal thickness in treated porcine burn wounds at PBD 21

The histological appearance of porcine burn wounds was consistent between replicates of the same burn condition. By PBD 14, partial or full nascent epidermis has formed in most of the burn wounds. Nascent epidermal thickness was measured on PBD 14 and 21 (Figure 5.13). I determined the nascent epidermis excluding stratum corneum and rete like ridges by taking measurements of 6 sections 150µm apart from one another (Ippagunta et al., 2016). Particularly, in the control groups (DeCtrl and Veh) the nascent epidermis remained hyper-thickened compared to treated groups. There was significant thicker nascent epidermal thickness in DeCtrl compared to NS on PBD 14 and PBD 21 ($p<0.05$). No significant difference was observed between control groups and treated groups on PBD 14 (Figure 5.13 a & d). On PBD 21, I observed a dose dependant effect in the thickness of nascent epidermis, showing that the lower dose of Cx43asODN (AS-30 µM) and Tonabersat (Tona-30 µM) had hyper-thickened epidermis similar to those in control groups hence no significant difference. Similarly, the 300µM of Cx43asODN (AS-300 µM) nascent epidermal thickness was reduced from both DeCtrl and Veh. The higher dose of Tonabersat (Tona-100 µM) treated wounds had a thinner nascent epidermis compared to DeCtrl on PBD 21 (Figure 5.13 b & e).

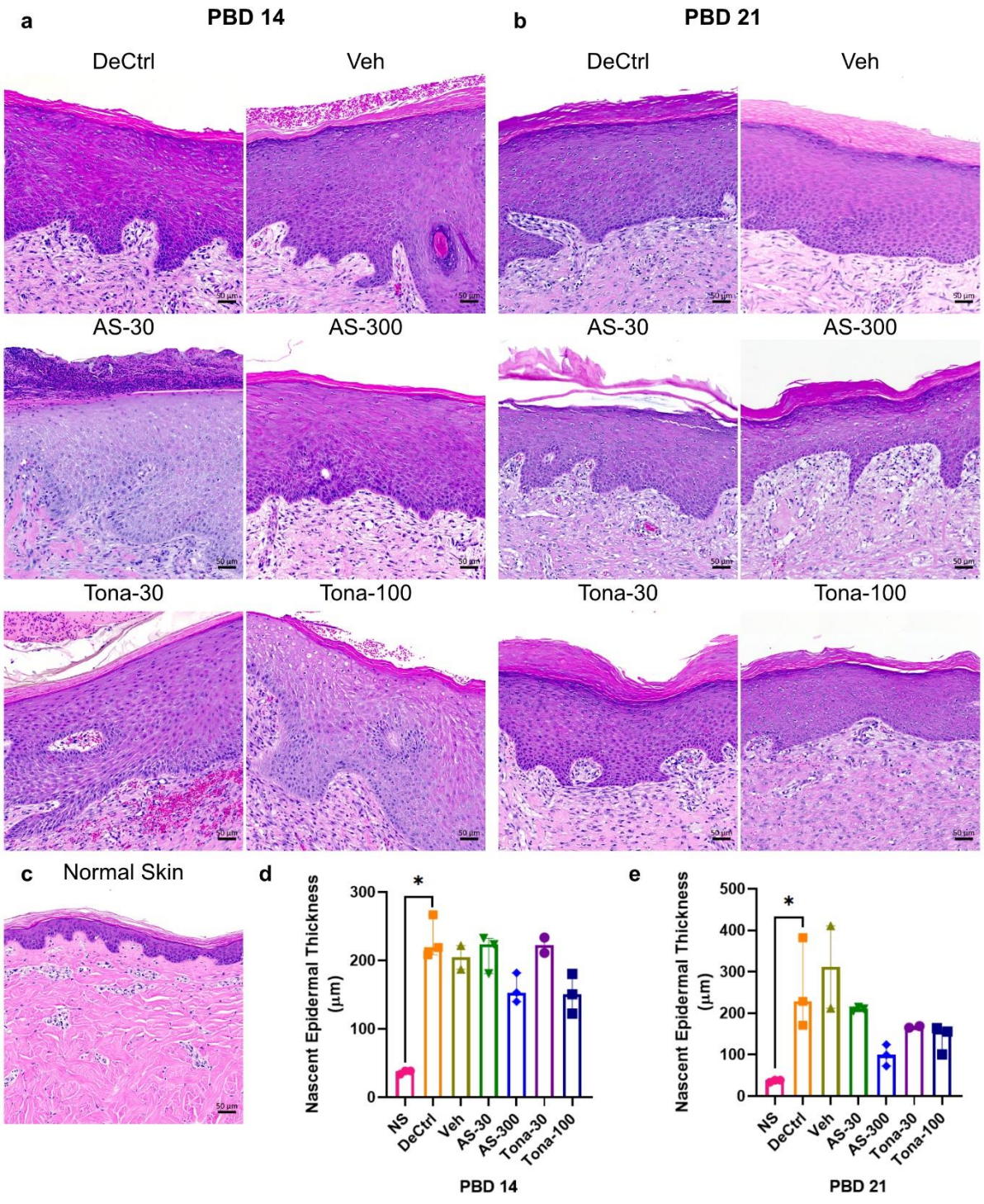

Figure 5.13 Nascent epidermal thickness on topically treated porcine burn wounds with Cx43asODN and Tonabersat.

(a) The panel represents H&E images of nascent epidermis from porcine burn wounds at PBD 14 and (b) PBD 21. (c) Representative of H&E image of porcine normal skin. Scale bar: 50μm. (d) Quantification of nascent epidermal thickness measurement at PBD 14 and (e) PBD 21. Data are presented as median and interquartile range (IQR). Statistical comparisons were made using Kruskal-Wallis Test ($p<0.05$). n= 3, 3, 2, 2, 3, 2 & 3 animals per group, in respective order as shown in graph).

5.3 Discussion

5.3.1 Cx43 and hemichannels in porcine burn injury

In this study, I discovered that the stasis zone of porcine burn injuries had higher protein levels of Cx43 gap junctions and hemichannels. Topical administration of either Cx43asODN or Tonabersat for four consecutive days caused a dose-dependent downregulation of Cx43 protein level. However, hemichannel protein levels did not alter in the zone of stasis. These findings were in line with those of Wang and colleagues, who found that endogenous Cx43 expression was elevated *in vitro* in pig cardiomyocytes stimulated with Ca^{2+} was inhibited by 50% with siRNA targeting Cx43 (N. Wang et al., 2012). Full thickness excisional wounds have been shown by western blot to have elevated Cx43 in a pig cutaneous injury model. With the administration of ACT1 peptide, this increase was reversed, and histological examination demonstrated decreased neutrophil recruitment, improved vascularization, and decreased scarring and wound area as compared to controls (Ghatnekar et al., 2009). An ischaemic condition in pig hearts enhanced the permeability of Cx43 gap junctions and hemichannels (Schulz et al., 2003), and this has been linked to the swelling of cardiomyocyte cells in response to simulated ischaemia (Schulz et al., 2007). In addition, treatment with octanol or 18 alpha glycyrrthetinic acid (18-α-GA), reduced the opening of hemichannels and consequently diminished cell swelling during ischaemia (Schulz et al., 2007). Treatment with Gap26 or 27 inhibited functional Cx43 hemichannels and hemichannel currents promoted by intracellular Ca^{2+} elevation (N. Wang et al., 2012). Furthermore, Gap19 also inhibited Cx43 hemichannels present in *in vivo* pig ventricular cardiomyocytes (D'Hondt et al., 2014). These findings support the hypothesis that downregulating Cx43 and hemichannel protein levels in the zone of stasis generates protection against disease progression.

5.3.2 P2X7 and NLRP3 activation in porcine burn injury

I have demonstrated that there is increased NLRP3 and Cas-1 expression in porcine burn injury in the zone of stasis. By targeting Cx43 with Cx43asODN or Tonabersat, I was able to show a trend in reduction of NLRP3 and Cas-1 expression in the zone of stasis. The data from Chapter 4 has shown that Cx43 targeted therpeutics reduced NLRP3 and Cas-1 expression in rat burn injury. This could be extrapolated that the similar effect may be taking place in porcine burn injury.

Extracellular ATP release is mediated by the constant opening of pathological hemichannels. Numerous studies have shown that external ATP activates P2 purinergic receptors, including P2X purinergic receptors like P2X4 and P2X7, and P2Y purinergic receptors, such as P2Y12 receptors, as a physiological cellular communication that causes a flux of Na^+, Ca^{2+}, and K^+ ions (Acosta et al., 2021; Lohman & Isakson, 2014; Mugisho, Rupenthal, et al., 2019). In a study of primary cultures of porcine bladder urothelial cells, acrolein-induced inflammatory damage had increased cell toxicity, increased P2X7 expression, and disrupted the tight junction protein ZO-1. However, this effect was abolished with the treatment of the selective P2X7R antagonist A804598, thus retained cell integrity and prevented degradation of tight junctions (Taidi et al., 2022). Similarly, another study reported on porcine theca cells from antral follicles, extracellular ATP induced cell death and DNA fragmentation was mediated by P2X7. Treatment with non-specific antagonist of P2X7, pyridoxal phosphate-6-azo (benzene-2,4-disulfonic acid) tetrasodium salt (PPADS), reversed this effect, suggesting a possible role for signalling via ATP during follicular development (Vazquez-Cuevas et al., 2006). Injury to the endothelium of harvested human saphenous veins has been shown to cause grafting failure and functional impairment of the vasomotor, thrombosis and inflammation. Using a rat model of overstretched aorta injury to

understand surgical traction injury has shown stretch injury of vascular tissue led to impaired endothelial-dependent relaxation via P2X7 activation. Treatment with purinergic P2X7 receptor inhibitors, brilliant blue FCF (FCF) and A740003, or apyrase, an enzyme that catalyses the hydrolysis of ATP, reduced nitric oxide production via the p38 MAPK signalling pathway and thus restored endothelial function (Komalavilas et al., 2017). In recent times, a substantial link has been found between Cx43 hemichannels and the P2X7 receptor. However, to my best knowledge no studies have demonstrated this connection in burn injuries. Despite the fact that I did not quantify ATP release from the porcine burn wounds, studies have demonstrated that ATP levels are higher during the first few hours after burn injury and cause burn progression (Bayliss et al., 2014). Hence, it can be postulated that extracellular ATP release from Cx43 hemichannels triggered activation of P2X7 in the zone of stasis, as demonstrated by increased Cx43 hemichannel and P2X7 protein levels. Furthermore, upon treatment with Cx43asODN, the protein expression of P2X7 was downregulated in a dose dependent manner. Burn wounds treated with a low concentration of Tonabersat (30μM) had marginally downregulated P2X7 expression very early on during burn injury. Xu and colleagues reported that the release of extracellular ATP from Cx43 hemichannels triggers P2X7 activation in tubular epithelial cells (Xu et al., 2022). Additionally, blockade of Cx43 hemichannels using the mimetic peptide Gap26 reduced ATP release. This suggests that preventing hemichannel opening reduces P2X7 activation.

Increasing evidence has suggested that P2X7 activation activates the NLRP3 inflammasome complex by recruiting and activating Caspase-1 and increasing production of mature IL-1β in models of diabetic retinopathy, liver, and central nervous systems (Albalawi et al., 2017; Kong et al., 2022; Tao et al., 2020). Pig peripheral blood mononuclear cells treated *in vitro* with LPS and

ATP produced more IL-1β, as demonstrated by van Hout and colleagues. However, the NLRP3 inhibitor MCC950 eliminated this secretion in a dose-dependent manner. In addition, increased NLRP3 mediated IL-1β production and increased neutrophil infiltration were dramatically suppressed when MCC950 was administered intravenously to pigs with transluminal balloon occluded hearts, preserving cardiac function and reducing infarct size (van Hout et al., 2017).

In this study, it was not possible to find a good antibody to study the expression of IL-1β in pig tissue. However, NLRP3 and Cas-1 protein expression in porcine burn injury indicates the possible activation of NLRP3 inflammasome complex in the zone of stasis. Based on previous studies and current findings from rat burn injury, it can be postulated that the reduced protein expression of NLRP3 and Cas-1 could mediate reduction in IL-1β in the zone of stasis of porcine burn injury. It is also important to note that the NLRP3 inflammasome in the porcine study is similar to human NLRP3 (Tohno et al., 2016). Hence, studying the role of Cx43 mediated NLRP3 inflammasome activation in the porcine burn injury model is clinically relevant.

5.3.3 Inflammation in porcine burn injury

I demonstrated that inflammation was increased in the zone of stasis as indicated by increased MPO in the early phases of burn wound healing. The extent and complexity of the inflammatory response in a burn injury is what determines the severity of the condition. Histamine, free radicals, and inflammatory cytokines are released as part of the first response, which causes vasodilation and secondary tissue damage. This draws neutrophils to the site, to kickstart chemotactic signalling to recruit macrophages (Korkmaz et al., 2017; Lateef et al., 2019). Increases in Cx43 protein level in neutrophils and macrophages have been reported in a number of studies (Branes et al., 2002;

Eugenin et al., 2003). In this study, I confirmed with immunostaining of sister sections with Cx43, MPO and H&E, multi-lobed nuclei that Cx43 and hemichannel protein expression was upregulated in neutrophils in the zone of stasis (Figure 5.5 and Figure 5.7). Earlier research confirms that that activated neutrophils exhibit elevated Cx43 expression (Eltzschig et al., 2006). The expression of elevated Cx43 and increased neutrophil migration to inflamed lungs were observed in a study of lung injury in mouse models that had been exposed to inflammation by intratracheal instillations of LPS. Gap26 treatment of inflamed lungs reduced neutrophil transmigration by 65%, indicating that Cx43 may be involved in mediating inflammation (Sarieddine et al., 2009). Furthermore, they also demonstrated using *in vitro* assays that adhesion of neutrophils was regulated by gap junctional coupling via Cx43 with endothelial cells and with addition of Gap26 adhesion was decreased (Sarieddine et al., 2009). Cx43asODN treatment of burn wounds in neonatal mice has demonstrated a reduction in the propagation of tissue damage and neutrophil infiltration around the wound after injury by reducing vasodilation and leakage of capillaries (Coutinho et al., 2005). However, in this study treatment with Cx43 targeted therpeutics did not alter MPO positive cells in porcine burn injury. The treatment effect on inflammatory response could not be determined due to the limited sample size. In addition, it was a major challenge to idenity working antibodies to target other immune cells such as macrophages on porcine tissues. The inclusion of additional immune cell markers will provide a more comprehensive and accurate assessment of the true effect of Cx43 targeted therapy in porcine burn injury. As a result, the investigation was restricted to one marker to study inflammation in the region. However, data from rat burn model (Chapter 4) have shown a decrease in MPO positive cells in the zone of stasis. This can be extrapolated to provide insights into the inflammatory response in porcine burn wounds targeted with Cx43 therapeutics, aiding in the assessment of therapeutic interventions in a broader context.

Furthermore, the accumulation of ATP may activate P2X7 in neutrophils, which leads to ATP induced loss of intracellular K^+, NLRP3 inflammasome activation and IL-1β secretion, triggering a secondary cascade of inflammation (Karmakar et al., 2016). In a rat model of experimental gout, the neutrophilic NLRP3 inflammasome has been proposed as a key source of IL-1β, causing increased inflammation and discomfort (Goldberg et al., 2017). Purified neutrophils from patient donors activated with a TNF/bacterialPly combination were treated with the specific NLRP3 inhibitor MCC950, which prevented the generation of IL-1β (Hassane et al., 2017). In our investigation, it was discovered that early stages of burn injury had elevated P2X7/NLRP3/Cas-1 expression in the zone of stasis, which could be dominated by neutrophils. However, treatment with Cx43asODN or Tonabersat reduced this expression in these cells, indicating that targeting NLRP3 via the Cx43/P2X7/NLRP3 pathway may reduce neutrophil response in the zone of stasis.

5.3.4 Reduced αSMA and HSP47 expression improved collagen content and nascent epidermal thickness in porcine burn injury

Burn injuries can lead to fibrotic scar contracture by the presence of increased numbers of myofibroblasts that express αSMA. Myofibroblast differentiation is categorized in two stages: proto-myofibroblasts and differentiated myofibroblasts that express αSMA (Desmouliere et al., 2005; Gabbiani, 2003). It is believed that alterations in the mechanical and organizational characteristics of the ECM and cytokine release by the inflammatory response causes proto-myofibroblast to develop after an injury (Hinz, 2007; Tomasek et al., 2002). Myofibroblasts have been shown to be the predominant cell type in granulation tissue after burn injury and to express increased levels of αSMA (Wang et al., 2011). ECM remodelling causes fibroblast differentiate into myofibroblast in response to profibrotic factors such as TGFβ1 to induce expression of αSMA (Asazuma-Nakamura et al., 2009; Hinz, 2007). It was discovered that TGβ1 induced αSMA

expression increases concurrently with Cx43 in *in vivo* neonatal rat cardiac fibroblasts (Asazuma-Nakamura et al., 2009). Downregulating Cx43 with Cx43asODN reversed this result, suggesting that Cx43 contributes to TGFβ1 signalling to regulate α-SMA expression. (Asazuma-Nakamura et al., 2009). Additionally, the expression of PAI-1 and αSMA was decreased in a peritoneal adhesion mouse model after Cx43 was downregulated with a single application of Cx43asODN (Chua et al., 2022).

In addition, studies have shown that the involvement of purinergic receptors and the NLRP3 inflammasome pathway induce fibrosis. According to research by Lu and colleagues, ATP binding to P2Y2 receptors mediated by Cx43 or Cx45 hemichannels increased collagen accumulation and αSMA synthesis by 60% via activation of the ERK signalling pathway. Additionally, treatment with carbenoxolone, a non-specific gap junction inhibitor, inhibited Cx43 or Cx45 expression and reduced mRNA expression of profibrotic markers such as plasminogen activator inhibitor-1 (PAI-1) and monocyte chemotactic protein-1, which in turn lowered the synthesis of αSMA in cardiac fibroblasts (Lu et al., 2012). Bracey and colleagues have reported that TGFβ1 stimulates cardiac fibroblasts to express NLRP3 and activate αSMA. Notably, NLRP3 regulation through myofibroblast differentiation in NLRP3 deficient mice protected against cardiac fibrosis and preserved cardiac architecture (Bracey et al., 2014). Moreover, streptozotocin (STZ) induced diabetes increases NLRP3 expression, leading to increased IL-1β and IL-18 levels that are associated with myofibroblast differentiation and αSMA expression. However, treatment with H3 relaxin inhibited NLRP3 inflammasome activation and attenuated αSMA and fibrosis markers (Zhang et al., 2017).

HSP47 is a marker of collagen synthesis and excessive collagen production leads to fibrosis. Numerous studies have reported that upregulation of HSP47 correlates to increased fibrosis (Chen et al., 2007; Kitamura et al., 2011; Mishima et al., 2003; Otsuka et al., 2017; Xiao et al., 2012). Furthermore, in a study of a porcine excisional wound model, HSP47 expression was upregulated during the healing process and correlated with the synthesis of collagen (Wang et al., 2002). It has been documented that in keloid scar, upregulation of HSP47 mRNA and protein has been correlated to increased collagen type I and III expression, suggesting the potential role in the development and progression of fibrosis (Naitoh et al., 2001). In addition, increasing evidence has reported the potential interaction between NLRP3 and HSP47. Arsenic stimulation both *in vitro* and *in vivo* caused an elevated expression of NLRP3 and HSP47 in a study of liver fibrosis. Blocking the activity of the NLRP3 inflammasome in hepatic stellate cells, resulted in reduced expression of HSP47 and the profibrotic markers collagen type I and αSMA (Yuan et al., 2022). Similarly, in a study of dermal fibrosis, delivery of HSP47 siRNA using a nanoparticle platform was shown to reduce HSP47 protein expression and profibrotic markers NOX4, collagen type I and αSMA (Morry et al., 2015). These studies support Cx43asODN or Tonabersat treatment in porcine burn wounds to have reduced HSP47 and αSMA expression via the NLRP3 inflammasome pathway in a dose dependent manner. Furthermore, histological analysis with Masson's Trichrome has also shown that better collagen preservation was observed in deeper layers of burn wounds of those treated with Cx43asODN or Tonabersat.

Hypertrophic scars can form in response to burn injuries, impaired wound healing or from inadequate wound care therapies (Tredget et al., 2014). Enhanced epidermal thickness, increased expression of keratinocyte proliferation and activation markers such as keratins 5, 6, and 16 and

17 are some of the characteristics of hypertrophic scars (Hakvoort et al., 1999). In addition, pro-inflammatory cytokines, fibrogenic and growth factors, influence the state of a healing epidermis (Hakvoort et al., 1999). In a study of porcine full thickness burn hypertrophic scar model, they found that the nascent epidermis was thicker than that of those treated with Shikonin spray, which has anti-tumorigenic, antioxidant, anti-bacterial, and anti-inflammatory properties. Furthermore, they found the differentiation marker cytokeratin 10 and proliferative marker p63 expression to be markedly reduced in the epidermis of hypertrophic scars treated with Shikonin (Deng et al., 2018). In chronic wounds, diabetic ulcers and venous leg ulcers, hyper-thickened epidermis is correlated with increasing Cx43 expression (Becker et al., 2012). Downregulation of Cx43 with Cx43asODN enhanced epidermal keratinocyte migration and fibroblast migration from the wound edge of excisional and incisional skin wound mouse models (Mori et al., 2006).

It has been reported that the αSMA expression in a porcine burn scar directly correlates to the severity of the burn condition, thickness of scar tissues, re-epithelialisation time and depth of burn (Wang et al., 2011). Here, I have demonstrated that wounds treated with Cx43asODN or Tonabersat had decreased expression of αSMA and HSP47 fibrosis, as well as improved collagen content confirmed with Masson's Trichrome staining and decreased nascent epidermal thickness, indicating an overall improved healing in treated wounds. These findings are consistent with those of Wang and colleagues (Wang et al., 2011).

In addition, targeting the zone of stasis has been shown to be beneficial for the treatment of burn injuries. Yucel et al., demonstrated that systemic pentoxifylline (PTX) treatment in rat comb burn model reduced inflammation and cell death in the zone of stasis. This in turn reduced the necrotic area, accelerated re-epithelization, and improved rat burn wound healing (Yucel et al., 2019).

Furthermore, Federick et al., showed that Clostridium collagenase treatment to porcine skin burn wounds prevented the conversion of tissue in the zone of stasis via faster resolution in neutrophils and limiting necrosis and apoptosis (Frederick et al., 2021). In addition, Clostridium collagenase treatment prevented destruction of dermal collagen and burn conversion that often led to a significant delay in healing (Frederick et al., 2021). These findings support that the targeting the zone of stasis for burn therapies prevents burn progression and improves wound healing outcomes.

5.4 Conclusion

To my best knowledge, this is the first study to test Cx43 targeted therapeutics in a pig scald burn injury. Here I have shown that upon burn wound injury, there is elevated Cx43 and hemichannel expression in zone of stasis. With the treatment of low and high concentrations of Cx43asODN or Tonabersat, I was able to reduce Cx43 expression. However, there was no changes in P2X7 and inflammation in the zone of stasis of porcine burn injury. Concomitantly, NLRP3 and Cas-1 expression was marginally reduced in a dose dependent manner. Due to the limitation of the study, such as small sample size, extrapolation from Chapter 4 on topical application Cx43 targeted theraputics on rat burn injury could possibly indicate that Cx43 gap junction and hemichannels may play a role in the activation of NLRP3 inflammasome. Concomitantly, early intervention with Cx43asODN or Tonabersat improved collagen content on PBD 14. Although all of the wounds have re-epithelialized by PBD 21, it is important to note that there is reduction in epidermal thickness in wounds treated with Cx43asODN or Tonabersat compared to control groups. Despite the major limitation of sample size, I demonstrated that early intervention with Cx43 targeted therapeutics in the zone of stasis may be beneficial in the treatment of burn injuries and could be used for future clinical applications.

Chapter 6: Preliminary study of Cx43asODN or Tonabersat scaffold delivery prevents burn progression in porcine burn injury

6.1 Introduction

As burn injury management can be challenging because of its pathophysiology, high mortality rate and long hospital stay, research to create new management methods or study the prevention of burn progression is of utmost importance (Hwee et al., 2016; Ngim & Ghulam, 1994). In chapter 5, I have discussed in detail porcine skin and porcine scald burn injury. In summary, porcine models have emerged as promising models due to the close resemblance of anatomical and physiological features to human skin, which makes pig skin optimal for studies of cutaneous biology and healing. Pre-clinical testing of pharmacological drugs was made possible with the use of porcine models prior to human testing (Sullivan et al., 2001). Furthermore, pig models have generally improved our knowledge of both normal and pathological wound healing and have produced a plethora of preliminary data, supporting the further development of these models (Seaton et al., 2015).

I have previously discussed the role of Cx43 gap junctions and hemichannels in porcine disease models of the heart (Stirm et al., 2021), lungs (Weber et al., 2019), kidney (Zhang et al., 2020), and skin (Ghatnekar et al., 2009). In general, the upregulation of Cx43 was associated with increased inflammation and fibrosis, whilst downregulation of Cx43 and hemichannels showed improved disease conditions and better wound healing in these studies. Although the NLRP3 inflammasome was not directly reported in porcine skin related studies, it is important to note that

others have reported it in porcine models of lung, kidney and heart conditions, whereby NLRP3 mediated IL-1β production has caused conditions to worsen as a result of secondary inflammatory response in the extracellular milieu (van Hout et al., 2017; Weber et al., 2019; Zhang et al., 2020). However, no studies have reported the possible role of Cx43 and NLRP3 activation in porcine burn injury. In this chapter, I explore and investigate the possible role of Cx43 and NLRP3 inflammasome pathway in porcine burn injury. In chapter 5, I delivered Cx43asODN and Tonabersat in a topical gel to porcine burn wounds and have observed improved wound healing via the Cx43 mediated NLRP3 pathway. To understand if Cx43asODN and Tonabersat could be delivered using a scaffold dressing method, I began with a pilot study to utilise PCL/PEG polymers as the backbone for these therapeutic drugs.

6.1.1 PCL/PEG scaffold in porcine studies

In the realm of burn management and research, significant challenges persist in addressing tissue damage, pain, delayed wound healing, fluid loss, bacterial infections, and the careful selection of appropriate materials for burn wound dressings. Wound dressing made of non-biodegradable and non-toxic materials such as polyurethane and hydrocolloid has been widely used on burn patients to provide an earlier epithelial cover as an exterior film and control wound exudate and create a moist healing environment (Noor et al., 2022). However, the non-biodegradable dressing offer minimal drug release when loaded with therapeutic drugs. Biodegradable dressings are often preferred in the burn wound care management as these dressings offer numerous benefits. These dressings gradually break down, reducing the need for frequent dressing changes, which alleviates pain and discomfort for burn patients. Additionally, they have a lower risk of adhering to the wound bed, decreasing the chances of injury of tissues during dressing changes (Dhivya et al.,

2015). Biodegradable dressings provide a supportive scaffold for cell attachment, proliferation, and tissue regeneration, promoting essential wound healing processes like granulation tissue formation. Moreover, these dressings act as a barrier against infection, vital in burn wound care (Negut et al., 2020). Biodegradable dressings are environmentally friendly as they naturally degrade, and their ease of application makes them suitable for complex anatomical areas (Rai et al., 2021; Velasco et al., 2015). In addition, biodegradable scaffold dressings offer a higher burst release of therapeutics over an extended period than a non-biodegradable dressing could offer. In the burn care management, the choice of suitable of dressings depends on the burn depth, size and exudate levels. Hence it involves a combination of different dressings and scaffold at various stages of burn wound healing to optimize outcomes (Kim et al., 2022).

One of the most often utilized biocompatible polymeric materials in recent years is polyethylene glycol (PEG), a critical component of many different types of medications and therapeutics that are already in clinical use and FDA authorized (Dethe et al., 2022). The hydrophilicity of PEG makes it ideal to be used in wound healing applications to maintain a moist environment at the wound site (Lan et al., 2023). In addition, the physical and chemical properties of PEG scaffolds such as mechanical strength, degradation rate, pore size can be easily modified to match the requirements of the wound site (Dethe et al., 2022; K. Luo et al., 2020). Polycaprolactone (PCL) another commonly used FDA approved compound has good mechanical strength, stable and gradual biodegradability, and biological compatibility, making it a useful material for wound healing. Very good drug and protein delivery properties are produced when PCL matrix is coupled with bioactive materials, which is another promising property for the application of wound healing and infection control (Al Samad et al., 2016). There are a few ways these synthetic polymers could

aid in drug release as sustained release of drugs is beneficial for regenerative studies. Drug release kinetics are determined by the degradation of the polymer when drugs are integrated into the scaffold matrix. The desired drug is infused into the scaffold, and when the polymer breaks down, the drug is released. When polymer/drug layers are applied to scaffold surfaces, diffusion and degradation of the covering polymer control the release (Yu et al., 2015). Furthermore, it is important to note that some strategies could give a strong burst release over a short period of time and others could reduce the burst release effect and extend the length of release time (Rambhia & Ma, 2015).

In a study of the local delivery to pig ear skin, zinc phthalocyanine nanoparticles composed of poly(ethylene glycol)-block-poly(caprolactone) (PEG-b-PCL) amphiphilic deblock copolymer were successful in penetrating viable skin layers (Conte et al., 2015). Another study explored the use of electrospun poly(ethylene (PEG)/polycaprolactone (PCL) nanofibrous scaffolds loaded with ibuprofen *in vitro*. They reported that continuous drug release of Ibuprofen from the scaffold, had no negative effects on the survival of fibroblasts. Additionally, a small number of adherent cells with rounded shape and proliferating cells on these nanofibrous scaffolds suggested their anti-adhesive properties, indicating that the scaffold could possibly be used as physical barriers for post-operative dressing while eluting ibuprofen to reduce abdominal adhesion and inflammation (Kheilnezhad & Hadjizadeh, 2022).

Biosynthesized gold nanoparticles (Au NPs) have been reported to be effective in promoting wound healing. In a rat incisional model, Au NPs were modified and incorporated with PEG/PCL polymers to form an Au-PEG/PCL scaffold. Their findings show that the Au-PEG/PCL scaffold was successful in encouraging keratinocyte proliferation and reducing the development of scars.

In particular, the polymeric Au-PEG/PCL scaffold showed internal implantation in rats and a reduction in inflammation in the wounded area, supporting its usage as a safe and highly effective biological wound healing agent (Wang et al., 2018). Although, various drugs were used in combination with PCL/PEG with or without additional polymers, it is important to note that the use of PCL/PEG polymer combination is known for its biocompatibility, and its potential for drug delivery makes it attractive for the use in cutaneous biology. No studies have been reported on the use of Cx43asODN or Tonabersat as a form of scaffold dressing.

6.1.2 Hypothesis

I hypothesise that the delivery of Cx43asODN or Tonabersat in a PCL/PEG scaffold will reduce Cx43 gap junctions and hemichannel protein levels, reducing NLRP3 inflammasome activation and preventing burn progression.

6.1.3 Aims

The main aim of this chapter is to show that Cx43 targeted therapeutics loaded PCL/PEG scaffold on porcine burn wounds can prevent the Cx43 upregulation and NLRP3 inflammasome complex activation.

1. Fabricate Cx43 therapeutics loaded PCL/PEG scaffold and understand release profile.
2. Quantifying Cx43 and hemichannel expression in porcine burn injury.
3. Quantifying the expression of NLRP3 inflammasome markers and skin fibrosis makers.
4. Qualitative observations of collagen content and nascent epidermal thickness in porcine burn injury treated with Cx43 targeted therapeutics.

6.2 Results

6.2.1 Scaffold release profile of AS-S and Tona-S

Scanning electron microscopy of Plain Scaffold (P-S), Cx43asODN (AS-S) and Tonabersat Scaffold (Tona-S) displayed smooth, continuous, bead-free, and randomly oriented nanofibers when Cx43asODN or Tonabersat was combined with PCL/PEG polymers (Figure 6.1 a, b & c). However, frequency distribution of fiber diameter revealed that addition of Cx43asODN or Tonabersat to PCL/PEG polymer produced more finer fibers (ranging between 0.4 to 0.8µm) (Figure 6.1 d, e & f).

Scaffold release profile provides valuable information on how loaded drugs or therapeutic agents are released from a scaffold over a period of time. The scaffold release profile assessed the daily concentration of Cx43asODN and Tonabersat eluted from the scaffold releasing. The scaffold release profile showed a burst release of 139 µg/ml (47µM) on day 1 of Cx43asODN scaffold (AS-S) with a gradual release of Cx43asODN over day 3 and 4. Whereas, Tonabersat Scaffold (Tona-S) had a scaffold burst release effect on Day 1 and 2 (19 ug/ml (48 µM) and 47 µg/ml (120 µM),respectively) and then subsequently a gradual release of Tonabersat over the next few days (Figure 6.1 g & h). Notably, the eluted amount from the scaffolds were less than the gel application of 300µM Cx43asODN and 100µM Tonabersat delivered each day for 4 consecutive days.

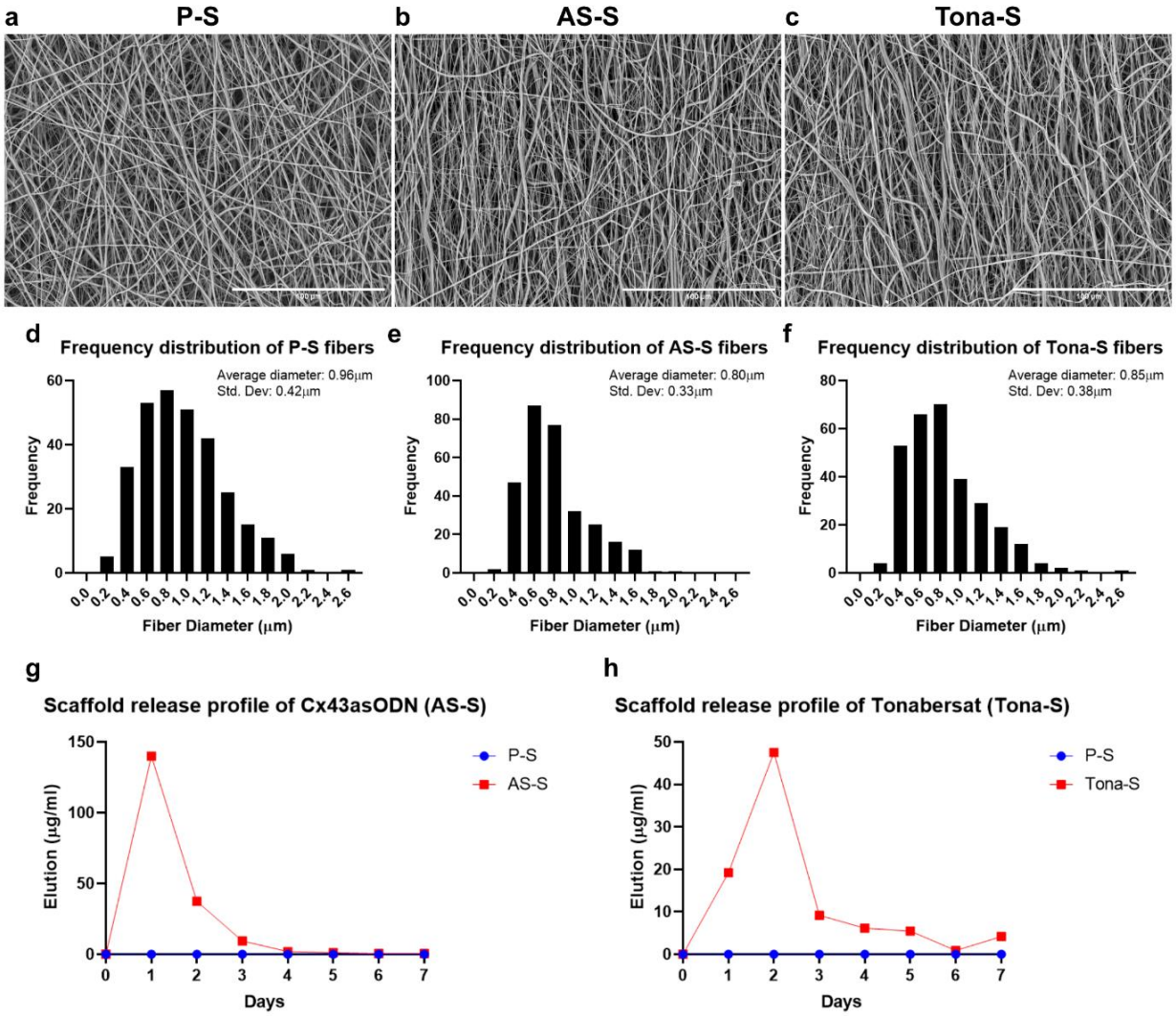

Figure 6.1 SEM and Scaffold release profile of Cx43asODN (AS-S) and Tonabersat (Tona-S) over 7 days.

SEM images of (a) Plain Scaffold (P-S), (b) Cx43asODN Scaffold (AS-S) and (c) Tonabersat Scaffold (Tona-S) Magnification: x500. Scale bar: 100µm. Fiber distribution of (a) Plain Scaffold (P-S), (b) Cx43asODN Scaffold (AS-S) and (c) Tonabersat Scaffold (Tona-S) (g) Scaffold release profile of Cx43asODN (AS-S) showing a burst effect on day 1 of scaffold release and gradual release on day 2, 3 & 4. (h) Scaffold release profile of Tonabersat (Tona-S) showing a burst effect on Day 1 & 2 with gradual release on subsequent days.

6.2.2 Cx43 targeted therapeutics scaffolds reduced ring of inflammation and preserved hair follicles in porcine scald burn injury

Cx43asODN and Tonabersat electrospun scaffold dressing were tested on the pilot burn animals as listed in (Table 2.2). Following four continuous days of Cx43asODN and Tonabersat treatment, wound healing progression was monitored by photography of the wounds on PBD 1, 4, 7, 14 & 21. The red ring of inflammation around the wound that was evidently visible on PBD 1 was reduced in PBD 4 wounds that were treated with AS-S and Tona-S. On PBD 7, 14 and 21, there was a similar trend of smaller wound size in the AS-S and Tona-S treated groups. Although statistically not significant, overall burn wound size was reduced in the treated groups as compared to control groups (Figure 6.2 & Figure 6.3 a). Wounds treated with AS-S or Tona-S had visibly higher numbers of hair follicles preserved in the wound area on PBD 21 (Figure 6.2 & Figure 6.3b).

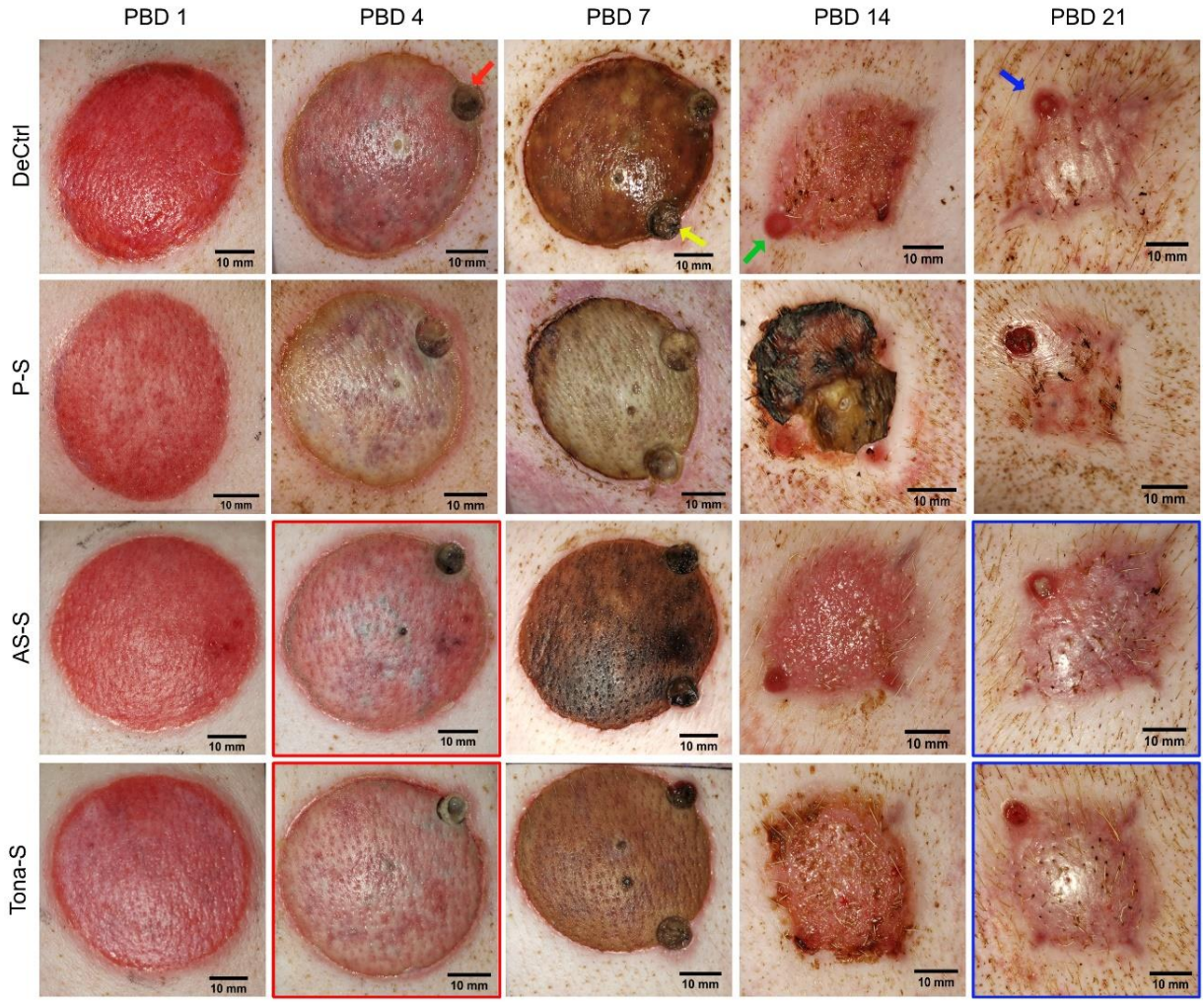

Figure 6.2 Macroscopic images of wound healing process of scaffold treated porcine burn wounds.

DeCtrl: Debrided Control (n=3 animals); P-S: Plain Scaffold (n=1 animal), AS-S: Cx43asODN Scaffold (n=3 animals), Tona-S: Tonabersat Scaffold (n=2 animals). Red arrow: biopsy excision of PBD 1, yellow arrow: biopsy excision of PBD 4, green arrow: biopsy excision of PBD 7, blue arrow: biopsy excision of PBD 14. Red box shows indicates, reduced red ring of inflammation around wound. Blue box indicates hair follicle preservations in wounds. Scale bar: 10mm.

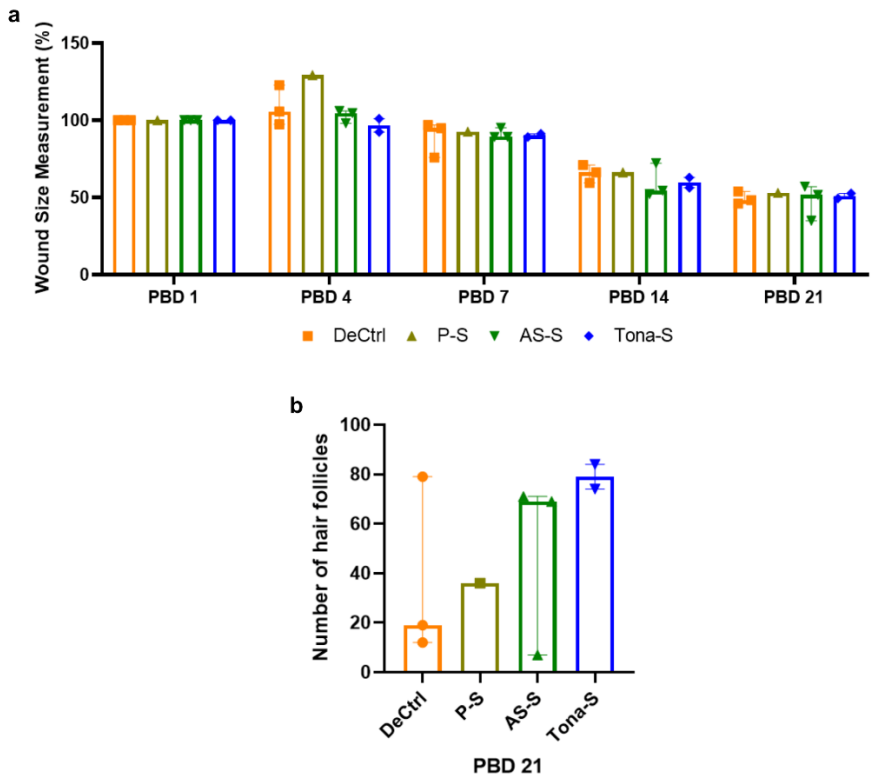

Figure 6.3 Marginally reduced wound size and increase in number of hair follicles in Cx43asODN and Tonabersat treated porcine burn wounds.
(a) Wound size measurement of porcine burn wounds treated with Cx43asODN and Tonabersat treated burn wounds on PBD 1, 4, 7, 14 & 21. DeCtrl: Debrided Control (n=3 animals); P-S: Plain Scaffold (n=1 animal), AS-S: Cx43asODN Scaffold (n=3 animals), Tona-S: Tonabersat Scaffold (n=2 animals). Data are presented as median and interquartile range (IQR). Statistical comparisons were made using Kruskal-Wallis Test.

6.2.3 Upregulated Cx43 expression did not alter with scaffold treatment in porcine burn injury

As shown in chapter 5, upon wound injury there was an increase in Cx43 protein levels in DeCtrl compared to normal skin (NS) on PBD 4 ($p=0.052$) and PBD 7 ($p<0.05$) (Figure 6.4). I then explored the use of AS-S and Tona-S as scaffold delivery treatment in porcine scald burn injury.

On PBD 4, I observed that Cx43 protein levels were reduced in wounds treated with AS-S compared to Veh control wounds ($p=0.8972$), however no difference from DeCtrl ($p>0.9999$) (Figure 6.4 b & d). Similarly, Tona-S treated wounds Cx43 expression levels were no different from DeCtrl and P-S (>0.9999) (Figure 6.4 b & d). On PBD 7, wounds treated with AS-S and Tona-S had no difference as compared to DeCtrl or Veh control (Figure 6.4 c & e). These results may suggest that scaffold delivery with Cx43asODN reduces expression of Cx43 at early timepoints after burn injury.

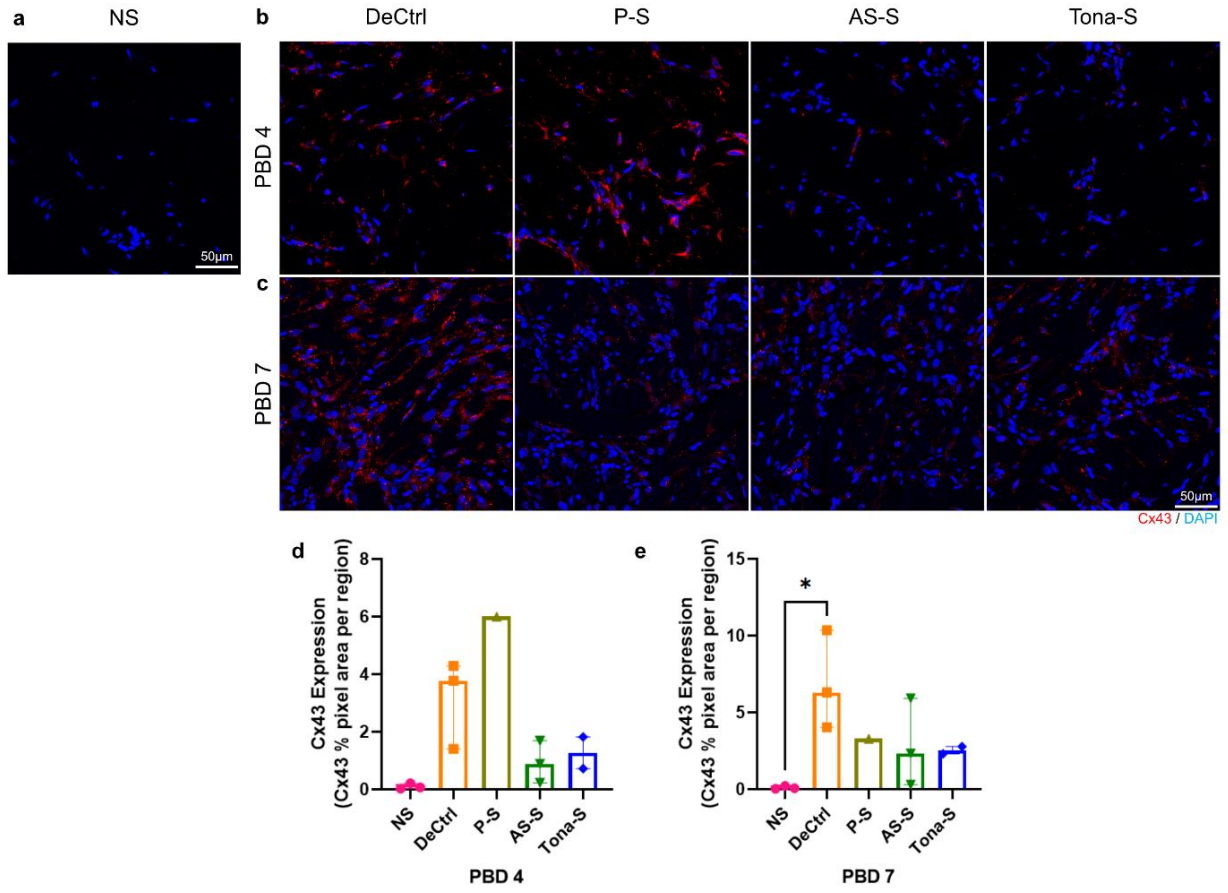

Figure 6.4 Scaffold delivery of Cx43 targeted therapeutics reduced Cx43 protein expression in zone of stasis on PBD 4.

Representative immunofluorescence images of Cx43 expression in (a) normal skin (NS), (b) in zone of stasis at PBD 4 and (c) PBD 7. DeCtrl: Debrided control, P-S: Plain scaffold, AS-S: Cx43asODN Scaffold and Tona-S: Tonabersat Scaffold. Magnification: 40x. Scale bar: 50µm. (d) Image analysis graph of Cx43 expression in the zone of stasis on PBD 4 and (e) PBD 7. Image analysis graph shows an increased expression between NS vs DeCtrl (n=3 animals per group) on PBD 4, & 7. Image analysis reveals lower Cx43 protein expression in the zone of stasis of treated (AS-S, Tona-S, n=3 & 2 animals, respectively) compared to the DeCtrl and P-S (n=1) on PBD 4 & 7. Data are expressed as median and interquartile range (IQR). Statistical comparisons were made using Kruskal-Wallis Test. (*$p<0.05$).

6.2.4 Cx43 targeted therapeutic scaffolds did not alter hemichannel expression in the zone of stasis

After establishing that Cx43 targeted therapeutics were able to reduce Cx43 protein expression, I then explored the hemichannel expression in the zone of stasis. I observed that there is an increased expression of hemichannels upon wound injury in DeCtrl in comparison to NS on PBD 4 ($p=0.0871$) (Figure 6.5 a, b & d). However, treatment with AS-S or Tona-S did not make a difference from DeCtrl in hemichannel expression on PBD 4 ($p=0.9999$) (Figure 6.5 b & d). On PBD 7, AS-S or Tona-S did not have any difference from DeCtrl or Veh control ($p=0.9999$). Hemichannel expression in Tona-S treated wounds were higher than P-S ($p=0.6675$) (Figure 6.5 c & e).

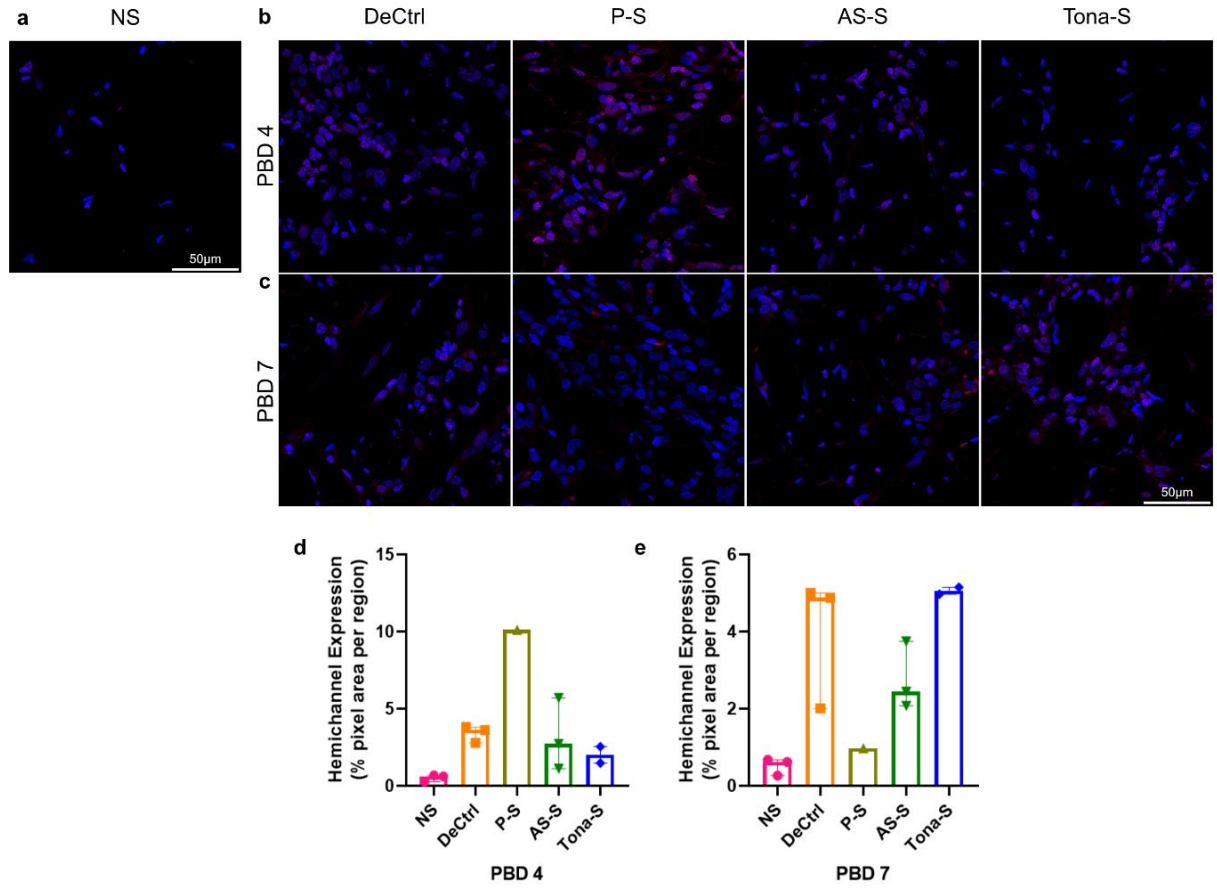

Figure 6.5 Scaffold delivery of Cx43 targeted therapeutics did not reduce hemichannel protein expression in zone of stasis on PBD 4 & 7.

Representative immunofluorescence images of hemichannel expression in (a) normal skin (NS), (b) in zone of stasis at PBD 4 and (c) PBD 7. DeCtrl: Debrided control, P-S: Plain scaffold, AS-S: Cx43asODN Scaffold and Tona-S: Tonabersat Scaffold. Magnification: 63x. Scale bar: 50µm. (d) Image analysis graph of hemichannel expression in the zone of stasis on PBD 4. (e) Image analysis graph of hemichannel expression on PBD 7. Image analysis graph shows an increased expression between NS vs DeCtrl (n=3 animals per group) on PBD 4 & 7. Image analysis reveals lower hemichannel protein expression in the zone of stasis of treated (AS-S, Tona-S, n=3 & 2 animals, respectively) compared to the DeCtrl and P-S (n=1) on PBD 4 & 7. Data are expressed as median and interquartile range (IQR). Statistical comparisons were made using Kruskal-Wallis Test. (*$p<0.05$).

6.2.5 MPO positive cells did not reduce in the zone of stasis of scaffold treated wounds

To quantify inflammation, i performed immunofluorescence staining using MPO. I found that on PBD 4, there is a significant increase in MPO positive cells in DeCtrl wounds compared to NS ($p<0.05$) (Figure 6.6 a, b & d). Upon treatment with AS-S or Tona-S, the MPO positive cells in the treated groups of AS-S or Tona-S did not reduce compared to DeCtrl and Veh ($p>0.9999$) (Figure 6.6 b & d). On PBD 7, there was no difference between control groups and treated groups ($p>0.9999$) (Figure 6.6 c & e).

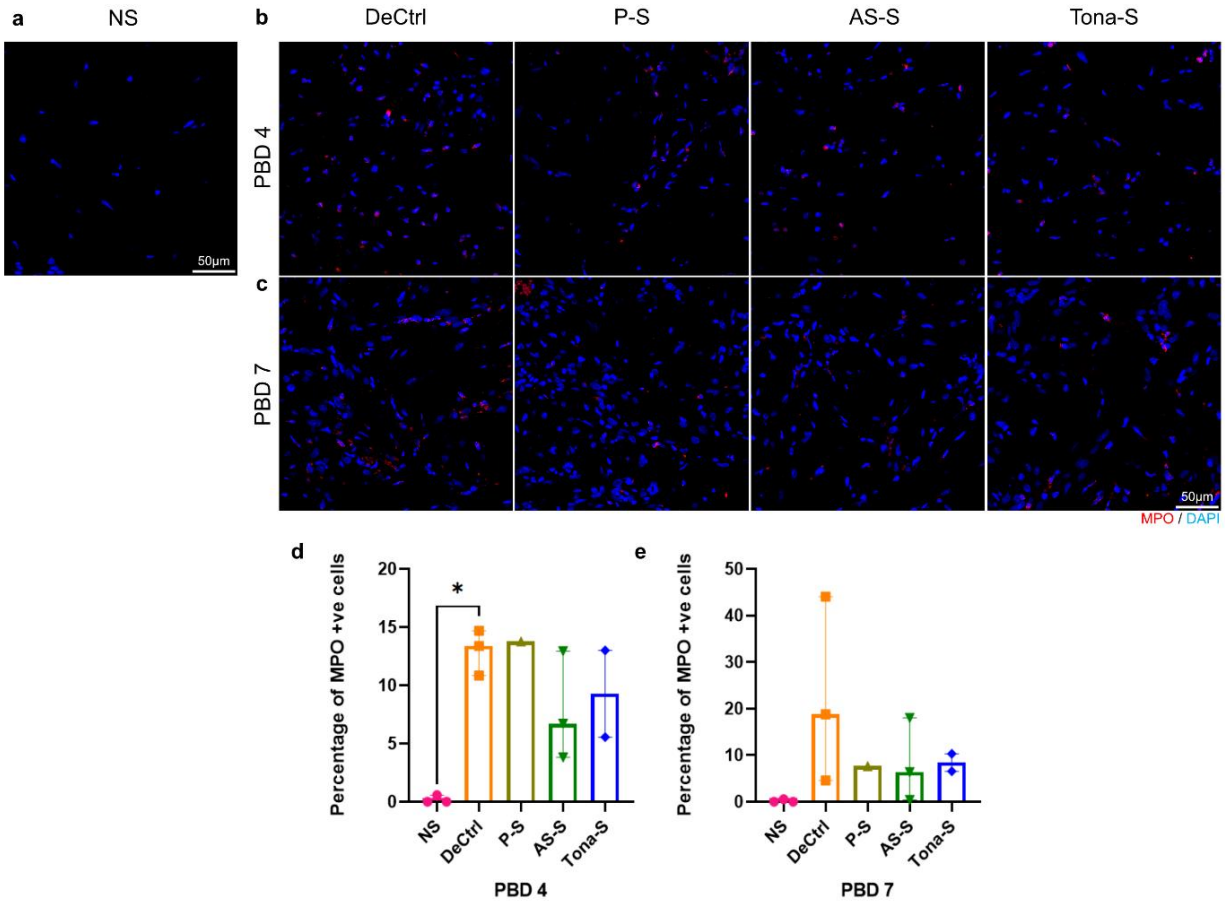

Figure 6.6 Scaffold delivery of Cx43 targeted therapeutics did not reduce percentage of MPO positive cells in zone of stasis on PBD 4 & 7.

Representative immunofluorescence images of percentage of MPO positive cells in (a) normal skin (NS), (b) in zone of stasis at PBD 4 and (c) PBD 7. DeCtrl: Debrided control, P-S: Plain scaffold, AS-S: Cx43asODN Scaffold and Tona-S: Tonabersat Scaffold. Magnification: 40x. Scale bar: 50µm. (d) Image analysis graph of percentage of MPO cells in the zone of stasis on PBD 4 and (e) PBD 7. Image analysis graph shows an increased percentage of MPO positive cells between NS vs DeCtrl (n=3 animals per group) on PBD 4 & 7. Image analysis shows comparison of MPO expression in the zone of stasis of treated (AS-S, Tona-S, n=3 & 2 animals, respectively) compared to the DeCtrl and P-S (n=1) on PBD 4 & 7. Data are expressed as median and interquartile range (IQR). Statistical comparisons were made using Kruskal-Wallis Test. (*$p<0.05$).

6.2.6 Significant increase P2X7 receptor expression was observed in porcine burn injury

To investigate P2X7 expression in the zone of stasis of porcine burn injury, I performed immunofluorescence staining and have found that P2X7 was indeed elevated in burn wounds compared to NS on PBD 4 ($p<0.05$) (Figure 6.7 a, b & d). Treatment with AS-S or Tona-S no difference in P2X7 expression as compared to DeCtrl ($p=0.8462$ and $p=0.5683$, respectively) (Figure 6.7 b & d). In addition, no difference was observed in treated groups and Veh control groups on PBD 4. Similarly, the expression levels of P2X7 were not different between treated and controls on PBD 7 suggesting that P2X7 is regulated in a Cx43 independent manner as observed in Chapter 4 in the rat burn model (Figure 6.7 c & e).

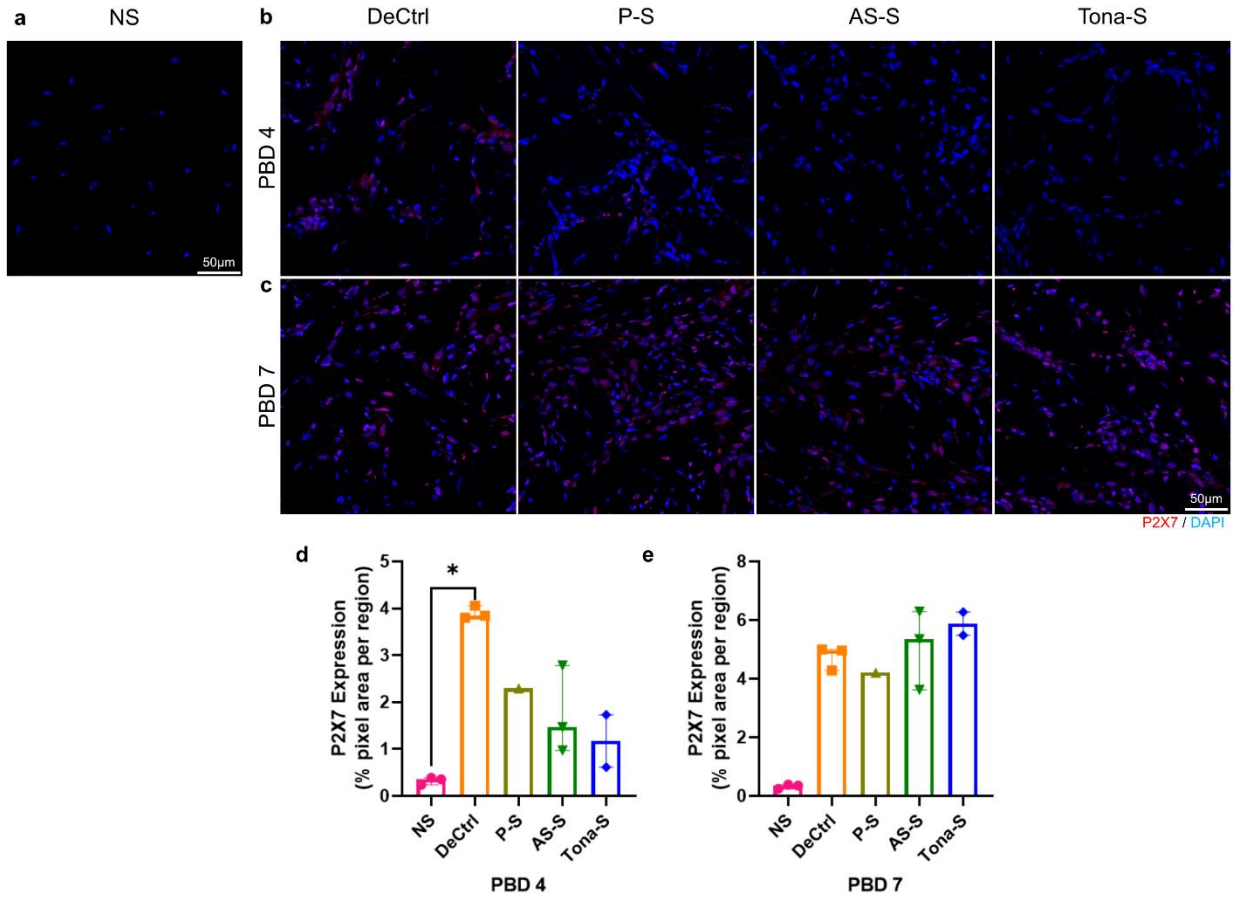

Figure 6.7 Scaffold delivery of Cx43 targeted therapeutics reduced P2X7 expression in zone of stasis on PBD 4.

Representative immunofluorescence images of P2X7 expression in (a) normal skin (NS), (b) in zone of stasis at PBD 4 and (c) PBD 7. DeCtrl: Debrided control, P-S: Plain scaffold, AS-S: Cx43asODN Scaffold and Tona-S: Tonabersat Scaffold. Magnification: 40x. Scale bar: 50µm. (d) Image analysis graph of P2X7 expression in the zone of stasis on PBD 4 and (e) PBD 7. Image analysis graph shows an increased P2X7 expression between NS vs DeCtrl (n=3 animals per group) on PBD 4 & 7. Image analysis reveals P2X7 expression comparison of treated (AS-S, Tona-S, n=3 & 2 animals, respectively) compared to the DeCtrl and P-S (n=1) on PBD 4 & 7. Data are expressed as median and interquartile range (IQR). Statistical comparisons were made using Kruskal-Wallis Test. (*$p<0.05$).

6.2.7 Cx43 targeted therapeutic scaffolds did not show a difference in NLRP3 expression in the zone stasis

To investigate if the NLRP3 inflammasome complex is activated and Cx43 targeted therapeutics influences activation of inflammasome complex, I investigated the expression of NLRP3 & Cas-1 in the zone of stasis (Figure 6.8 & Figure 6.9). Following porcine burn injury, I observed significant increase in NLRP3 expression in DeCtrl wounds compared to NS on PBD 4 (Figure 6.8 a, b & d). Upon treatment with AS-S or Tona-S, I did not observe a difference than DeCtrl and Veh controls on PBD 4 and 7 (Figure 6.8 b, c, d & e).

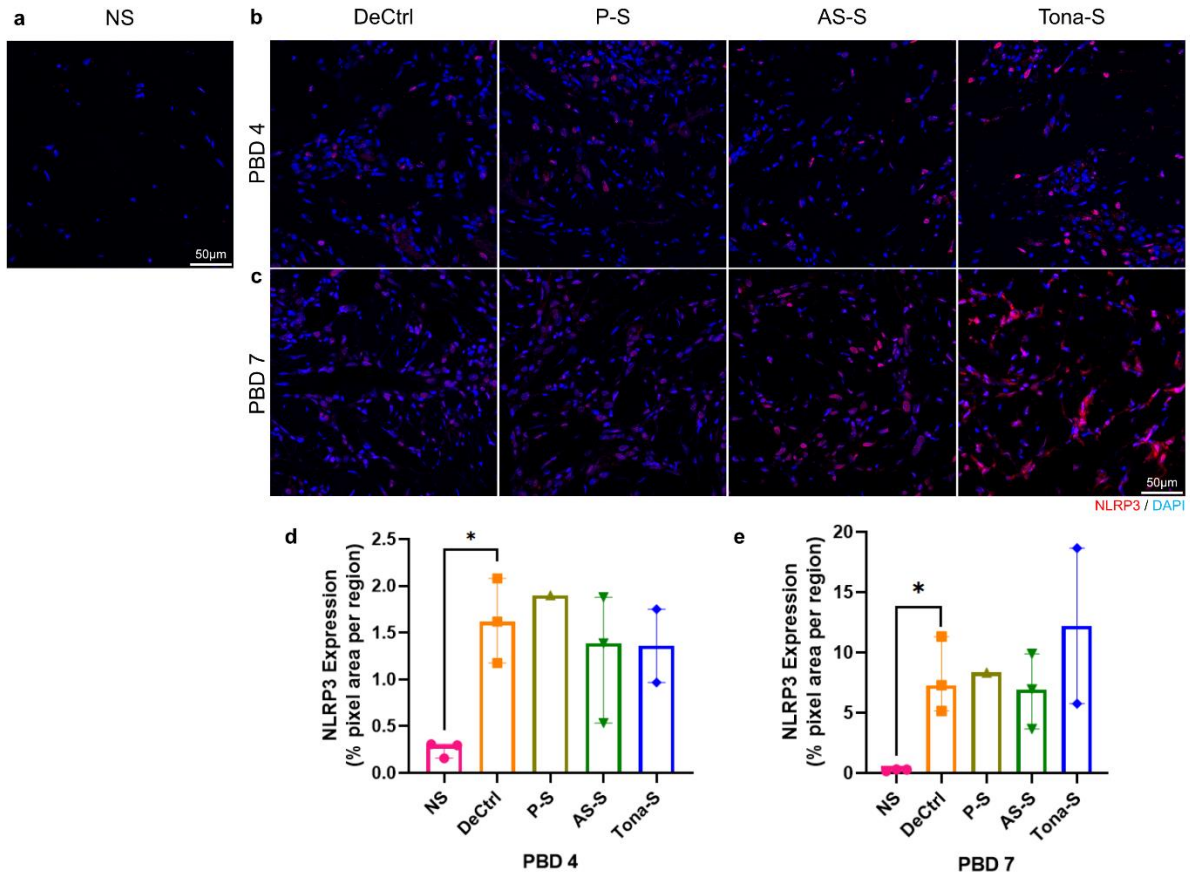

Figure 6.8 Scaffold delivery of Cx43 targeted therapeutics did not change NLRP3 expression in zone of stasis on PBD 4 & 7.

Representative immunofluorescence images of NLRP3 expression in (a) normal skin (NS), (b) in zone of stasis at PBD 4 and (c) PBD 7. DeCtrl: Debrided control, P-S: Plain scaffold, AS-S: Cx43asODN Scaffold and Tona-S: Tonabersat Scaffold. Magnification: 40x. Scale bar: 50μm. (d) Image analysis graph of NLRP3 expression in the zone of stasis on PBD 4 and (e) PBD 7. Image analysis graph shows an increased NLRP3 expression between NS vs DeCtrl (n=3 animals per group) on PBD 4 & 7. Image analysis reveals no difference in NLRP3 protein expression in the zone of stasis of treated (AS-S, Tona-S, n=3 & 2 animals, respectively) compared to the DeCtrl and P-S (n=1) on PBD 4 & 7. Data are expressed as median and interquartile range (IQR). Statistical comparisons were made using Kruskal-Wallis Test. (*$p<0.05$).

6.2.8 Cx43 targeted therapeutic scaffolds did not reduce Cas-1 expression in the zone stasis

During the NLRP3 inflammasome complex formation, Cas-1 is recruited and tightly regulated and subsequently results in secretion of mature IL-1β. Here I observed that following porcine burn injury, there was a significant increase in Cas-1 expression in DeCtrl wounds as compared to NS on PBD 4 ($p<0.05$) but no difference on PBD 7 (Figure 6.9). Upon treatment with AS-S Cas-1 expression did not alter compared to DeCtrl and P-S (Figure 6.9 b & d). Treatment with Tona-S had slight reduction in Cas-1 expression as compared to DeCtrl ($p=0.6309$) but not from P-S. However, on PBD 7, there is no difference between treated and control groups (Figure 6.9 c & e).

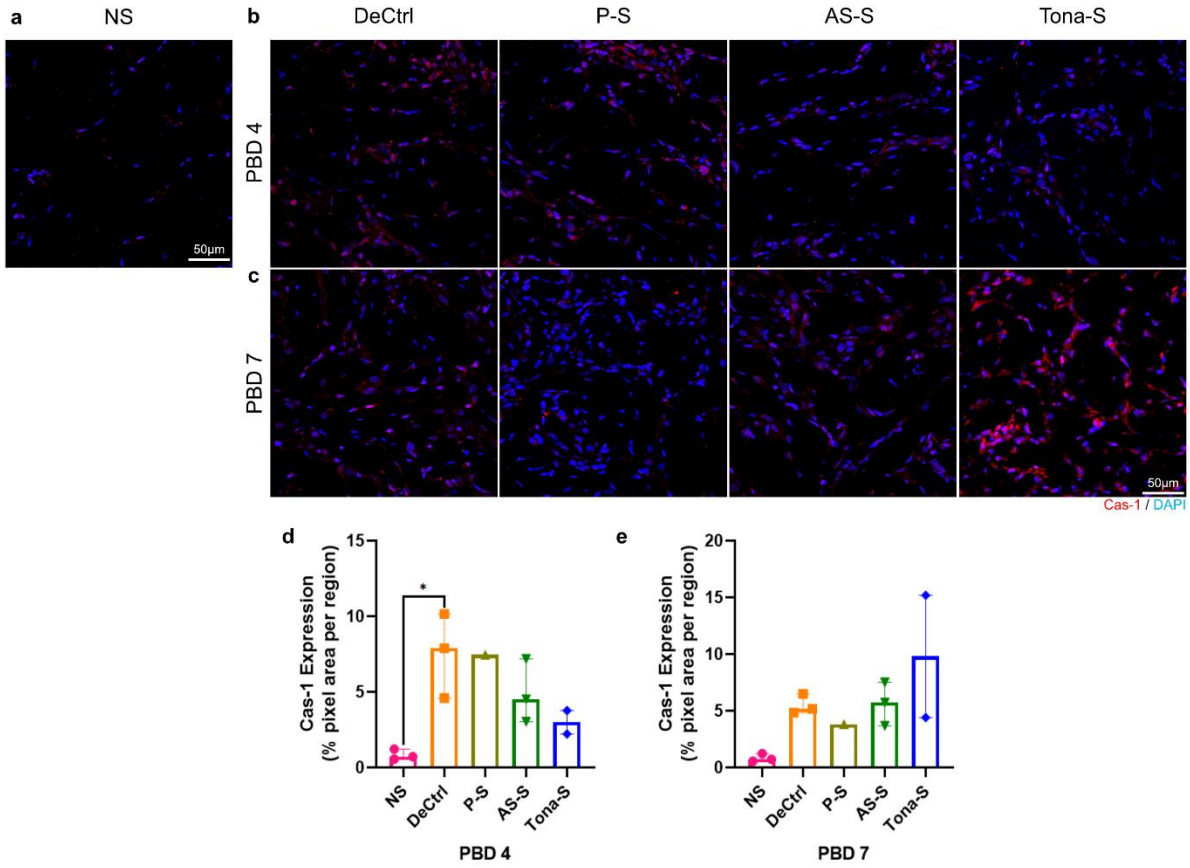

Figure 6.9 Scaffold delivery of Cx43 targeted therapeutics did not reduce Cas-1 expression in zone of stasis on PBD 4.

Representative immunofluorescence images of Cas-1 expression in (a) normal skin (NS), (b) in zone of stasis at PBD 4 and (c) PBD 7. DeCtrl: Debrided control, P-S: Plain scaffold, AS-S: Cx43asODN Scaffold and Tona-S: Tonabersat Scaffold. Magnification: 40x. Scale bar: 50µm. (d) Image analysis graph of Cas-1 expression in the zone of stasis on PBD 4 reveals lower in Cas-1 protein expression in the zone of stasis of treated (AS-S, Tona-S, n=3 & 2 animals, respectively) compared to the DeCtrl (n=3) and P-S (n=1). (e) Image analysis graph of Cas-1 expression in the zone of stasis on PBD 7 reveals no difference in Cas-1 protein expression in the zone of stasis of treated (AS-S, Tona-S, n=3 & 2 animals, respectively) compared to the DeCtrl (n=3) and P-S (n=1). Data are expressed as median and interquartile range (IQR). Statistical comparisons were made using Kruskal-Wallis Test. (*$p<0.05$).

6.2.9 Cx43 targeted therapeutic scaffolds did not reduce skin fibrosis markers in porcine burn injury

To determine whether skin fibrosis is increased in porcine burn injury, αSMA and HSP47 were investigated. I observed a slight increase in αSMA and HSP47 expression in DeCtrl wounds on PBD 14 and significant increase on PBD 21 compared to NS ($p=0.1045$ and $p<0.01$) (Figure 6.10). There is no difference in αSMA expression between AS-S or Tona-S compared to DeCtrl and P-S on PBD 14 and 21, (Figure 6.10 b & e). Similarly, when I assessed HSP47 expression with treated with AS-S or Tona-S, there was no difference in expression when compared to DeCtrl and P-S on PBD 14 and 21 (Figure 6.10 f & g).

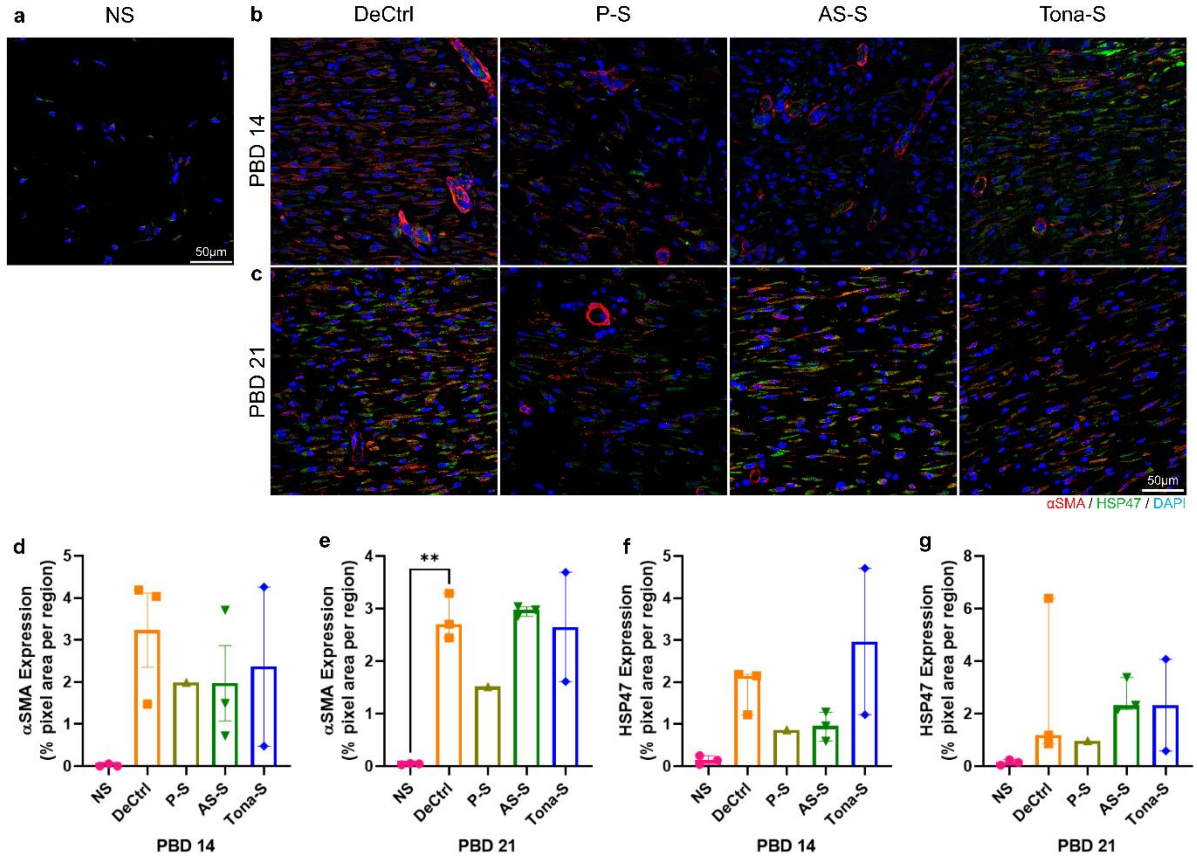

Figure 6.10 Scaffold delivery of Cx43 targeted therapeutics did not reduce αSMA and HSP47 expression in zone of stasis on PBD 14 & 21.

Representative immunofluorescence images of co-labelled αSMA (red) and HSP47 (green) expression in (a) normal skin (NS), (b) Debrided Ctrl: DeCtrl, P-S: Plain Scaffold, AS-S: Cx43asODN scaffold, Tona-S: Tonabersat scaffold on PBD 14 and (c) PBD 21. Magnification: 40x. Scale bar: 50µm. (d) Image analysis graph of αSMA expression on PBD 14 and (e) PBD 21. (f) Image analysis graph of HSP47 expression on PBD 14 and (g) PBD 21. Comparisons were made between NS vs DeCtrl (n=3 animals per group) on PBD 14 & 21. Comparison of treated (AS-S & Tona-S, n=3 & 2 animals, respectively) to DeCtrl & Veh (n=3 & 2, respectively) on PBD 14 & 21. Data are expressed as median and interquartile range (IQR). Statistical comparisons were made using Kruskal-Wallis Test. (*$p<0.05$).

6.2.10 Cx43 targeted therapeutic scaffolds did not improve collagen content in the deep dermis of porcine burn injury

To quantify percentage of collagen content in porcine burn injury, I analysed tissues stained with Masson's Trichrome. I divided the tissues into three portions, namely, upper dermis, mid dermis, and deep dermis. In upper dermis, DeCtrl wounds and treated wounds of AS-S or Tona-S had least collagen deposition with infiltration of myofibroblasts and inflammatory cells as compared to the treated groups, however, not significant (Figure 6.11 a & d). Similarly, this was also observed in mid dermis. In deep dermis, wounds treated with P-S, AS-S and Tona-S displayed normal collagen pattern as compared to DeCtrl (Figure 6.11 c & d). Even though there is no significant difference across controls and treated wounds, it is important to note increase presence of cells potentially to be myofibroblasts or inflammatory cells in DeCtrl, AS-S and Tona-S wounds (Figure 6.11).

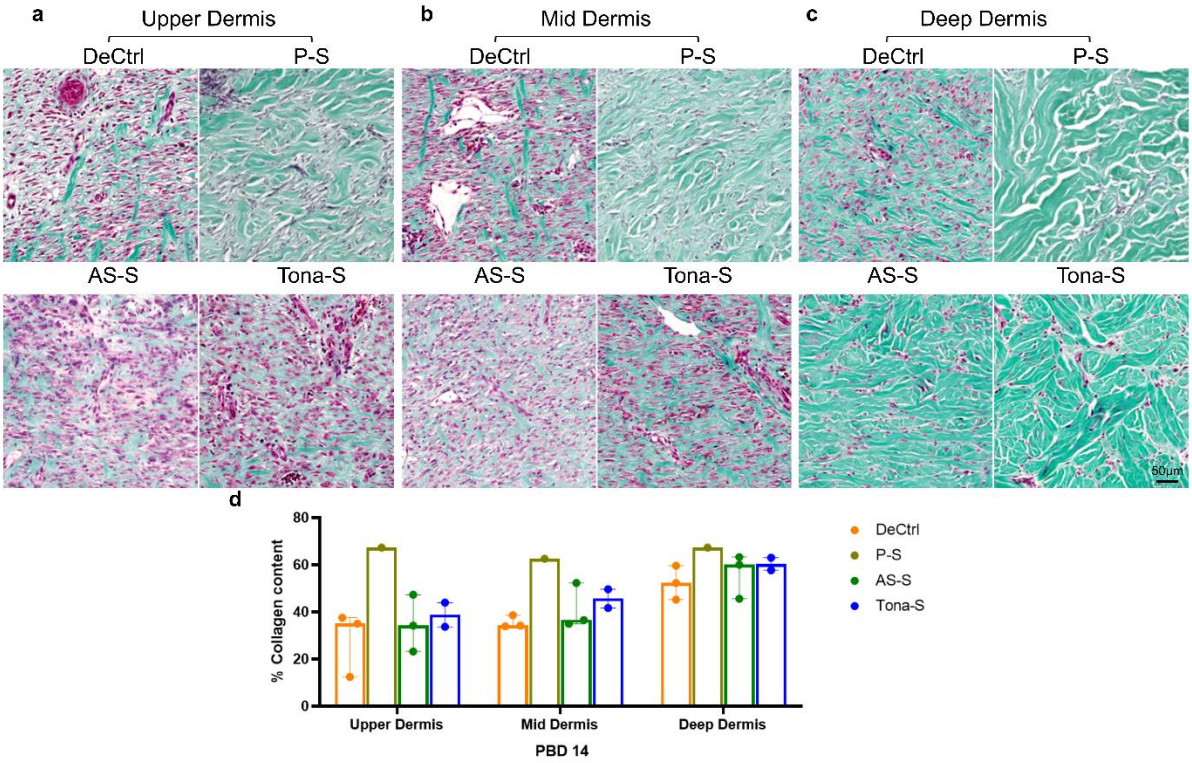

Figure 6.11 Scaffold delivery of Cx43 targeted therapeutics did not improve collagen content in porcine burn injury on PBD 14.

The panel shows representative Masson's Trichrome stained images of (a) upper dermis (b) mid dermis and (c) deep dermis of porcine burn injury on PBD 14. Debrided Ctrl: DeCtrl, P-S: Plain Scaffold, AS-S: Cx43asODN scaffold, Tona-S: Tonabersat scaffold. Staining: Collagen—green; nuclei—black; muscle fibres and cytoplasm—red. (d) Image analysis of collagen content from Masson's Trichrome stained images of upper dermis, mid dermis & deep dermis (DeCtrl, Veh, P-S. AS-S & Tona-S; n=3, 2, 1, 3 & 2 animals, respectively). Data are expressed as median and interquartile range (IQR). Statistical comparisons were made using Kruskal-Wallis Test – not significant. Scale bar: 50µm.

6.2.11 Reduction in nascent epidermal thickness in scaffold treated wounds

As described above, the nascent epidermal thickness was measured on PBD 14 and 21 for burn wounds treated with scaffold dressings. There was significant thicker nascent epidermal thickness in DeCtrl compared to NS on PBD 14 and PBD 21 ($p<0.05$). Particularly, in the control groups (DeCtrl and Plain Scaffold (P-S)) the nascent epidermis remained hyper-thickened compared to treated groups. However, no significant difference was observed between control groups and treated groups on PBD 14 (Figure 6.12 a & d). The Cx43asODN and Tonabersat scaffold dressing treated wounds had thinner nascent epidermis compared to DeCtrl and P-S on PBD 21 (Figure 6.12 a & d), though not significant. On PBD 21, the Cx43asODN and Tonabersat scaffold dressing treated wounds nascent epidermal thickness thinned down close to those in normal skin (Figure 6.12 b, c & e).

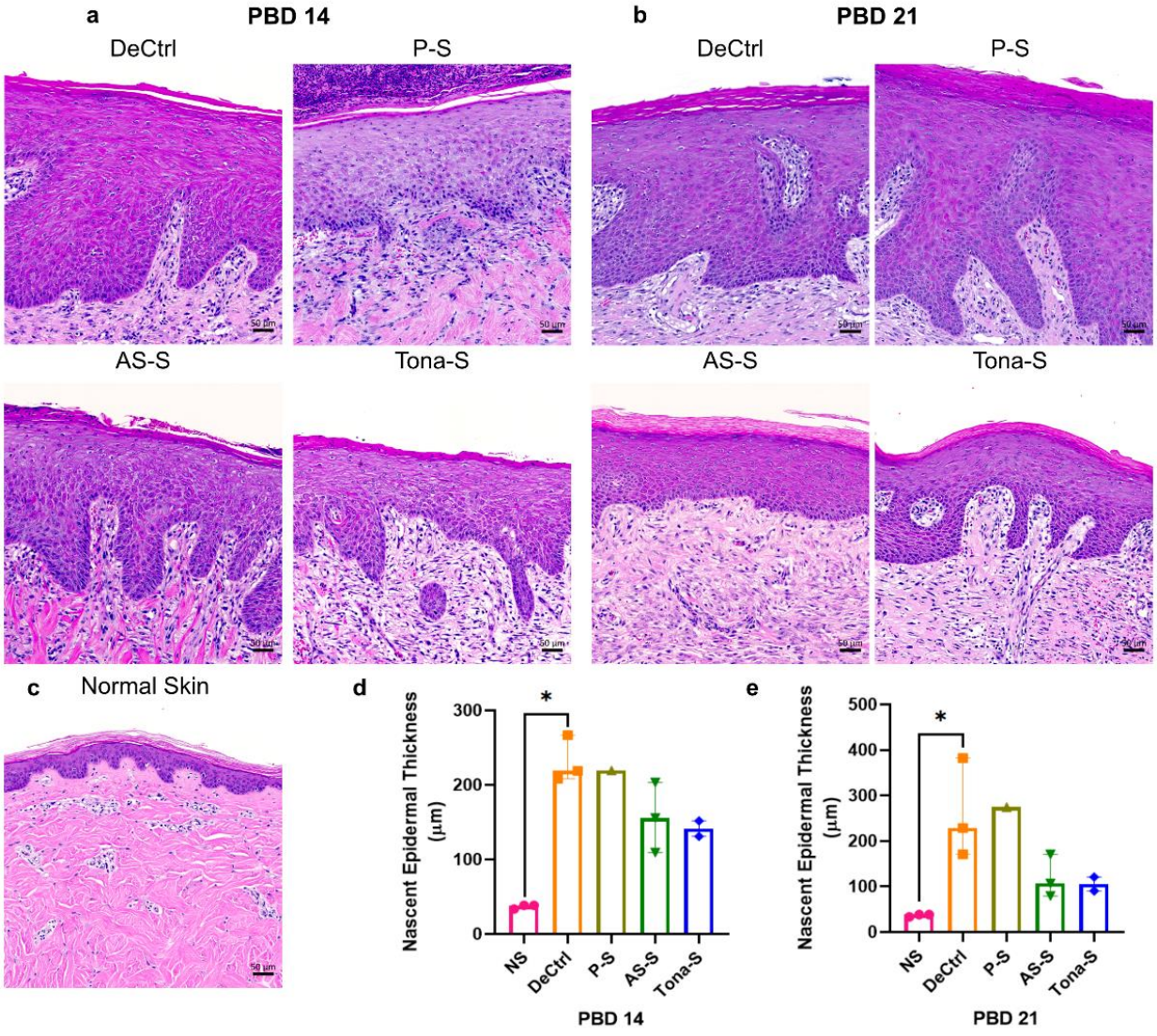

Figure 6.12 Nascent epidermal thickness of scaffold treated porcine burn wounds with AS-S and Tona-S.

(a) The panel represents H&E images of nascent epidermis from porcine burn wounds at PBD 14 and (b) PBD 21. (c) Representative of H&E image of porcine normal skin. Scale bar: 50µm. (d) Quantification of nascent epidermal thickness measurement at PBD 14 and (e) PBD 21. Data are expressed as median and interquartile range (IQR). Statistical comparisons were made using Kruskal-Wallis Test ($p<0.05$), n= 3, 3, 1, 3 & 2 animals per group, in respective order as shown in graph).

6.3 Discussion

In chapter 5, I have demonstrated that Cx43 plays a role in porcine burn injury whereby topical application of Cx43asODN or Tonabersat downregulated Cx43 and hemichannel protein expression. However, no changes was observed to NLRP3 inflammasome markers and inflammation in the zone of stasis of porcine burn injury. Concomitantly, early intervention with Cx43asODN or Tonabersat improved collagen content and epidermal thickness on PBD 14. In this chapter, to improve the therapeutic delivery method to porcine burn injury, I employed scaffold PCL/PEG dressing to deliver Cx43asODN or Tonabersat. I observed that there was an early burst release effect of the therapeutics from the PCL/PEG scaffold. I also observed the downregulation of Cx43 in treated groups of AS-S or Tona-S. However, treatment with Cx43 therapeutic loaded scaffolds did not alter expression of hemichannel and NLRP3 and its inflammasome complex markers. Importantly, the reduction of Cx43 and hemichannels on PBD 4 was not sustained up to PBD 7, as shown in this immunofluorescence analysis, which might be contributed by the early burst effect of scaffold release of therapeutics. Hence, this drug delivery profile could have affected the upstream signalling leading to burn progression while having little effect on porcine burn wound healing. On the other hand, AS-S and Tona-S act as protective barriers for burn wounds and promote re-epithelialisation which could have assisted with keratinocyte migration over the healing period and reduced nascent epidermal thickness. However, the prevention of burn progression or improvement to burn wound healing with PCL/PEG dressing with Cx43 targeted therapeutics remains inconclusive. Data from the Cx43 targeted therapeutics in rat burn injury (Chapter 4) can be extrapolated that the further optimization of PCL/PEG scaffold loaded with

Cx43asODN or Tonabersat may reduce the NLRP3 inflammasome complex formation and improve burn wound healing.

PCL and PEG continue to be of great interest for tissue engineering. In *ex vivo* models of porcine skin, retinol (vitamin A) was delivered in block copolymer poly(caprolactone)-block-poly(ethylene glycol) PCL-b-PEG and poly(lactide)-block-poly(ethylene glycol) copolymer (PLA-b-PEG). It was found that both copolymers enhanced skin absorption of all-trans retinol through the stratum corneum into the epidermis and dermis. In contrast to PCL-b-PEG, skin absorption from PLA-b-PEG nanoparticles was improved further. This was caused by the physical differences between PLA and PCL, which were solid glassy materials at ambient temperature and semisolid amorphous materials, respectively (Laredj-Bourezg et al., 2015). This provides insights on PLA being a possible candidate in future for therapeutic release of Cx43asODN or Tonabersat.

Chrysin, a natural bioactive flavonoid extract from plants, honey and propolis is known to have anti-inflammatory and antioxidant properties (Mohammadi et al., 2019). LPS stimulated J774A1 mouse macrophages seeded on Chrysin loaded PCL/PEG nanofibrous mat have been shown to have reduced overexpression of IL-6, IL-1β, TNF-α and excessive production of nitric oxide (NO) in these cells (Deldar et al., 2018). Additionally, human foreskin fibroblast cells were more resilient to oxidative stress when grown on chrysin-loaded PCL/PEG nanofibrous mats. These findings suggest that natural substance delivery via integration with PCL/PEG nanofibrous mats can enhance wound healing by promoting cell proliferation and reducing anti-oxidative and anti-inflammatory properties (Deldar et al., 2018). Curcumin is a natural polyphenolic compound that is known to have anti-cancer, anti-microbial and anti-inflammatory properties (Mohammadi et al., 2019). Due to the poor solubility state of these chrysin and curcumin compounds, it was attempted

to be delivered in a sustained manner in combination with PCL/PEG to fabricate into chrysin–curcumin-loaded PCL-PEG nanofibers. A rat excisional wound model, treated with chrysin–curcumin-loaded PCL-PEG nanofibers, demonstrated reduced inflammation and faster wound closure (Mohammadi et al., 2019). In a diabetic mouse burn model, burn wounds were treated with recombinant human epidermal growth factor (EGF) conjugated to the surface of PCL-PEG-PCL electrospun nanofibers (Choi et al., 2008). They found accelerated wound closure and increased keratinocyte EGF expression in burn wounds treated with EGF conjugated PCL-PEG-PCL nanofibers compared to control groups (Choi et al., 2008).

In another study with combination of other polymers, Diclofenac incorporated PCL/PEG/chitosan/keratin sutures have demonstrated to have outstanding tensile strength as well as quick and sustained drug release in a different study with combinations of other polymers. Furthermore, HaCaT cell PCL/PEG/chitosan/keratin/Diclofenac suture *in vitro* tests showed enhanced cell proliferation, viability, and migration, indicating a possible utility in clinical settings (Deng et al., 2021). These studies provide vital information on the potential therapeutic use of PCL/PEG scaffolds. This preliminary study has paved the way to explore and fine tune the use of PCL/PEG or other combinations of synthetic polymers for the treatment of burn wounds.

Other than PCL/PEG combination, several studies have provided insights on polymer combination using poly(lactic-co-glycolic acid (PLGA) that has shown to have good scaffold release profile. Gilmartin and colleagues have demonstrated that the use of PCL and PLGA scaffolds coated in Cx43asODN in rat excisional wound models. They have found that combination scaffold of PCL and PLGA coated for four times with Cx43asODN had sustained scaffold release profile over 7 days than PCL or PLGA coated scaffolds. In situ Cx43asODN PCL/PLGA scaffold had reduced

Cx43 expression at wound edges, a reduction in inflammatory response, and foreign body response with significant improvement in rate of re-epithelialisation and contracture, suggesting that this might be applicable to venous leg ulcers in clinical application (Gilmartin et al., 2016).

In an another study on diabetic rat wound model, hyaluronic acid (HA)/poly(lactic-co-glycolic acid, PLGA) core/shell fiber matrices loaded with epigallocatechin-3-O-gallate (EGCG) (HA/PLGA-E) were fabricated by coaxial electrospinning. In comparison to no treatment or HA/PLGA, they discovered that the wound areas were dramatically reduced by the coverage with HA/PLGA-E matrices due to accelerated re-epithelialization and neovascularization, as well as increased collagen deposition, suggesting it to be a good candidate for diabetic wound healing (Shin et al., 2016).

Dhall and colleagues have explored the use of alginate sponge dressings (ASD) containing insulin encapsulated in PLGA microparticles that provide a sustained release of bioactive insulin for >20 days. In a rat burn model, they have demonstrated that treatment with these dressings containing 0.04 mg insulin/cm^2 every three days for nine days, promoted wound closure with reduced oxidative stress and inflammation. Moreover, they found that insulin promoted collagen deposition and maturation, with the fibers arranged more like a basket weave than aligned and cross-linked to indicate scar tissue (Dhall et al., 2015).

It is noteworthy that these combinations of synthetic polymers could be useful in the treatment of burn injury. Future work should include improving the drug release profile of the PCL/PEG scaffold or using it in combination with other polymers to achieve better wound healing outcomes when tested *in vivo*. This pilot study has provided insights on the limitations and how we could

improve in the future. I have addressed the limitations in a general view and specific limitations of topical application and scaffold therapeutic delivery in porcine burn model in the following chapter.

Chapter 7: Summary and conclusion

Burn wounds continue to worsen after the initial injury resulting in burn progression (Singh et al., 2007). Burn injuries are a global public health problem, accounting for an estimated 180,000 deaths from severe burns annually. Hence, active research is warranted for the study of burn progression and burn prevention. Our previous research has shown that Cx43 is increased in burn injury and contributes to the transmission of cell death signals and inflammation after burn injury (Coutinho et al., 2005; Feng et al., 2020). However, more research regarding this limited understanding of Cx43 and burn injuries is yet to be further investigated.

The thesis hypothesised that Cx43 plays a pivotal role in the response to a burn injury that promotes inflammation, and that the treatment with Cx43asODN or Tonabersat will either transiently reduce Cx43 gap junction protein or block Cx43 hemichannel activity, respectively, to mitigate burn progression and enhance wound healing.

In **Chapter 3**, a rat deep partial burn model was established. This was chosen based on the reproducibility of burn wounds and histological features that serve as clinical indications of burn injury in humans. This was accomplished with the use of a scoring matrix proposed by Medina et al (Medina et al., 2018). The immediate damage to the epidermis, the coagulated dermis, the cell damage to the hair follicles, the neutrophil infiltration into the burn area that delineates the necrotic tissue area, and the possibly surviving area with large, rounded adipocytes in the middle dermis are the histological characteristics of a rat deep partial thickness burn. Results from this chapter showed that the initial partial thickness burn damage at 55°C for 10 s progressed to a deep partial thickness burn, indicating that the initial zone of stasis was transformed into a zone of necrosis.

Furthermore, a 10s burn wound at 85°C showed more severe burns, indicating that the burn production model was accurate in simulating different burn depths. In a rat burn model, higher levels of Cx43 expression were seen in the epidermis and dermis, indicating that Cx43 may be involved in the progression of burns. In order to stop or retard the course of burns, it may be possible in the future to target Cx43 expression in rat burn injuries.

Using the 55°C 10 s burn model, topical application Cx43 targeted therapeutics of Cx43asODN or Tonabersat was carried out in **Chapter 4** to explore the role of Cx43 in rat burn injury. Early stages of burn wound healing saw an increased inflammatory response, elevated Cx43 and hemichannel expression in the zone of stasis. Targeting Cx43 prevented burn progression and accelerated early wound healing. The topical administration of Cx43asODN, which targets the mRNA of Cx43, decreased the amounts of Cx43 gap junctional and hemichannels protein, further demonstrating the importance of Cx43. A hemichannel blocker, Tonabersat has also been shown to drastically lower hemichannel protein levels. Concomitantly, marginally and transiently reduced P2X7 expression and NLRP3 inflammasome complex markers expression, which in turn resulted in less IL-1β production in rat burn injury. Additionally, to accelerate wound healing, Cx43/P2X7-mediated NLRP3 inflammasome suppression decreased the inflammatory response in the initial stages of burn injury. Furthermore, there was notable a reduction in αSMA and HSP47 skin fibrosis markers, along with MMP-9. In wounds treated with Cx43asODN or Tonabersat, histological examination of rat burn injury showed improved collagen preservation and synthesis and decreased nascent epidermal thickness. Although wound contraction is the primary process by which the rat skin heals, the results from **Chapter 4** set the stage for preclinical testing. Overall, this research points to a potential role for the P2X7-activated NLRP3 inflammasome pathway via

Cx43 in the early stages of burn wound healing. This suggests that inhibiting the Cx43 hemichannels may be a useful therapeutic target for halting the course of burn progression and enhancing recovery.

The role of Cx43 in pig burn injury and whether Cx43 targeted therapies may be helpful for porcine burn wounds were investigated in light of the results from the rat burn injury study. Experiments were conducted in **Chapter 5** using an improved scald burn model, originally developed by Andrews et al. (Andrews et al., 2016). This study, as far as I am aware, was the first to investigate Cx43 targeted therapies in a pig scald burn lesion. Results from this chapter demonstrated that in the zone of stasis, following a scald burn wound injury, Cx43 and hemichannel expression are enhanced. However, the potential influence of the F-127 Pluronic gel as a carrier must be carefully considered. Administration of low and high concentrations of Cx43asODN or Tonabersat downregulated Cx43 and hemichannel expression and reduced downstream players such as P2X7 and NLRP3 inflammasome activation in the zone of stasis. In addition, this decreased the number of MPO positive neutrophils. Early treatment with Cx43asODN or Tonabersat also halted the progression of burns and preserved the collagen content in deeper layers of dermis on PBD 14. Although all of the wounds have re-epithelialized by PBD 21, it is important to note that there is an earlier reduction in epidermal thickness in wounds treated with Cx43asODN or Tonabersat compared to control groups.

Alongside topical gel application of Cx43asODN or Tonabersat in porcine scald burn injury, I also investigated the delivery of Cx43asODN or Tonabersat in an electrospun PCL/PEG scaffold dressing that is another form of topical application in **Chapter 6**. The early burst release effect of Cx43asODN or Tonabersat from PCL/PEG scaffold downregulated Cx43 gap junctions and

hemichannels. This concomitantly reduced P2X7 expression, and subsequently reduced NLRP3 and Cas-1 expression on PBD 4. However, it was revealed that the reduction of Cx43 and hemichannels on PBD 4 did not last until PBD 7, which may have been caused by the initial burst effect from the therapeutic scaffolds. This might have caused a mild decrease in the upstream signalling that caused the scald burn wound progression, while having little impact on the healing of pig burn wounds. Additionally, the absence of direct measurement of ATP release from wounds following treatment leaves some uncertainty about the role of Cx43 in triggering P2X7 that requires further validation. Moreover, Cx43 therapeutics incorporated PCL/PEG scaffolds that served as a barrier protection for the burn wounds, facilitated re-epithelialization, and may have aided in keratinocyte migration throughout the healing process and decreased nascent epidermal thickness. The use of a single P-S scaffold as a control in **Chapter 6** poses challenges in interpreting therapeutic effects. Despite the significant sample size limitation, the results from **Chapter 6** show that early intervention with Cx43 targeted therapies in the zone of stasis is actually helpful in the treatment of burn injuries and may be applied in other clinical settings. Future research may examine different polymer combinations such as PLA or PLGA to fabricate Cx43asODN or Tonabersat scaffolds or attempt the use of microneedles to enhance the delivery of drugs to burn wounds. The translation of the porcine study results to human burns is complex due to varied clinical scenarios. Despite these limitations, the study indicates the potential benefits of Cx43asODN and Tonabersat in burn injury treatment and calls for further research, especially beyond 21 days, to explore their effects on hypertrophic scar formation.

Considering these findings collectively, the preliminary investigation involving targeted therapeutics for Cx43 in the porcine burn model suggests a need for further exploration. However,

at this juncture, the rat burn model with Cx43 targeted therapy appears to be a more suitable model than the porcine burn model. Notably, the topical application method proves to be a more effective delivery system compared to the scaffold dressing, as further refinements are required to enhance the scaffold release profile. Future work could explore further optimization of scaffold dressing that could potentially release drugs in a sustained manner over a period of time along with other delivery strategies such as encapsulation or microneedles to enhance drug delivery efficiency. Overall, the result from this thesis indicates that Cx43 gap junctions and hemichannels play a crucial role in the progression of burns by regulating the recruitment of early inflammatory cells, activation of P2X7, and activation of the NLRP3 inflammasome complex in the zone of stasis. A reduction in the protein levels of Cx43, hemichannels, P2X7 and NLRP3 markers in the zone of stasis, indicates the prevention of burn conversion from turning into a necrotic zone. These findings also indicate this regulatory role is likely to be mediated by Cx43 in the zone of stasis, suggesting that zone of stasis plays a major role and early intervention is key to salvage this zone to improve burn wound healing outcomes. In addition, further investigation into the contribution of Cx43 and other P2 purinergic family members involvement in the inflammasome activation will open up new strategies for fine-tuning connexin-based therapeutics to prevent burn progression. In addition, NLRP3 inflammasome activation is implicated in pyroptosis cell death (Wang et al., 2022). Future work could investigate the interaction between Cx43, NLRP3 and pyroptosis in burn wounds.

7.1 Limitations

The characterisation of the rat burn model in **Chapter 3** revealed a number of limitations. Qualitative measurement with inflammatory score and a single marker MPO to identify neutrophils in burn wounds was used to study the leukocyte infiltration (Figure 3.7 & Figure 3.10). To better understand the presence of immune cells during the burn progression and wound healing phase, additional antibody markers for various immune cells may be helpful. Another limitation is that the depth of burn in the dermis was not determined as it was challenging to distinguish between dead and dying tissue area and measure the depth precisely based on H&E stained tissues. The use of special histology stains such as Masson's Trichrome or Picrosirius Red may be useful to idenitify the depth of burn better and include as a measure of quantification.

In **Chapter 4**, the study was limited by the inability to show ATP release via the Cx43 triggering P2X7. Measurement of ATP from tissue homogenates after topical treatment with Cx43 targeted therapeutics may validate and strengthen that ATP release via Cx43 triggers P2X7. I recognise that the expression of the P2X7 protein levels alone may not be good indicator to determine its activity. Specific functional assays are required to measure specific cellular responses or events triggered by P2X7 receptor. However, carrying out these tests directly in tissues is typically more challenging. Immunolabeling techniques such as immunofluorescence provide insightful information about the localization and receptor expression within the tissues despite the inability to directly measure the activity. The study of IL-1β in tissues is limited by the secretion to be diluted or washed away within the tissue milieu. Even though Cx43 targeted therapeutics decreased the expression of IL-1β, localized secretion could be swiftly scattered or carried away by interstitial fluids, which would limit its accumulation and detection. The use of specialized

methods like ELISA to comprehend the contributions of IL-1β to the immune response and its function in certain burn tissue microenvironments. In addition, validation of M1 and M2 macrophages in rat burn wounds treated with Cx43 treatments will strengthen the pro-inflammatory and anti-inflammatory state of the tissues.

Research on burn wound healing in rats has provided valuable insights into the cause and progression of burn injuries. However, the use of small sized rat burn wounds may not accurately represent the classical burn features observed in humans. In addition, the structure and anatomy of rat skin differ significantly from human skin, with the presence of the panniculus carnosus muscle layer distinguishing it from human skin. The panniculus carnosus heals wounds through contraction, unlike re-epithelialization seen in humans. Furthermore, the rats used in this study varied in weight from 200 to 250g. The thickness of the skin increases with animal size. Because of the disparity in dermal thickness, the burn injuries inflicted on smaller rats seemed to be slightly deeper than those on larger animals. Hence, analysing the data from the burn wounds in rats requires careful consideration.

One of the key limitations in the **Chapter 5 and 6** is that the sample size is small. Using a larger sample size would be preferred to strengthen the statistical power of the study. However, despite the small sample size and trend results, it overall gives some confidence that the results obtained from **Chapter 4** topical application of Cx43asODN and Tonabersat in rat burn injury is consistent with the similar wound healing directions that were observed from **Chapter 5** with the topical application in porcine burn injury. Despite the small sample size limitation, dose dependent differences in protein expression were found in the treated wounds as compared to controls. However, it is also important to note that the F-127 Pluronic gel as a carrier has been reported to

have a positive effect on wound healing (Paustian et al., 1993). Caution must be taken when analysing the data. Nevertheless, our results have shown that the positive effect observed from Cx43asODN and Tonabersat had minimal influence from the F-127 Pluronic gel. Furthermore, protein quantification using western blotting is necessary to determine that Tonabersat can lower hemichannel protein levels as opposed to blocking the pathogenic Cx43 hemichannel channel in porcine injury treated with gel topical application and scaffold dressing. However, the region of interest in this study, the zone of stasis, cannot be distinguished when using the western blotting technique. Another limitation was that I did not directly measure ATP release in the wounds after treatment application. This would have strengthened our data that indeed the ATP release via the Cx43 had triggered the P2X7. In addition, finding good specifc antibodies for pig tissue immunolabeling was another difficult task. The results on the inflammatory response in pig burn wounds may have been strengthened by the use of specific immune cell markers.

In addition, in **Chapter 6**, using a single P-S scaffold as a control was a huge limitation as it was hard to determine if the therapeutic effect observed from AS-S and Tona-S on PBD 4 was truly from the scaffold release or if the scaffolds acted as a simple protective barrier. Extrapolation from the scaffold release profile has shown that the concentration of drugs eluted from the scaffold was far less than that of topically delivered therapeutics to porcine burn. This could be a reason for the results from porcine topical application having a better outcome than scaffold application in porcine burn. Further optimization of scaffold dressings is required to improve theraeputic release profile.

Although I attempted to tightly control burn creation, it is not possible to completely standardize the burn creation as variances were introduced by the langer lines of the pigs. Langer lines are also

known as cleavage lines or tension lines on the body that represent the natural orientation of the collagen fibers in the skin which was first described by anatomist Karl Langer in the mid-19th century (Wilhelmi et al., 1999). These lines are greatly affected by the musculoskeletal movements which affects the rate of healing and scarring process. In a study using micropig, they have observed that excisional wounds created at cephalic area contracted and healed faster than those in the caudal area (Kwak et al., 2014). In our study, the P-S control was positioned at the cephalic area, and this could be a reason for it to heal faster and not show any difference from the treated wounds. A larger sample size and randomisation of wounds could reduce confounding factors from Langer lines.

For the creation of burn wounds, I adopted the methodology published by Andrews and team (Andrews et al., 2016). The key difference from their study and ours is that the age and breed of the pigs utilised in this study differs from Andrews et al., 2016 publication where they have used juvenile pigs weighing around 27kg whereas our pigs were bigger and weighed more than 50kg. Hence, the dermal thickness in our model was thicker, and that could have potentially introduced some differences. Even though we chose a temperature that was shown to create deep partial thickness, it may have created a less severe burn than was reported in their study. In addition, I did not measure the temperature of skin during and after burn creation and hence I could not control for the differences in burn creation. Using a higher temperature to create a deeper wound may have been desirable for this porcine burn study.

Results found in pig studies may not translate directly into humans as the clinical implications reported in human burns are varied. It is impossible to determine the temperature of exposure and the duration of exposure for human burn injuries in order to directly compare to porcine burn

development (Singer et al., 2020). In clinical settings, scald burn injury often occurs in patients older than 65 after encountering boiling water and steam (Tracy et al., 2020), and in children (Battle et al., 2016). It has been reported that scald burns were less severe compared to contact burns. In addition, some scald and contact burns are smaller in surface area than in flame burns (Singer et al., 2020). However, it is not ethical to expose animals to flame burns or dipping them into hot water to create a larger surface area to best reproduce human burns.

Although this study has used scald burns, the findings from this study has shown that using either Cx43asODN or Tonabersat could be beneficial in the treatment of burn injury. I have validated the use of Cx43asODN and Tonabersat in a rodent burn model **(Chapter 4)**, which has shown to have promising outcomes in terms of prevention of burn progression and better wound healing outcomes. However, the size and placement of multiple wounds on the rat model introduces high variances in burn wound creation, hence I limited it to four wounds per animal in the rat burn model and worked with concentrations that were previously reported for Cx43asODN and Tonabersat. In the porcine burn model, I was able to work on multiple wounds on each pig. I had the opportunity to validate the use the high and low doses for topical application of Cx43asODN and Tonabersat as a pilot study in the porcine scald burn model. The porcine burn wounds were also followed up until PBD 21. Histological features have shown that the wounds are still undergoing remodelling. It will be beneficial to study wound healing beyond 21 days to better understand if the therapeutic effect of early intervention with Cx43asODN and Tonabersat affects hypertrophic scar formation.

Publications

Journal Papers

Thangaveloo, M, Feng, J., Phillips, A. R., & Becker, D. L. (2024) Targeted Cx43 therapeutics reduce inflammasome activation in rat burn injury. *(Under Review)*

Thangaveloo, M, Lim, D., Aw, Amelia., Kannan, B., Lim, B. H. S., Phillips, A. R., & Becker, D. L. (2024) Sustained delivery of Cx43 Therapeutics in porcine burn injury prevents burn progression. *(In preparation)*.

Kwek, M. S. Y.*, **Thangaveloo, M**.*, Phillips, A. R., & Becker, D. L. (2023) Targetting Cx43 to reduce the severity of pressure ulcer progression. *Cells*, *12*(24). *(Co-first authors)*

Zheng, X. T., Yang, Z., Sutarlie, L., **Thangaveloo, M**., Yu, Y., Salleh, N. A. B. M., Chin, J. S., Xiong., Z, Becker, D. L., Tee, B. C. K., & Su, X. (2023) Battery-Free and AI-enabled Multiplexed Sensor Patches for In situ Wound Monitoring. *Science Advances*, *9*(24), eadg6670.

Chua, J.W., **Thangaveloo, M**., Lim, D., Madden, L. E., Phillips, A. R., & Becker, D. L. (2022). Connexin43 in post-surgical peritoneal adhesion formation. *Life (Basel)*, *12*(11).

Kwek, M. S. Y., **Thangaveloo, M**., Hui, S. L. B., Madden, L. E., Phillips, A. R., & Becker, D. L. (2021). Characterisation of an ischaemia reperfusion model for the formation of a stage I pressure ulcer in mouse skin. *Journal of Tissue Viability*, *30*(3), 352-362.

Feng, J., **Thangaveloo, M**., Ong, Y. S., Chong, S. J., Joethy, J. V., & Becker, D. L. (2020). Connexin 43 upregulation in burns promotes burn conversion through spread of apoptotic death signals. *Burns*, *46*(6), 1389-1397.

Poster Presentation

Thangaveloo, M, Feng, J., Becker, D. L. (2022) Targeted Cx43 therapeutics reduces inflammasome activation in burn injury. 26th to 30th September 2022. EMBO conference: The molecular and cellular basis of Regeneration and tissue repair: Spain.

References

Abbas, O. L., Ozatik, O., Gonen, Z. B., Ogut, S., Entok, E., Ozatik, F. Y., Bahar, D., Bakir, Z. B., & Musmul, A. (2018). Prevention of Burn Wound Progression by Mesenchymal Stem Cell Transplantation: Deeper Insights Into Underlying Mechanisms. *Ann Plast Surg*, *81*(6), 715-724. https://doi.org/10.1097/SAP.0000000000001620

Abdullahi, A., Amini-Nik, S., & Jeschke, M. G. (2014). Animal models in burn research. *Cell Mol Life Sci*, *71*(17), 3241-3255. https://doi.org/10.1007/s00018-014-1612-5

Abudara, V., Bechberger, J., Freitas-Andrade, M., De Bock, M., Wang, N., Bultynck, G., Naus, C. C., Leybaert, L., & Giaume, C. (2014). The connexin43 mimetic peptide Gap19 inhibits hemichannels without altering gap junctional communication in astrocytes. *Front Cell Neurosci*, *8*, 306. https://doi.org/10.3389/fncel.2014.00306

Acosta, M. L., Mat Nor, M. N., Guo, C. X., Mugisho, O. O., Coutinho, F. P., Rupenthal, I. D., & Green, C. R. (2021). Connexin therapeutics: blocking connexin hemichannel pores is distinct from blocking pannexin channels or gap junctions. *Neural Regen Res*, *16*(3), 482-488. https://doi.org/10.4103/1673-5374.290097

Aghdam, S. Y., Kenchegowda, D., Sharma, N. K., Holmes-Hampton, G. P., Legesse, B., Moroni, M., & Ghosh, S. P. (2020). Dysregulated Cardiac IGF-1 Signaling and Antioxidant Response Are Associated with Radiation Sensitivity. *Int J Mol Sci*, *21*(14). https://doi.org/10.3390/ijms21145049

Agrawal, S., Temsamani, J., Galbraith, W., & Tang, J. (1995). Pharmacokinetics of antisense oligonucleotides. *Clin Pharmacokinet*, *28*(1), 7-16. https://doi.org/10.2165/00003088-199528010-00002

Ahn, C. S., & Maitz, P. K. (2012). The true cost of burn. *Burns*, *38*(7), 967-974. https://doi.org/10.1016/j.burns.2012.05.016

Aijaz, A., Vinaik, R., & Jeschke, M. G. (2022). Large animal models of thermal injury. *Methods Cell Biol*, *168*, 191-219. https://doi.org/10.1016/bs.mcb.2021.12.015

Akershoek, J. J. J., Brouwer, K. M., Vlig, M., Boekema, B., Beelen, R. H. J., Middelkoop, E., & Ulrich, M. M. W. (2018). Early intervention by Captopril does not improve wound healing of partial thickness burn wounds in a rat model. *Burns*, *44*(2), 429-435. https://doi.org/10.1016/j.burns.2017.08.008

Al Samad, A., Bethry, A., Koziolova, E., Netopilik, M., Etrych, T., Bakkour, Y., Coudane, J., El Omar, F., & Nottelet, B. (2016). PCL-PEG graft copolymers with tunable amphiphilicity as efficient drug delivery systems. *J Mater Chem B*, *4*(37), 6228-6239. https://doi.org/10.1039/c6tb01841f

Albalawi, F., Lu, W., Beckel, J. M., Lim, J. C., McCaughey, S. A., & Mitchell, C. H. (2017). The P2X7 Receptor Primes IL-1beta and the NLRP3 Inflammasome in Astrocytes Exposed to Mechanical Strain. *Front Cell Neurosci*, *11*, 227. https://doi.org/10.3389/fncel.2017.00227

Almad, A. A., Taga, A., Joseph, J., Gross, S. K., Welsh, C., Patankar, A., Richard, J. P., Rust, K., Pokharel, A., Plott, C., Lillo, M., Dastgheyb, R., Eggan, K., Haughey, N., Contreras, J. E., & Maragakis, N. J. (2022). Cx43 hemichannels contribute to astrocyte-mediated toxicity in sporadic and familial ALS. *Proc Natl Acad Sci U S A*, *119*(13), e2107391119. https://doi.org/10.1073/pnas.2107391119

Alsaab, H., Alzhrani, R. M., & Boddu, S. H. (2016). Evaluation of the percutaneous absorption of chlorpromazine from PLO gels across porcine ear and human abdominal skin. *Drug Dev Ind Pharm*, *42*(8), 1258-1266. https://doi.org/10.3109/03639045.2015.1122610

Alven, S., & Aderibigbe, B. A. (2020). Chitosan and Cellulose-Based Hydrogels for Wound Management. *Int J Mol Sci*, *21*(24). https://doi.org/10.3390/ijms21249656

Alves, N. G., Motawe, Z. Y., Yuan, S. Y., & Breslin, J. W. (2018). Endothelial Protrusions in Junctional Integrity and Barrier Function. *Curr Top Membr*, *82*, 93-140. https://doi.org/10.1016/bs.ctm.2018.08.006

Andrews, C. J., & Cuttle, L. (2017). Comparing the reported burn conditions for different severity burns in porcine models: a systematic review. *Int Wound J*, *14*(6), 1199-1212. https://doi.org/10.1111/iwj.12786

Andrews, C. J., Kempf, M., Kimble, R., & Cuttle, L. (2016). Development of a Consistent and Reproducible Porcine Scald Burn Model. *PLoS One*, *11*(9), e0162888. https://doi.org/10.1371/journal.pone.0162888

Andrews, C. J., Kimble, R. M., Kempf, M., & Cuttle, L. (2017). Evidence-based injury prediction data for the water temperature and duration of exposure for clinically relevant deep dermal scald injuries. *Wound Repair Regen*, *25*(5), 792-804. https://doi.org/10.1111/wrr.12577

Arda, M. S., Kocman, A. E., Soztutar, E., Baksan, B., & Cetin, C. (2017). A new apparatus for standardization of experimental burn models. *Burns*, *43*(6), 1322-1329. https://doi.org/10.1016/j.burns.2017.01.014

Artlett, C. M. (2012). The Role of the NLRP3 Inflammasome in Fibrosis. *Open Rheumatol J*, *6*, 80-86. https://doi.org/10.2174/1874312901206010080

Asazuma-Nakamura, Y., Dai, P., Harada, Y., Jiang, Y., Hamaoka, K., & Takamatsu, T. (2009). Cx43 contributes to TGF-beta signaling to regulate differentiation of cardiac fibroblasts into myofibroblasts. *Exp Cell Res*, *315*(7), 1190-1199. https://doi.org/10.1016/j.yexcr.2008.12.021

Bae, J. Y., Lee, S. W., Shin, Y. H., Lee, J. H., Jahng, J. W., & Park, K. (2017). P2X7 receptor and NLRP3 inflammasome activation in head and neck cancer. *Oncotarget*, *8*(30), 48972-48982. https://doi.org/10.18632/oncotarget.16903

Bajwa, N., Sung, S., Ennis, D. B., Fishbein, M. C., Nowroozi, B. N., Ruan, D., Maccabi, A., Alger, J., John, M. A. S., Grundfest, W. S., & Taylor, Z. D. (2017). Terahertz Imaging of Cutaneous Edema: Correlation With Magnetic Resonance Imaging in Burn Wounds. *IEEE Trans Biomed Eng*, *64*(11), 2682-2694. https://doi.org/10.1109/TBME.2017.2658439

Banerjee, J., Seetharaman, S., Wrice, N. L., Christy, R. J., & Natesan, S. (2019). Delivery of silver sulfadiazine and adipose derived stem cells using fibrin hydrogel improves infected burn wound regeneration. *PLoS One*, *14*(6), e0217965. https://doi.org/10.1371/journal.pone.0217965

Basile, D. P., Anderson, M. D., & Sutton, T. A. (2012). Pathophysiology of acute kidney injury. *Compr Physiol*, *2*(2), 1303-1353. https://doi.org/10.1002/cphy.c110041

Battle, C. E., Evans, V., James, K., Guy, K., Whitley, J., & Evans, P. A. (2016). Epidemiology of burns and scalds in children presenting to the emergency department of a regional burns unit: a 7-year retrospective study. *Burns Trauma*, *4*, 19. https://doi.org/10.1186/s41038-016-0047-7

Bayliss, J., Delarosa, S., Wu, J., Peterson, J. R., Eboda, O. N., Su, G. L., Hemmila, M., Krebsbach, P. H., Cederna, P. S., Wang, S. C., Xi, C., & Levi, B. (2014). Adenosine triphosphate hydrolysis reduces neutrophil infiltration and necrosis in partial-thickness scald burns in mice. *J Burn Care Res*, *35*(1), 54-61. https://doi.org/10.1097/BCR.0b013e31829b36d6

Becic, F., Mulabegovic, N., Mornjakovic, Z., Kapic, E., Prasovic, S., Becic, E., & Kusturica, J. (2005). Topical treatment of standardised burns with herbal remedies in model rats. *Bosn J Basic Med Sci*, *5*(4), 50-57. https://doi.org/10.17305/bjbms.2005.3233

Becker, D. L., Thrasivoulou, C., & Phillips, A. R. (2012). Connexins in wound healing; perspectives in diabetic patients. *Biochim Biophys Acta*, *1818*(8), 2068-2075. https://doi.org/10.1016/j.bbamem.2011.11.017

Bhattacharyya, A., Torre, P., Yadav, P., Boostanpour, K., Chen, T. Y., Tsukui, T., Sheppard, D., Muramatsu, R., Seed, R. I., Nishimura, S. L., Jung, J. B., Tang, X. Z., Allen, C. D. C., & Bhattacharya, M. (2022). Macrophage Cx43 Is Necessary for Fibroblast Cytosolic Calcium and Lung Fibrosis After Injury. *Front Immunol*, *13*, 880887. https://doi.org/10.3389/fimmu.2022.880887

Bracey, N. A., Gershkovich, B., Chun, J., Vilaysane, A., Meijndert, H. C., Wright, J. R., Jr., Fedak, P. W., Beck, P. L., Muruve, D. A., & Duff, H. J. (2014). Mitochondrial NLRP3 protein induces reactive oxygen species to promote Smad protein signaling and fibrosis independent from the inflammasome. *J Biol Chem*, *289*(28), 19571-19584. https://doi.org/10.1074/jbc.M114.550624

Brandner, J. M., Houdek, P., Husing, B., Kaiser, C., & Moll, I. (2004). Connexins 26, 30, and 43: differences among spontaneous, chronic, and accelerated human wound healing. *Journal of Investigative Dermatology*, *122*(5), 1310-1320. https://doi.org/10.1111/j.0022-202X.2004.22529.x

Brandner, J. M., Zacheja, S., Houdek, P., Moll, I., & Lobmann, R. (2008). Expression of matrix metalloproteinases, cytokines, and connexins in diabetic and nondiabetic human keratinocytes before and after transplantation into an ex vivo wound-healing model. *Diabetes Care*, *31*(1), 114-120. https://doi.org/10.2337/dc07-1304

Branes, M. C., Contreras, J. E., & Saez, J. C. (2002). Activation of human polymorphonuclear cells induces formation of functional gap junctions and expression of connexins. *Med Sci Monit*, *8*(8), BR313-323. https://www.ncbi.nlm.nih.gov/pubmed/12165735

Brans, T. A., Dutrieux, R. P., Hoekstra, M. J., Kreis, R. W., & du Pont, J. S. (1994). Histopathological evaluation of scalds and contact burns in the pig model. *Burns*, *20 Suppl 1*, S48-51. https://doi.org/10.1016/0305-4179(94)90090-6

Braza, M. E., & Fahrenkopf, M. P. (2022). Split-Thickness Skin Grafts. In *StatPearls*. https://www.ncbi.nlm.nih.gov/pubmed/31855388

Brink, J. A., Sheets, P. W., Dines, K. A., Etchison, M. R., Hanke, C. W., & Sadove, A. M. (1986). Quantitative assessment of burn injury in porcine skin with high-frequency ultrasonic imaging. *Invest Radiol*, *21*(8), 645-651. https://doi.org/10.1097/00004424-198608000-00008

Browning, J. A., & Cindass, R. (2022). Burn Debridement, Grafting, and Reconstruction. In *StatPearls*. https://www.ncbi.nlm.nih.gov/pubmed/31869181

Buckley, C., Zhang, X., Wilson, C., & McCarron, J. G. (2021). Carbenoxolone and 18beta-glycyrrhetinic acid inhibit inositol 1,4,5-trisphosphate-mediated endothelial cell calcium signalling and depolarise mitochondria. *Br J Pharmacol*, *178*(4), 896-912. https://doi.org/10.1111/bph.15329

Burke, S., Nagajyothi, F., Thi, M. M., Hanani, M., Scherer, P. E., Tanowitz, H. B., & Spray, D. C. (2014). Adipocytes in both brown and white adipose tissue of adult mice are functionally connected via gap junctions: implications for Chagas disease. *Microbes Infect*, *16*(11), 893-901. https://doi.org/10.1016/j.micinf.2014.08.006

Busuioc, C. J., Mogosanu, G. D., Popescu, F. C., Lascar, I., Parvanescu, H., & Mogoanta, L. (2013). Phases of the cutaneous angiogenesis process in experimental third-degree skin burns: histological and immunohistochemical study. *Rom J Morphol Embryol*, *54*(1), 163-171. https://www.ncbi.nlm.nih.gov/pubmed/23529325

Butts, C. C., Holmes, J. H., & Carter, J. E. (2020). Surgical Escharotomy and Decompressive Therapies in Burns. *J Burn Care Res*, *41*(2), 263-269. https://doi.org/10.1093/jbcr/irz152

Cai, E. Z., Ang, C. H., Raju, A., Tan, K. B., Hing, E. C., Loo, Y., Wong, Y. C., Lee, H., Lim, J., Moochhala, S. M., Hauser, C. A., & Lim, T. C. (2014). Creation of consistent burn wounds: a rat model. *Arch Plast Surg*, *41*(4), 317-324. https://doi.org/10.5999/aps.2014.41.4.317

Cai, J., Guan, H., Jiao, X., Yang, J., Chen, X., Zhang, H., Zheng, Y., Zhu, Y., Liu, Q., & Zhang, Z. (2021). NLRP3 inflammasome mediated pyroptosis is involved in cadmium exposure-induced neuroinflammation through the IL-1β/IkB-α-NF-κB-NLRP3 feedback loop in swine. *Toxicology*, *453*, 152720. https://doi.org/https://doi.org/10.1016/j.tox.2021.152720

Campelo, A. P. B. S., Campelo, M. W. S., Britto, G. A. d. C., Ayala, A. P., Guimarães, S. B., & Vasconcelos, P. R. L. d. (2011). An optimized animal model for partial and total skin thickness burns studies. *Acta Cirurgica Brasileira*, *26*, 38-42.

http://www.scielo.br/scielo.php?script=sci_arttext&pid=S0102-86502011000700008&nrm=iso

http://www.scielo.br/pdf/acb/v26s1/08.pdf

Chan, W. N., Evans, J. M., Hadley, M. S., Herdon, H. J., Jerman, J. C., Parsons, A. A., Read, S. J., Stean, T. O., Thompson, M., & Upton, N. (1999a). Identification of (-)-cis-6-acetyl-4S-(3-chloro-4-fluoro-benzoylamino)- 3,4-dihydro-2,2-dimethyl-2H-benzo[b]pyran-3S-ol as a potential antimigraine agent. *Bioorg Med Chem Lett*, *9*(2), 285-290. https://doi.org/10.1016/s0960-894x(98)00728-8

Chan, W. N., Evans, J. M., Hadley, M. S., Herdon, H. J., Jerman, J. C., Parsons, A. A., Read, S. J., Stean, T. O., Thompson, M., & Upton, N. (1999b). Identification of (−)-cis-6-acetyl-4S-(3-chloro-4-fluoro-benzoylamino)-3,4-dihydro-2,2-dimethyl-2H-benzo[b]pyran-3S-ol as a potential antimigraine agent. *Bioorganic & Medicinal Chemistry Letters*, *9*(2), 285-290. https://doi.org/https://doi.org/10.1016/S0960-894X(98)00728-8

Chang, Y.-c., Chang, H.-Y., Hahn, R., Lee, E., Svoboda, K., Gordon, M., & Gerecke, D. (2015). Connexin 43 Antisense Therapy Modulates Connexin Expression and Wound Repair in Nitrogen Mustard Injured Mouse Skin. *The FASEB Journal*, *29*(S1), 876.873. https://doi.org/https://doi.org/10.1096/fasebj.29.1_supplement.876.3

Chen, B., Yang, L., Chen, J., Chen, Y., Zhang, L., Wang, L., Li, X., Li, Y., & Yu, H. (2019). Inhibition of Connexin43 hemichannels with Gap19 protects cerebral ischemia/reperfusion injury via the JAK2/STAT3 pathway in mice. *Brain Res Bull*, *146*, 124-135. https://doi.org/10.1016/j.brainresbull.2018.12.009

Chen, J. J., Zhao, S., Cen, Y., Liu, X. X., Yu, R., & Wu, D. M. (2007). Effect of heat shock protein 47 on collagen accumulation in keloid fibroblast cells. *Br J Dermatol*, *156*(6), 1188-1195. https://doi.org/10.1111/j.1365-2133.2007.07898.x

Chen, W., Zhu, S., Wang, Y., Li, J., Qiang, X., Zhao, X., Yang, H., D'Angelo, J., Becker, L., Wang, P., Tracey, K. J., & Wang, H. (2019). Enhanced Macrophage Pannexin 1 Expression and Hemichannel Activation Exacerbates Lethal Experimental Sepsis. *Sci Rep*, *9*(1), 160. https://doi.org/10.1038/s41598-018-37232-z

Chen, Z. C., Wu, S. S., Su, W. Y., Lin, Y. C., Lee, Y. H., Wu, W. H., Chen, C. H., & Wen, Z. H. (2016). Anti-inflammatory and burn injury wound healing properties of the shell of Haliotis diversicolor. *BMC Complement Altern Med*, *16*(1), 487. https://doi.org/10.1186/s12906-016-1473-6

Chi, Y., Liu, X., & Chai, J. (2021). A narrative review of changes in microvascular permeability after burn. *Ann Transl Med*, *9*(8), 719. https://doi.org/10.21037/atm-21-1267

Chiang, R. S., Borovikova, A. A., King, K., Banyard, D. A., Lalezari, S., Toranto, J. D., Paydar, K. Z., Wirth, G. A., Evans, G. R., & Widgerow, A. D. (2016). Current concepts related to hypertrophic scarring in burn injuries. *Wound Repair Regen*, *24*(3), 466-477. https://doi.org/10.1111/wrr.12432

Chitnis, D., Dickerson, C., Munster, A. M., & Winchurch, R. A. (1996). Inhibition of apoptosis in polymorphonuclear neutrophils from burn patients. *J Leukoc Biol*, *59*(6), 835-839. https://doi.org/10.1002/jlb.59.6.835

Choe, G., Park, J., Park, H., & Lee, J. Y. (2018). Hydrogel Biomaterials for Stem Cell Microencapsulation. *Polymers (Basel)*, *10*(9). https://doi.org/10.3390/polym10090997

Choi, C., Saha, A., An, S., Cho, Y. K., Kim, H., Noh, M., & Lee, Y. H. (2022). Macrophage-Specific Connexin 43 Knockout Protects Mice from Obesity-Induced Inflammation and Metabolic Dysfunction. *Front Cell Dev Biol*, *10*, 925971. https://doi.org/10.3389/fcell.2022.925971

Choi, J. S., Leong, K. W., & Yoo, H. S. (2008). In vivo wound healing of diabetic ulcers using electrospun nanofibers immobilized with human epidermal growth factor (EGF). *Biomaterials*, *29*(5), 587-596. https://doi.org/10.1016/j.biomaterials.2007.10.012

Choudhury, S., Surendran, N., & Das, A. (2021). Recent advances in the induced pluripotent stem cell-based skin regeneration. *Wound Repair Regen*, *29*(5), 697-710. https://doi.org/10.1111/wrr.12925

Chua, J. W., Thangaveloo, M., Lim, D. X. E., Madden, L. E., Phillips, A. R. J., & Becker, D. L. (2022). Connexin43 in Post-Surgical Peritoneal Adhesion Formation. *Life (Basel)*, *12*(11). https://doi.org/10.3390/life12111734

Church, D., Elsayed, S., Reid, O., Winston, B., & Lindsay, R. (2006). Burn wound infections. *Clin Microbiol Rev*, *19*(2), 403-434. https://doi.org/10.1128/CMR.19.2.403-434.2006

Clark, R. A. F., Fenner, J., Sasson, A., McClain, S. A., Singer, A. J., & Tonnesen, M. G. (2018). Blood vessel occlusion with erythrocyte aggregates causes burn injury progression-microvasculature dilation as a possible therapy. *Exp Dermatol*, *27*(6), 625-629. https://doi.org/10.1111/exd.13518

Cogliati, B., Vinken, M., Silva, T. C., Araujo, C. M. M., Aloia, T. P. A., Chaible, L. M., Mori, C. M. C., & Dagli, M. L. Z. (2015). Connexin 43 deficiency accelerates skin wound healing and extracellular matrix remodeling in mice. *J Dermatol Sci*, *79*(1), 50-56. https://doi.org/10.1016/j.jdermsci.2015.03.019

Conte, C., Costabile, G., d'Angelo, I., Pannico, M., Musto, P., Grassia, G., Ialenti, A., Tirino, P., Miro, A., Ungaro, F., & Quaglia, F. (2015). Skin transport of PEGylated poly(epsilon-caprolactone) nanoparticles assisted by (2-hydroxypropyl)-beta-cyclodextrin. *J Colloid Interface Sci*, *454*, 112-120. https://doi.org/10.1016/j.jcis.2015.05.010

Contreras, J. E., Saez, J. C., Bukauskas, F. F., & Bennett, M. V. (2003). Gating and regulation of connexin 43 (Cx43) hemichannels. *Proc Natl Acad Sci U S A*, *100*(20), 11388-11393. https://doi.org/10.1073/pnas.1434298100

Contreras, J. E., Sanchez, H. A., Eugenin, E. A., Speidel, D., Theis, M., Willecke, K., Bukauskas, F. F., Bennett, M. V., & Saez, J. C. (2002). Metabolic inhibition induces opening of unapposed connexin 43 gap junction hemichannels and reduces gap junctional

communication in cortical astrocytes in culture. *Proc Natl Acad Sci U S A*, *99*(1), 495-500. https://doi.org/10.1073/pnas.012589799

Contreras, J. E., Sanchez, H. A., Veliz, L. P., Bukauskas, F. F., Bennett, M. V., & Saez, J. C. (2004). Role of connexin-based gap junction channels and hemichannels in ischemia-induced cell death in nervous tissue. *Brain Res Brain Res Rev*, *47*(1-3), 290-303. https://doi.org/10.1016/j.brainresrev.2004.08.002

Coutinho, F. P., Green, C. R., Acosta, M. L., & Rupenthal, I. D. (2020). Xentry-Gap19 inhibits Connexin43 hemichannel opening especially during hypoxic injury. *Drug Deliv Transl Res*, *10*(3), 751-765. https://doi.org/10.1007/s13346-020-00763-y

Coutinho, F. P., Green, C. R., & Rupenthal, I. D. (2018). Intracellular oligonucleotide delivery using the cell penetrating peptide Xentry. *Sci Rep*, *8*(1), 11256. https://doi.org/10.1038/s41598-018-29556-7

Coutinho, P., Qiu, C., Frank, S., Wang, C. M., Brown, T., Green, C. R., & Becker, D. L. (2005). Limiting burn extension by transient inhibition of Connexin43 expression at the site of injury. *Br J Plast Surg*, *58*(5), 658-667. https://doi.org/10.1016/j.bjps.2004.12.022

Cronin, M., Anderson, P. N., Cook, J. E., Green, C. R., & Becker, D. L. (2008). Blocking connexin43 expression reduces inflammation and improves functional recovery after spinal cord injury. *Mol Cell Neurosci*, *39*(2), 152-160. https://doi.org/10.1016/j.mcn.2008.06.005

Cronin, M., Anderson, P. N., Green, C. R., & Becker, D. L. (2006). Antisense delivery and protein knockdown within the intact central nervous system. *Front Biosci*, *11*, 2967-2975. https://doi.org/10.2741/2025

Cross, S. E., Naylor, I. L., Coleman, R. A., & Teo, T. C. (1995). An experimental model to investigate the dynamics of wound contraction. *Br J Plast Surg*, *48*(4), 189-197. https://doi.org/10.1016/0007-1226(95)90001-2

Cuttle, L., Kempf, M., Phillips, G. E., Mill, J., Hayes, M. T., Fraser, J. F., Wang, X. Q., & Kimble, R. M. (2006). A porcine deep dermal partial thickness burn model with hypertrophic scarring. *Burns*, *32*(7), 806-820. https://doi.org/10.1016/j.burns.2006.02.023

D'Arpa, P., & Leung, K. P. (2017). Toll-Like Receptor Signaling in Burn Wound Healing and Scarring. *Adv Wound Care (New Rochelle)*, *6*(10), 330-343. https://doi.org/10.1089/wound.2017.0733

D'Hondt, C., Iyyathurai, J., Himpens, B., Leybaert, L., & Bultynck, G. (2014). Cx43-hemichannel function and regulation in physiology and pathophysiology: insights from the bovine corneal endothelial cell system and beyond. *Front Physiol*, *5*, 348. https://doi.org/10.3389/fphys.2014.00348

Dahiya, P. (2009). Burns as a model of SIRS. *FBL*, *14*(13), 4962-4967. https://doi.org/10.2741/3580

Dahlof, C. G., Hauge, A. W., & Olesen, J. (2009). Efficacy and safety of tonabersat, a gap-junction modulator, in the acute treatment of migraine: a double-blind, parallel-group, randomized study. *Cephalalgia*, *29 Suppl 2*, 7-16. https://doi.org/10.1111/j.1468-2982.2009.01975.x

Damodaram, S., Thalakoti, S., Freeman, S. E., Garrett, F. G., & Durham, P. L. (2009). Tonabersat inhibits trigeminal ganglion neuronal-satellite glial cell signaling. *Headache*, *49*(1), 5-20. https://doi.org/10.1111/j.1526-4610.2008.01262.x

Decrock, E., De Vuyst, E., Vinken, M., Van Moorhem, M., Vranckx, K., Wang, N., Van Laeken, L., De Bock, M., D'Herde, K., Lai, C. P., Rogiers, V., Evans, W. H., Naus, C. C., & Leybaert, L. (2009). Connexin 43 hemichannels contribute to the propagation of apoptotic cell death in a rat C6 glioma cell model. *Cell Death Differ*, *16*(1), 151-163. https://doi.org/10.1038/cdd.2008.138

Deldar, Y., Pilehvar-Soltanahmadi, Y., Dadashpour, M., Montazer Saheb, S., Rahmati-Yamchi, M., & Zarghami, N. (2018). An in vitro examination of the antioxidant, cytoprotective and anti-inflammatory properties of chrysin-loaded nanofibrous mats for potential wound healing applications. *Artif Cells Nanomed Biotechnol*, *46*(4), 706-716. https://doi.org/10.1080/21691401.2017.1337022

Delvaeye, T., De Smet, M. A. J., Verwaerde, S., Decrock, E., Czekaj, A., Vandenbroucke, R. E., Lemeire, K., Goncalves, A., Declercq, W., Vandenabeele, P., Krysko, D. V., & Leybaert, L. (2019). Blocking connexin43 hemichannels protects mice against tumour necrosis factor-induced inflammatory shock. *Sci Rep*, *9*(1), 16623. https://doi.org/10.1038/s41598-019-52900-4

Deng, X., Chen, Q., Qiang, L., Chi, M., Xie, N., Wu, Y., Yao, M., Zhao, D., Ma, J., Zhang, N., & Xie, Y. (2018). Development of a Porcine Full-Thickness Burn Hypertrophic Scar Model and Investigation of the Effects of Shikonin on Hypertrophic Scar Remediation. *Front Pharmacol*, *9*, 590. https://doi.org/10.3389/fphar.2018.00590

Deng, X., Gould, M., & Ali, M. A. (2021). Fabrication and characterisation of melt-extruded chitosan/keratin/PCL/PEG drug-eluting sutures designed for wound healing. *Mater Sci Eng C Mater Biol Appl*, *120*, 111696. https://doi.org/10.1016/j.msec.2020.111696

Desmouliere, A., Chaponnier, C., & Gabbiani, G. (2005). Tissue repair, contraction, and the myofibroblast. *Wound Repair Regen*, *13*(1), 7-12. https://doi.org/10.1111/j.1067-1927.2005.130102.x

Desplantez, T., Verma, V., Leybaert, L., Evans, W. H., & Weingart, R. (2012). Gap26, a connexin mimetic peptide, inhibits currents carried by connexin43 hemichannels and gap junction channels. *Pharmacol Res*, *65*(5), 546-552. https://doi.org/10.1016/j.phrs.2012.02.002

Dethe, M. R., A, P., Ahmed, H., Agrawal, M., Roy, U., & Alexander, A. (2022). PCL-PEG copolymer based injectable thermosensitive hydrogels. *J Control Release*, *343*, 217-236. https://doi.org/10.1016/j.jconrel.2022.01.035

Dhall, S., Silva, J. P., Liu, Y., Hrynyk, M., Garcia, M., Chan, A., Lyubovitsky, J., Neufeld, R. J., & Martins-Green, M. (2015). Release of insulin from PLGA-alginate dressing stimulates

regenerative healing of burn wounds in rats. *Clin Sci (Lond)*, *129*(12), 1115-1129. https://doi.org/10.1042/CS20150393

Dhivya, S., Padma, V. V., & Santhini, E. (2015). Wound dressings - a review. *Biomedicine (Taipei)*, *5*(4), 22. https://doi.org/10.7603/s40681-015-0022-9

Di Fusco, D., Dinallo, V., Marafini, I., Figliuzzi, M. M., Romano, B., & Monteleone, G. (2019). Antisense Oligonucleotide: Basic Concepts and Therapeutic Application in Inflammatory Bowel Disease. *Front Pharmacol*, *10*, 305. https://doi.org/10.3389/fphar.2019.00305

Di, W. L., Rugg, E. L., Leigh, I. M., & Kelsell, D. P. (2001). Multiple epidermal connexins are expressed in different keratinocyte subpopulations including connexin 31. *Journal of Investigative Dermatology*, *117*(4), 958-964. https://doi.org/10.1046/j.0022-202x.2001.01468.x

Doktor, F., Prager, P., Wiedemann, P., Kohen, L., Bringmann, A., & Hollborn, M. (2018). Hypoxic expression of NLRP3 and VEGF in cultured retinal pigment epithelial cells: contribution of P2Y(2) receptor signaling. *Purinergic Signal*, *14*(4), 471-484. https://doi.org/10.1007/s11302-018-9631-6

Dorsett-Martin, W. A. (2004). Rat models of skin wound healing: a review. *Wound Repair Regen*, *12*(6), 591-599. https://doi.org/10.1111/j.1067-1927.2004.12601.x

Dosch, M., Zindel, J., Jebbawi, F., Melin, N., Sanchez-Taltavull, D., Stroka, D., Candinas, D., & Beldi, G. (2019). Connexin-43-dependent ATP release mediates macrophage activation during sepsis. *Elife*, *8*. https://doi.org/10.7554/eLife.42670

Du, Z. J., Cui, G. Q., Zhang, J., Liu, X. M., Zhang, Z. H., Jia, Q., Ng, J. C., Peng, C., Bo, C. X., & Shao, H. (2017). Inhibition of gap junction intercellular communication is involved in silica nanoparticles-induced H9c2 cardiomyocytes apoptosis via the mitochondrial pathway. *Int J Nanomedicine*, *12*, 2179-2188. https://doi.org/10.2147/IJN.S127904

Elbadawy, H. M., Mirabelli, P., Xeroudaki, M., Parekh, M., Bertolin, M., Breda, C., Cagini, C., Ponzin, D., Lagali, N., & Ferrari, S. (2016). Effect of connexin 43 inhibition by the mimetic peptide Gap27 on corneal wound healing, inflammation and neovascularization. *Br J Pharmacol*, *173*(19), 2880-2893. https://doi.org/10.1111/bph.13568

Eltzschig, H. K., Eckle, T., Mager, A., Kuper, N., Karcher, C., Weissmuller, T., Boengler, K., Schulz, R., Robson, S. C., & Colgan, S. P. (2006). ATP release from activated neutrophils occurs via connexin 43 and modulates adenosine-dependent endothelial cell function. *Circ Res*, *99*(10), 1100-1108. https://doi.org/10.1161/01.RES.0000250174.31269.70

Eugenin, E. A., Branes, M. C., Berman, J. W., & Saez, J. C. (2003). TNF-alpha plus IFN-gamma induce connexin43 expression and formation of gap junctions between human monocytes/macrophages that enhance physiological responses. *J Immunol*, *170*(3), 1320-1328. https://doi.org/10.4049/jimmunol.170.3.1320

Evans, W. H., & Boitano, S. (2001). Connexin mimetic peptides: specific inhibitors of gap-junctional intercellular communication. *Biochem Soc Trans*, *29*(Pt 4), 606-612. https://doi.org/10.1042/bst0290606

Fagan, J. M., Ganguly, M., Stockman, H., Ferland, L. H., & Toner, M. (1999). Posttranslational modifications of cardiac and skeletal muscle proteins by reactive oxygen species after burn injury in the rat. *Ann Surg*, *229*(1), 106-114. https://doi.org/10.1097/00000658-199901000-00014

Faniku, C., O'Shaughnessy, E., Lorraine, C., Johnstone, S. R., Graham, A., Greenhough, S., & Martin, P. E. M. (2018). The Connexin Mimetic Peptide Gap27 and Cx43-Knockdown Reveal Differential Roles for Connexin43 in Wound Closure Events in Skin Model Systems. *Int J Mol Sci*, *19*(2). https://doi.org/10.3390/ijms19020604

Farroha, A., Frew, Q., El-Muttardi, N., Philp, B., & Dziewulski, P. (2013). The use of Biobrane(R) to dress split-thickness skin graft in paediatric burns. *Ann Burns Fire Disasters*, *26*(2), 94-97. https://www.ncbi.nlm.nih.gov/pubmed/24133404

Feng, J., See, J. L., Choke, A., Ooi, A., & Chong, S. J. (2018). Biobrane for burns of the pubic region: minimizing dressing changes. *Mil Med Res*, *5*(1), 29. https://doi.org/10.1186/s40779-018-0177-2

Feng, J., Thangaveloo, M., Ong, Y. S., Chong, S. J., Joethy, J. V., & Becker, D. L. (2020). Connexin 43 upregulation in burns promotes burn conversion through spread of apoptotic death signals. *Burns*. https://doi.org/10.1016/j.burns.2020.03.011

Fitzgerald, D. J., Fusenig, N. E., Boukamp, P., Piccoli, C., Mesnil, M., & Yamasaki, H. (1994). Expression and function of connexin in normal and transformed human keratinocytes in culture. *Carcinogenesis*, *15*(9), 1859-1865. https://doi.org/10.1093/carcin/15.9.1859

Frantseva, M. V., Kokarovtseva, L., Naus, C. G., Carlen, P. L., MacFabe, D., & Perez Velazquez, J. L. (2002). Specific gap junctions enhance the neuronal vulnerability to brain traumatic injury. *J Neurosci*, *22*(3), 644-653. https://www.ncbi.nlm.nih.gov/pubmed/11826094

https://www.ncbi.nlm.nih.gov/pmc/articles/PMC6758478/pdf/ns0302000644.pdf

Frederick, R. E., Bearden, R., Jovanovic, A., Jacobson, N., Sood, R., & Dhall, S. (2021). Clostridium Collagenase Impact on Zone of Stasis Stabilization and Transition to Healthy Tissue in Burns. *Int J Mol Sci*, *22*(16). https://doi.org/10.3390/ijms22168643

Gabbiani, G. (2003). The myofibroblast in wound healing and fibrocontractive diseases. *J Pathol*, *200*(4), 500-503. https://doi.org/10.1002/path.1427

Garcia-Dorado, D., Rodriguez-Sinovas, A., & Ruiz-Meana, M. (2004). Gap junction-mediated spread of cell injury and death during myocardial ischemia-reperfusion. *Cardiovasc Res*, *61*(3), 386-401. https://doi.org/10.1016/j.cardiores.2003.11.039

Garcia, V. G., de Lima, M. A., Okamoto, T., Milanezi, L. A., Junior, E. C., Fernandes, L. A., de Almeida, J. M., & Theodoro, L. H. (2010). Effect of photodynamic therapy on the healing of cutaneous third-degree-burn: histological study in rats. *Lasers Med Sci*, *25*(2), 221-228. https://doi.org/10.1007/s10103-009-0694-z

Ghasemiyeh, P., & Mohammadi-Samani, S. (2019). Hydrogels as Drug Delivery Systems; Pros and Cons (Review Article). *5*, 7-24. https://doi.org/10.30476/tips.2019.81604.1002

Ghatnekar, G. S., O'Quinn, M. P., Jourdan, L. J., Gurjarpadhye, A. A., Draughn, R. L., & Gourdie, R. G. (2009). Connexin43 carboxyl-terminal peptides reduce scar progenitor and promote regenerative healing following skin wounding. *Regen Med*, *4*(2), 205-223. https://doi.org/10.2217/17460751.4.2.205

Gilmartin, D. J., Soon, A., Thrasivoulou, C., Phillips, A. R., Jayasinghe, S. N., & Becker, D. L. (2016). Sustained Release of Cx43 Antisense Oligodeoxynucleotides from Coated Collagen Scaffolds Promotes Wound Healing. *Adv Healthc Mater*, *5*(14), 1786-1799. https://doi.org/10.1002/adhm.201600175

Glass, B. J. (2014). *The role of connexins in tissue injury repair* UCL (University College London)].

Goadsby, P. J., Ferrari, M. D., Csanyi, A., Olesen, J., Mills, J. G., & Tonabersat, T. O. N. S. G. (2009). Randomized, double-blind, placebo-controlled, proof-of-concept study of the cortical spreading depression inhibiting agent tonabersat in migraine prophylaxis. *Cephalalgia*, *29*(7), 742-750. https://doi.org/10.1111/j.1468-2982.2008.01804.x

Golberg, A., Villiger, M., Khan, S., Quinn, K. P., Lo, W. C. Y., Bouma, B. E., Mihm, M. C., Jr., Austen, W. G., Jr., & Yarmush, M. L. (2016). Preventing Scars after Injury with Partial Irreversible Electroporation. *Journal of Investigative Dermatology*, *136*(11), 2297-2304. https://doi.org/10.1016/j.jid.2016.06.620

Goldberg, E. L., Asher, J. L., Molony, R. D., Shaw, A. C., Zeiss, C. J., Wang, C., Morozova-Roche, L. A., Herzog, R. I., Iwasaki, A., & Dixit, V. D. (2017). beta-Hydroxybutyrate Deactivates Neutrophil NLRP3 Inflammasome to Relieve Gout Flares. *Cell Rep*, *18*(9), 2077-2087. https://doi.org/10.1016/j.celrep.2017.02.004

Goliger, J. A., & Paul, D. L. (1994). Expression of gap junction proteins Cx26, Cx31.1, Cx37, and Cx43 in developing and mature rat epidermis. *Dev Dyn*, *200*(1), 1-13. https://doi.org/10.1002/aja.1002000102

Gombault, A., Baron, L., & Couillin, I. (2012). ATP release and purinergic signaling in NLRP3 inflammasome activation. *Front Immunol*, *3*, 414. https://doi.org/10.3389/fimmu.2012.00414

Goodenough, D. A., Goliger, J. A., & Paul, D. L. (1996). Connexins, connexons, and intercellular communication. *Annu Rev Biochem*, *65*, 475-502. https://doi.org/10.1146/annurev.bi.65.070196.002355

Gorman, P. J., Saggers, G., Ehrlich, P., Mackay, D. R., & Graham, W. P., 3rd. (1999). Effects of topical nitroglycerin and flurbiprofen in the rat comb burn model. *Ann Plast Surg*, *42*(5), 529-532. https://doi.org/10.1097/00000637-199905000-00011

Goto, M., Samonte, V., Ravindranath, T., Sayeed, M. M., & Gamelli, R. L. (2006). Burn injury exacerbates hemodynamic and metabolic responses in rats with polymicrobial sepsis. *J Burn Care Res*, *27*(1), 50-59. https://doi.org/10.1097/01.bcr.0000192568.77001.b1

Gravante, G., Delogu, D., Palmieri, M. B., Santeusanio, G., Montone, A., & Esposito, G. (2008). Inverse relationship between the apoptotic rate and the time elapsed from thermal injuries

in deep partial thickness burns. *Burns*, *34*(2), 228-233. https://doi.org/10.1016/j.burns.2007.03.014

Gravante, G., Palmieri, M. B., Esposito, G., Delogu, D., Santeusanio, G., Filingeri, V., & Montone, A. (2006). Apoptotic cells are present in ischemic zones of deep partial-thickness burns. *J Burn Care Res*, *27*(5), 688-693. https://doi.org/10.1097/01.BCR.0000238101.94950.EC

Gravante, G., Palmieri, M. B., Esposito, G., Delogu, D., Santeusanio, G., Filingeri, V., & Montone, A. (2007). Apoptotic death in deep partial thickness burns vs. normal skin of burned patients. *J Surg Res*, *141*(2), 141-145. https://doi.org/10.1016/j.jss.2006.07.031

Grek, C. L., Montgomery, J., Sharma, M., Ravi, A., Rajkumar, J. S., Moyer, K. E., Gourdie, R. G., & Ghatnekar, G. S. (2017). A Multicenter Randomized Controlled Trial Evaluating a Cx43-Mimetic Peptide in Cutaneous Scarring. *Journal of Investigative Dermatology*, *137*(3), 620-630. https://doi.org/10.1016/j.jid.2016.11.006

Grupcheva, C. N., Laux, W. T., Rupenthal, I. D., McGhee, J., McGhee, C. N., & Green, C. R. (2012). Improved corneal wound healing through modulation of gap junction communication using connexin43-specific antisense oligodeoxynucleotides. *Invest Ophthalmol Vis Sci*, *53*(3), 1130-1138. https://doi.org/10.1167/iovs.11-8711

Guo, H. F., Ali, R. M., Hamid, R. A., Zaini, A. A., & Khaza'ai, H. (2017). A new model for studying deep partial-thickness burns in rats. *Int J Burns Trauma*, *7*(6), 107-114. https://www.ncbi.nlm.nih.gov/pubmed/29119063

https://www.ncbi.nlm.nih.gov/pmc/articles/PMC5665842/pdf/ijbt0007-0107.pdf

Guo, S., & Dipietro, L. A. (2010). Factors affecting wound healing. *J Dent Res*, *89*(3), 219-229. https://doi.org/10.1177/0022034509359125

Guo, S. X., Jin, Y. Y., Fang, Q., You, C. G., Wang, X. G., Hu, X. L., & Han, C. M. (2015). Beneficial effects of hydrogen-rich saline on early burn-wound progression in rats. *PLoS One*, *10*(4), e0124897. https://doi.org/10.1371/journal.pone.0124897

Gurung, S., & Skalko-Basnet, N. (2009). Wound healing properties of Carica papaya latex: in vivo evaluation in mice burn model. *J Ethnopharmacol*, *121*(2), 338-341. https://doi.org/10.1016/j.jep.2008.10.030

Hakvoort, T. E., Altun, V., Ramrattan, R. S., van der Kwast, T. H., Benner, R., van Zuijlen, P. P., Vloemans, A. F., & Prens, E. P. (1999). Epidermal participation in post-burn hypertrophic scar development. *Virchows Arch*, *434*(3), 221-226. https://doi.org/10.1007/s004280050331

Hansbrough, J., Tenenhaus, M., Wikstrom, T., Braide, M., Rennekampff, O. H., Kiessig, V., & Bjursten, L. M. (1996). Effects of recombinant bactericidal/permeability-increasing protein (rBPI23) on neutrophil activity in burned rats. *J Trauma*, *40*(6), 886-892; discussion 892-883. https://doi.org/10.1097/00005373-199606000-00005

Hansbrough, J. F., Wikstrom, T., Braide, M., Tenenhaus, M., Rennekampff, O. H., Kiessig, V., & Bjursten, L. M. (1996). Neutrophil activation and tissue neutrophil sequestration in a rat model of thermal injury. *J Surg Res*, *61*(1), 17-22. https://doi.org/10.1006/jsre.1996.0074

Hassane, M., Demon, D., Soulard, D., Fontaine, J., Keller, L. E., Patin, E. C., Porte, R., Prinz, I., Ryffel, B., Kadioglu, A., Veening, J. W., Sirard, J. C., Faveeuw, C., Lamkanfi, M., Trottein, F., & Paget, C. (2017). Neutrophilic NLRP3 inflammasome-dependent IL-1beta secretion regulates the gammadeltaT17 cell response in respiratory bacterial infections. *Mucosal Immunol*, *10*(4), 1056-1068. https://doi.org/10.1038/mi.2016.113

Hastie, L. E., Patton, W. F., Hechtman, H. B., & Shepro, D. (1997). Filamin redistribution in an endothelial cell reoxygenation injury model. *Free Radic Biol Med*, *22*(6), 955-966. https://doi.org/10.1016/s0891-5849(96)00482-0

Hawat, G., Helie, P., & Baroudi, G. (2012). Single intravenous low-dose injections of connexin 43 mimetic peptides protect ischemic heart in vivo against myocardial infarction. *J Mol Cell Cardiol*, *53*(4), 559-566. https://doi.org/10.1016/j.yjmcc.2012.07.008

Hayati, F., Ghamsari, S. M., Dehghan, M. M., & Oryan, A. (2018). Effects of carbomer 940 hydrogel on burn wounds: an in vitro and in vivo study. *J Dermatolog Treat*, *29*(6), 593-599. https://doi.org/10.1080/09546634.2018.1426823

Hazrati, M., Mehrabani, D., Japoni, A., Montaseri, H., Azarpira, N., Hamidian-shirazi, A. R., & Tanideh, N. (2010). Effect of Honey on Healing of Pseudomonas aeruginosa Infected Burn Wounds in Rat. *Journal of Applied Animal Research*, *37*, 161-165. https://doi.org/10.1080/09712119.2010.9707117

Herdon, H. J., Jerman, J. C., Stean, T. O., Middlemiss, D. N., Chan, W. N., Vong, A. K., Evans, J. M., Thompson, M., & Upton, N. (1997). Characterization of the binding of [3H]-SB-204269, a radiolabelled form of the new anticonvulsant SB-204269, to a novel binding site in rat brain membranes. *Br J Pharmacol*, *121*(8), 1687-1691. https://doi.org/10.1038/sj.bjp.0701331

Hettiaratchy, S., & Dziewulski, P. (2004). ABC of burns: pathophysiology and types of burns. *BMJ*, *328*(7453), 1427-1429. https://doi.org/10.1136/bmj.328.7453.1427

Hinz, B. (2007). Formation and function of the myofibroblast during tissue repair. *Journal of Investigative Dermatology*, *127*(3), 526-537. https://doi.org/10.1038/sj.jid.5700613

Hoang Thi, T. T., Pilkington, E. H., Nguyen, D. H., Lee, J. S., Park, K. D., & Truong, N. P. (2020). The Importance of Poly(ethylene glycol) Alternatives for Overcoming PEG Immunogenicity in Drug Delivery and Bioconjugation. *Polymers (Basel)*, *12*(2). https://doi.org/10.3390/polym12020298

Hoorelbeke, D., Decrock, E., De Smet, M., De Bock, M., Descamps, B., Van Haver, V., Delvaeye, T., Krysko, D. V., Vanhove, C., Bultynck, G., & Leybaert, L. (2020). Cx43 channels and signaling via IP(3)/Ca(2+), ATP, and ROS/NO propagate radiation-induced DNA damage to non-irradiated brain microvascular endothelial cells. *Cell Death Dis*, *11*(3), 194. https://doi.org/10.1038/s41419-020-2392-5

Hossler, F. E. (2014). Skin. In *Ultrastructure atlas of human tissues*. Wiley-Blackwell. https://doi.org/https://doi.org/10.1002/9781118284551

Huang, Y., Mao, Z., Zhang, Z., Obata, F., Yang, X., Zhang, X., Huang, Y., Mitsui, T., Fan, J., Takeda, M., & Yao, J. (2019). Connexin43 Contributes to Inflammasome Activation and Lipopolysaccharide-Initiated Acute Renal Injury via Modulation of Intracellular Oxidative Status. *Antioxid Redox Signal*, *31*(16), 1194-1212. https://doi.org/10.1089/ars.2018.7636

Hwee, J., Song, C., Tan, K. C., Tan, B. K., & Chong, S. J. (2016). The trends of burns epidemiology in a tropical regional burns centre. *Burns*, *42*(3), 682-686. https://doi.org/10.1016/j.burns.2015.10.019

Inzaugarat, M. E., Johnson, C. D., Holtmann, T. M., McGeough, M. D., Trautwein, C., Papouchado, B. G., Schwabe, R., Hoffman, H. M., Wree, A., & Feldstein, A. E. (2019). NLR Family Pyrin Domain-Containing 3 Inflammasome Activation in Hepatic Stellate Cells Induces Liver Fibrosis in Mice. *Hepatology*, *69*(2), 845-859. https://doi.org/10.1002/hep.30252

Ippagunta, S. K., Gangwar, R., Finkelstein, D., Vogel, P., Pelletier, S., Gingras, S., Redecke, V., & Hacker, H. (2016). Keratinocytes contribute intrinsically to psoriasis upon loss of Tnip1 function. *Proc Natl Acad Sci U S A*, *113*(41), E6162-E6171. https://doi.org/10.1073/pnas.1606996113

Irmak, F., Kurt Yazar, S., Sirvan, S. S., Serin, M., Ozagari, A., & Karasoy Yesilada, A. (2018). Beneficial effects of Salvia miltiorrhiza in the healing of burn wounds: an experimental study in rats. *J Plast Surg Hand Surg*, *52*(4), 229-233. https://doi.org/10.1080/2000656X.2018.1461631

Isakson, B. E., Evans, W. H., & Boitano, S. (2001). Intercellular Ca2+ signaling in alveolar epithelial cells through gap junctions and by extracellular ATP. *Am J Physiol Lung Cell Mol Physiol*, *280*(2), L221-228. https://doi.org/10.1152/ajplung.2001.280.2.L221

Jackson, D. M. (1953). The diagnosis of the depth of burning. *Br J Surg*, *40*(164), 588-596. https://doi.org/10.1002/bjs.18004016413

Jeschke, M. G. (2016). Postburn Hypermetabolism: Past, Present, and Future. *J Burn Care Res*, *37*(2), 86-96. https://doi.org/10.1097/BCR.0000000000000265

Jeschke, M. G., van Baar, M. E., Choudhry, M. A., Chung, K. K., Gibran, N. S., & Logsetty, S. (2020). Burn injury. *Nat Rev Dis Primers*, *6*(1), 11. https://doi.org/10.1038/s41572-020-0145-5

Jiang, J., Hoagland, D., Palatinus, J. A., He, H., Iyyathurai, J., Jourdan, L. J., Bultynck, G., Wang, Z., Zhang, Z., Schey, K., Poelzing, S., McGowan, F. X., & Gourdie, R. G. (2019). Interaction of alpha Carboxyl Terminus 1 Peptide With the Connexin 43 Carboxyl Terminus Preserves Left Ventricular Function After Ischemia-Reperfusion Injury. *J Am Heart Assoc*, *8*(16), e012385. https://doi.org/10.1161/JAHA.119.012385

Jing, Y., Wu, F., Li, D., Yang, L., Li, Q., & Li, R. (2018). Metformin improves obesity-associated inflammation by altering macrophages polarization. *Mol Cell Endocrinol*, *461*, 256-264. https://doi.org/10.1016/j.mce.2017.09.025

Johnson, R. M., & Richard, R. (2003). Partial-thickness burns: identification and management. *Adv Skin Wound Care*, *16*(4), 178-187; quiz 188-179. https://doi.org/10.1097/00129334-200307000-00010

Junker, J. P., Kamel, R. A., Caterson, E. J., & Eriksson, E. (2013). Clinical Impact Upon Wound Healing and Inflammation in Moist, Wet, and Dry Environments. *Adv Wound Care (New Rochelle)*, *2*(7), 348-356. https://doi.org/10.1089/wound.2012.0412

Kakagia, D. D., & Karadimas, E. J. (2018). The Efficacy of Versajet Hydrosurgery System in Burn Surgery. A Systematic Review. *J Burn Care Res*, *39*(2), 188-200. https://doi.org/10.1097/BCR.0000000000000561

Kakugawa, T., Mukae, H., Hishikawa, Y., Ishii, H., Sakamoto, N., Ishimatsu, Y., Fujii, T., Koji, T., & Kohno, S. (2010). Localization of HSP47 mRNA in murine bleomycin-induced pulmonary fibrosis. *Virchows Arch*, *456*(3), 309-315. https://doi.org/10.1007/s00428-009-0876-x

Kameritsch, P., & Pogoda, K. (2020). The Role of Connexin 43 and Pannexin 1 During Acute Inflammation. *Front Physiol*, *11*, 594097. https://doi.org/10.3389/fphys.2020.594097

Kanapathy, M., Simpson, R., Madden, L., Thrasivoulou, C., Mosahebi, A., Becker, D. L., & Richards, T. (2018). Upregulation of epidermal gap junctional proteins in patients with venous disease. *Br J Surg*, *105*(1), 59-67. https://doi.org/10.1002/bjs.10653

Karim, A. S., Shaum, K., & Gibson, A. L. F. (2020). Indeterminate-Depth Burn Injury-Exploring the Uncertainty. *J Surg Res*, *245*, 183-197. https://doi.org/10.1016/j.jss.2019.07.063

Karmakar, M., Katsnelson, M. A., Dubyak, G. R., & Pearlman, E. (2016). Neutrophil P2X7 receptors mediate NLRP3 inflammasome-dependent IL-1beta secretion in response to ATP. *Nat Commun*, *7*, 10555. https://doi.org/10.1038/ncomms10555

Kelley, N., Jeltema, D., Duan, Y., & He, Y. (2019). The NLRP3 Inflammasome: An Overview of Mechanisms of Activation and Regulation. *Int J Mol Sci*, *20*(13). https://doi.org/10.3390/ijms20133328

Kheilnezhad, B., & Hadjizadeh, A. (2022). Ibuprofen-Loaded Electrospun PCL/PEG Nanofibrous Membranes for Preventing Postoperative Abdominal Adhesion. *ACS Appl Bio Mater*, *5*(4), 1766-1778. https://doi.org/10.1021/acsabm.2c00126

Kieken, F., Mutsaers, N., Dolmatova, E., Virgil, K., Wit, A. L., Kellezi, A., Hirst-Jensen, B. J., Duffy, H. S., & Sorgen, P. L. (2009). Structural and molecular mechanisms of gap junction remodeling in epicardial border zone myocytes following myocardial infarction. *Circ Res*, *104*(9), 1103-1112. https://doi.org/10.1161/CIRCRESAHA.108.190454

Kim, D. E., Phillips, T. M., Jeng, J. C., Rizzo, A. G., Roth, R. T., Stanford, J. L., Jablonski, K. A., & Jordan, M. H. (2001). Microvascular assessment of burn depth conversion during varying

resuscitation conditions. *J Burn Care Rehabil*, *22*(6), 406-416. https://doi.org/10.1097/00004630-200111000-00011

Kim, H., Shin, S., & Han, D. (2022). Review of History of Basic Principles of Burn Wound Management. *Medicina (Kaunas)*, *58*(3). https://doi.org/10.3390/medicina58030400

Kim, J., Yang, Y. L., Jeong, Y., & Jang, Y. S. (2020). Middle East Respiratory Syndrome-Coronavirus Infection into Established hDPP4-Transgenic Mice Accelerates Lung Damage Via Activation of the Pro-Inflammatory Response and Pulmonary Fibrosis. *J Microbiol Biotechnol*, *30*(3), 427-438. https://doi.org/10.4014/jmb.1910.10055

Kim, J. E., Lee, J., Jang, M., Kwak, M. H., Go, J., Kho, E. K., Song, S. H., Sung, J. E., Lee, J., & Hwang, D. Y. (2015). Accelerated healing of cutaneous wounds using phytochemically stabilized gold nanoparticle deposited hydrocolloid membranes. *Biomater Sci*, *3*(3), 509-519. https://doi.org/10.1039/c4bm00390j

Kim, J. Y., Dunham, D. M., Supp, D. M., Sen, C. K., & Powell, H. M. (2016). Novel burn device for rapid, reproducible burn wound generation. *Burns*, *42*(2), 384-391. https://doi.org/10.1016/j.burns.2015.08.027

Kim, Y., Davidson, J. O., Gunn, K. C., Phillips, A. R., Green, C. R., & Gunn, A. J. (2016). Role of Hemichannels in CNS Inflammation and the Inflammasome Pathway. *Adv Protein Chem Struct Biol*, *104*, 1-37. https://doi.org/10.1016/bs.apcsb.2015.12.001

Kim, Y., Griffin, J. M., Harris, P. W., Chan, S. H., Nicholson, L. F., Brimble, M. A., O'Carroll, S. J., & Green, C. R. (2017). Characterizing the mode of action of extracellular Connexin43 channel blocking mimetic peptides in an in vitro ischemia injury model. *Biochim Biophys Acta Gen Subj*, *1861*(2), 68-78. https://doi.org/10.1016/j.bbagen.2016.11.001

Kim, Y., Griffin, J. M., Nor, M. N. M., Zhang, J., Freestone, P. S., Danesh-Meyer, H. V., Rupenthal, I. D., Acosta, M., Nicholson, L. F. B., O'Carroll, S. J., & Green, C. R. (2017). Tonabersat Prevents Inflammatory Damage in the Central Nervous System by Blocking Connexin43 Hemichannels. *Neurotherapeutics*, *14*(4), 1148-1165. https://doi.org/10.1007/s13311-017-0536-9

King, D. R., Sedovy, M. W., Leng, X., Xue, J., Lamouille, S., Koval, M., Isakson, B. E., & Johnstone, S. R. (2021). Mechanisms of Connexin Regulating Peptides. *Int J Mol Sci*, *22*(19). https://doi.org/10.3390/ijms221910186

Kiong, K. L., Chong, S. J., & Tan, B. K. (2015). Biobrane for burns of the ear--a novel technique. *Burns*, *41*(2), 414. https://doi.org/10.1016/j.burns.2014.10.002

Kitamura, H., Yamamoto, S., Nakase, H., Matsuura, M., Honzawa, Y., Matsumura, K., Takeda, Y., Uza, N., Nagata, K., & Chiba, T. (2011). Role of heat shock protein 47 in intestinal fibrosis of experimental colitis. *Biochem Biophys Res Commun*, *404*(2), 599-604. https://doi.org/10.1016/j.bbrc.2010.12.006

Knuth, C. M., Auger, C., & Jeschke, M. G. (2021). Burn-induced hypermetabolism and skeletal muscle dysfunction. *Am J Physiol Cell Physiol*, *321*(1), C58-C71. https://doi.org/10.1152/ajpcell.00106.2021

Kobayashi, H., Ebisawa, K., Kambe, M., Kasai, T., Suga, H., Nakamura, K., Narita, Y., Ogata, A., & Kamei, Y. (2018). Effects of exosomes derived from the induced pluripotent stem cells on skin wound healing. *Nagoya J Med Sci*, *80*(2), 141-153. https://doi.org/10.18999/nagjms.80.2.141

Komalavilas, P., Luo, W., Guth, C. M., Jolayemi, O., Bartelson, R. I., Cheung-Flynn, J., & Brophy, C. M. (2017). Vascular surgical stretch injury leads to activation of P2X7 receptors and impaired endothelial function. *PLoS One*, *12*(11), e0188069. https://doi.org/10.1371/journal.pone.0188069

Kong, H., Zhao, H., Chen, T., Song, Y., & Cui, Y. (2022). Targeted P2X7/NLRP3 signaling pathway against inflammation, apoptosis, and pyroptosis of retinal endothelial cells in diabetic retinopathy. *Cell Death Dis*, *13*(4), 336. https://doi.org/10.1038/s41419-022-04786-w

Korkmaz, H. I., Ulrich, M. M. W., van Wieringen, W. N., Vlig, M., Emmens, R. W., Meyer, K. W., Sinnige, P., Krijnen, P. A. J., van Zuijlen, P. P. M., & Niessen, H. W. M. (2017). The Local and Systemic Inflammatory Response in a Pig Burn Wound Model With a Pivotal Role for Complement. *J Burn Care Res*, *38*(5), e796-e806. https://doi.org/10.1097/BCR.0000000000000486

Kulp, G. A., Tilton, R. G., Herndon, D. N., & Jeschke, M. G. (2012). Hyperglycemia exacerbates burn-induced liver inflammation via noncanonical nuclear factor-kappaB pathway activation. *Mol Med*, *18*(1), 948-956. https://doi.org/10.2119/molmed.2011.00357

Kuroda, K., & Tajima, S. (2004). HSP47 is a useful marker for skin fibroblasts in formalin-fixed, paraffin-embedded tissue specimens. *J Cutan Pathol*, *31*(3), 241-246. https://doi.org/10.1111/j.0303-6987.2003.00166.x

Kuroda, T., Harada, T., Tsutsumi, H., & Kobayashi, M. (1997). Hypernatremia deepens the demarcating borderline of leukocytic infiltration in the burn wound. *Burns*, *23*(5), 432-437. https://doi.org/10.1016/s0305-4179(97)00016-8

Kwak, M., Son, D., Kim, J., & Han, K. (2014). Static Langer's line and wound contraction rates according to anatomical regions in a porcine model. *Wound Repair Regen*, *22*(5), 678-682. https://doi.org/10.1111/wrr.12206

Kwek, M. S. Y., Thangaveloo, M., Hui, S. L. B., Madden, L. E., Phillips, A. R., & Becker, D. L. (2021). Characterisation of an ischemia reperfusion model for the formation of a stage I pressure ulcer in mouse skin. *J Tissue Viability*, *30*(3), 352-362. https://doi.org/10.1016/j.jtv.2021.03.004

Lagos-Cabre, R., Brenet, M., Diaz, J., Perez, R. D., Perez, L. A., Herrera-Molina, R., Quest, A. F. G., & Leyton, L. (2018). Intracellular Ca(2+) Increases and Connexin 43 Hemichannel Opening Are Necessary but Not Sufficient for Thy-1-Induced Astrocyte Migration. *Int J Mol Sci*, *19*(8). https://doi.org/10.3390/ijms19082179

Laird, D. W. (2006). Life cycle of connexins in health and disease. *Biochem J*, *394*(Pt 3), 527-543. https://doi.org/10.1042/BJ20051922

Laird, D. W., & Lampe, P. D. (2018). Therapeutic strategies targeting connexins. *Nat Rev Drug Discov*, *17*(12), 905-921. https://doi.org/10.1038/nrd.2018.138

Lan, Z., Kar, R., Chwatko, M., Shoga, E., & Cosgriff-Hernandez, E. (2023). High porosity PEG-based hydrogel foams with self-tuning moisture balance as chronic wound dressings. *J Biomed Mater Res A*, *111*(4), 465-477. https://doi.org/10.1002/jbm.a.37498

Laredj-Bourezg, F., Bolzinger, M. A., Pelletier, J., Valour, J. P., Rovere, M. R., Smatti, B., & Chevalier, Y. (2015). Skin delivery by block copolymer nanoparticles (block copolymer micelles). *Int J Pharm*, *496*(2), 1034-1046. https://doi.org/10.1016/j.ijpharm.2015.11.031

Latarjet, J. (1995). A simple guide to burn treatment. International Society for Burn Injuries in collaboration with the World Health Organization. *Burns*, *21*(3), 221-225. https://doi.org/10.1016/0305-4179(95)80015-g

Lateef, Z., Stuart, G., Jones, N., Mercer, A., Fleming, S., & Wise, L. (2019). The Cutaneous Inflammatory Response to Thermal Burn Injury in a Murine Model. *Int J Mol Sci*, *20*(3). https://doi.org/10.3390/ijms20030538

Law, L. Y., Zhang, W. V., Stott, N. S., Becker, D. L., & Green, C. R. (2006). In vitro optimization of antisense oligodeoxynucleotide design: an example using the connexin gene family. *J Biomol Tech*, *17*(4), 270-282. https://www.ncbi.nlm.nih.gov/pubmed/17028167

https://www.ncbi.nlm.nih.gov/pmc/articles/PMC2291797/pdf/0170270.pdf

Lebeaux, D., Chauhan, A., Rendueles, O., & Beloin, C. (2013). From in vitro to in vivo Models of Bacterial Biofilm-Related Infections. *Pathogens*, *2*(2), 288-356. https://doi.org/10.3390/pathogens2020288

Legemate, C. M., Goei, H., Middelkoop, E., Oen, I., Nijhuis, T. H. J., Kwa, K. A. A., van Zuijlen, P. P. M., Beerthuizen, G., Nieuwenhuis, M. K., van Baar, M. E., & van der Vlies, C. H. (2018). Long-term scar quality after hydrosurgical versus conventional debridement of deep dermal burns (HyCon trial): study protocol for a randomized controlled trial. *Trials*, *19*(1), 239. https://doi.org/10.1186/s13063-018-2599-2

Legemate, C. M., Kwa, K. A. A., Goei, H., Pijpe, A., Middelkoop, E., van Zuijlen, P. P. M., Beerthuizen, G., Nieuwenhuis, M. K., van Baar, M. E., van der Vlies, C. H., & HyCon Study, G. (2022). Hydrosurgical and conventional debridement of burns: randomized clinical trial. *Br J Surg*, *109*(4), 332-339. https://doi.org/10.1093/bjs/znab470

Leu, J. G., Chen, S. A., Chen, H. M., Wu, W. M., Hung, C. F., Yao, Y. D., Tu, C. S., & Liang, Y. J. (2012). The effects of gold nanoparticles in wound healing with antioxidant epigallocatechin gallate and alpha-lipoic acid. *Nanomedicine*, *8*(5), 767-775. https://doi.org/10.1016/j.nano.2011.08.013

Li, Q., Fukuda, K., Lu, Y., Nakamura, Y., Chikama, T., Kumagai, N., & Nishida, T. (2003). Enhancement by neutrophils of collagen degradation by corneal fibroblasts. *J Leukoc Biol*, *74*(3), 412-419. https://doi.org/10.1189/jlb.0801757

Li, X., Zhao, H., Tan, X., Kostrzewa, R. M., Du, G., Chen, Y., Zhu, J., Miao, Z., Yu, H., Kong, J., & Xu, X. (2015). Inhibition of connexin43 improves functional recovery after ischemic brain injury in neonatal rats. *Glia*, *63*(9), 1553-1567. https://doi.org/10.1002/glia.22826

Li, Z., Zhou, F., Li, Z., Lin, S., Chen, L., Liu, L., & Chen, Y. (2018). Hydrogel Cross-Linked with Dynamic Covalent Bonding and Micellization for Promoting Burn Wound Healing. *ACS Appl Mater Interfaces*, *10*(30), 25194-25202. https://doi.org/10.1021/acsami.8b08165

Lin, J. H., Weigel, H., Cotrina, M. L., Liu, S., Bueno, E., Hansen, A. J., Hansen, T. W., Goldman, S., & Nedergaard, M. (1998). Gap-junction-mediated propagation and amplification of cell injury. *Nat Neurosci*, *1*(6), 494-500. https://doi.org/10.1038/2210

Lindberg, M. R., & Lamps, L. W. (2018). Dermis. In M. R. Lindberg & L. W. Lamps (Eds.), *Diagnostic Pathology: Normal Histology (Second Edition)* (pp. 46-49). Elsevier. https://doi.org/https://doi.org/10.1016/B978-0-323-54803-8.50015-2

Lindblom, L., Cassuto, J., Yregard, L., Mattsson, U., Tarnow, P., & Sinclair, R. (2000). Role of nitric oxide in the control of burn perfusion. *Burns*, *26*(1), 19-23. https://doi.org/10.1016/s0305-4179(99)00106-0

Liu, W., Yang, D., Shi, J., Wen, P., Zhang, J., Wang, Z., Hu, B., Shi, X., Cao, S., Guo, W., & Zhang, S. (2021). Caspase-1 Inhibitor Reduces Pyroptosis Induced by Brain Death in Kidney. *Front Surg*, *8*, 760989. https://doi.org/10.3389/fsurg.2021.760989

Liu, Y., Zhou, S., Gao, Y., & Zhai, Y. (2019). Electrospun nanofibers as a wound dressing for treating diabetic foot ulcer. *Asian Journal of Pharmaceutical Sciences*, *14*(2), 130-143. https://doi.org/https://doi.org/10.1016/j.ajps.2018.04.004

Lohman, A. W., & Isakson, B. E. (2014). Differentiating connexin hemichannels and pannexin channels in cellular ATP release. *FEBS Lett*, *588*(8), 1379-1388. https://doi.org/10.1016/j.febslet.2014.02.004

Lopez, W., Ramachandran, J., Alsamarah, A., Luo, Y., Harris, A. L., & Contreras, J. E. (2016). Mechanism of gating by calcium in connexin hemichannels. *Proc Natl Acad Sci U S A*, *113*(49), E7986-E7995. https://doi.org/10.1073/pnas.1609378113

Louie, H. H., Shome, A., Kuo, C. Y., Rupenthal, I. D., Green, C. R., & Mugisho, O. O. (2021). Connexin43 hemichannel block inhibits NLRP3 inflammasome activation in a human retinal explant model of diabetic retinopathy. *Exp Eye Res*, *202*, 108384. https://doi.org/10.1016/j.exer.2020.108384

Lu, D., Soleymani, S., Madakshire, R., & Insel, P. A. (2012). ATP released from cardiac fibroblasts via connexin hemichannels activates profibrotic P2Y2 receptors. *FASEB J*, *26*(6), 2580-2591. https://doi.org/10.1096/fj.12-204677

Lucero, C. M., Andrade, D. C., Toledo, C., Diaz, H. S., Pereyra, K. V., Diaz-Jara, E., Schwarz, K. G., Marcus, N. J., Retamal, M. A., Quintanilla, R. A., & Del Rio, R. (2020). Cardiac remodeling and arrhythmogenesis are ameliorated by administration of Cx43 mimetic peptide Gap27 in heart failure rats. *Sci Rep*, *10*(1), 6878. https://doi.org/10.1038/s41598-020-63336-6

Luo, H., Liu, T., Yang, H., Ye, H., & Luo, X. (2020). Expression of Collagen (Types I, III, and V), HSP47, MMP-2, and TIMP-1 in Retrobulbar Adipose Tissue of Patients with Thyroid-Associated Orbitopathy. *J Ophthalmol*, *2020*, 4929634. https://doi.org/10.1155/2020/4929634

Luo, K., Wang, L., Chen, X., Zeng, X., Zhou, S., Zhang, P., & Li, J. (2020). Biomimetic Polyurethane 3D Scaffolds Based on Polytetrahydrofuran Glycol and Polyethylene Glycol for Soft Tissue Engineering. *Polymers (Basel)*, *12*(11). https://doi.org/10.3390/polym12112631

Lyon, H., Shome, A., Rupenthal, I. D., Green, C. R., & Mugisho, O. O. (2020). Tonabersat Inhibits Connexin43 Hemichannel Opening and Inflammasome Activation in an In Vitro Retinal Epithelial Cell Model of Diabetic Retinopathy. *Int J Mol Sci*, *22*(1). https://doi.org/10.3390/ijms22010298

Mahato, R. I., Cheng, K., & Guntaka, R. V. (2005). Modulation of gene expression by antisense and antigene oligodeoxynucleotides and small interfering RNA. *Expert Opin Drug Deliv*, *2*(1), 3-28. https://doi.org/10.1517/17425247.2.1.3

Mancuso, M., Pasquali, E., Leonardi, S., Rebessi, S., Tanori, M., Giardullo, P., Borra, F., Pazzaglia, S., Naus, C. C., Di Majo, V., & Saran, A. (2011). Role of connexin43 and ATP in long-range bystander radiation damage and oncogenesis in vivo. *Oncogene*, *30*(45), 4601-4608. https://doi.org/10.1038/onc.2011.176

Martin, P. E., & van Steensel, M. (2015). Connexins and skin disease: insights into the role of beta connexins in skin homeostasis. *Cell Tissue Res*, *360*(3), 645-658. https://doi.org/10.1007/s00441-014-2094-3

Mat Nor, M. N., Rupenthal, I. D., Green, C. R., & Acosta, M. L. (2020). Connexin Hemichannel Block Using Orally Delivered Tonabersat Improves Outcomes in Animal Models of Retinal Disease. *Neurotherapeutics*, *17*(1), 371-387. https://doi.org/10.1007/s13311-019-00786-5

McDouall, A., Zhou, K. Q., Bennet, L., Green, C. R., Gunn, A. J., & Davidson, J. O. (2022). Connexins, Pannexins and Gap Junctions in Perinatal Brain Injury. *Biomedicines*, *10*(6). https://doi.org/10.3390/biomedicines10061445

McKenzie, B. A., Dixit, V. M., & Power, C. (2020). Fiery Cell Death: Pyroptosis in the Central Nervous System. *Trends Neurosci*, *43*(1), 55-73. https://doi.org/10.1016/j.tins.2019.11.005

McNamara, A. R., Zamba, K. D., Sokolich, J. C., Jaskille, A. D., Light, T. D., Griffin, M. A., & Meyerholz, D. K. (2010). Apoptosis is Differentially Regulated by Burn Severity and Dermal Location. *Journal of Surgical Research*, *162*(2), 258-263. https://doi.org/https://doi.org/10.1016/j.jss.2009.01.038

Medina, J. L., Fourcaudot, A. B., Sebastian, E. A., Shankar, R., Brown, A. W., & Leung, K. P. (2018). Standardization of deep partial-thickness scald burns in C57BL/6 mice. *Int J Burns Trauma*, *8*(2), 26-33. https://www.ncbi.nlm.nih.gov/pubmed/29755839

https://www.ncbi.nlm.nih.gov/pmc/articles/PMC5943616/pdf/ijbt0008-0026.pdf

Menegat, T. A., Oliveira, A. F., Majewski, M. G. C., Blanes, L., Juliano, Y., Novo, N. F., & Ferreira, L. M. (2019). Experimental models of scald burns. A scope review. *Acta Cir Bras*, *34*(10), e201901007. https://doi.org/10.1590/s0102-865020190100000007

Menon, S., Chan, Q., Bertinetti, M., Harvey, J. G., Hei, E. R., & Holland, A. J. (2016). A novel device to create consistent deep dermal burns in a porcine model. *Int J Burns Trauma*, *6*(2), 26-29. https://www.ncbi.nlm.nih.gov/pubmed/27335694

Metcalfe, A. D., & Ferguson, M. W. (2007). Tissue engineering of replacement skin: the crossroads of biomaterials, wound healing, embryonic development, stem cells and regeneration. *J R Soc Interface*, *4*(14), 413-437. https://doi.org/10.1098/rsif.2006.0179

Meyer, W., Schwarz, R., & Neurand, K. (1978). The skin of domestic mammals as a model for the human skin, with special reference to the domestic pig. *Curr Probl Dermatol*, *7*, 39-52. https://doi.org/10.1159/000401274

Meyerholz, D. K., Piester, T. L., McNamara, A. R., Sokolich, J. C., Jaskille, A. D., Orion, K. C., Zamba, K. D., & Light, T. D. (2009). Pharmacologic modification to resuscitation fluid after thermal injury--is drotrecogin alfa the answer to arrest burn depth progression? *J Trauma*, *67*(5), 996-1003. https://doi.org/10.1097/TA.0b013e3181b83b3b

Meyerholz, D. K., Piester, T. L., Sokolich, J. C., Zamba, G. K., & Light, T. D. (2009). Morphological parameters for assessment of burn severity in an acute burn injury rat model. *Int J Exp Pathol*, *90*(1), 26-33. https://doi.org/10.1111/j.1365-2613.2008.00617.x

Mishima, Y., Miyazaki, M., Abe, K., Ozono, Y., Shioshita, K., Xia, Z., Harada, T., Taguchi, T., Koji, T., & Kohno, S. (2003). Enhanced expression of heat shock protein 47 in rat model of peritoneal fibrosis. *Perit Dial Int*, *23*(1), 14-22. https://www.ncbi.nlm.nih.gov/pubmed/12691502

Mitsunaga Junior, J. K., Gragnani, A., Ramos, M. L., & Ferreira, L. M. (2012). Rat an experimental model for burns: a systematic review. *Acta Cir Bras*, *27*(6), 417-423. https://doi.org/10.1590/s0102-86502012000600010

Mohammadi, Z., Sharif Zak, M., Majdi, H., Mostafavi, E., Barati, M., Lotfimehr, H., Ghaseminasab, K., Pazoki-Toroudi, H., Webster, T. J., & Akbarzadeh, A. (2019). The effect of chrysin-curcumin-loaded nanofibres on the wound-healing process in male rats. *Artif Cells Nanomed Biotechnol*, *47*(1), 1642-1652. https://doi.org/10.1080/21691401.2019.1594855

Mokos, Z. B., Jovic, A., Grgurevic, L., Dumic-Cule, I., Kostovic, K., Ceovic, R., & Marinovic, B. (2017). Current Therapeutic Approach to Hypertrophic Scars. *Front Med (Lausanne)*, *4*, 83. https://doi.org/10.3389/fmed.2017.00083

Monstrey, S., Hoeksema, H., Verbelen, J., Pirayesh, A., & Blondeel, P. (2008). Assessment of burn depth and burn wound healing potential. *Burns*, *34*(6), 761-769. https://doi.org/10.1016/j.burns.2008.01.009

Moore, K., Ghatnekar, G., Gourdie, R. G., & Potts, J. D. (2014). Impact of the controlled release of a connexin 43 peptide on corneal wound closure in an STZ model of type I diabetes. *PLoS One*, *9*(1), e86570. https://doi.org/10.1371/journal.pone.0086570

Morgun, E. I., & Vorotelyak, E. A. (2020). Epidermal Stem Cells in Hair Follicle Cycling and Skin Regeneration: A View From the Perspective of Inflammation. *Front Cell Dev Biol*, *8*, 581697. https://doi.org/10.3389/fcell.2020.581697

Mori, R., Power, K. T., Wang, C. M., Martin, P., & Becker, D. L. (2006). Acute downregulation of connexin43 at wound sites leads to a reduced inflammatory response, enhanced keratinocyte proliferation and wound fibroblast migration. *J Cell Sci*, *119*(Pt 24), 5193-5203. https://doi.org/10.1242/jcs.03320

Morisaki, N., Ohuchi, A., & Moriwaki, S. (2013). The role of neprilysin in regulating the hair cycle. *PLoS One*, *8*(2), e55947. https://doi.org/10.1371/journal.pone.0055947

Moritz, A. R., & Henriques, F. C. (1947). Studies of Thermal Injury: II. The Relative Importance of Time and Surface Temperature in the Causation of Cutaneous Burns. *Am J Pathol*, *23*(5), 695-720. https://www.ncbi.nlm.nih.gov/pubmed/19970955

Morry, J., Ngamcherdtrakul, W., Gu, S., Goodyear, S. M., Castro, D. J., Reda, M. M., Sangvanich, T., & Yantasee, W. (2015). Dermal delivery of HSP47 siRNA with NOX4-modulating mesoporous silica-based nanoparticles for treating fibrosis. *Biomaterials*, *66*, 41-52. https://doi.org/10.1016/j.biomaterials.2015.07.005

Mugisho, O. O., Green, C. R., Squirrell, D. M., Bould, S., Danesh-Meyer, H. V., Zhang, J., Acosta, M. L., & Rupenthal, I. D. (2019). Connexin43 hemichannel block protects against the development of diabetic retinopathy signs in a mouse model of the disease. *J Mol Med (Berl)*, *97*(2), 215-229. https://doi.org/10.1007/s00109-018-1727-5

Mugisho, O. O., Rupenthal, I. D., Paquet-Durand, F., Acosta, M. L., & Green, C. R. (2019). Targeting connexin hemichannels to control the inflammasome: the correlation between connexin43 and NLRP3 expression in chronic eye disease. *Expert Opin Ther Targets*, 1-9. https://doi.org/10.1080/14728222.2019.1673368

Myers, K. J., & Dean, N. M. (2000). Sensible use of antisense: how to use oligonucleotides as research tools. *Trends Pharmacol Sci*, *21*(1), 19-23. https://doi.org/10.1016/s0165-6147(99)01420-0

Nadworny, P. L., Wang, J., Tredget, E. E., & Burrell, R. E. (2008). Anti-inflammatory activity of nanocrystalline silver in a porcine contact dermatitis model. *Nanomedicine*, *4*(3), 241-251. https://doi.org/10.1016/j.nano.2008.04.006

Naitoh, M., Hosokawa, N., Kubota, H., Tanaka, T., Shirane, H., Sawada, M., Nishimura, Y., & Nagata, K. (2001). Upregulation of HSP47 and collagen type III in the dermal fibrotic disease, keloid. *Biochem Biophys Res Commun*, *280*(5), 1316-1322. https://doi.org/10.1006/bbrc.2001.4257

Nakase, T., Fushiki, S., & Naus, C. C. (2003). Astrocytic gap junctions composed of connexin 43 reduce apoptotic neuronal damage in cerebral ischemia. *Stroke*, *34*(8), 1987-1993. https://doi.org/10.1161/01.STR.0000079814.72027.34

National Library of Medicine, U. S. (2016, January 28 - 2020, May 27). *A Study of Granexin Gel in the Treatment of Diabetic Foot Ulcer. ClinicalTrials.gov Identifier: NCT02667327*. https://clinicaltrials.gov/ct2/show/study/NCT02667327

Negut, I., Dorcioman, G., & Grumezescu, V. (2020). Scaffolds for Wound Healing Applications. *Polymers (Basel)*, *12*(9). https://doi.org/10.3390/polym12092010

Neves, S. M., Nicolau, R. A., Filho, A. L., Mendes, L. M., & Veloso, A. M. (2014). Digital photogrammetry and histomorphometric assessment of the effect of non-coherent light (light-emitting diode) therapy (lambda640 +/- 20 nm) on the repair of third-degree burns in rats. *Lasers Med Sci*, *29*(1), 203-212. https://doi.org/10.1007/s10103-013-1312-7

Ngim, R. C., & Ghulam, A. K. (1994). Current logistics of acute burn care in Singapore. *Singapore Med J*, *35*(3), 257-262. https://www.ncbi.nlm.nih.gov/pubmed/7997898

Nielsen, M. S., Axelsen, L. N., Sorgen, P. L., Verma, V., Delmar, M., & Holstein-Rathlou, N. H. (2012). Gap junctions. *Compr Physiol*, *2*(3), 1981-2035. https://doi.org/10.1002/cphy.c110051

Noor, A., Afzal, A., Masood, R., Khaliq, Z., Ahmad, S., Ahmad, F., Qadir, M.-B., & Irfan, M. (2022). Dressings for burn wound: a review. *Journal of Materials Science*, *57*(12), 6536-6572. https://doi.org/10.1007/s10853-022-07056-4

O'Carroll, S. J., Alkadhi, M., Nicholson, L. F. B., & Green, C. R. (2008). Connexin43 Mimetic Peptides Reduce Swelling, Astrogliosis, and Neuronal Cell Death after Spinal Cord Injury. *Cell Communication & Adhesion*, *15*(1-2), 27-42. https://doi.org/10.1080/15419060802014164

O'Quinn, M. P., Palatinus, J. A., Harris, B. S., Hewett, K. W., & Gourdie, R. G. (2011). A peptide mimetic of the connexin43 carboxyl terminus reduces gap junction remodeling and induced arrhythmia following ventricular injury. *Circ Res*, *108*(6), 704-715. https://doi.org/10.1161/CIRCRESAHA.110.235747

Oka, T., Ohta, K., Kanazawa, T., & Nakamura, K.-I. (2016). Interaction between Macrophages and Fibroblasts during Wound Healing of Burn Injuries in Rats. *The Kurume Medical Journal*, *62*(3.4), 59-66. https://doi.org/10.2739/kurumemedj.MS00003

Oksuz, S., Ulkur, E., Oncul, O., Kose, G. T., Kucukodac, Z., & Urhan, M. (2013). The effect of subcutaneous mesenchymal stem cell injection on statis zone and apoptosis in an experimental burn model. *Plast Reconstr Surg*, *131*(3), 463-471. https://doi.org/10.1097/PRS.0b013e31827c6d6f

Ongstad, E. L., O'Quinn, M. P., Ghatnekar, G. S., Yost, M. J., & Gourdie, R. G. (2013). A Connexin43 Mimetic Peptide Promotes Regenerative Healing and Improves Mechanical Properties in Skin and Heart. *Adv Wound Care (New Rochelle)*, *2*(2), 55-62. https://doi.org/10.1089/wound.2011.0341

Orellana, J. A., Avendano, B. C., & Montero, T. D. (2014). Role of connexins and pannexins in ischemic stroke. *Curr Med Chem*, *21*(19), 2165-2182. https://doi.org/10.2174/09298673216661312281917l4

Osikov, M. V., Telesheva, L. F., & Likhacheva, A. G. (2014). Effect of local application of epidermal growth factor on innate immunity and cell composition of destruction focus in experimental thermal injury. *Bull Exp Biol Med*, *157*(3), 307-310. https://doi.org/10.1007/s10517-014-2552-7

Otsuka, M., Shiratori, M., Chiba, H., Kuronuma, K., Sato, Y., Niitsu, Y., & Takahashi, H. (2017). Treatment of pulmonary fibrosis with siRNA against a collagen-specific chaperone HSP47 in vitamin A-coupled liposomes. *Exp Lung Res*, *43*(6-7), 271-282. https://doi.org/10.1080/01902148.2017.1354946

Ousey, K., Cutting, K. F., Rogers, A. A., & Rippon, M. G. (2016). The importance of hydration in wound healing: reinvigorating the clinical perspective. *J Wound Care*, *25*(3), 122, 124-130. https://doi.org/10.12968/jowc.2016.25.3.122

Ozcan, C., Ergun, O., Celik, A., Corduk, N., & Ozok, G. (2002). Enzymatic debridement of burn wound with collagenase in children with partial-thickness burns. *Burns*, *28*(8), 791-794. https://doi.org/10.1016/s0305-4179(02)00191-2

Palackic, A., Jay, J. W., Duggan, R. P., Branski, L. K., Wolf, S. E., Ansari, N., & El Ayadi, A. (2022). Therapeutic Strategies to Reduce Burn Wound Conversion. *Medicina (Kaunas)*, *58*(7). https://doi.org/10.3390/medicina58070922

Pantalone, D., Bergamini, C., Martellucci, J., Alemanno, G., Bruscino, A., Maltinti, G., Sheiterle, M., Viligiardi, R., Panconesi, R., Guagni, T., & Prosperi, P. (2021). The Role of DAMPS in Burns and Hemorrhagic Shock Immune Response: Pathophysiology and Clinical Issues. Review. *Int J Mol Sci*, *22*(13). https://doi.org/10.3390/ijms22137020

Parihar, A., Parihar, M. S., Milner, S., & Bhat, S. (2008). Oxidative stress and anti-oxidative mobilization in burn injury. *Burns*, *34*(1), 6-17. https://doi.org/10.1016/j.burns.2007.04.009

Parsons, A. A., Bingham, S., Raval, P., Read, S., Thompson, M., & Upton, N. (2001). Tonabersat (SB-220453) a novel benzopyran with anticonvulsant properties attenuates trigeminal nerve-induced neurovascular reflexes. *Br J Pharmacol*, *132*(7), 1549-1557. https://doi.org/10.1038/sj.bjp.0703932

Paustian, P. W., McPherson, J. C., 3rd, Haase, R. R., Runner, R. R., Plowman, K. M., Ward, D. F., Nguyen, T. H., & McPherson, J. C., Jr. (1993). Intravenous Pluronic F-127 in early burn wound treatment in rats. *Burns*, *19*(3), 187-191. https://doi.org/10.1016/0305-4179(93)90146-y

Paw, M., Borek, I., Wnuk, D., Ryszawy, D., Piwowarczyk, K., Kmiotek, K., Wojcik-Pszczola, K. A., Pierzchalska, M., Madeja, Z., Sanak, M., Blyszczuk, P., Michalik, M., & Czyz, J. (2017). Connexin43 Controls the Myofibroblastic Differentiation of Bronchial Fibroblasts from Patients with Asthma. *Am J Respir Cell Mol Biol*, *57*(1), 100-110. https://doi.org/10.1165/rcmb.2015-0255OC

Pearson, R. A., Dale, N., Llaudet, E., & Mobbs, P. (2005). ATP released via gap junction hemichannels from the pigment epithelium regulates neural retinal progenitor proliferation. *Neuron*, *46*(5), 731-744. https://doi.org/10.1016/j.neuron.2005.04.024

Peinnequin, A., Mouret, C., Birot, O., Alonso, A., Mathieu, J., Clarencon, D., Agay, D., Chancerelle, Y., & Multon, E. (2004). Rat pro-inflammatory cytokine and cytokine related mRNA quantification by real-time polymerase chain reaction using SYBR green. *BMC Immunol*, *5*, 3. https://doi.org/10.1186/1471-2172-5-3

Pelegrin, P. (2021). P2X7 receptor and the NLRP3 inflammasome: Partners in crime. *Biochem Pharmacol*, *187*, 114385. https://doi.org/10.1016/j.bcp.2020.114385

Pessolato, A. G., Martins Ddos, S., Ambrosio, C. E., Mancanares, C. A., & de Carvalho, A. F. (2011). Propolis and amnion reepithelialise second-degree burns in rats. *Burns*, *37*(7), 1192-1201. https://doi.org/10.1016/j.burns.2011.05.016

Plikus, M. V., & Chuong, C. M. (2008). Complex hair cycle domain patterns and regenerative hair waves in living rodents. *Journal of Investigative Dermatology*, *128*(5), 1071-1080. https://doi.org/10.1038/sj.jid.5701180

Pober, J. S., & Sessa, W. C. (2014). Inflammation and the blood microvascular system. *Cold Spring Harb Perspect Biol*, *7*(1), a016345. https://doi.org/10.1101/cshperspect.a016345

Pollok, S., Pfeiffer, A. C., Lobmann, R., Wright, C. S., Moll, I., Martin, P. E., & Brandner, J. M. (2011). Connexin 43 mimetic peptide Gap27 reveals potential differences in the role of Cx43 in wound repair between diabetic and non-diabetic cells. *J Cell Mol Med*, *15*(4), 861-873. https://doi.org/10.1111/j.1582-4934.2010.01057.x

Poplimont, H., Georgantzoglou, A., Boulch, M., Walker, H. A., Coombs, C., Papaleonidopoulou, F., & Sarris, M. (2020). Neutrophil Swarming in Damaged Tissue Is Orchestrated by Connexins and Cooperative Calcium Alarm Signals. *Curr Biol*, *30*(14), 2761-2776 e2767. https://doi.org/10.1016/j.cub.2020.05.030

Poranki, D., Goodwin, C., & Van Dyke, M. (2016). Assessment of Deep Partial Thickness Burn Treatment with Keratin Biomaterial Hydrogels in a Swine Model. *Biomed Res Int*, *2016*, 1803912. https://doi.org/10.1155/2016/1803912

Prindeze, N. J., Hoffman, H. A., Ardanuy, J. G., Zhang, J., Carney, B. C., Moffatt, L. T., & Shupp, J. W. (2016). Active Dynamic Thermography is a Sensitive Method for Distinguishing Burn Wound Conversion. *Journal of Burn Care & Research*, *37*(6), e559-e568. https://doi.org/10.1097/BCR.0000000000000296

Prohaska, J., & Cook, C. (2022). Skin Grafting. In *StatPearls*. https://www.ncbi.nlm.nih.gov/pubmed/30422469

Qing, C., Xinyi, Z., Xuefei, Y., Xindong, X., & Jianhua, F. (2021). The Specific Connexin 43-Inhibiting Peptide Gap26 Improved Alveolar Development of Neonatal Rats With Hyperoxia Exposure. *Front Pharmacol*, *12*, 587267. https://doi.org/10.3389/fphar.2021.587267

Qing, L., Fu, J., Wu, P., Zhou, Z., Yu, F., & Tang, J. (2019). Metformin induces the M2 macrophage polarization to accelerate the wound healing via regulating AMPK/mTOR/NLRP3 inflammasome singling pathway. *Am J Transl Res*, *11*(2), 655-668. https://www.ncbi.nlm.nih.gov/pubmed/30899369

Qiu, C., Coutinho, P., Frank, S., Franke, S., Law, L. Y., Martin, P., Green, C. R., & Becker, D. L. (2003). Targeting connexin43 expression accelerates the rate of wound repair. *Curr Biol*, *13*(19), 1697-1703. https://doi.org/10.1016/j.cub.2003.09.007

Rae, L., Fidler, P., & Gibran, N. (2016). The Physiologic Basis of Burn Shock and the Need for Aggressive Fluid Resuscitation. *Crit Care Clin*, *32*(4), 491-505. https://doi.org/10.1016/j.ccc.2016.06.001

Rai, P., Mehrotra, S., Priya, S., Gnansounou, E., & Sharma, S. K. (2021). Recent advances in the sustainable design and applications of biodegradable polymers. *Bioresour Technol*, *325*, 124739. https://doi.org/10.1016/j.biortech.2021.124739

Ramadan, R., Vromans, E., Anang, D. C., Goetschalckx, I., Hoorelbeke, D., Decrock, E., Baatout, S., Leybaert, L., & Aerts, A. (2020). Connexin43 Hemichannel Targeting With TAT-Gap19 Alleviates Radiation-Induced Endothelial Cell Damage. *Front Pharmacol*, *11*, 212. https://doi.org/10.3389/fphar.2020.00212

Ramakrishnan, R., Chouhan, D., Vijayakumar Sreelatha, H., Arumugam, S., Mandal, B. B., & Krishnan, L. K. (2022). Silk Fibroin-Based Bioengineered Scaffold for Enabling Hemostasis and Skin Regeneration of Critical-Size Full-Thickness Heat-Induced Burn Wounds. *ACS Biomater Sci Eng*, *8*(9), 3856-3870. https://doi.org/10.1021/acsbiomaterials.2c00328

Rambhia, K. J., & Ma, P. X. (2015). Controlled drug release for tissue engineering. *J Control Release*, *219*, 119-128. https://doi.org/10.1016/j.jconrel.2015.08.049

Ramsey, M. L., Walker, B., & Patel, B. C. (2022). Full Thickness Skin Grafts. In *StatPearls*. https://www.ncbi.nlm.nih.gov/pubmed/30422470

Rapaport, F. T., Bachvaroff, R. J., Grullon, J., Kunz, H., & Gill, T. J., 3rd. (1982). Genetics of natural resistance to thermal injury. *Ann Surg*, *195*(3), 294-304. https://doi.org/10.1097/00000658-198203000-00009

Ray Jalian, H., Tam, J., Vuong, L. N., Fisher, J., Garibyan, L., Mihm, M. C., Zurakowski, D., Evans, C. L., & Rox Anderson, R. (2015). Selective Cryolysis of Sebaceous Glands. *Journal of Investigative Dermatology*, *135*(9), 2173-2180. https://doi.org/10.1038/jid.2015.148

Razzaque, M. S., Kumari, S., Foster, C. S., & Ahmed, A. R. (2003). Expression profiles of collagens, HSP47, TGF-beta1, MMPs and TIMPs in epidermolysis bullosa acquisita. *Cytokine*, *21*(5), 207-213. https://doi.org/10.1016/s1043-4666(03)00034-6

Reddy, A. S., Abraham, A., McClain, S. A., Clark, R. A., Ralen, P., Sandoval, S., & Singer, A. J. (2015). The Role of Necroptosis in Burn Injury Progression in a Rat Comb Burn Model.

Academic emergency medicine : official journal of the Society for Academic Emergency Medicine, *22*(10), 1181-1186. https://doi.org/10.1111/acem.12768

Retamal, M. A., Froger, N., Palacios-Prado, N., Ezan, P., Saez, P. J., Saez, J. C., & Giaume, C. (2007). Cx43 hemichannels and gap junction channels in astrocytes are regulated oppositely by proinflammatory cytokines released from activated microglia. *J Neurosci*, *27*(50), 13781-13792. https://doi.org/10.1523/JNEUROSCI.2042-07.2007

Richard, G. (2000). Connexins: a connection with the skin. *Exp Dermatol*, *9*(2), 77-96. https://doi.org/10.1034/j.1600-0625.2000.009002077.x

Rijken, F., & Bruijnzeel, P. L. (2009). The pathogenesis of photoaging: the role of neutrophils and neutrophil-derived enzymes. *J Investig Dermatol Symp Proc*, *14*(1), 67-72. https://doi.org/10.1038/jidsymp.2009.15

Rinaldi, C., & Wood, M. J. A. (2018). Antisense oligonucleotides: the next frontier for treatment of neurological disorders. *Nat Rev Neurol*, *14*(1), 9-21. https://doi.org/10.1038/nrneurol.2017.148

Riquelme, M. A., Kar, R., Gu, S., & Jiang, J. X. (2013). Antibodies targeting extracellular domain of connexins for studies of hemichannels. *Neuropharmacology*, *75*, 525-532. https://doi.org/10.1016/j.neuropharm.2013.02.021

Risek, B., Klier, F. G., & Gilula, N. B. (1992). Multiple gap junction genes are utilized during rat skin and hair development. *Development*, *116*(3), 639-651. https://www.ncbi.nlm.nih.gov/pubmed/1289057

https://dev.biologists.org/content/develop/116/3/639.full.pdf

Rock, K. L., & Kono, H. (2008). The inflammatory response to cell death. *Annu Rev Pathol*, *3*, 99-126. https://doi.org/10.1146/annurev.pathmechdis.3.121806.151456

Rodjakovic, D., Salm, L., & Beldi, G. (2021). Function of Connexin-43 in Macrophages. *Int J Mol Sci*, *22*(3). https://doi.org/10.3390/ijms22031412

Rodriguez-Sinovas, A., Cabestrero, A., Lopez, D., Torre, I., Morente, M., Abellan, A., Miro, E., Ruiz-Meana, M., & Garcia-Dorado, D. (2007). The modulatory effects of connexin 43 on cell death/survival beyond cell coupling. *Prog Biophys Mol Biol*, *94*(1-2), 219-232. https://doi.org/10.1016/j.pbiomolbio.2007.03.003

Roger, E., Boutin, L., & Chadjichristos, C. E. (2022). The Role of Connexin 43 in Renal Disease: Insights from In Vivo Models of Experimental Nephropathy. *Int J Mol Sci*, *23*(21). https://doi.org/10.3390/ijms232113090

Roy, S., Santra, S., Das, A., Dixith, S., Sinha, M., Ghatak, S., Ghosh, N., Banerjee, P., Khanna, S., Mathew-Steiner, S., Ghatak, P. D., Blackstone, B. N., Powell, H. M., Bergdall, V. K., Wozniak, D. J., & Sen, C. K. (2020). Staphylococcus aureus Biofilm Infection Compromises Wound Healing by Causing Deficiencies in Granulation Tissue Collagen. *Ann Surg*, *271*(6), 1174-1185. https://doi.org/10.1097/SLA.0000000000003053

Ruigrok, M. J. R., El Amasi, K. E. M., Leeming, D. J., Sand, J. M. B., Frijlink, H. W., Hinrichs, W. L. J., & Olinga, P. (2021). Silencing Heat Shock Protein 47 (HSP47) in Fibrogenic Precision-Cut Lung Slices: A Surprising Lack of Effects on Fibrogenesis? *Front Med (Lausanne)*, *8*, 607962. https://doi.org/10.3389/fmed.2021.607962

Saeidinia, A., Keihanian, F., Lashkari, A. P., Lahiji, H. G., Mobayyen, M., Heidarzade, A., & Golchai, J. (2017). Partial-thickness burn wounds healing by topical treatment: A randomized controlled comparison between silver sulfadiazine and centiderm. *Medicine (Baltimore)*, *96*(9), e6168. https://doi.org/10.1097/MD.0000000000006168

Sahu, G., Sukumaran, S., & Bera, A. K. (2014). Pannexins form gap junctions with electrophysiological and pharmacological properties distinct from connexins. *Sci Rep*, *4*, 4955. https://doi.org/10.1038/srep04955

Sahu, K., Kaurav, M., & Pandey, R. S. (2017). Protease loaded permeation enhancer liposomes for treatment of skin fibrosis arisen from second degree burn. *Biomed Pharmacother*, *94*, 747-757. https://doi.org/10.1016/j.biopha.2017.07.141

Saitoh, M., Oyamada, M., Oyamada, Y., Kaku, T., & Mori, M. (1997). Changes in the expression of gap junction proteins (connexins) in hamster tongue epithelium during wound healing and carcinogenesis. *Carcinogenesis*, *18*(7), 1319-1328. https://doi.org/10.1093/carcin/18.7.1319

Sakallioglu, A. E., Basaran, O., Ozdemir, B. H., Arat, Z., Yucel, M., & Haberal, M. (2006). Local and systemic interactions related to serum transforming growth factor-beta levels in burn wounds of various depths. *Burns*, *32*(8), 980-985. https://doi.org/10.1016/j.burns.2006.04.018

Sakamoto, M., Morimoto, N., Ogino, S., Jinno, C., Kawaguchi, A., Kawai, K., & Suzuki, S. (2016). Preparation of Partial-Thickness Burn Wounds in Rodents Using a New Experimental Burning Device. *Ann Plast Surg*, *76*(6), 652-658. https://doi.org/10.1097/sap.0000000000000655

Salgado, R. M., Alcantara, L., Mendoza-Rodriguez, C. A., Cerbon, M., Hidalgo-Gonzalez, C., Mercadillo, P., Moreno, L. M., Alvarez-Jimenez, R., & Krotzsch, E. (2012). Post-burn hypertrophic scars are characterized by high levels of IL-1beta mRNA and protein and TNF-alpha type I receptors. *Burns*, *38*(5), 668-676. https://doi.org/10.1016/j.burns.2011.12.012

Sarieddine, M. Z., Scheckenbach, K. E., Foglia, B., Maass, K., Garcia, I., Kwak, B. R., & Chanson, M. (2009). Connexin43 modulates neutrophil recruitment to the lung. *J Cell Mol Med*, *13*(11-12), 4560-4570. https://doi.org/10.1111/j.1582-4934.2008.00654.x

Sarrouilhe, D., Dejean, C., & Mesnil, M. (2014). Involvement of gap junction channels in the pathophysiology of migraine with aura. *Front Physiol*, *5*, 78. https://doi.org/10.3389/fphys.2014.00078

Sayan, M., & Mossman, B. T. (2016). The NLRP3 inflammasome in pathogenic particle and fibre-associated lung inflammation and diseases. *Part Fibre Toxicol*, *13*(1), 51. https://doi.org/10.1186/s12989-016-0162-4

Schaefer, T. J., & Nunez Lopez, O. (2023). Burn Resuscitation and Management. In *StatPearls*. https://www.ncbi.nlm.nih.gov/pubmed/28613546

Schneider, M. R., & Wolf, E. (2016). Genetically engineered pigs as investigative and translational models in dermatology. *British Journal of Dermatology*, *174*(1), 237-239. https://doi.org/10.1111/bjd.14092

Schulz, R., Boengler, K., Totzeck, A., Luo, Y., Garcia-Dorado, D., & Heusch, G. (2007). Connexin 43 in ischemic pre- and postconditioning. *Heart Fail Rev*, *12*(3-4), 261-266. https://doi.org/10.1007/s10741-007-9032-3

Schulz, R., Görge, P. M., Görbe, A., Ferdinandy, P., Lampe, P. D., & Leybaert, L. (2015). Connexin 43 is an emerging therapeutic target in ischemia/reperfusion injury, cardioprotection and neuroprotection. *Pharmacology & Therapeutics*, *153*, 90-106. https://doi.org/https://doi.org/10.1016/j.pharmthera.2015.06.005

Schulz, R., Gres, P., Skyschally, A., Duschin, A., Belosjorow, S., Konietzka, I., & Heusch, G. (2003). Ischemic preconditioning preserves connexin 43 phosphorylation during sustained ischemia in pig hearts in vivo. *FASEB J*, *17*(10), 1355-1357. https://doi.org/10.1096/fj.02-0975fje

Scott, C. A., & Kelsell, D. P. (2011). Key functions for gap junctions in skin and hearing. *Biochem J*, *438*(2), 245-254. https://doi.org/10.1042/BJ20110278

Scott, C. A., Tattersall, D., O'Toole, E. A., & Kelsell, D. P. (2012). Connexins in epidermal homeostasis and skin disease. *Biochim Biophys Acta*, *1818*(8), 1952-1961. https://doi.org/10.1016/j.bbamem.2011.09.004

Seaton, M., Hocking, A., & Gibran, N. S. (2015). Porcine models of cutaneous wound healing. *ILAR J*, *56*(1), 127-138. https://doi.org/10.1093/ilar/ilv016

Shakespeare, P. (2001). Burn wound healing and skin substitutes. *Burns*, *27*(5), 517-522. https://www.ncbi.nlm.nih.gov/pubmed/11451610

Sharma, K. S., Ralston, D., Giblin, V., & MacNeil, S. (2019). Engineering of Accepted Skin-Equivalent Tissue for Tissue Repair: Current State and Perspectives. In R. L. Reis (Ed.), *Encyclopedia of Tissue Engineering and Regenerative Medicine* (pp. 285-298). Academic Press. https://doi.org/https://doi.org/10.1016/B978-0-12-801238-3.65568-X

Shimizu, H., Sakimoto, T., & Yamagami, S. (2019). Pro-inflammatory role of NLRP3 inflammasome in experimental sterile corneal inflammation. *Sci Rep*, *9*(1), 9596. https://doi.org/10.1038/s41598-019-46116-9

Shin, Y. C., Shin, D. M., Lee, E. J., Lee, J. H., Kim, J. E., Song, S. H., Hwang, D. Y., Lee, J. J., Kim, B., Lim, D., Hyon, S. H., Lim, Y. J., & Han, D. W. (2016). Hyaluronic Acid/PLGA Core/Shell Fiber Matrices Loaded with EGCG Beneficial to Diabetic Wound Healing. *Adv Healthc Mater*, *5*(23), 3035-3045. https://doi.org/10.1002/adhm.201600658

Shpichka, A., Butnaru, D., Bezrukov, E. A., Sukhanov, R. B., Atala, A., Burdukovskii, V., Zhang, Y., & Timashev, P. (2019). Skin tissue regeneration for burn injury. *Stem Cell Res Ther*, *10*(1), 94. https://doi.org/10.1186/s13287-019-1203-3

Shupp, J. W., Nasabzadeh, T. J., Rosenthal, D. S., Jordan, M. H., Fidler, P., & Jeng, J. C. (2010). A review of the local pathophysiologic bases of burn wound progression. *J Burn Care Res*, *31*(6), 849-873. https://doi.org/10.1097/BCR.0b013e3181f93571

Sierawska, O., Malkowska, P., Taskin, C., Hrynkiewicz, R., Mertowska, P., Grywalska, E., Korzeniowski, T., Torres, K., Surowiecka, A., Niedzwiedzka-Rystwej, P., & Struzyna, J. (2022). Innate Immune System Response to Burn Damage-Focus on Cytokine Alteration. *Int J Mol Sci*, *23*(2). https://doi.org/10.3390/ijms23020716

Silberstein, S. D. (2009). Tonabersat, a novel gap-junction modulator for the prevention of migraine. *Cephalalgia*, *29 Suppl 2*, 28-35. https://doi.org/10.1111/j.1468-2982.2009.01973.x

Siller-Jackson, A. J., Burra, S., Gu, S., Xia, X., Bonewald, L. F., Sprague, E., & Jiang, J. X. (2008). Adaptation of connexin 43-hemichannel prostaglandin release to mechanical loading. *J Biol Chem*, *283*(39), 26374-26382. https://doi.org/10.1074/jbc.M803136200

Singer, A. J., McClain, S. A., Taira, B. R., Guerriero, J. L., & Zong, W. (2008). Apoptosis and necrosis in the ischemic zone adjacent to third degree burns. *Academic emergency medicine : official journal of the Society for Academic Emergency Medicine*, *15*(6), 549-554. https://doi.org/10.1111/j.1553-2712.2008.00115.x

Singer, A. J., Taira, B. R., Anderson, R., McClain, S. A., & Rosenberg, L. (2011). Reepithelialization of mid-dermal porcine burns after rapid enzymatic debridement with Debrase(R). *J Burn Care Res*, *32*(6), 647-653. https://doi.org/10.1097/BCR.0b013e31822dc467

Singer, A. J., Zhou, J. W., Osman, O. B., Harris, Z. B., Khani, M. E., Baer, E., Zhang, N., McClain, S. A., & Arbab, M. H. (2020). Comparison of comparable scald and contact burns in a porcine model: A preliminary report. *Wound Repair Regen*, *28*(6), 789-796. https://doi.org/10.1111/wrr.12848

Singer, D. D., Singer, A. J., Gordon, C., & Brink, P. (2013). The effects of rat mesenchymal stem cells on injury progression in a rat model. *Academic emergency medicine : official journal of the Society for Academic Emergency Medicine*, *20*(4), 398-402. https://doi.org/10.1111/acem.12116

Singh, M., Nuutila, K., Minasian, R., Kruse, C., & Eriksson, E. (2016). Development of a precise experimental burn model. *Burns*, *42*(7), 1507-1512. https://doi.org/10.1016/j.burns.2016.02.019

Singh, V., Devgan, L., Bhat, S., & Milner, S. M. (2007). The pathogenesis of burn wound conversion. *Ann Plast Surg*, *59*(1), 109-115. https://doi.org/10.1097/01.sap.0000252065.90759.e6

Song, S., Qiu, D., Luo, F., Wei, J., Wu, M., Wu, H., Du, C., Du, Y., Ren, Y., Chen, N., Duan, H., & Shi, Y. (2018). Knockdown of NLRP3 alleviates high glucose or TGFB1-induced EMT in human renal tubular cells. *J Mol Endocrinol*, *61*(3), 101-113. https://doi.org/10.1530/JME-18-0069

Spray, D. C., Hanstein, R., Lopez-Quintero, S. V., Stout, R. F., Jr., Suadicani, S. O., & Thi, M. M. (2013). Gap junctions and Bystander Effects: Good Samaritans and executioners. *Wiley Interdiscip Rev Membr Transp Signal*, *2*(1), 1-15. https://doi.org/10.1002/wmts.72

Srinivas, S. M., de Boer, J. F., Park, H., Keikhanzadeh, K., Huang, H. E., Zhang, J., Jung, W. Q., Chen, Z., & Nelson, J. S. (2004). Determination of burn depth by polarization-sensitive optical coherence tomography. *J Biomed Opt*, *9*(1), 207-212. https://doi.org/10.1117/1.1629680

Stackowicz, J., Gaudenzio, N., Serhan, N., Conde, E., Godon, O., Marichal, T., Starkl, P., Balbino, B., Roers, A., Bruhns, P., Jonsson, F., Moguelet, P., Georgin-Lavialle, S., Broderick, L., Hoffman, H. M., Galli, S. J., & Reber, L. L. (2021). Neutrophil-specific gain-of-function mutations in Nlrp3 promote development of cryopyrin-associated periodic syndrome. *J Exp Med*, *218*(10). https://doi.org/10.1084/jem.20201466

Stanojcic, M., Chen, P., Harrison, R. A., Wang, V., Antonyshyn, J., Zuniga-Pflucker, J. C., & Jeschke, M. G. (2014). Leukocyte infiltration and activation of the NLRP3 inflammasome in white adipose tissue following thermal injury. *Crit Care Med*, *42*(6), 1357-1364. https://doi.org/10.1097/CCM.0000000000000209

Steffens, D., Leonardi, D., Soster, P. R., Lersch, M., Rosa, A., Crestani, T., Scher, C., de Morais, M. G., Costa, J. A., & Pranke, P. (2014). Development of a new nanofiber scaffold for use with stem cells in a third degree burn animal model. *Burns*, *40*(8), 1650-1660. https://doi.org/10.1016/j.burns.2014.03.008

Stirm, M., Fonteyne, L. M., Shashikadze, B., Lindner, M., Chirivi, M., Lange, A., Kaufhold, C., Mayer, C., Medugorac, I., Kessler, B., Kurome, M., Zakhartchenko, V., Hinrichs, A., Kemter, E., Krause, S., Wanke, R., Arnold, G. J., Wess, G., Nagashima, H., . . . Wolf, E. (2021). A scalable, clinically severe pig model for Duchenne muscular dystrophy. *Dis Model Mech*, *14*(12). https://doi.org/10.1242/dmm.049285

Stoica, A. E., Chircov, C., & Grumezescu, A. M. (2020). Hydrogel Dressings for the Treatment of Burn Wounds: An Up-To-Date Overview. *Materials (Basel)*, *13*(12). https://doi.org/10.3390/ma13122853

Strudwick, X. L., & Cowin, A. J. (2017). The Role of the Inflammatory Response in Burn Injury. In *Hot Topics in Burn Injuries* (pp. 37-57). IntechOpen: London. https://doi.org/DOI: 10.5772/intechopen.71330

Suadicani, S. O., De Pina-Benabou, M. H., Urban-Maldonado, M., Spray, D. C., & Scemes, E. (2003). Acute downregulation of Cx43 alters P2Y receptor expression levels in mouse spinal cord astrocytes. *Glia*, *42*(2), 160-171. https://doi.org/10.1002/glia.10197

Sullivan, T. P., Eaglstein, W. H., Davis, S. C., & Mertz, P. (2001). The pig as a model for human wound healing. *Wound Repair Regen*, *9*(2), 66-76. https://doi.org/10.1046/j.1524-475x.2001.00066.x

Summer, G. J., Romero-Sandoval, E. A., Bogen, O., Dina, O. A., Khasar, S. G., & Levine, J. D. (2008). Proinflammatory cytokines mediating burn-injury pain. *Pain*, *135*(1-2), 98-107. https://doi.org/10.1016/j.pain.2007.05.012

Sun, G., Zhang, X., Shen, Y. I., Sebastian, R., Dickinson, L. E., Fox-Talbot, K., Reinblatt, M., Steenbergen, C., Harmon, J. W., & Gerecht, S. (2011). Dextran hydrogel scaffolds enhance angiogenic responses and promote complete skin regeneration during burn wound healing. *Proc Natl Acad Sci U S A*, *108*(52), 20976-20981. https://doi.org/10.1073/pnas.1115973108

Sutcliffe, J. E., Chin, K. Y., Thrasivoulou, C., Serena, T. E., O'Neil, S., Hu, R., White, A. M., Madden, L., Richards, T., Phillips, A. R., & Becker, D. L. (2015). Abnormal connexin expression in human chronic wounds. *Br J Dermatol*, *173*(5), 1205-1215. https://doi.org/10.1111/bjd.14064

Taidi, Z., Mansfield, K. J., Sana-Ur-Rehman, H., Moore, K. H., & Liu, L. (2022). Protective Effect of Purinergic P2X7 Receptor Inhibition on Acrolein-Induced Urothelial Cell Damage. *Front Physiol*, *13*, 885545. https://doi.org/10.3389/fphys.2022.885545

Tao, Y., Wang, N., Qiu, T., & Sun, X. (2020). The Role of Autophagy and NLRP3 Inflammasome in Liver Fibrosis. *Biomed Res Int*, *2020*, 7269150. https://doi.org/10.1155/2020/7269150

Tarzemany, R., Jiang, G., Jiang, J. X., Larjava, H., & Hakkinen, L. (2017). Connexin 43 Hemichannels Regulate the Expression of Wound Healing-Associated Genes in Human Gingival Fibroblasts. *Sci Rep*, *7*(1), 14157. https://doi.org/10.1038/s41598-017-12672-1

Tarzemany, R., Jiang, G., Larjava, H., & Hakkinen, L. (2015). Expression and function of connexin 43 in human gingival wound healing and fibroblasts. *PLoS One*, *10*(1), e0115524. https://doi.org/10.1371/journal.pone.0115524

Tavares Pereira Ddos, S., Lima-Ribeiro, M. H., de Pontes-Filho, N. T., Carneiro-Leao, A. M., & Correia, M. T. (2012). Development of animal model for studying deep second-degree thermal burns. *J Biomed Biotechnol*, *2012*, 460841. https://doi.org/10.1155/2012/460841

Tenenhaus, M., Bhavsar, D., & Rennekampff, H. O. (2007). Treatment of deep partial thickness and indeterminate depth facial burn wounds with water-jet debridement and a biosynthetic dressing. *Injury*, *38 Suppl 5*, S39-45. https://doi.org/10.1016/j.injury.2007.10.039

Tewari, P., Kealey, C. P., Bennett, D. B., Bajwa, N., Barnett, K. S., Singh, R. S., Culjat, M. O., Stojadinovic, A., Grundfest, W. S., & Taylor, Z. D. (2012). In vivo terahertz imaging of rat skin burns. *J Biomed Opt*, *17*(4), 040503. https://doi.org/10.1117/1.JBO.17.4.040503

Tohno, M., Shimosato, T., Aso, H., & Kitazawa, H. (2011). Immunobiotic Lactobacillus strains augment NLRP3 expression in newborn and adult porcine gut-associated lymphoid tissues. *Vet Immunol Immunopathol*, *144*(3-4), 410-416. https://doi.org/10.1016/j.vetimm.2011.09.010

Tohno, M., Shinkai, H., Toki, D., Okumura, N., Tajima, K., & Uenishi, H. (2016). Identification of the Q969R gain-of-function polymorphism in the gene encoding porcine NLRP3 and its distribution in pigs of Asian and European origin. *Immunogenetics*, *68*(9), 693-701. https://doi.org/10.1007/s00251-016-0917-y

Tomasek, J. J., Gabbiani, G., Hinz, B., Chaponnier, C., & Brown, R. A. (2002). Myofibroblasts and mechano-regulation of connective tissue remodelling. *Nat Rev Mol Cell Biol*, *3*(5), 349-363. https://doi.org/10.1038/nrm809

Tonkin, R. S., Bowles, C., Perera, C. J., Keating, B. A., Makker, P. G. S., Duffy, S. S., Lees, J. G., Tran, C., Don, A. S., Fath, T., Liu, L., O'Carroll, S. J., Nicholson, L. F. B., Green, C. R., Gorrie, C., & Moalem-Taylor, G. (2018). Attenuation of mechanical pain hypersensitivity by treatment with Peptide5, a connexin-43 mimetic peptide, involves inhibition of NLRP3 inflammasome in nerve-injured mice. *Exp Neurol*, *300*, 1-12. https://doi.org/10.1016/j.expneurol.2017.10.016

Tracy, L. M., Singer, Y., Schrale, R., Gong, J., Darton, A., Wood, F., Kurmis, R., Edgar, D., Cleland, H., & Gabbe, B. J. (2020). Epidemiology of burn injury in older adults: An Australian and New Zealand perspective. *Scars Burn Heal*, *6*, 2059513120952336. https://doi.org/10.1177/2059513120952336

Tredget, E. E., Levi, B., & Donelan, M. B. (2014). Biology and principles of scar management and burn reconstruction. *Surg Clin North Am*, *94*(4), 793-815. https://doi.org/10.1016/j.suc.2014.05.005

Trufant, J. W., Marzolf, S., Leach, B. C., & Cook, J. (2016). The utility of full-thickness skin grafts (FTSGs) for auricular reconstruction. *J Am Acad Dermatol*, *75*(1), 169-176. https://doi.org/10.1016/j.jaad.2016.01.028

Upadhyay, N. K., Kumar, R., Mandotra, S. K., Meena, R. N., Siddiqui, M. S., Sawhney, R. C., & Gupta, A. (2009). Safety and healing efficacy of Sea buckthorn (Hippophae rhamnoides L.) seed oil on burn wounds in rats. *Food Chem Toxicol*, *47*(6), 1146-1153. https://doi.org/10.1016/j.fct.2009.02.002

Upton, N., Blackburn, T. P., Campbell, C. A., Cooper, D., Evans, M. L., Herdon, H. J., King, P. D., Ray, A. M., Stean, T. O., Chan, W. N., Evans, J. M., & Thompson, M. (1997). Profile of SB-204269, a mechanistically novel anticonvulsant drug, in rat models of focal and generalized epileptic seizures. *Br J Pharmacol*, *121*(8), 1679-1686. https://doi.org/10.1038/sj.bjp.0701330

Valiunas, V., Polosina, Y. Y., Miller, H., Potapova, I. A., Valiuniene, L., Doronin, S., Mathias, R. T., Robinson, R. B., Rosen, M. R., Cohen, I. S., & Brink, P. R. (2005). Connexin-specific cell-to-cell transfer of short interfering RNA by gap junctions. *J Physiol*, *568*(Pt 2), 459-468. https://doi.org/10.1113/jphysiol.2005.090985

van Hout, G. P., Bosch, L., Ellenbroek, G. H., de Haan, J. J., van Solinge, W. W., Cooper, M. A., Arslan, F., de Jager, S. C., Robertson, A. A., Pasterkamp, G., & Hoefer, I. E. (2017). The selective NLRP3-inflammasome inhibitor MCC950 reduces infarct size and preserves

cardiac function in a pig model of myocardial infarction. *Eur Heart J*, *38*(11), 828-836. https://doi.org/10.1093/eurheartj/ehw247

Vaughn, L., & Beckel, N. (2012). Severe burn injury, burn shock, and smoke inhalation injury in small animals. Part 1: burn classification and pathophysiology. *J Vet Emerg Crit Care (San Antonio)*, *22*(2), 179-186. https://doi.org/10.1111/j.1476-4431.2012.00727.x

Vazquez-Cuevas, F. G., Juarez, B., Garay, E., & Arellano, R. O. (2006). ATP-induced apoptotic cell death in porcine ovarian theca cells through P2X7 receptor activation. *Mol Reprod Dev*, *73*(6), 745-755. https://doi.org/10.1002/mrd.20447

Velasco, M. A., Narvaez-Tovar, C. A., & Garzon-Alvarado, D. A. (2015). Design, materials, and mechanobiology of biodegradable scaffolds for bone tissue engineering. *Biomed Res Int*, *2015*, 729076. https://doi.org/10.1155/2015/729076

Vinaik, R., Abdullahi, A., Barayan, D., & Jeschke, M. G. (2020). NLRP3 inflammasome activity is required for wound healing after burns. *Transl Res*, *217*, 47-60. https://doi.org/10.1016/j.trsl.2019.11.002

Vinaik, R., Stanojcic, M., & Jeschke, M. G. (2018). NLRP3 Inflammasome Modulates Post-Burn Lipolysis and Hepatic Fat Infiltration via Fatty Acid Synthase. *Sci Rep*, *8*(1), 15197. https://doi.org/10.1038/s41598-018-33486-9

Vinken, M. (2015). Introduction: connexins, pannexins and their channels as gatekeepers of organ physiology. *Cellular and molecular life sciences : CMLS*, *72*(15), 2775-2778. https://doi.org/10.1007/s00018-015-1958-3

Vinken, M., Vanhaecke, T., Papeleu, P., Snykers, S., Henkens, T., & Rogiers, V. (2006). Connexins and their channels in cell growth and cell death. *Cell Signal*, *18*(5), 592-600. https://doi.org/10.1016/j.cellsig.2005.08.012

Walker, H. L., & Mason, A. D., Jr. (1968). A standard animal burn. *J Trauma*, *8*(6), 1049-1051. https://doi.org/10.1097/00005373-196811000-00006

Wan, L., Jiang, D., Correa-Gallegos, D., Ramesh, P., Zhao, J., Ye, H., Zhu, S., Wannemacher, J., Volz, T., & Rinkevich, Y. (2021). Connexin43 gap junction drives fascia mobilization and repair of deep skin wounds. *Matrix Biol*, *97*, 58-71. https://doi.org/10.1016/j.matbio.2021.01.005

Wang, A., Zheng, N., Jia, Q., Chen, Y., & Xu, S. (2022). S100A9-containing serum exosomes obtained from patients with burn injuries promote myocardial cell pyroptosis through NLRP3. *Exp Ther Med*, *24*(5), 646. https://doi.org/10.3892/etm.2022.11583

Wang, D., Wang, H., Gao, H., Zhang, H., Zhang, H., Wang, Q., & Sun, Z. (2020). P2X7 receptor mediates NLRP3 inflammasome activation in depression and diabetes. *Cell Biosci*, *10*, 28. https://doi.org/10.1186/s13578-020-00388-1

Wang, F., Xu, Y., Lv, C., Han, C., & Li, Y. (2018). Enhanced wound healing activity of PEG/PCL copolymer combined with bioactive nanoparticles in wound care after anorectal surgery:

Via bio-inspired methodology. *J Photochem Photobiol B*, *187*, 54-60. https://doi.org/10.1016/j.jphotobiol.2018.07.018

Wang, J., Wang, C. Z., Salsbury, J. R., Zhang, J., Enkhbaatar, P., Herndon, D. N., El Ayadi, A., & Ansari, N. H. (2021). Thermal injury induces early blood vessel occlusion in a porcine model of brass comb burn. *Sci Rep*, *11*(1), 12457. https://doi.org/10.1038/s41598-021-91874-0

Wang, J. F., Olson, M. E., Winkfein, R. J., Kulyk, W. M., Wright, J. B., & Hart, D. A. (2002). Molecular and cell biology of porcine HSP47 during wound healing: complete cDNA sequence and regulation of gene expression. *Wound Repair Regen*, *10*(4), 230-240. https://doi.org/10.1046/j.1524-475x.2002.10406.x

Wang, N., De Bock, M., Antoons, G., Gadicherla, A. K., Bol, M., Decrock, E., Evans, W. H., Sipido, K. R., Bukauskas, F. F., & Leybaert, L. (2012). Connexin mimetic peptides inhibit Cx43 hemichannel opening triggered by voltage and intracellular Ca2+ elevation. *Basic Res Cardiol*, *107*(6), 304. https://doi.org/10.1007/s00395-012-0304-2

Wang, N., De Vuyst, E., Ponsaerts, R., Boengler, K., Palacios-Prado, N., Wauman, J., Lai, C. P., De Bock, M., Decrock, E., Bol, M., Vinken, M., Rogiers, V., Tavernier, J., Evans, W. H., Naus, C. C., Bukauskas, F. F., Sipido, K. R., Heusch, G., Schulz, R., . . . Leybaert, L. (2013). Selective inhibition of Cx43 hemichannels by Gap19 and its impact on myocardial ischemia/reperfusion injury. *Basic Res Cardiol*, *108*(1), 309. https://doi.org/10.1007/s00395-012-0309-x

Wang, T., Zhu, X., Xue, X., & Wu, D. (2012). Hydrogel sheets of chitosan, honey and gelatin as burn wound dressings. *Carbohydrate Polymers*, *88*(1), 75-83. https://doi.org/https://doi.org/10.1016/j.carbpol.2011.11.069

Wang, W., Wang, X., Chun, J., Vilaysane, A., Clark, S., French, G., Bracey, N. A., Trpkov, K., Bonni, S., Duff, H. J., Beck, P. L., & Muruve, D. A. (2013). Inflammasome-independent NLRP3 augments TGF-beta signaling in kidney epithelium. *J Immunol*, *190*(3), 1239-1249. https://doi.org/10.4049/jimmunol.1201959

Wang, X. Q., Kravchuk, O., Winterford, C., & Kimble, R. M. (2011). The correlation of in vivo burn scar contraction with the level of alpha-smooth muscle actin expression. *Burns*, *37*(8), 1367-1377. https://doi.org/10.1016/j.burns.2011.07.018

Wang, Z., Ye, Q., Yu, S., & Akhavan, B. (2023). Poly Ethylene Glycol (PEG)-Based Hydrogels for Drug Delivery in Cancer Therapy: A Comprehensive Review. *Adv Healthc Mater*, *12*(18), e2300105. https://doi.org/10.1002/adhm.202300105

Warby, R., & Maani, C. V. (2020). Burns Classification. In *StatPearls*. https://www.ncbi.nlm.nih.gov/pubmed/30969595

Weber, B., Mendler, M. R., Lackner, I., von Zelewski, A., Hofler, S., Baur, M., Braun, C. K., Hummler, H., Schwarz, S., Pressmar, J., & Kalbitz, M. (2019). Lung injury after asphyxia and hemorrhagic shock in newborn piglets: Analysis of structural and inflammatory changes. *PLoS One*, *14*(7), e0219211. https://doi.org/10.1371/journal.pone.0219211

Wheat, J. C., & Wolf, J. S., Jr. (2009). Advances in bioadhesives, tissue sealants, and hemostatic agents. *Urol Clin North Am*, *36*(2), 265-275, x. https://doi.org/10.1016/j.ucl.2009.02.002

WHO. (2018). *Burns*. https://www.who.int/news-room/fact-sheets/detail/burns

Wiggins-Dohlvik, K., & Tharakan, B. (2018). A Rat Burn Injury Model for Studying Changes in Microvascular Permeability. *Methods Mol Biol*, *1717*, 93-100. https://doi.org/10.1007/978-1-4939-7526-6_8

Wilhelmi, B. J., Blackwell, S. J., & Phillips, L. G. (1999). Langer's lines: to use or not to use. *Plast Reconstr Surg*, *104*(1), 208-214. https://www.ncbi.nlm.nih.gov/pubmed/10597698

Williams, F. N., Herndon, D. N., & Jeschke, M. G. (2009). The hypermetabolic response to burn injury and interventions to modify this response. *Clin Plast Surg*, *36*(4), 583-596. https://doi.org/10.1016/j.cps.2009.05.001

Wiszniewski, L., Limat, A., Saurat, J. H., Meda, P., & Salomon, D. (2000). Differential expression of connexins during stratification of human keratinocytes. *Journal of Investigative Dermatology*, *115*(2), 278-285. https://doi.org/10.1046/j.1523-1747.2000.00043.x

Wong, R., Geyer, S., Weninger, W., Guimberteau, J. C., & Wong, J. K. (2016). The dynamic anatomy and patterning of skin. *Exp Dermatol*, *25*(2), 92-98. https://doi.org/10.1111/exd.12832

Wong, V. W., Sorkin, M., Glotzbach, J. P., Longaker, M. T., & Gurtner, G. C. (2011). Surgical approaches to create murine models of human wound healing. *J Biomed Biotechnol*, *2011*, 969618. https://doi.org/10.1155/2011/969618

Wright, C. S., Pollok, S., Flint, D. J., Brandner, J. M., & Martin, P. E. (2012). The connexin mimetic peptide Gap27 increases human dermal fibroblast migration in hyperglycemic and hyperinsulinemic conditions in vitro. *J Cell Physiol*, *227*(1), 77-87. https://doi.org/10.1002/jcp.22705

Wright, C. S., van Steensel, M. A., Hodgins, M. B., & Martin, P. E. (2009). Connexin mimetic peptides improve cell migration rates of human epidermal keratinocytes and dermal fibroblasts in vitro. *Wound Repair Regen*, *17*(2), 240-249. https://doi.org/10.1111/j.1524-475X.2009.00471.x

Wu, B., Zhang, F., Jiang, W., & Zhao, A. (2021). Nanosilver Dressing in Treating Deep II Degree Burn Wound Infection in Patients with Clinical Studies. *Comput Math Methods Med*, *2021*, 3171547. https://doi.org/10.1155/2021/3171547

Wu, D., Choi, J. C., Coselli, J., Shen, Y. H., & LeMaire, S. A. (2013). NLRP3 Inflammasome Activates Matrix Metalloproteinase-9: Potential Role in Smooth Muscle Cell Dysfunction in Thoracic Aortic Disease. *Journal of Surgical Research*, *179*(2), 204. https://doi.org/https://doi.org/10.1016/j.jss.2012.10.360

Wu, L., Chen, K., Xiao, J., Xin, J., Zhang, L., Li, X., Li, L., Si, J., Wang, L., & Ma, K. (2020). Angiotensin II induces RAW264.7 macrophage polarization to the M1-type through the

connexin 43/NF-kappaB pathway. *Mol Med Rep*, *21*(5), 2103-2112. https://doi.org/10.3892/mmr.2020.11023

Wu, R., Du, D., Bo, Y., Zhang, M., Zhang, L., & Yan, Y. (2019). Hsp90alpha promotes the migration of iPSCs-derived keratinocyte to accelerate deep second-degree burn wound healing in mice. *Biochem Biophys Res Commun*, *520*(1), 145-151. https://doi.org/10.1016/j.bbrc.2019.09.120

Xiao, H. B., Liu, R. H., Ling, G. H., Xiao, L., Xia, Y. C., Liu, F. Y., Li, J., Liu, Y. H., Chen, Q. K., Lv, J. L., Zhan, M., Yang, S. K., Kanwar, Y. S., & Sun, L. (2012). HSP47 regulates ECM accumulation in renal proximal tubular cells induced by TGF-beta1 through ERK1/2 and JNK MAPK pathways. *Am J Physiol Renal Physiol*, *303*(5), F757-765. https://doi.org/10.1152/ajprenal.00470.2011

Xiao, M., Li, L., Li, C., Liu, L., Yu, Y., & Ma, L. (2016). 3,4-Methylenedioxy-beta-Nitrostyrene Ameliorates Experimental Burn Wound Progression by Inhibiting the NLRP3 Inflammasome Activation. *Plast Reconstr Surg*, *137*(3), 566e-575e. https://doi.org/10.1097/01.prs.0000479972.06934.83

Xu, H., Wang, M., Li, Y., Shi, M., Wang, Z., Cao, C., Hong, Y., Hu, B., Zhu, H., Zhao, Z., Chu, X., Zhu, F., Deng, X., Wu, J., Zhao, F., Guo, J., Wang, Y., Pei, G., Zhu, F., . . . Zeng, R. (2022). Blocking connexin 43 and its promotion of ATP release from renal tubular epithelial cells ameliorates renal fibrosis. *Cell Death Dis*, *13*(5), 511. https://doi.org/10.1038/s41419-022-04910-w

Xu, W., Liu, K., Li, T., Zhang, W., Dong, Y., Lv, J., Wang, W., Sun, J., Li, M., Wang, M., Zhao, Z., & Liang, Y. (2019). An in situ hydrogel based on carboxymethyl chitosan and sodium alginate dialdehyde for corneal wound healing after alkali burn. *J Biomed Mater Res A*, *107*(4), 742-754. https://doi.org/10.1002/jbm.a.36589

Xue, M., & Jackson, C. J. (2015). Extracellular Matrix Reorganization During Wound Healing and Its Impact on Abnormal Scarring. *Adv Wound Care (New Rochelle)*, *4*(3), 119-136. https://doi.org/10.1089/wound.2013.0485

Yan, Y., Jiang, J., Zhang, M., Chen, Y., Wang, X., Huang, M., & Zhang, L. (2019). Effect of iPSCs-derived keratinocytes on healing of full-thickness skin wounds in mice. *Exp Cell Res*, *385*(1), 111627. https://doi.org/10.1016/j.yexcr.2019.111627

Ye, J., Zeng, B., Zhong, M., Li, H., Xu, L., Shu, J., Wang, Y., Yang, F., Zhong, C., Ye, X., He, X., & Ouyang, D. (2021). Scutellarin inhibits caspase-11 activation and pyroptosis in macrophages via regulating PKA signaling. *Acta Pharm Sin B*, *11*(1), 112-126. https://doi.org/10.1016/j.apsb.2020.07.014

Ye, Q., Chen, S., & Wang, D. (2021). Metabolic Regulation of the NLRP3 Inflammasome. *Infectious Microbes & Diseases*, *3*(4). https://journals.lww.com/imd/Fulltext/2021/12000/Metabolic_Regulation_of_the_NLRP3_Inflammasome.3.aspx

Yin, X., Feng, L., Ma, D., Yin, P., Wang, X., Hou, S., Hao, Y., Zhang, J., Xin, M., & Feng, J. (2018). Roles of astrocytic connexin-43, hemichannels, and gap junctions in oxygen-

glucose deprivation/reperfusion injury induced neuroinflammation and the possible regulatory mechanisms of salvianolic acid B and carbenoxolone. *J Neuroinflammation*, *15*(1), 97. https://doi.org/10.1186/s12974-018-1127-3

Yu, Y., Chen, J., Chen, R., Cao, L., Tang, W., Lin, D., Wang, J., & Liu, C. (2015). Enhancement of VEGF-Mediated Angiogenesis by 2-N,6-O-Sulfated Chitosan-Coated Hierarchical PLGA Scaffolds. *ACS Appl Mater Interfaces*, *7*(18), 9982-9990. https://doi.org/10.1021/acsami.5b02324

Yuan, W., Qiu, T., Yao, X., Wu, C., Shi, Y., Wang, N., Zhang, J., Jiang, L., Liu, X., Yang, G., Bai, J., & Sun, X. (2022). Hsp47 acts as a bridge between NLRP3 inflammasome and hepatic stellate cells activation in arsenic-induced liver fibrosis. *Toxicol Lett*, *370*, 7-14. https://doi.org/10.1016/j.toxlet.2022.07.816

Yucel, B., Coruh, A., & Deniz, K. (2019). Salvaging the Zone of Stasis in Burns by Pentoxifylline: An Experimental Study in Rats. *J Burn Care Res*, *40*(2), 211-219. https://doi.org/10.1093/jbcr/irz005

Zawacki, B. E., & Jones, R. J. (1967). Standard depth burns in the rat: the importance of the hair growth cycle. *Br J Plast Surg*, *20*(4), 347-354. https://doi.org/10.1016/s0007-1226(67)80065-1

Zeng, Q., Macri, L. K., Prasad, A., Clark, R. A. F., Zeugolis, D. I., Hanley, C., Garcia, Y., & Pandit, A. (2011). 5.534 - Skin Tissue Engineering. In P. Ducheyne (Ed.), *Comprehensive Biomaterials* (pp. 467-499). Elsevier. https://doi.org/https://doi.org/10.1016/B978-0-08-055294-1.00186-0

Zhang, C., Zhang, Q., Yang, D., Qiao, Y., Wang, B., Yan, J., Li, Z., Huang, Z., Zhou, Y., Hu, K., & Zhang, Y. (2022). Chitosan degradation products promote healing of burn wounds of rat skin. *Front Bioeng Biotechnol*, *10*, 1002437. https://doi.org/10.3389/fbioe.2022.1002437

Zhang, J., Guan, J., Niu, X., Hu, G., Guo, S., Li, Q., Xie, Z., Zhang, C., & Wang, Y. (2015). Exosomes released from human induced pluripotent stem cells-derived MSCs facilitate cutaneous wound healing by promoting collagen synthesis and angiogenesis. *J Transl Med*, *13*, 49. https://doi.org/10.1186/s12967-015-0417-0

Zhang, P., Zou, B., Liou, Y. C., & Huang, C. (2021). The pathogenesis and diagnosis of sepsis post burn injury. *Burns Trauma*, *9*, tkaa047. https://doi.org/10.1093/burnst/tkaa047

Zhang, T., Wu, K. Y., Ma, N., Wei, L. L., Garstka, M., Zhou, W., & Li, K. (2020). The C5a/C5aR2 axis promotes renal inflammation and tissue damage. *JCI Insight*, *5*(7). https://doi.org/10.1172/jci.insight.134081

Zhang, X., Pan, L., Yang, K., Fu, Y., Liu, Y., Chi, J., Zhang, X., Hong, S., Ma, X., & Yin, X. (2017). H3 Relaxin Protects Against Myocardial Injury in Experimental Diabetic Cardiomyopathy by Inhibiting Myocardial Apoptosis, Fibrosis and Inflammation. *Cell Physiol Biochem*, *43*(4), 1311-1324. https://doi.org/10.1159/000481843

Zhang, X. F., & Cui, X. (2017). Connexin 43: Key roles in the skin. *Biomed Rep*, *6*(6), 605-611. https://doi.org/10.3892/br.2017.903

Zheng, B., Shen, C., Sun, J., Guo, W., Jin, Y., & Niu, Y. (2019). Developing a Simple Burn Model in Rats of Different Ages. *J Burn Care Res*, *40*(5), 639-647. https://doi.org/10.1093/jbcr/irz072

Zhong, Z., Zhai, Y., Liang, S., Mori, Y., Han, R., Sutterwala, F. S., & Qiao, L. (2013). TRPM2 links oxidative stress to NLRP3 inflammasome activation. *Nat Commun*, *4*, 1611. https://doi.org/10.1038/ncomms2608

Zhou, Q., Wang, Y., Lu, Z., He, C., Li, L., You, M., Wang, L., Cao, T., Zhao, Y., Li, Q., Mou, A., Shu, W., He, H., Zhao, Z., Liu, D., Zhu, Z., Gao, P., & Yan, Z. (2022). Cx43 acts as a mitochondrial calcium regulator that promotes obesity by inducing macrophages polarization. In: Research Square.

Zhou, Y., Zhang, X. L., Lu, S. T., Zhang, N. Y., Zhang, H. J., Zhang, J., & Zhang, J. (2022). Human adipose-derived mesenchymal stem cells-derived exosomes encapsulated in pluronic F127 hydrogel promote wound healing and regeneration. *Stem Cell Res Ther*, *13*(1), 407. https://doi.org/10.1186/s13287-022-02980-3

Zhu, Y., Chen, X., Lu, Y., Fan, S., Yang, Y., Chen, Q., Huang, Q., Xia, L., Wei, Y., Zheng, J., & Liu, X. (2021). Diphenyleneiodonium enhances P2X7 dependent non-opsonized phagocytosis and suppresses inflammasome activation via blocking CX43-mediated ATP leakage. *Pharmacol Res*, *166*, 105470. https://doi.org/10.1016/j.phrs.2021.105470

Ziegler, B., Fischer, S., Pieper, D., Mathes, T., Kneser, U., & Hirche, C. (2020). Evidence and Trends in Burn Wound Debridement: An Evidence Map. *Plast Surg (Oakv)*, *28*(4), 232-242. https://doi.org/10.1177/2292550320928553

Zohdi, R. M., Zakaria, Z. A., Yusof, N., Mustapha, N. M., & Abdullah, M. N. (2011). Sea cucumber (Stichopus hermanii) based hydrogel to treat burn wounds in rats. *J Biomed Mater Res B Appl Biomater*, *98*(1), 30-37. https://doi.org/10.1002/jbm.b.31828